Complexation, Coupling, and Cleavage of Organonitriles, Alkynes, Dinitrogen, Hydrostannanes or Phosphines by Three-Coordinate Molybdenum(III) Complexes

by

Yi-Chou Tsai

Submitted to the Department of Chemistry
in partial fulfillment of the requirements for the degree of

Doctor of Philosophy in Chemistry

at the

MASSACHUSETTS INSTITUTE OF TECHNOLOGY
[February 2002]
October 2001

Author .....
Department of Chemistry
September 20, 2001

Certified by .....
Christopher C. Cummins
Professor of Chemistry
Thesis Supervisor

Accepted by .....
Robert W. Field
Chairman, Department Committee on Graduate Students

This doctoral thesis has been examined by a Committee of the Department of Chemistry as follows:

Professor Stephen J. Lippard _____

Professor Christopher C. Cummins _____

Professor Richard R. Schrock _____

Dedicated to my beloved wife Jui-Fen (Nora)

Complexation, Coupling, and Cleavage of Organonitriles, Alkynes, Dinitrogen, Hydrostannanes, and Phosphines by Three-Coordinate Molybdenum(III) Complexes

Yi-Chou Tsai

Submitted to the Department of Chemistry, October 2001

Massachusetts Institute of Technology

in Partial Fullfillment of the Requirements

for the Degree of Doctor of Philosophy of Chemistry

Thesis Supervisor: Christopher C. Cummins

Title: Professor of Chemistry

Abstract

Chapter 1. Complexation, Coupling, and Cleavage of Organonitriles by a Masked Three-Coordinate Molybdenum(III) Complex: Spectroscopic Characterization and Mechanistic Investigations

The hydride ligand in Mo(H)(η^2-Me_2CNAr)(N[^{i}Pr]Ar)$_2$ (**1**) formed via β-hydrogen elimination is characterized by electron paramagnetic resonance (EPR) spectra that show coupling to a single hydrogen nucleus, $A_{iso}{}^1H$ = 16.4 G. The deutero analog Mo(D)(η^2-Me_2CNAr)(N[$CDMe_2$]Ar)$_2$ (**1-d_3**) was prepared and EPR spectra show the expected coupling to a single deuteron, $A_{iso}{}^2H$ = 2.4 G. The β-hydrogen elimination in **1** is a reversible process as confirmed by variable-temperature ^2H NMR spectroscopy. Consequently, **1** behaves as a source of Mo(N[^{i}Pr]Ar)$_3$ (**2**). Addition of 1 equiv of organic nitrile (NCR) to **1** yields the dimeric complexes [**2-NCR**]$_2$, which can be oxidized by one or two electrons on the electrochemical time scale. The paramagnetic cation [**2-NCPh**]$_2{}^+$ was structurally characterized as its triodide salt, but a salt of the corresponding dicationic dimer could not be obtained. The nitrile coupling process is believed to occur through the radical monomer **2-η^1-NCR**. In contrast to the condition favoring nitrile coupling, a slow addition of 1/3 equiv of benzonitrile to **1** results in scission of the N≡C triple bond and the formation of the bridging nitride complex **2$_2$-μ-N** and benzylidyne **2-CPh**. In addition to coupling and cleavage, nitriles can coordinate to **2** via η^1 or η^2 binding modes. Treatment of Mo(H)(η^2-$(CD_3)_2CNAr$)(N[^{i}Pr-d_6]Ar)$_2$ (**1-d_{18}**) with 2 equiv of 2,4,6-trimethylbenzonitrile (NCMes) gives the paramagnetic blue complex **2-(η^1-NCMes)$_2$**. The structure of **2-(η^1-NCMes)$_2$** was established by X-ray diffraction., and the geometry at molybdenum is best described as trigonal bipyrimidal with the two nitrile ligands occupying axial positions. Addition of 1 equiv of 9-anthracenecarbonitrile (NCAnth) to **1** gives an asymmetric head-to-tail dimer [**2-NCAnth**]$_2$, which was characterized by X-ray crystallography as well. Furthermore, addition of 1 equiv of $NCNMe_2$ to **1** or Mo(N[^{t}Bu-d_6]Ar)$_3$ (**3**) produces paramagnetic complexes **2-** or **3-η^2-NCNMe$_2$**. The structure of **3-η^2-**$NCNMe_2$ was confirmed by X-ray crystallography. By comparing the EPR and ^2H NMR data of complexes **2-(η^1-NCMes)$_2$**, **2-** and **3-η^2-NCNMe$_2$**, it is shown that **2-(η^1-NCPh)$_2$** and **2-(η^2-NCPh)** are formed in solution when NCPh is added to **1**, while only **3-η^2-NCPh** is seen in the reaction of **3** with NCPh.

Chapter 2. Interaction of Styrene and Alkynes with a Masked Three-Coordinate Molybdenum(III) Complex: Preparation of Well-Defined Alkyne Metathesis Catalysts and Related Chemistry

Addition of one equiv of styrene or alkynes to Mo(H)(η^2-Me_2CNAr)(N[^{i}Pr]Ar)$_2$ (Ar = 3,5-$C_6H_3Me_2$) (**1**) produces paramagnetic complexes (η^2-H_2CCHPh)Mo(N[^{i}Pr]Ar)$_3$ (**2-η^2-H_2CCHPh**) or (η^2-R^1CCR^2)Mo(N[^{i}Pr]Ar)$_3$) (**2-η^2-R^1CCR^2**). The molecular structure of **2-η^2-H_2CCHPh** was determined by X-ray diffraction study and it shows that styrene coordinates to Mo in η^2 manner. Interestingly, the structure of **2-η^2-H_2CCHPh** shows three β-agostic Mo$\cdots$HC interactions, which are confirmed by DFT calculations. The experimental EPR spectra and simulation data of **2-η^2-H_2CCHPh** indicate the unpaired-electron interacts with Mo and the three vinylic styrene hydrogens. The rate of formation of **2-η^2-R^1CCR^2** is dependent on the steric bulk of the alkyne, i.e. the bulkier the alkyne, the slower the reaction. With appropriate acetylenic groups (R^1 = H, R^2 = Ph or ^{n}Pr), complexes **2-η^2-R^1CCR^2** can dimerize to form (μ-bis(carbene))dimolybdenum complexes (μ-$CR^2CHCHCR^2$)**2$_2$** ([**2-R^2CCR^1**]$_2$). Complexes **2-η^2-R^1CCR^2** can be oxidized upon addition of one-half equiv of I_2 to form the iodide salts [**2-η^2-R^1CCR^2**][I]. Addition of one equiv of super hydride $LiHBEt_3$ to the iodide salts of [**2-η^2-R^1CCR^2**]$^+$ produced (η^2-R^1HCCR^2)Mo(N[^{i}Pr]Ar)$_3$)(η^2-vinyl) complexes. Alternatively, complex **2-η^2-$H_2CCSiMe_3$** can be prepared by adding 0.5 equiv of Ph_2SnH_2 to **2-η^2-$HCCSiMe_3$**. Heating **2-η^2-$H_2CCSiMe_3$** induced isomerization to form the Schrock-type alkylidyne complex **2-CCH_2SiMe_3**. Alcoholysis of **2-CCH_2SiMe_3** gave trialkoxymolybdenum(VI) alkylidyne complexes upon addition of 3 equiv of alcohol. These new carbyne complexes were found to be good catalysts for alkyne metathesis.

Chapter 3. Dinitrogen Cleavage by Three-Coordinate Molybdenum(III) Complexes Accelerated by Lewis Bases

Dinitrogen cleavage (1 atm, 25 °C) by Mo(H)(η^2-$(CD_3)_2CNAr$)(N[^{i}Pr-d_6]Ar)$_2$ (**1**) or Mo(N[^{t}Bu-d_6]Ar)$_3$ (**3**) (Ar = 3,5-$C_6H_3Me_2$) yielding half equiv of [Mo(N[^{i}Pr-d_6]Ar)$_3$](μ-N) (**2$_2$-μ-N**) or two

equiv of Mo(N[^{t}Bu-d_6]Ar)$_3$)(**3-N**) is found to be accelerated in the presence of one equiv of a Lewis bases, e.g. 2,6-dimethylpyrazine, pyridine, 4-dimethylaminopyridine, 1-methylimidazole, or potassium hydride. From a ^{2}H NMR spectroscopy study, 2,6-dimethylpyrazine, pyridine, 4-dimethylaminopyridine or 1-methylimidazole were found to be able to reversibly bind complex **1** in solution. Presumably, a base coordinates to **1** yielding an adduct **2-L** (L = 2,6-dimethylpyrazine, pyridine, 4-dimethylaminopyridine or 1-methylimidazole) and dinitrogen binds to these adducts **2-L** more readily than **2**. On the other hand, no interactions have been observed between compound **3** and pyridine, 4-dimethylaminopyridine or 1-methylimidazole based on NMR time scale, while 2,6-dimethylpyrazine was found to bind to **3** reversibly. In neat 2,4,6-collidine, complex **1** or **3** remains intact and, therefore, the rate of dinitrogen cleavage is not effected. This observation strongly supports the above hypothesis. The rate of dinitrogen cleavage is dependent on the size and basicity of Lewis bases and it increases as the following order: 2,6-dimethylpyrazine, pyridine, 4-dimethylaminopyridine, 1-methylimidazole, and potassium hydride. Potassium hydride is found to be the most effective base for accelerating dinitrogen cleavage by **1** or **3**, and it furthermore reduces purple **2$_2$-μ-N** to it's corresponding green potassium salt [**2$_2$-μ-N**]$^-$.

Chapter 4. Activation of E-H Bonds (E = Sn or P) by Three-Coordinate Molybdenum(III) Complexes

Addition of one equiv of HSnR$_3$ (R = ^{n}Bu or Ph) to Mo(H)(η^2-Me$_2$CNAr)(N[^{i}Pr]Ar)$_2$ (**1**) produced a paramagnetic hydrido stannyl complex Mo(η^2-HSnR$_3$)(N[^{i}Pr]Ar)$_3$ (**2-η^2-HSnR$_3$**. The X-ray diffraction study indicates that HSn^{n}Bu$_3$ binds Mo in η^2 manner. Interestingly, the strength of the interaction between Mo and Sn-H is dependent on the nature of the Sn-H bond. A greater degree of oxidative addition was observed in complex **2-η^2-HSnPh$_3$**. In contrast to the results of the reactions of **1** with HSnR$_3$, Mo(N[^{t}Bu-d$_6$]Ar)$_3$ (**3**) reacted with HSnR$_3$ to yield a mixture of Mo(H)(N[^{t}Bu]Ar)$_3$ (**3-H**), Mo(SnR$_3$)(N[^{t}Bu]Ar)$_3$ (**3-SnR$_3$**), and R$_3$SnSnR$_3$ (R = ^{n}Bu or Ph). Complex (**3-SnPh$_3$**) was also synthesized independently upon salt metathesis from the reaction of Mo(I)(N[^{t}Bu]Ar)$_3$ with KSnPh$_3$ and fully chracterized. Addition of one equiv of H$_2$SnR$_2$ to **1** resulted in a vigorous evolution of hydrogen and produced the green diamagnetic compounds (μ-

$SnR_2SnR_2)[Mo(N[^iPr]Ar)_3]_2$ ($[\mathbf{2\text{-}SnR_2}]_2$) (R = ^{n}Bu or Ph). The formation of $[\mathbf{2\text{-}SnR_2}]_2$ probably occurs *via* the dimerization of a stannylidene intermediate. Compounds $[\mathbf{2\text{-}SnR_2}]_2$ are thermally unstable in solution and decompose rapidly to give **1** and $(SnR_2)_n$ (R = ^{n}Bu or Ph) at room temperature. Addition of one half equiv of H_2SnR_2 to **3** produced a paramagnetic metal hydride complex **3-H** and organotin by-product $(SnR_2)_n$. In contrast to the different reactivities of **1** and **3** towards $HSnR_3$ and H_2SnR_2, both **1** and **3** reacted with PH_2Ph to yield $Mo(PHPh)(N[^iPr]Ar)_3$ (**2-PHPh**) and $Mo(PHPh)(N[^tBu\text{-}d_6]Ar)_3$ (**3-PHPh**), respectively. The formation of **2-PHPh** or **3-PHPh** occurs *via* bimetallic oxidative addition in reactions of **1** or **3** with PH_2Ph to form the intermediates **2-H** and **2-PHPh** or **3-H** and **3-PHPh**, respectively. Subsequently, **2-H** or **3-H** reacted with PH_2Ph to produce **2-PHPh** or **3-PHPh**. Owing to the steric bulk of **3**, however, a greater amount of PH_2Ph is necessary for eliminating **3-H** and increasing the yield of **3-PHPh**.

Table of Contents

Chapter 1.

Complexation, Coupling, and Cleavage of Organonitriles by a Masked Three-Coordinate Molybdenum(III) Complex: Spectroscopic Characterization and Mechanistic Investigations

Chapter 2.

Interaction of Styrene and Alkynes with a Masked Three-Coordinate Molybdenum(III) Complex: Preparation of Well-Defined Alkyne Metathesis Catalysts and Related Chemistry

Chapter 4.

Activation of E-H Bonds (E = Sn or P) by Three-Coordinate Molybdenum(III) Complexes

List of Figures

Chapter 1.

Complexation, Coupling, and Cleavage of Organonitriles by a Masked Three-Coordinate Molybdenum(III) Complex: Spectroscopic Characterization and Mechanistic Investigations

11 X-band EPR spectra of **2-η^2-OCPh$_2$** (top) Experimental conditions: Microwave frequency ν = 9.351 GHz, Power = 1 mW, Modulation amplitude = 5 G, **3-η^2-NCNMe$_2$** (middle) Experimental conditions: Microwave frequency ν = 9.707 GHz, Power = 1 mW, Modulation amplitude = 5 G, and **2-η^2-NCPh** (bottom) Experimental conditions: Microwave frequency ν = 9.351 GHz, Power = 1 mW, Modulation amplitude = 5 G. All spectra were recorded in frozen toluene solution at T = 110 K. The inset shows the isotropic spectrum of **2-η^2-NCPh** in liquid solution at T = 260 K. Experimental conditions: Microwave frequency ν = 9.351 GHz, Power = 1 mW, Modulation amplitude = 5 G.....52

12 Cyclic voltammogram of **[2-NCPh]**$_2$.....56

13 Thermal ellipsoid plot (35% probability) of **[2-NCPh]**$_2$[I_3]. Selected distances (Å) and angles (°): Mo(1)-N(1), 1.921(5); Mo(1)-N(2), 1.918(5); Mo(1)-N(3), 1.929(5); Mo(1)-N(4), 1.740(5); C(4)-C(4)*, 1.368(12); I(1)-I(2), 2.938(1); I(2)-I(3), 2.896(1); N(1)-Mo(1)-N(2), 110.7(2); N(2)-Mo(1)-N(3), 110.2(2); N(3)-Mo(1)-N(1), 113.2(2); N(4)-Mo(1)-N(1), 107.5(2); N(4)-Mo(1)-N(2), 107.4(2); N(3)-Mo-N(4), 109.6(2); C(4)-N(4)-Mo(1), 175.6(5); N(4)-C(4)-C(4)*, 120.6(7); I(3)-I(2)-I(1), 177.22(3).....58

14 Pictured are molecular orbitals 116, 115, 112 and 106, clockwise from upper left. These correspond to the LUMO, SOMO, Mo-imine backbonding, and hydridic orbitals, respectively, of the model system Mo(H)(Me_2CNPh)($NMePh)_2$ derived from X-ray and neutron diffraction studies of complex **1**. The calculation employed *C*1 symmetry for the model system in agreement with the solid state structure determinations. EPR hyperfine couplings from the calculation are as follows: A_{iso}(Mo) = 52 MHz, A_{iso}(H) = 49 MHz, $A_{iso}(N_{imine})$ = 3.9 MHz, $A_{iso}(N_{amide})$ = 7.2 and 6.5 MHz. All of the foregoing are in good agreement with values determined experimentally with the exception of A_{iso}(H); the origin of the latter

Chapter 2.

Interaction of Styrene and Alkynes with a Masked Three-coordinate Molybdenum(III) Complex: Preparation of Well-Defined Alkyne Metathesis Catalysts and Related Chemistry

Chapter 3.

Dinitrogen Cleavage by Three-Coordinate Molybdenum(III) Complexes Accelerated by Lewis Bases

Chapter 4.

Activation of E-H Bonds (E = Sn or P) by Three-Coordinate Molybdenum(III) Complexes

List of Schemes

Chapter 1.

Complexation, Coupling, and Cleavage of Organonitriles by a Masked Three-Coordinate Molybdenum(III) Complex: Spectroscopic Characterization and Mechanistic Investigations

Chapter 2.

Interaction of Styrene and Alkynes with a Masked Three-Coordinate Molybdenum(III) Complex: Preparation of Well-Defined Alkyne Metathesis Catalysts and Related Chemistry

List of Tables

Chapter 1.

Complexation, Coupling, and Cleavage of Organonitriles by a Masked Three-Coordinate Molybdenum(III) Complex: Spectroscopic Characterization and Mechanistic Investigations

Chapter 2.

Interaction of Styrene and Alkynes with a Masked Three-Coordinate Molybdenum(III) Complex: Preparation of Well-Defined Alkyne Metathesis Catalysts and Related Chemistry

Chapter 4.

Activation of E-H Bonds (E = Sn or P) by Three-Coordinate Molybdenum(III) Complexes

List of Abbreviations Used in the Text

Ad	adamantyl
Anal	elemental analysis
Anth	Anthracence
Ar	3,5-$C_6H_3Me_2$
br	broad
Calcd	calculated
CCD	charged coupled device
cm^{-1}	wavenumber
Cy	cyclohexyl
d	day(s), doublet
d^n	numbers of d-electrons
deg(°)	degrees
EPR	Electron Paramagnetic Resonance
equiv	equivalents
FT	Fourier transform
Fc/Fc^+	Ferrocene/Ferrocenium
G	Gauss
g	grams
GOF	goodness of fit
h	hour(s)
^1H	proton
^2H	deuteron
HOMO	highest occupied molecular orbital
Hz	Hertz
^iPr	*iso*-Propyl
IR	infrared
LUMO	lowest unoccupied molecular orbital
M	moles/liter, mega
M	multiplet in NMR

Mes	2,4,6-$C_6H_2Me_3$
mg	milligram
min	minute(s)
mL	milliliter
mmol	millimole
MO	molecular orbital
NMR	nuclear magnetic resonance
ORTEP	Oak Ridge Thermal Elipsoid Plot
OTf	OSO_2CF_3
Ph	C_6H_5
ppm	parts per million
py	pyridine
q	quintet
R	$C(CD_3)_2(CH_3)$
R'	generic alkyl group
R"	generic alkyl group
RT	room temperature (≈ 25 °C)
s	singlet in NMR
SQuID	Superconducting Quantum Interference Device
t	triplet
THF	tetrahydrofuran
^{t}Bu	$C(CMe_3)$
VT	variable temperature
°C	degrees Celsius
Å	Angstrom (10^{-10} m)
χ	magnetic susceptibility
δ	chemical shift in ppm downfield from zero
$\Delta\nu_{1/2}$	peak width at half-height
η^x	x-hapto
μ	bridging ligand
μ_B	Bohr magnetons

μ_{eff}	effective magnetic moment
θ	Weiss constant, detector angle in crystallography
ρ_{calc}	calculated density
σ	background intensity

Chapter 1. Complexation, Coupling, and Cleavage of Organonitriles by a Masked Three-Coordinate Molybdenum(III) Complex: Spectroscopic Characterization and Mechanistic Investigations

October 29, 2001

1 Introduction

Three-coordinate transition metal complexes stabilized by sterically encumbering ligands are attractive targets for study with respect to the activation of small molecules.[1,2] For example, dinitrogen[3,4] and nitrous oxide[5,6] NN bond splitting reactions occur under mild conditions as mediated by the three-coordinate molybdenum(III) complex $Mo(N[R]Ar)_3$ (R = $C(CD_3)_2CH_3$ (**3**) or ^tBu and Ar = 3,5-$C_6H_3Me_2$). $Mo(N[R]Ar)_3$ has been used also as a platform for the synthesis of new triply bonded functional groups including a terminal phosphide[7] and a terminal carbide[8] stemming from activation of white phosphorus and carbon monoxide, respectively. Dramatic has been the effect of steric bulk on modulating dinitrogen cleavage reactivity, as has been probed with a family of ligands bearing more voluminous substituents (R = 2-adamantyl or 1-adamantyl).[6,9]

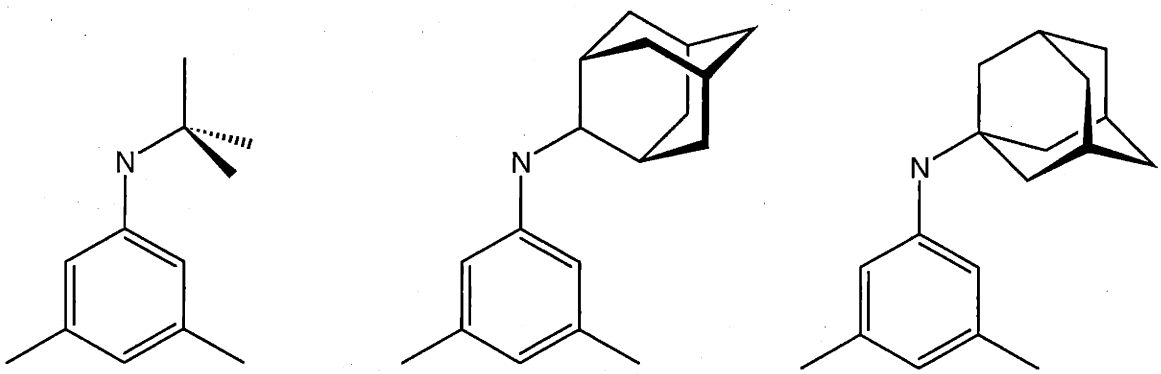

In addition to small-molecule activation, we are interested also in the activation of organic molecules typified by nitriles and alkynes. Unfortunately, the very steric bulk of the ligands that is responsible for the stability of the three-coordinate molybdenum complex occasionally can hinder or obstruct reactions with organic substrates. In a recent communication,[10] we reported the synthesis and reactivity of a novel cyclometallated molybdenum metallaaziridine hydride complex, $Mo(H)(\eta^2$-

$Me_2C{=}NAr)(N[^iPr]Ar)_2$ (1). This molybdenum complex is an excellent candidate for the activation of organic molecules due to its reduced steric bulk.

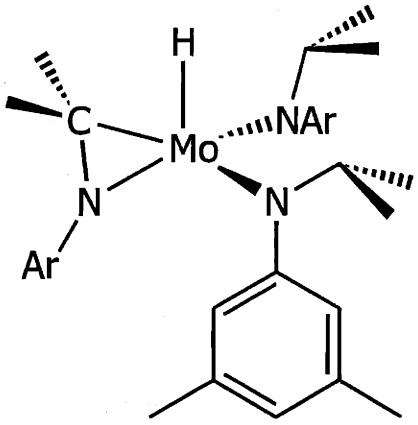

1

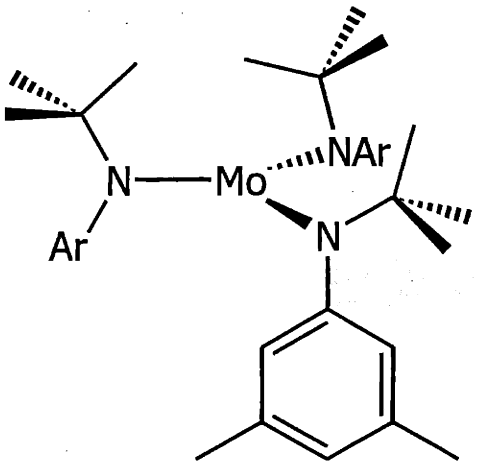

3

Nitriles represent a triple-bond functionality reminiscent of dinitrogen, carbon monoxide, isocyanides, and alkynes, and as such are used extensively as ligands in transition-metal chemistry. Owing to their weak σ-donor and π-acceptor abilities, nitriles often can be displaced readily to afford novel coordination and organometallic complexes. Nitriles are known to interact with a transtion metal in two different ways, these being the terminal end-on σ-complex, (η^1-NCR), and the side-on π-complex, (η^2-NCR).[11]

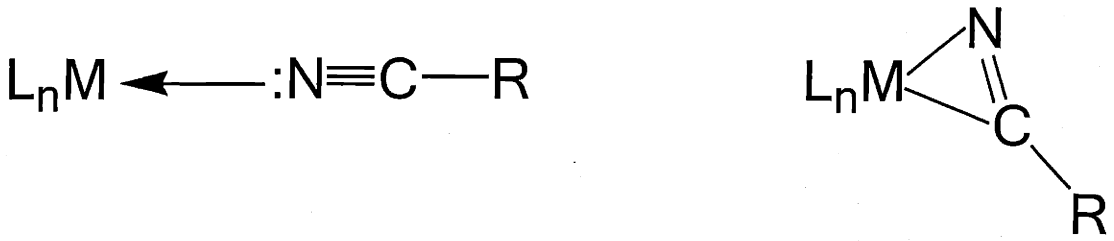

σ-complex

π-complex

η^1-NCR

η^2-NCR

Recent studies on transition-metal organonitrile complexes have revealed that coordinated nitriles can be endowed with rich reactivities.[11–17] Most of the metal-promoted reactions of nitriles reported to date are concerned with the nitrile ligands being coordinated to electron-deficient metal centers through their nitrogen terminus. Nitriles coordinated to π-donating metal complexes are expected to be susceptible to attack by electrophiles, due to the moderate π-accepting character of NCR. However, nitrile complexes with strongly π-donating low-valent metal centers are considerably limited in number, and the reactivity of nitriles in such complexes remains to be developed.[18–22]

As eported previously, either NCR coupling or C≡N triple bond scission mainfolds can be accessed by controlling the concentration of **1**.[10] These two types of reactions are rare,[23–32] and their mechanisms are of great interest.[33] Herein are reported synthetic and spectroscopic studies of the reactions between nitriles and the molybdenum metallaziridine hydride **1** carried out to define the nature of intermediates and complexs important to organonitrile transformations.

2 Results

2.1 EPR study of 1 and Mo(D)(η^2-Me_2CNAr)(N[CDMe_2]Ar)$_2$ (1-d_3)

The *tris*-anilide molybdenum(III) species Mo(N[R]Ar)$_3$ (R = ^{t}Bu, ^{1}Ad) reported previously are EPR-silent at 25 °C. Solution magnetic susceptibility measurements obtained by the method of Evans[34] are consistent with a quartet ground state for Mo(N[R]Ar)$_3$ (μ_{eff} = 3.82 (**3**) and 3.96 μ_B (R = ^{1}Ad)).[4,9] In contrast, complex **1** reported in this paper possesses an EPR-active $S = 1/2$ ground state. The magnetic moment of **1** was found to be 2.10 μ_B, close to the spin-only moment for a system containing one unpaired electron.[35]

The X-band EPR spectrum of **1** and its deuterated isotopomer **1-d_3** were subjected to an in-depth EPR spectroscopic investigation. The spectra were measured at low (110 K) and ambient (300 K) temperatures both in the solid state and in solution. Figures 1 and 2 show the solution spectra at 300 K and the respective simulations together with enlargements for clarity. The liquid solution spectra display intense signals centered at g = 1.982, flanked with additional satellites. The relatively small line width W of $\leq$ 2 G allows the detection of resolved hyperfine structure due to coupling of the unpaired electron with the nuclear spin of the less abundant $^{95/97}$Mo isotopes (25.5 %; $I = 5/2$). A coupling constant, $A_{iso}{}^{95/97}$Mo, of 32.6 G was obtained from the simulation.

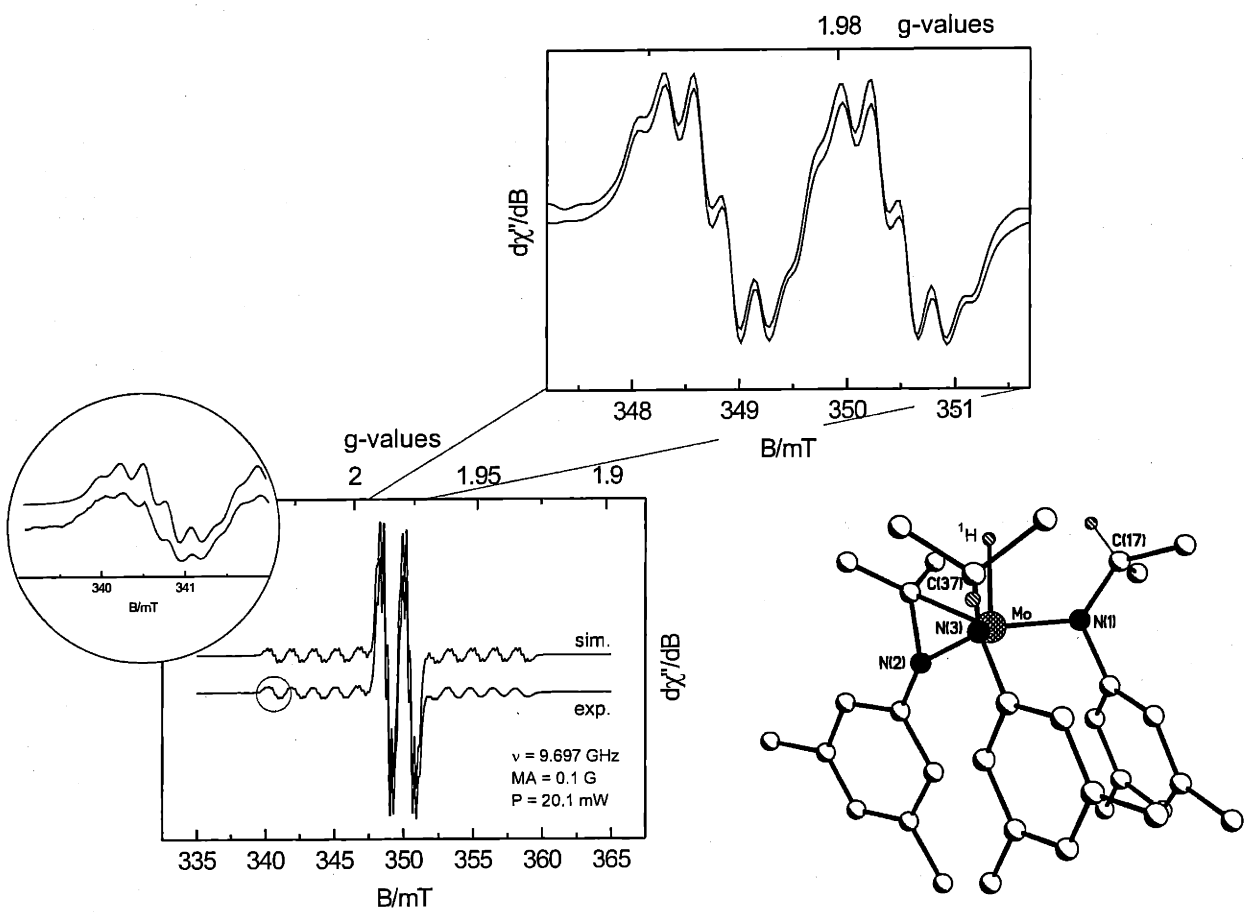

Figure 1: X-band EPR spectrum of **1** with inset of enlarged low-field signal (top) and enlargement of main signal (bottom) recorded in Et_2O/n-C_5H_{12} (1:1) at 300 K. Experimental conditions: microwave frequency ν: 9.697 GHz, Power: 20.1 mW, Modulation amplitude: 0.1 G. Simulated parameters: $g_{iso} = 1.9825$, $A_{iso}{}^{95/97}$Mo (25.5%) = 32.6 G (90.41 MHz), $A_{iso}{}^{1}$H (99.99%) = 16.4 G (45.48 MHz), $A_{iso}{}^{14}$N (99.63%) = 2.75 G (2 amido ligands, 7.63 MHz) and 1.35 G (imino ligand, 3.74 MHz), and line width = 1.94 G

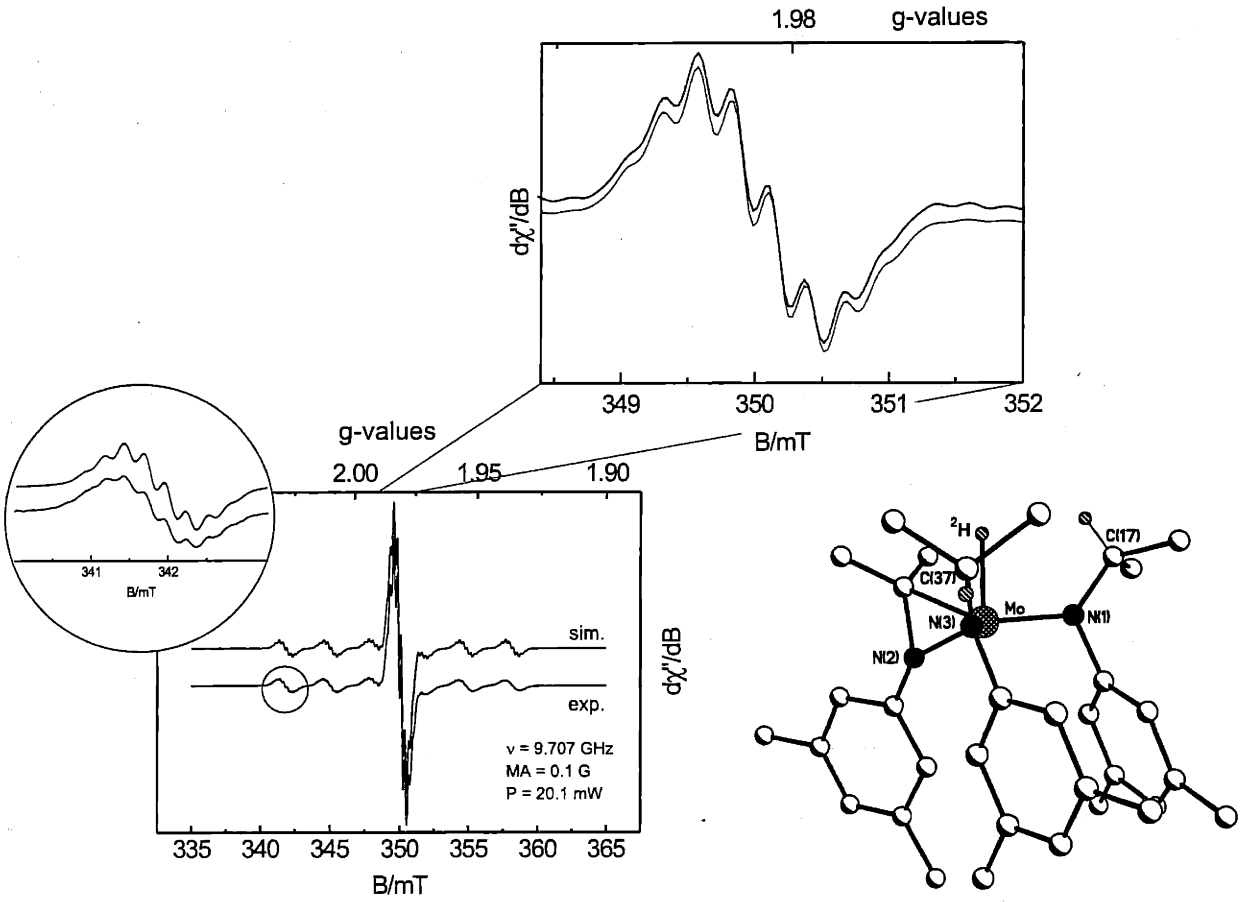

Figure 2: X-band EPR spectrum of **1-d_3** with inset of enlarged low-field signal (top) and enlargement of main signal (bottom) recorded in Et_2O/n-C_5H_{12} (1:1) at 300 K. Experimental conditions: microwave frequency ν: 9.707 GHz, Power: 20.1 mW, Modulation amplitude: 0.1 G. Simulated parameters: g_{iso} = 1.9825, $A_{iso}{}^{95/97}$Mo (25.5%) = 32.6 G (90.41 MHz), $A_{iso}{}^{2}$H (99.63%) = 2.4 G (6.66 MHz), $A_{iso}{}^{14}$N (99.63%) = 2.75 G (2 amido ligands, 7.63 MHz) and 1.35 G (imino ligand, 3.74 MHz), and line width = 1.94 G

The most prominent difference in the spectra is the splitting pattern envinced by **1** and its deutero analog **1-d_3**. The main signal at $g = 1.982$ as well as the six satellites in **1** are split into two equally intense signals through coupling of the electron spin with a nuclear spin of $I = 1/2$. The spectrum of the deuterated isotopomer **1-d_3** does not exhibit this additional strong super-hyperfine structure and this feature must therefore arise from coupling to the apical metal hydride ligand. A coupling constant, $A_{iso}{}^{1}H$, of 16.4 G was obtained from the simulation. Since $A_{iso}{}^{2}H$ is $\approx 1/7$ $A_{iso}{}^{1}H$, the spectrum of **1-d_3** was simulated under the assumption of a coupling constant $A_{mathrmiso}{}^{2}H$ of 2.4 G. Although the peak-peak line width and $A_{iso}{}^{2}H$ are comparable in magnitude (additional hyperfine splitting through coupling to the deuteride is not resolved), $A_{iso}{}^{2}H$ must be included in order to simulate dominant features such as characteristic shoulders and turning points in the spectrum. It also accounts for the line-broadening through unresolved hyperfine splitting. It is noteworthy that the spectrum of **1-d_3** was successfully simulated without changing any other parameters. From a simulation of the main signals at 1.982 as well as the low-field signals shown in Figures 1 and 2 (enlargement and inset) it has been possible to establish that in addition to the $^{95/97}$Mo and the H/D coupling, two different types of nitrogen nuclei interact with the electron spin. To account for the characteristic splitting pattern, a super-hyperfine coupling constant, $A_{iso}{}^{14}N$ (99.63 %; $I = 1$; $n = 2$) of 2.75 G was established. Additionally, a weaker coupling to a single nitrogen nucleus with $A_{iso}{}^{14}N$ of 1.35 G (n =1) was introduced. Although the latter interaction is significantly smaller than the inherent line-width, we have not been able to simulate the very sharp and characteristic resonances flanking the main signals at zero crossing as well as their relative intensities without introducing this weak interaction. To further verify the assignment, two strategies were employed: A variety of deuterated ligands (below) and the corresponding isotopomers of **1** were synthesized and investigated to rule out agostic interactions

and weak Mo-H couplings to ortho hydrogens of the Ar moiety. As anticipated, no effect on the EPR spectra was observed. Also, a DFT calculation on the geometry-optimized model compound $Mo(H)(Me_2CNPh)(NMePh)_2Mo(H)$ was employed. The obtained computional results indicate that the two amide nitrogen atoms carry twice as much spin density as the metallaaziridine N atom, suggesting a hyperfine coupling constant for the latter approximately half the value of that for the former. This is consistent with our findings.

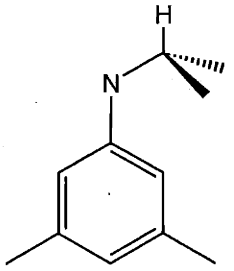

d_0

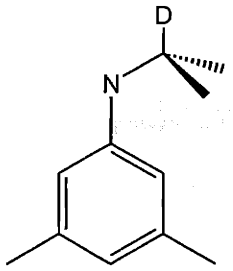

d_1

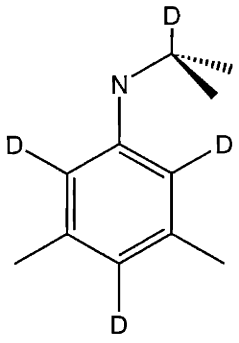

d_4

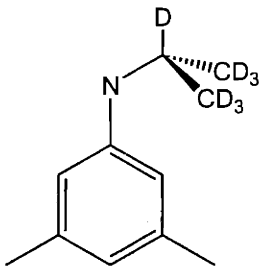

d_7

2.2 Variable temperature ^{2}H NMR spectroscopy investigations of Mo(H)(η^2-$(CD_3)_2CNAr$)(N[^{i}Pr-d_6]Ar)$_2$ (**1**-d_{18})

The crystal structure of **1** illustrates β-H elimination from one amido ligand and resulting pseudo-mirror molecular symmetry, consistent with the compound's ^{2}H NMR data consisting of three signals in a 1:1:1 ratio. Initially it was thought that the cyclometallated nature of **1** would inhibit the type of reaction chemistry observed for related three-coordinate derivatives, i.e. **3**. This proved not to be the case. In a previous report,[10] we described that **1** reductively splits dinitrogen under mild conditions, reacts with benzophenone to yield Mo(η^2-$OCPh_2$)(N[^{i}Pr]Ar)$_3$ (**2**-η^2-$\mathbf{OCPh_2}$), and couples and cleaves organic nitriles. Based on these observations, **1** is a very reactive species and serves as a source of the three-coordinate molybdenum(III) complex Mo(N[^{i}Pr]Ar)$_3$ (**2**), suggesting that the β-H elimination process is reversible. To further illustrate the β-hydrogen elimination process, a variable-temperature ^{2}H NMR study was undertaken on **1**-d_{18}. As illustrated in Figure 3, coalescence of two peaks at 8.3 and 5.8 ppm due to the diastereotopic $CH(CD_3)_2$ groups was observed at 70 °C, but coalescence of these with the original signal at −19.5 ppm (metallaaziridine $C(CD_3)_2$ moiety) is not achieved. Based on a simulation (Figure 4) complete coalescence is expected to be achieved at higher temperatures. Also consistent with the data in Figure 3 would be a fluxional process in which the metallaaziridine-hydride moiety rotates as a whole to achieve coplanarity with the Mo N_2 plane, but this is considered unlikely. After being cooled down to room temperature from 90 °C, **1**-d_{18} showed no signs of decomposition, an indication of the thermal stability of **1**-d_{18}.

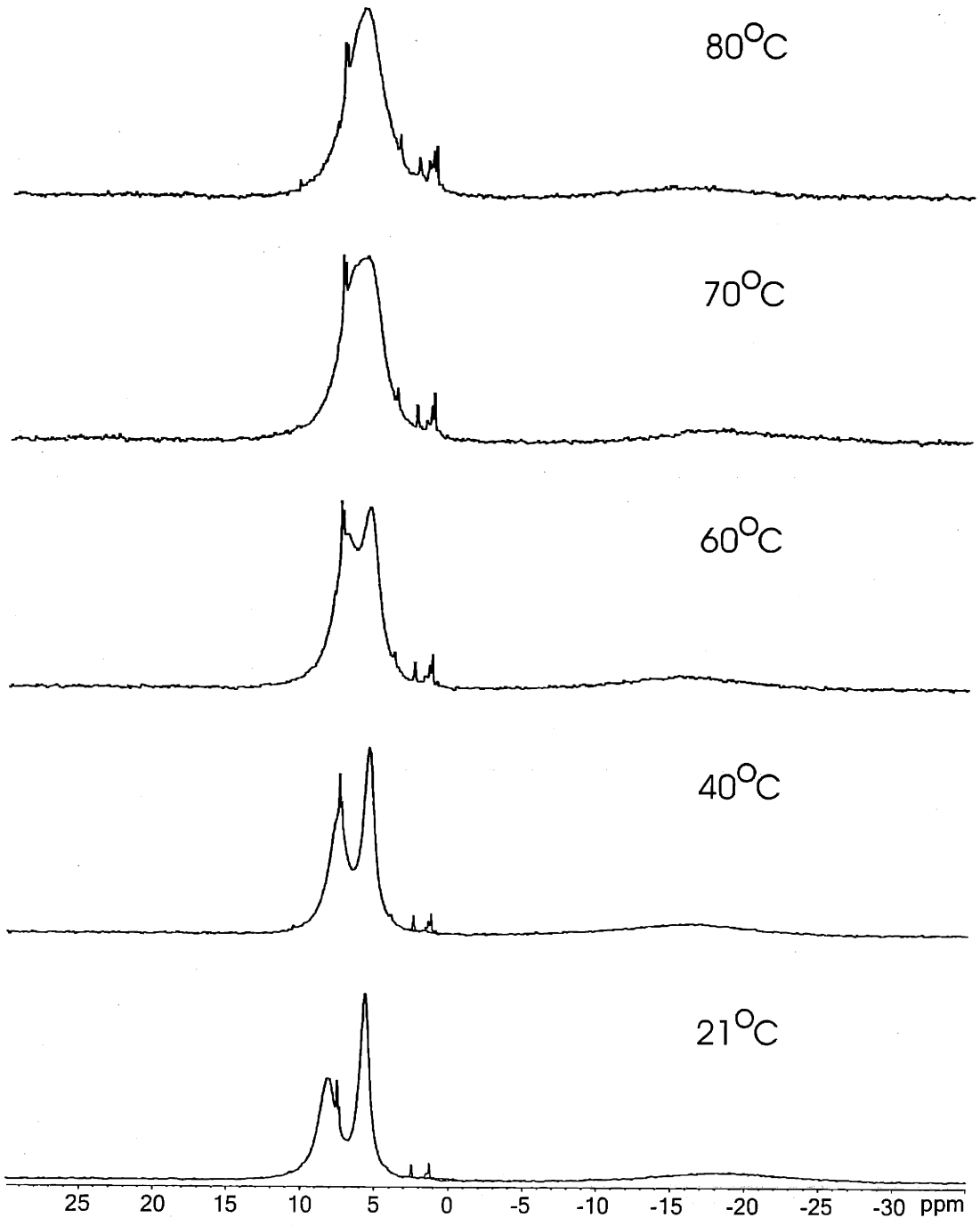

Figure 3: ^{2}H NMR spectra of **1**-d_{18} in toluene at different temperatures.

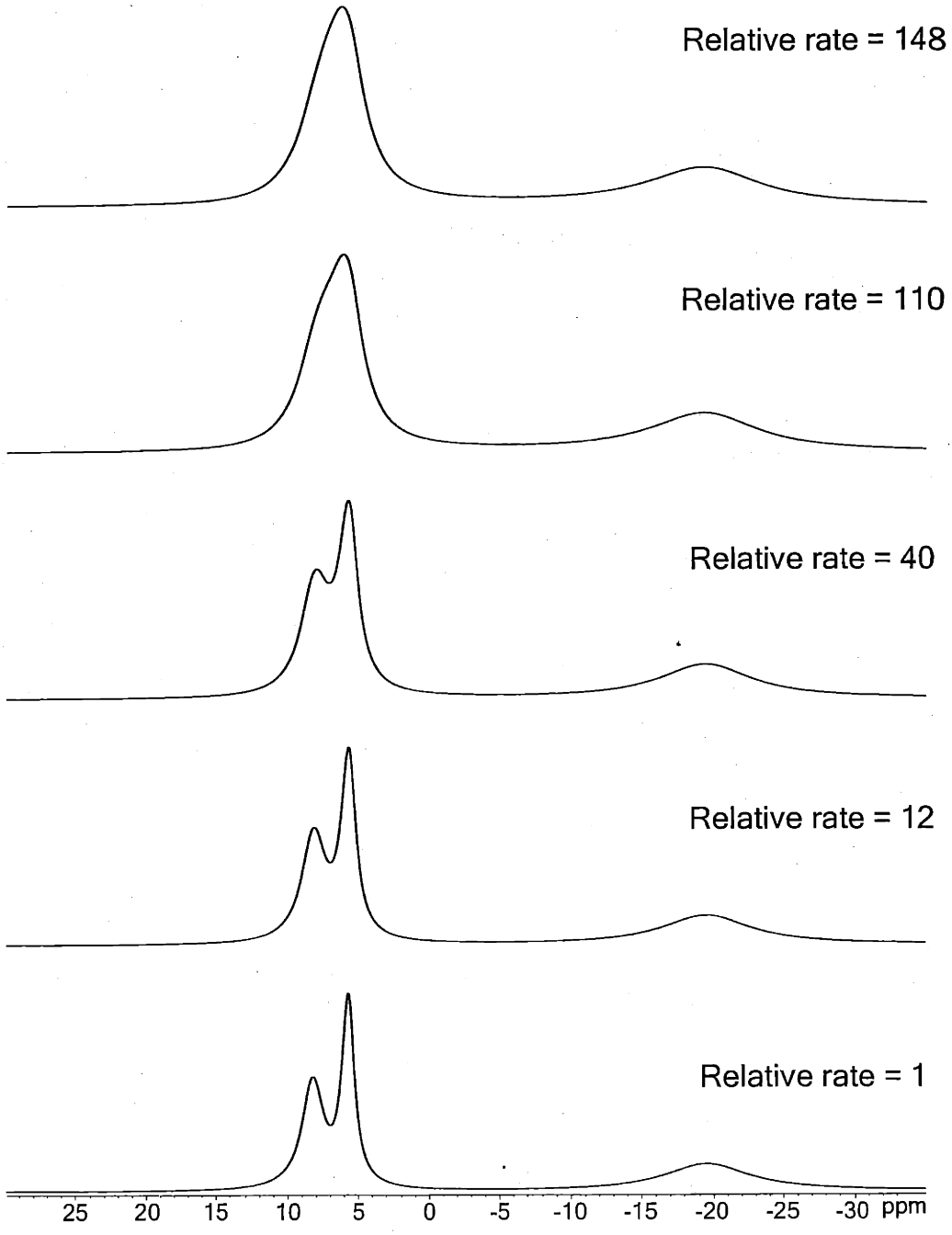

Figure 4: Simulated ^{2}H NMR spectra of **1**-d_{18} at different exchanging rates.

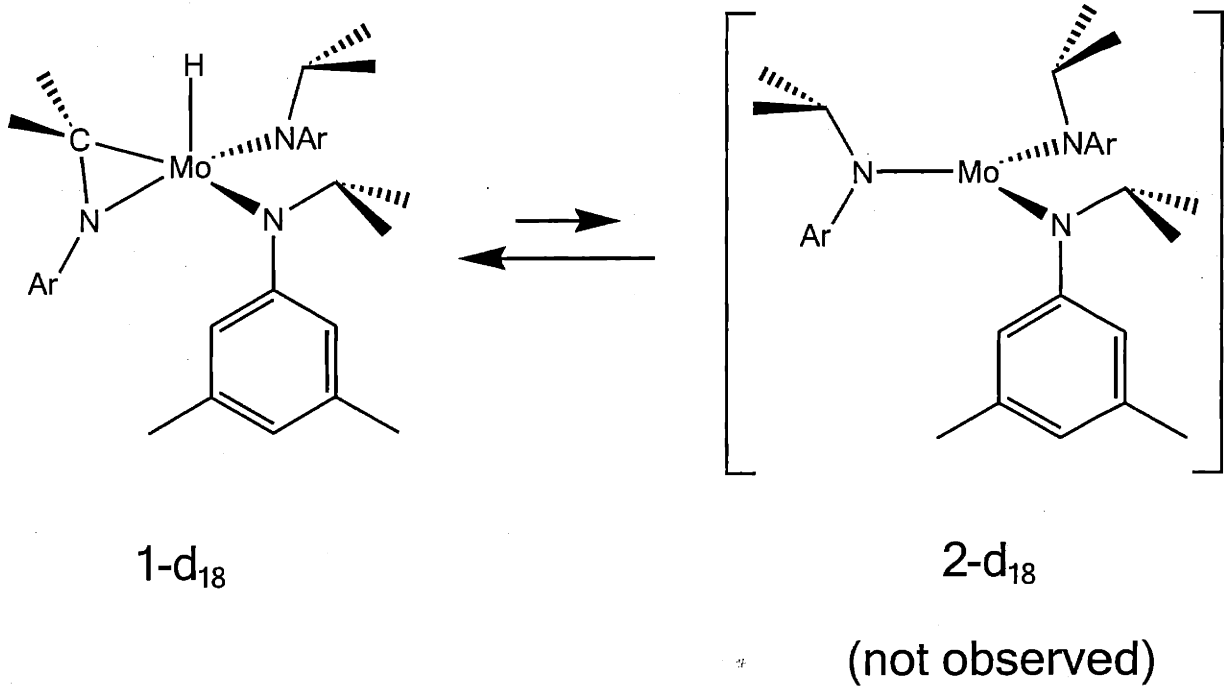

Scheme 1: Reversible β-H elimination.

2.3 Coupling of NCR

Addition of 1 equiv of NCR (R = Me, Et, ^{i}Pr, Ph, 4-methylphenyl, 4-fluorophenyl, 4-methoxyphenyl, 4-dimethylaminophenyl, perfluorophenyl) to a solution of **1** elicits a color change from orange-brown first to blue and then to green. On removal of solvent after stirring for 30 min, the nitrile coupling products [**2-NCR**]$_2$ were thereby obtained. By monitoring these reactions using ^{2}H NMR spectroscopy in conjuction with the use of **1-*d*$_{18}$**, three resonance signals were observed and monitored as a function of time. One of the signals is due to the diamagnetic nitrile-coupled dimer displaying steadily increasing intensity over the course of reaction, and the other two initially were unidentified and decreased over the time. On the other hand, the coupling reactions are fast when R =

4-fluorophenyl and perfluorophenyl, so no intermediates were observed. Presumably, **2-η^1-NCR**[25] is the intermediate that dimerizes over the time.

2.4 The reactions of NCR with 1-d_{18} or 3

Since two unidentified signals, which could be due to intermediates, **2-η^1-NCR** or **2-η^2-NCR** complexes, were detected during the NCR coupling reactions, it was surprised that insight could be gained into the mechanism of coupling and splitting of NCR by attempting to assign the two peaks. To prevent NCR from coupling, and to illustrate the nature of speculated intermediates **2-η^1-NCR** or **2-η^2-NCR**, bulky nitriles were employed as surrogate substrates.

Treatment of complex **1-d_{18}** wth 1 equiv of 2,4,6-trimethylbenzonitrile (NCMes) or trimethylacetonitrile (NC^{t}Bu) at room temperature resulted in the formation of an intense blue (NCMes) or purple (NC^{t}Bu) solution. When the nitrile is NCMes, ^{2}H NMR spectra of the reaction mixture revealed a new resonance at 3.21 ppm ($\Delta\nu_{1/2}$= 22.3 Hz) and residual **1-d_{18}** (4.08 ppm ($\Delta\nu_{1/2}$= 10.3 Hz for NC^{t}Bu). Complete disappearance of **1-d_{18}** was found to be effected upon addition of more than 2 equiv of NCMes or NC^{t}Bu. The solution reverted to **1-d_{18}** upon dilution, implying that the coordination of NCMes or NC^{t}Bu is reversible. Owing to the unstable nature of this blue compound in solution, excess NCMes was added to the solution in order to obtain a crystalline compound. The identity of the paramagnetic blue material was established by X-ray diffraction. The molecular structure of **2-(η^1-NCMes)$_2$** is shown in Figure 5, and selected bond distances and angles are given in the caption.

The geometry at molybdenum is essentially trigonal bipyramidal with the three amido ligands occupying equatorial positions and the two nitriles positioned axially. The N(4)-Mo-N(5) angle is 175.2 (2)°. The N(amido)-Mo-N(amido) angles all are close to 120° and the N(amido)-Mo-N(nitrile) angles are near 90°. The distances of Mo-N(4), 2.097(4) Å and Mo-N(5), 2.081(4) Å are longer than Mo-N(amido) distances (averaging 2.007(4) Å). The interatomic distances of N(4)-C(41) and N(5)-C(51) are 1.158(6) and 1.153(6) Å, which are very close for free NCR (1.150-1.160 Å).[36,37] The IR spectrum of solid **2-(η^1-NCMes)$_2$** in Nujol displays a stretch at 2218 cm^{-1} (The stretching frequency of the C≡N group for free a aromatic nitrile is in the range of 2240-2222 cm^{-1}).[38] These measurements suggest the interactions between Mo and the two NCMes ligands are simply σ-type. In other words, the two NCMes are σ-donor ligands. This weak interaction is consistent with instability of **2-(η^1-NCMes)$_2$**. SQuID magnetic susceptibility data for solid **2-(η^1-NCMes)$_2$** is $\mu_{\text{eff}} = 1.58\ \mu_B$, which is close to the spin-only value for a system containing one unpaired electron (1.73 μ_B). This result is reasonable since the lowest-lying orbitals of the trigonal bipyramidal **2-(η^1-NCMes)$_2$** should be a degenerate d_{xz} and d_{yz} pair of similar energy and the energy gap to the next higher energy orbitals with substantial d character should be large with respect to the electron-pairing energy. Therefore, three d electrons should occupy these two orbitals to give a low-spin species. Although no sign of **1-d_{18}** in the reaction of **1-d_{18}** with more than 2 equiv of NCMes or NC^{t}Bu, complex **2$_2$-μ-N** was formed after stirring these two reactions for overnight under a dinitrogen atmosphere. Since no alkylidyne complexes were detected, the formation of **2$_2$-μ-N** is attributed to the cleavage of dinitrogen by **1-d_{18}** under these conditions. Attempts to record EPR spectra on **2-(η^1-NCMes)$_2$** or **2-(η^1-NC^{t}Bu)$_2$** were unsuccessful. Only the signal of **1-d_{18}** was observed even though the amount of NCMes were up to 25 equiv, underscoring again the labile nature of the two nitrile ligands. Accordingly, the reaction between **2-(η^1-NCMes)$_2$** or **2-(η^1-**

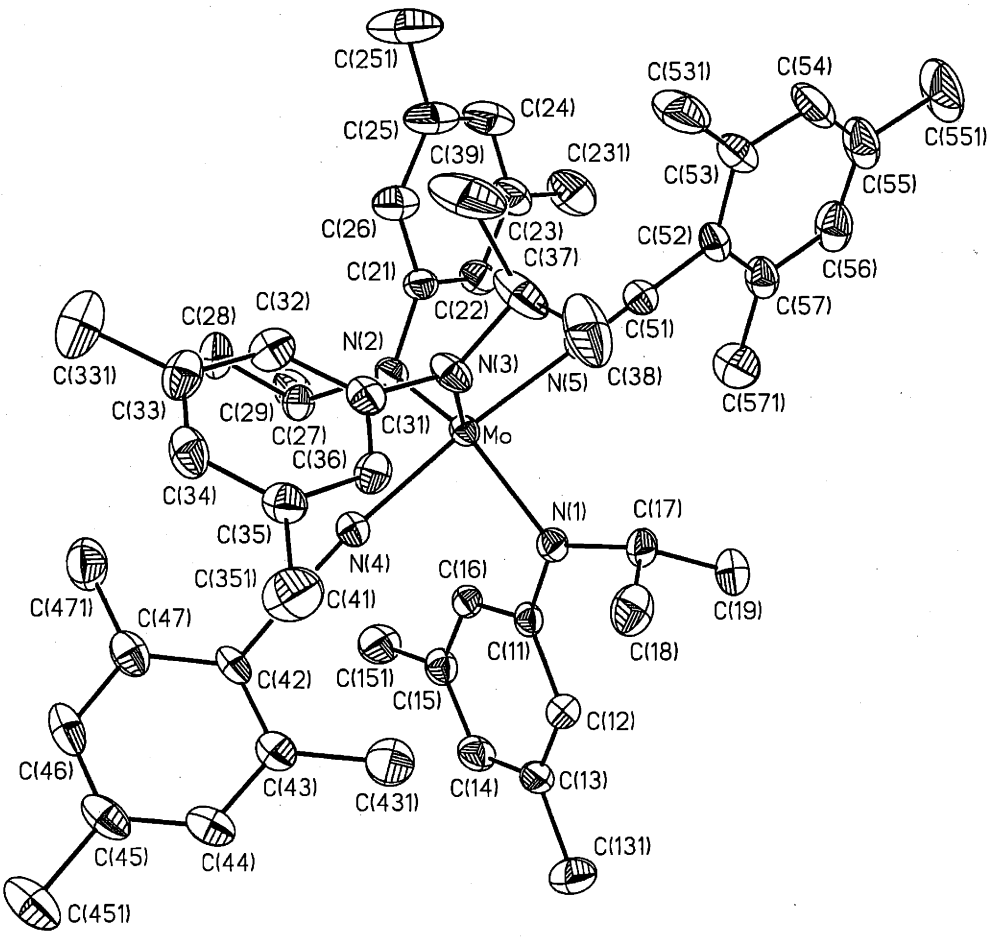

Figure 5: Thermal ellipsoid plot (35% probability) of **2-(η^1-NCMes)$_2$**. Selected distances (Å) and angles (°): Mo-N(1), 2.050(4); Mo-N(2), 1.992(4); Mo-N(3), 1.979(4); Mo-N(4), 2.097(4); Mo-N(5), 2.081(4); N(4)-C(41), 1.158(6); N(5)-C(51), 1.153(6); N(1)-Mo-N(2), 124.9(2); N(2)-Mo-N(3), 117.5(2); N(3)-Mo-N(1), 117.6(2); N(1)-Mo-N(4), 86.9(2); N(2)-Mo-N(4), 93.5(2); N(3)-Mo-N(4), 89.4(2); N(1)-Mo-N(5), 88.3(2); N(2)-Mo-N(5), 89.6(2); N(3)-Mo-N(5), 92.4(2).

NC^{t}Bu)$_2$ and 1 equiv of NCPh yielded irreversibly the coupling product [**2-NCPh**]$_2$ and 2 equiv of NCMes or NC^{t}Bu. On the other hand, owing to its steric bulk, the *tert*-butyl-substituted three-coordinate molybdenum complex **3**, does not exhibit any reaction toward 2-methylbenzonitrile, NCMes, or NC^{t}Bu.

Addition of 1 equiv of 9-anthracenecarbonitrile (NCAnth) in Et_2O to a solution of **1** yielded rapidly purple precipitate. ^{1}H NMR spectra in C_6D_6 display two different anilide ligand resonances in a 1:1 ratio, suggesting an asymmetric head-to-tail dimeric product [**2-NCAnth**]$_2$. A crystallographic study of this dimeric complex provided proof of this stuctural assignment. An ORTEP diagram of [**2-NCAnth**]$_2$ is depicted in Figure 6, and important bond distances and angles may be found in the caption. Unlike the symmetric coupling of other organonitriles (*vide supra*), in which the C-C bond forms between two carbons adjacent to nitrogen atoms, the bulk of anthracene prevents the coupling reaction from occurring at the β-carbon. Therefore, the formation of C(410)-C(8) irreversibly leads to the loss of aromaticity of one anthracene and the formation of an unusual diketimido ligand.[39,40] The geometry at molybdenum is best described as tetrahedral. The metrical parameters for the amido ligands in [**2-NCAnth**]$_2$ are all typical for complexes of this type.[10] However, the bond distances of Mo(1)-N(4) and Mo(2)-N(8), 1.917(5) and 1.835(5) Å, are significantly shorter than Mo-N(amido). Furthermore, the long C(4)-N(4) and C(8)-N(8) bonds, 1.213(7) and 1.291(7) Å, imply a case for strong back-bonding from molybdenum to empty N=C π^* orbitals.

Symmetrical NCR coupling can be avoided by varying the bulk of an NCR, and can also be prevented by including an electron-donating substituent. Addition of 1 equiv of $NCNMe_2$ in diethyl ether to **1-*d*$_{18}$** or **3** resulted in a color change from orange-brown or bright orange to olive or green solutions, respectively. ^{2}H NMR spectra displayed a new singlet resonance in

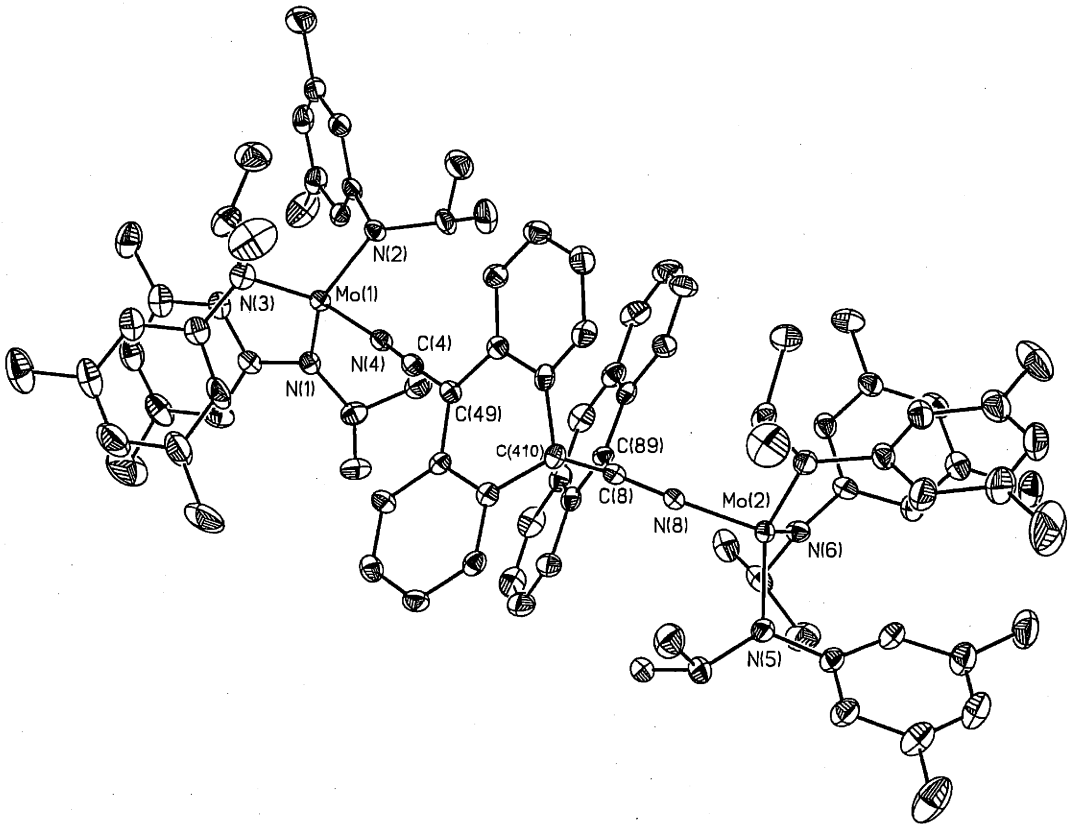

Figure 6: Thermal ellipsoid plot (35% probability) of [**2-NCAnth**]$_2$. Selected distances (Å) and angles (°): Mo(1)-N(1), 1.961(5); Mo(1)-N(2), 1.948(5); Mo(1)-N(3), 1.941(5); Mo(1)-N(4), 1.917(5); Mo(2)-N(5), 2.008(5); Mo(2)-N(6), 1.947(5); Mo(2)-N(7), 1.931(5); Mo(2)-N(8), 1.833(5); N(4)-C(4), 1.213(7); C(4)-C(49), 1.347(7); C(8)-N(8), 1.291(7); N(1)-Mo(1)-N(2), 111.6(2); N(2)-Mo(1)-N(3), 115.3(2); N(3)-Mo(1)-N(1), 118.7(2); N(4)-Mo(1)-N(1), 104.3(2); N(2)-Mo(1)-N(4), 97.1(2); N(3)-Mo(1)-N(4), 106.5(2); C(4)-N(4)-Mo(1), 168.4(5); N(4)-C(4)-C(49), 178.0(6).

both cases at 8.68 ($\Delta\nu_{1/2}$= 63.1 Hz) and 7.06 ($\Delta\nu_{1/2}$= 76.6 Hz) ppm whereas neither ^{1}H nor ^{2}H NMR spectra exhibited signs of the starting Mo complexes or formation of diamagnetic material. These observations suggest that either **2-** and **3-η^1-NCNMe$_2$** or **2-** and **3-η^2-NCNMe$_2$** were formed. An X-ray diffraction study was undertaken of compound that the new compounds **3-η^2-NCNMe$_2$**, which established the nitrile ligand to be side-bonded to the Mo (Figure 7). Relevant interatomic distances and angles may be found in the caption. The coordination environment about the molybdenum center is pseudo-tetrahedral, with the NCNMe$_2$ ligand occupying one coordination site and the C(3)-Mo-N(5) angle equal to 36.3 (2)°. The bond distances of Mo-C(3) and Mo-N(5) are 2.037(6), 2.030(5) Å. The C(3)-N(5) bond distance is 1.267(8) Å, which represents a lengthening of 0.117 Å relative to that of free nitriles. The C-N bond distance reported for the side-bonded nitrile complexes (Table 1) are in the range of 1.20-1.27 Å which compare to the C-N bond distance of **3-η^2-NCNMe$_2$** (1.267(8) Å). Furthermore, the angle N(5)-C(3)-N(4) of the coordinated nitrile of η^2-NCNMe$_2$ is reduced from 180°to 132.1(5)°, and falls in the range of the N-C-C angles (128-141°) reported for the complexes in Table 1. These metrical parameters are close to that expected for sp^2 hybridization at C atom. Consequently, coordination of the nitrile ligands in a side-bonded fashion in complexes in Table 1 lead to comparable lengthening in the C-N bond distances as well as very similar deformations in the C-C-N angles, suggesting a similar metal to coordinated nitrile bonding interaction which can best be described by η^2-coordination of the nitrile to generate a formal metalla-azacyclopropenyl. Like **2-η^2-PhCCPh** and **2-η^2-OCPh$_2$**, both of which have one unpaired electron,[10] solution magnetic susceptibility measurements of complexes **2-** and **3-η^2-NCNMe$_2$** using Evans method yielded magnetic moments 1.92 (**2-η^2-NCNMe$_2$**) and 1.83 (**3-η^2-NCNMe$_2$**) μ_B, typical of a system containing a single unpaired electron.

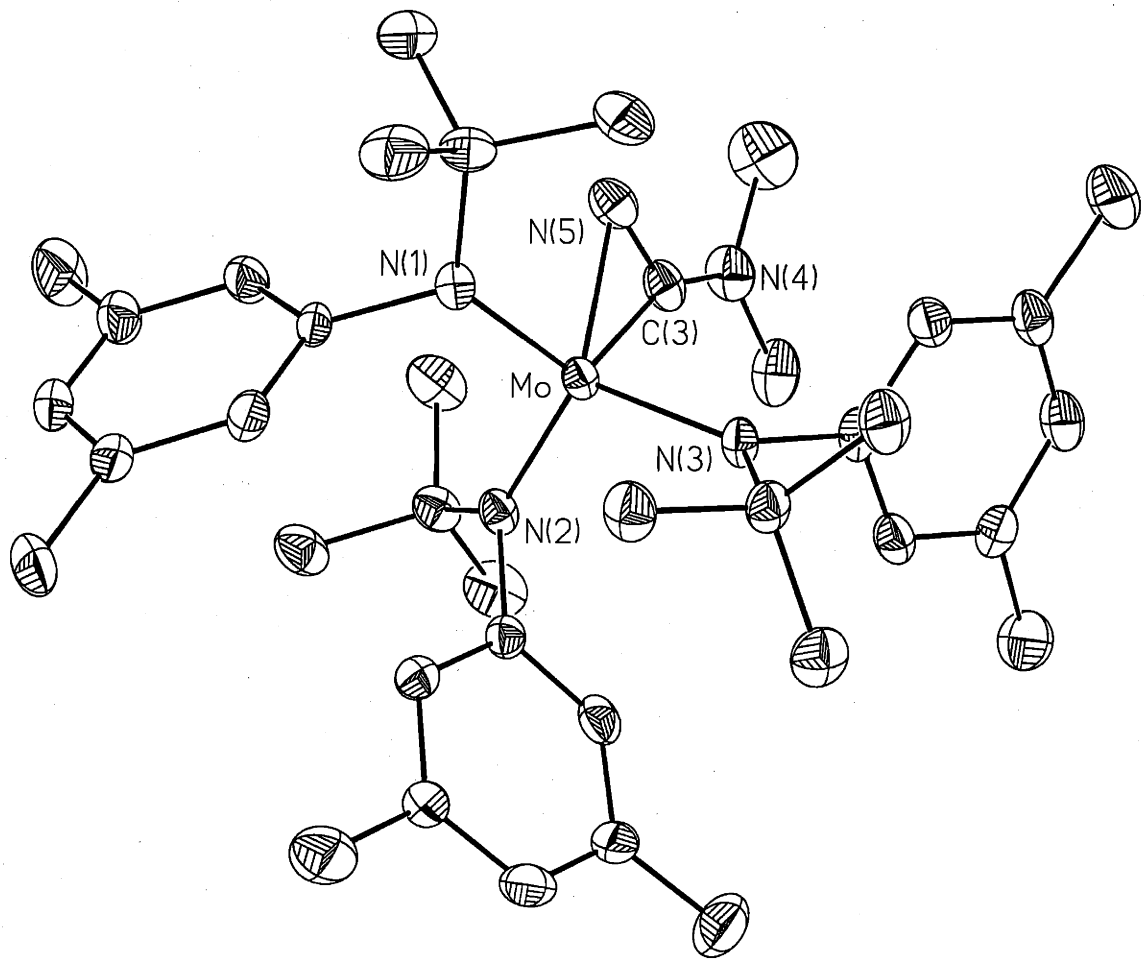

Figure 7: Thermal ellipsoid plot (35% probability) of **3**-η^2-**NCNMe$_2$**. Selected distances (Å) and angles (°): Mo-N(1), 2.035(4); Mo-N(2), 1.982(5); Mo-N(3), 1.967(4); Mo-N(5), 2.030(5); Mo-C(3), 2.037(6); C(3)-N(5), 1.267(8); N(4)-C(3), 1.346(8); N(1)-Mo-N(2), 114.0(2); N(2)-Mo-N(3), 111.8(2); N(3)-Mo-N(1), 109.6(2); N(1)-Mo-N(5), 86.3(2); N(2)-Mo-N(5), 122.3(2); N(3)-Mo-N(5), 110.1(2); N(1)-Mo-C(3), 122.3(2); N(2)-Mo-C(3), 98.9(2); N(3)-Mo-C(3), 99.1(2); N(5)-Mo-C(3), 36.3(2); Mo-N(5)-C(3), 72.1(4); Mo-C(3)-N(5), 71.5(3); N(5)-C(3)-N(4), 130.9(6); C(3)-N(4)-C(1), 120.1(6); C(3)-N(4)-C(2), 121.7(5); C(1)-N(4)-C(2), 118.0(6).

Complexes	M-C (Å)	M-N (Å)	C-N (Å)	C-C-N (°)
$MoCp_2(\eta^2\text{-NCMe})$[67]	2.124(8)	2.219(7)	1.200(10)	139.0 (7)
$[MoCl(\eta^2\text{-NCMe})(dmpe)_2][BPh_4]$[68]	1.981(7)	1.959(7)	1.217(8)	129.7(6)
$[WCl(bipy)(PMe_3)_3(\eta^2\text{-NCMe})][PF_6]$[69]	1.998(5)	2.008(4)	1.267(7)	129.6(5)
$WCl_2(PMe_3)_3(\eta^2\text{-NCMe})$[69,70]	1.98(1)	2.01(1)	1.27(1)	128(1)
$IrCp(PPh)_3(\eta^2\text{-NC-}(p\text{-}ClC_6H_4))$[71,72]	2.11(2)	2.17(2)	1.23(3)	138
$IrCp^*(CO)(\eta^2\text{-NC-}(p\text{-}ClC_6H_4))$[72]	2.040(8)	2.185(5)	1.209(11)	141
3-η^2-NCNMe$_2$ (this work)	2.037(6)	2.030(5)	1.267(8)	132.1(5) (N-C-N)

Table 1: Structural data of complexes with a M-η^2-NCR moiety.

2.5 ^{2}H NMR and EPR spectroscopy studies of the reactions of 1-d_{18} or 3 with NCPh

With the ^{2}H NMR spectra of **[2-NCPh]$_2$**, **2-(η^1-NCMes)$_2$**, **2-η^2-NCNMe$_2$**, and **3-η^2-NCNMe$_2$** (Figure 10) in hand, we can gain insight into the NCR coupling reactions mediated by **1-d_{18}** and **3**. Addition of 1 equiv of NCPh to **1-d_{18}** in Et_2O resulted rapidly in a color change from orange-brown to dark blue. The accompanying ^{2}H NMR spectrum (Figure 11, top) displays three peaks at 1.84 (**[2-NCPh]$_2$**), 4.77 ($\Delta\nu_{1/2}$= 10.2 Hz), and 8.52 ($\Delta\nu_{1/2}$= 38.8 Hz) ppm. After stirring for 1 h the peaks at 4.77 and 8.52 ppm disappeared while the peak at 1.84 ppm remained. When 2 equiv of NCPh was added to **1-d_{18}**, the intensity of the resonance signal at 4.77 ppm increased (Figure 11, bottom). In comparison with ^{2}H NMR spectroscopic data of complexes **2-(η^1-NCMes)$_2$** and **2-η^2-NCNMe$_2$**, assignments of the signals at 4.77 and 8.52 ppm were made as **2-(η^1-NCPh)$_2$** and **2-η^2-NCPh**, respectively. Contrary to the observations of reactions of **1-d_{18}** with NCPh, addition

of 1 or 2 equiv of NCPh to **3** resulted rapidly in a color change from orange to reddish-purple, showing only displayed two resonance signals at 2.38 ppm ([**3-NCPh**]$_2$) and 9.41 ppm in ^{2}H NMR spectra (Figure 12). The peak at 9.41 was assigned as **3-η^2-NCPh** in comparison with the chemical shift of **3-η^2-NCNMe$_2$**. The signal of complex **3-(η^1-NCPh)$_2$** could not be observed no matter the amount of NCPh, which is believed to be as a consequence of the steric bulk of (^{t}Bu groups.

With the EPR spectroscopic data of complexes **2-η^2-OCPh$_2$**, **2-η^2-NCNMe$_2$**, and **3-η^2-NCNMe$_2$** available, complex **2-η^2-NCPh** can be easily characterized in advance. All these four species each possesses an EPR active $S = 1/2$ ground state and therefore were subject to EPR spectroscopic investigations. Figure 13 displays the EPR spectra recorded in frozen solutions together with the simulations. Despite their chemical differences (^{i}Pr vs. ^{t}Bu anilide, η^2-OCPh$_2$ vs. η^2-NCNMe$_2$), their electronic structures reflected by the EPR spectra are remarkably similar. At 295 K in solution, both species each display an isotropic spectrum around $g_{iso} = 1.9475$ (**2-η^2-OCPh$_2$**) and 1.9396 (**3-η^2-NCNMe$_2$**), respectively. A six-line sub-spectrum is observed for the two counterparts due to coupling of the electron spin with the nuclear spin carrying $^{95/97}$Mo isotopes (I = 5/2, 25.5%). The isotropic hyperfine coupling constant $A_{iso}{}^{95/97}$Mo was determined to be 38.47 G (105 MHz) for **2-η^2-OCPh$_2$** and 37.00 G (101 MHz) for **3-η^2-NCNMe$_2$**. The complexes exhibit rhombic spectra in frozen toluene solution at 110 K (Figure 13). Simulation reveals very similar g- and A-tensors for both species (Table 2). The spectral appearance provides a fingerprint and might prove a useful tool in identifying similar species. It was expected that the reaction of **1** with NCPh to form the EPR-silent **2-(η^1-NCPh)$_2$** proceeds via an η^1-coordinated intermediate because of EPR spectroscopic property of complex **2-(η^1-NCMes)$_2$**. In order to establish this mechanism, freshly prepared solutions of **1** with an 1-fold excess of NCPh were investigated. Since

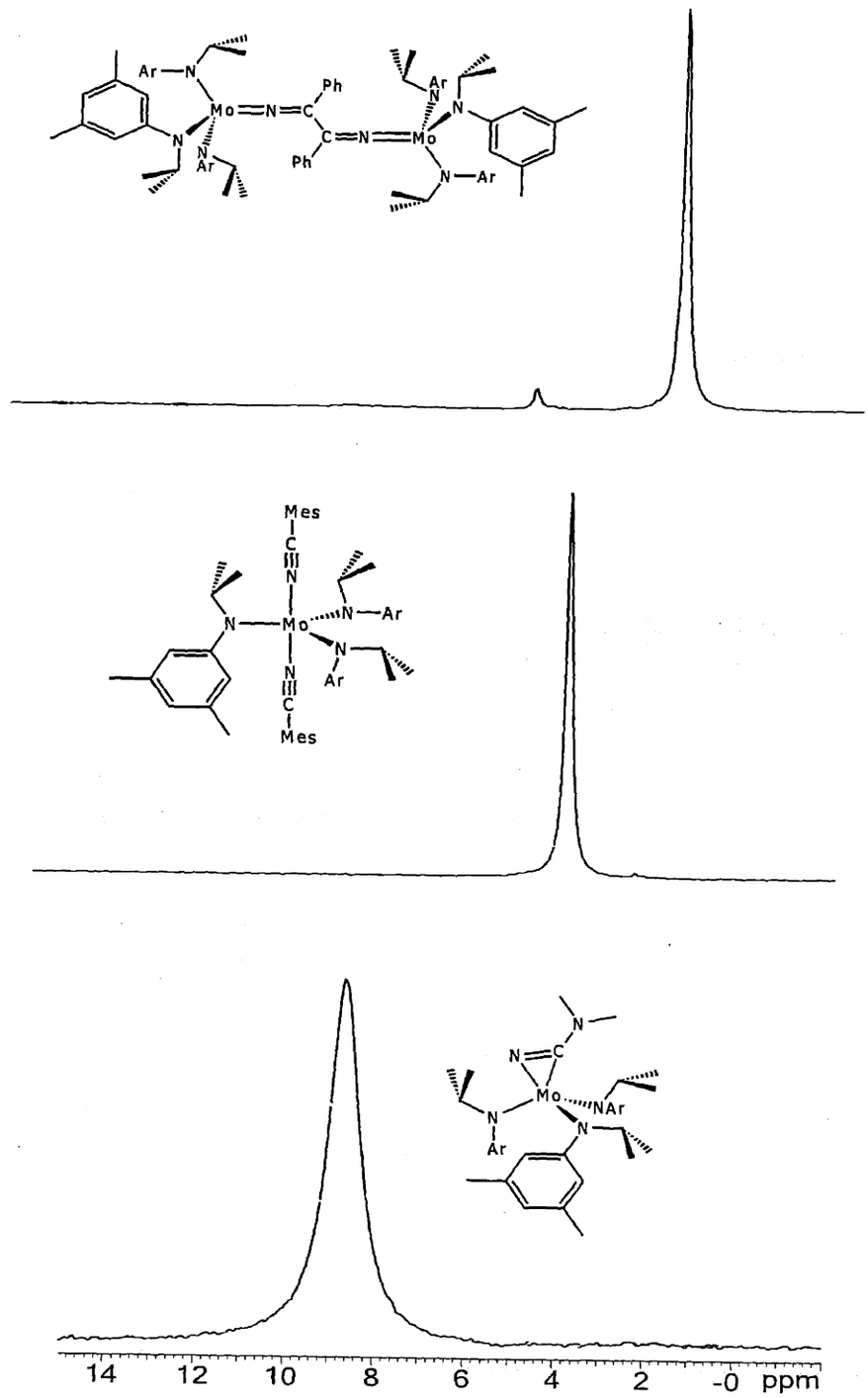

Figure 8: ^{2}H NMR spectra of [**2-NCPh**]$_2$, **2-**(η^1**-NCMes**)$_2$, and **2-**η^2**-NCNMe**$_2$ recorded in Et_2O.

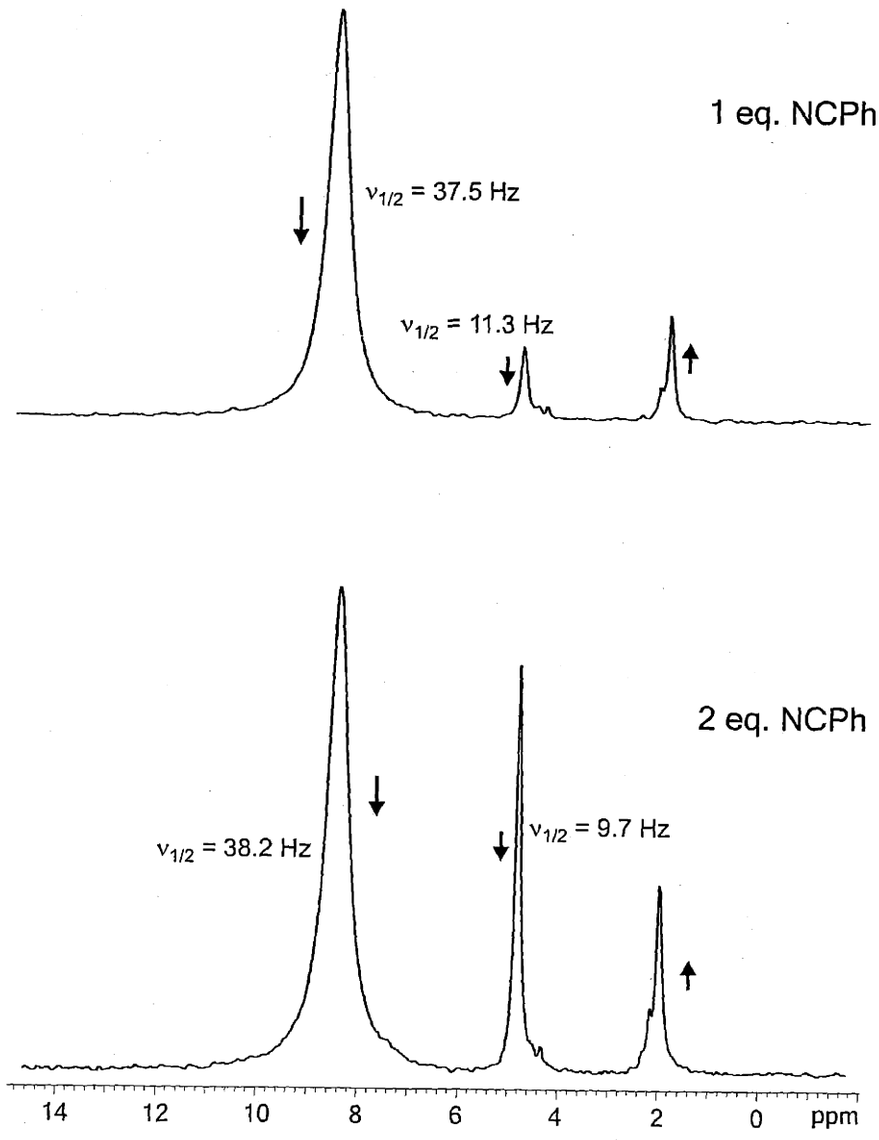

Figure 9: ^{2}H NMR spectra of mixtures of **1-d_{18}** with 1 and 2 equiv of NCPh recorded in Et_2O.

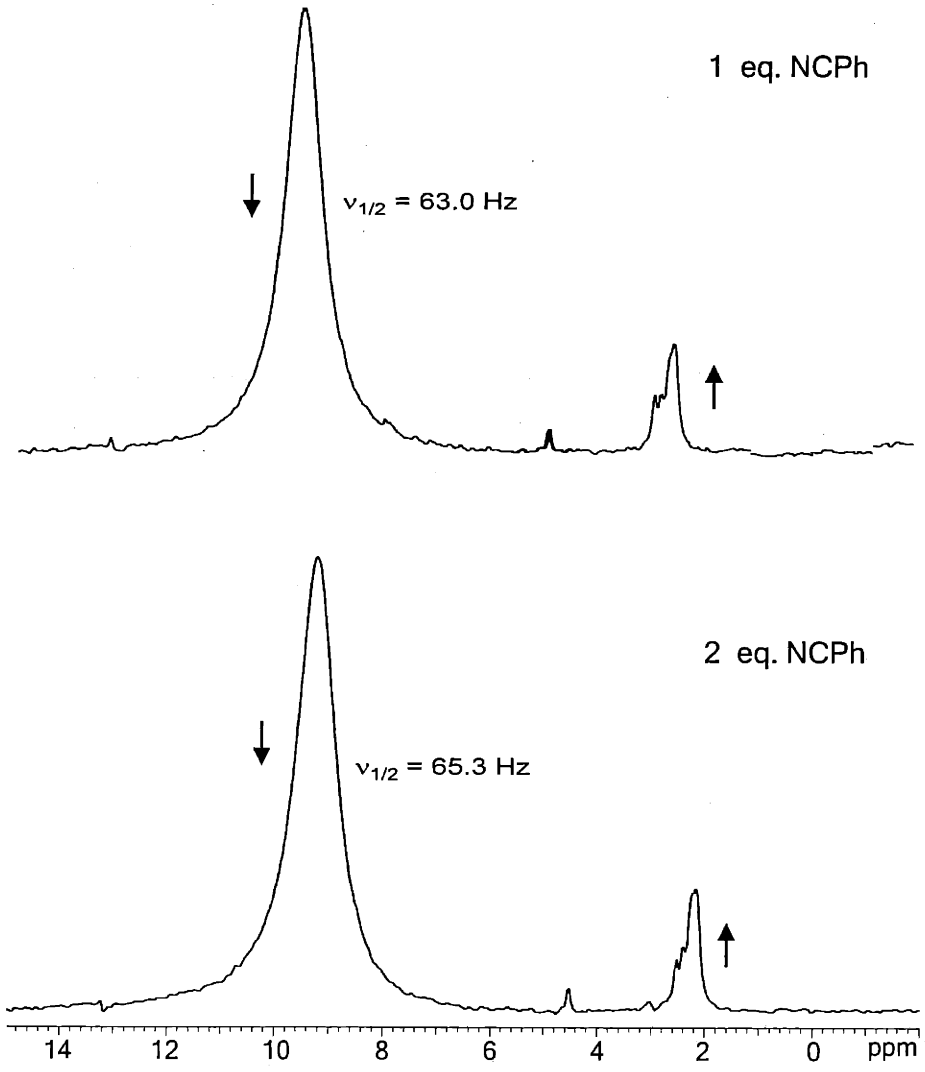

Figure 10: ^{2}H NMR spectra of mixtures of **3** with 1 and 2 equiv of NCPh recorded in Et_2O.

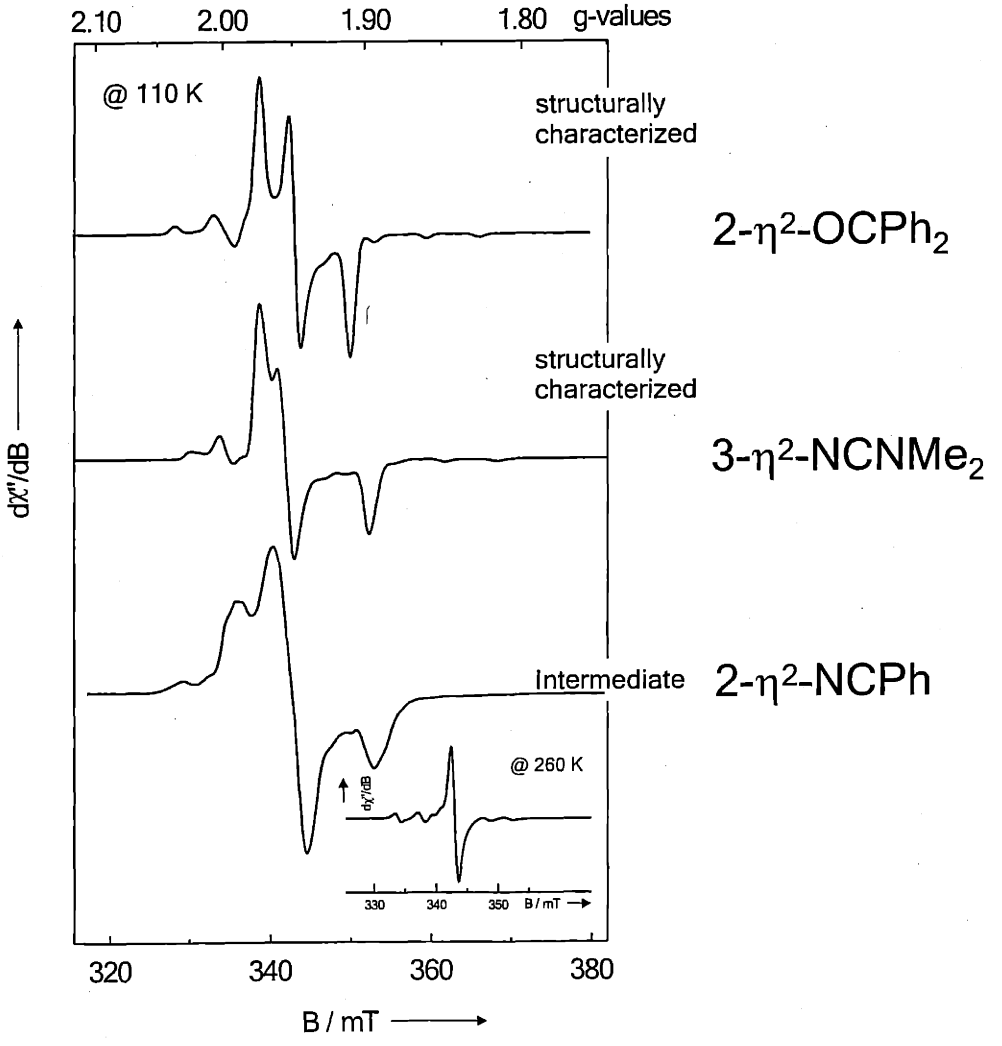

Figure 11: X-band EPR spectra of **2-η^2-OCPh$_2$** (top): microwave frequency ν = 9.351 GHz, power = 1 mW, modulation amplitude = 5 G, **3-η^2-NCNMe$_2$** (middle): microwave frequency ν = 9.707 GHz, power = 1 mW, modulation amplitude = 5 G, and **2-η^2-NCPh** (bottom): microwave frequency ν = 9.351 GHz, power = 1 mW, modulation amplitude = 5 G. All spectra were recorded in frozen toluene solution at T = 110 K. The inset shows the isotropic spectrum of **2-η^2-NCPh** in liquid solution at T = 260 K. Experimental conditions: microwave frequency ν = 9.351 GHz, power = 1 mW, modulation amplitude = 5 G.

Parameters	**2-η^2-OCPh$_2$**	**3-η^2-NCNMe$_2$**	**2-η^2-NCPh**
g_{iso}	1.9475	1.9396	1.9564
g_1	1.9790	1.9720	1.9770
g_2	1.9540	1.9541	1.9540
g_3	1.9165	1.8961	1.9048
g_{av}	1.9500	1.9410	1.9453
A_{iso}*/G (MHz)	38.47 (105)	37.00 (101)	
A_1/G (MHz)	39.02 (106.5)	34.07 (93.0)	
A_2/G (MHz)	25.79 (70.4)	27.84 (76.0)	
A_3/G (MHz)	59.17 (161.5)	56.61 (154.5)	
A_{av}/G (MHz)	41.30 (112.8)	39.47 (107.8)	

Table 2: Summary of EPR spectroscopic parameters of complexes **2-η^2-OCPh$_2$**, **3-η^2-NCNMe$_2$**, and **2-η^2-NCPh**.

(*): $^{95/97}$Mo, 25.5%

the EPR spectra of pure **1** in solution exhibit extremely small line widths (*vide supra*) compared to those of **2**-η^2-**OCPh**$_2$ and **3**-η^2-**NCNMe**$_2$, traces of unreacted **1** can be identified unambiguously. However, spectra of the mixture of **1** and excess NCPh showed a new isotropic signal at g_{iso} = 1.9564 ($A_{iso}{}^{95/97}$Mo = 27.9 G (77.5 MHz)) and unreacted **1** was not observed. This spectrum possesses a remarkable similarity to that of **2**-η^2-**OCPh**$_2$ and **3**-η^2-**NCNMe**$_2$ in toluene solution at 260 K. Even more indicative for the formation of an η^2-coordinated intermediate is the frozen solution spectrum. The spectrum recorded in toluene at 110 K displayed a rhombic signal with resonances g_1 = 1.9770, g_2 = 1.9540, and g_3 = 1.9048, which also resembles those of **2**-η^2-**OCPh**$_2$ and **3**-η^2-**NCNMe**$_2$.

2.6 Splitting of NCPh

Like the unobserved intermediate **3-N**$_2$ in the dinitrogen cleavage reaction by **3**,[4] the intermediates **2**-η^1-**NCR** in the reactions of **1** and NCR have not been experimentally detected either. In order to capture the invisible intermediate **2**-η^1-**NCPh** to form **2**$_2$-μ, η^1, η^1-**NCPh**, which is similar to the purple intermediate **3-N**$_2$, half equiv of NCPh was added to a diethyl ether solution of **1** and the reaction was stirred for 12 h. The analysis of the reaction mixture by ^{1}H and ^{13}C NMR spectroscopy revealed the formation of [**2-NCPh**]$_2$, **2**$_2$-μ-**N**, and **2-CPh** (^{13}C NMR spectrum shows a resonance for the α-C at 294.9 ppm), instead of the desired compound **2**$_2$-μ, η^1, η^1-**NCPh**. Since the coupling reaction of NCPh was not fast, the formation of [**2-NCPh**]$_2$ was depressed and the yields of compounds **2**$_2$-μ-**N** and **2-CPh** increased by solwoly adding one third equiv of NCPh in diethyl ether to **1**. ^{1}H NMR spectra revealed the crude mixture contained **2**$_2$-μ-**N**, **2-CPh**, and only small amount of [**2-NCPh**]$_2$ indeed.

2.7 Redox of [2-NCPh]$_2$

The ultimate goal of investigating NCR coupling was to split an N≡C bond and make an alkyne and complex **2-N** based on the following known results. First of all, acetonitrile can be reductively coupled in two-electron manner mediated by d^2 transition metal complexes.[23–27] Secondly, complex **1** can behave as a 3-electron reductant and it has been proved based on the dinitrogen and NCPh cleavage reactions. However, this did not turn out to be the case. The NCR coupling reactions mediated by **1** and **3** is a 1-electron (per Mo) redox reaction, and the product [**2-NCPh**]$_2$ is thermally and photochemically stable. On the other hand, it was found that the Mo(V) complex **3-NMes** decomposed to a nitrido Mo(VI) complex **3-N**.[4] Therefore, upon removal of 2 electron from [**2-NCPh**]$_2$ to give dicationic salt [**2-NCPh**]$_2^{2+}$ might result in a complete cleavage of NCPh and formation of **2-N** and PhCCPh. Virtually all [**2-NCR**]$_2$ where R = Me, Et, ^{i}Pr, Ph, and 4-methylphenyl exhibit rich electrochemical activity. As shown in Figure 8, [**2-NCPh**]$_2$ undergoes two successive reversible 1-electron oxidation to yield the mono- ($E_{1/2} = -1.109$ V vs Fc/Fc^+) and finally the dication ($E_{1/2} = -0.612$ V vs Fc/Fc^+). Electrochemical reversibility was demonstrated by the peak-to-peak separation between the resolved reduction and oxidation wave maxima (75 mV). It has been reported that the magnitude of the peak-to-peak separation ($\Delta E_{1/2}$) gives an indication of the interaction between two metal sites.[41–44] The Mo-Mo interaction increases as the value of $\Delta E_{1/2}$ increases.

$$[\text{IV IV}] + [\text{V V}] \rightleftharpoons 2\,[\text{IV V}] \qquad (1)$$

In eq 1, the abbreviations [IV IV], [IV V], and [V V] denote [**2-NCPh**]$_2$, [**2-NCPh**]$_2^+$, and [**2-NCPh**]$_2^{2+}$, respectively. From the value of $\Delta E_{1/2}$, the conproportionation equilibrium constants

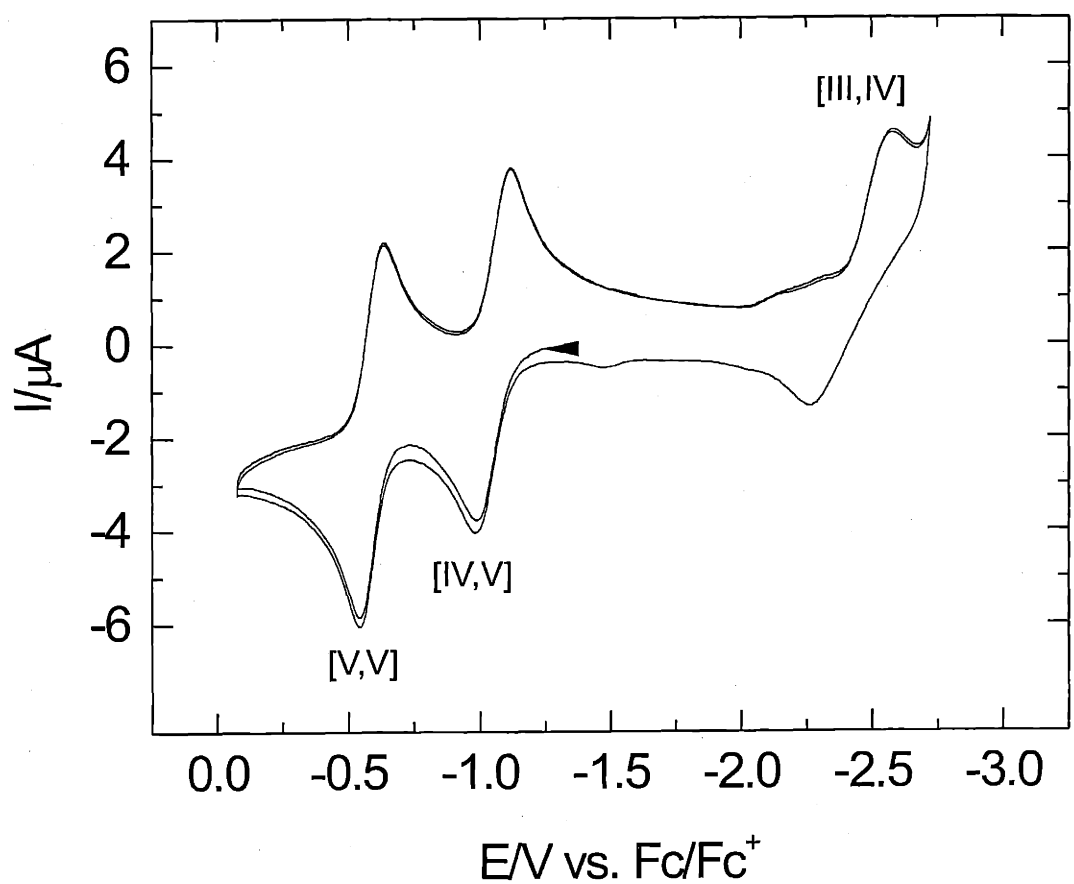

Figure 12: Cyclic voltammogram of [**2-NCPh**]$_2$ recorded in THF solution containing 0.50 M TBAP. Scan rate is 0.10 V s^{-1}.

K (2.6×10^8) can be calculated. The monoxidized salt was isolated by oxidizing [**2-NCPh**]$_2$ with mild oxidants such as I_2 and $[(C_5H_5)_2Fe][CF_3SO_3]$ to give [**2-NCPh**]$_2[I_3]$ and [**2-NCPh**]$_2[CF_3SO_3]$. Complex [**2-NCPh**]$_2[I_3]$ is EPR silent and has been determined to have 3 unpaired electrons (μ_{eff} = 3.74 μ_B) by Evans method. In Figure 9, the crystal structure of [**2-NCPh**]$_2[I_3]$ indicates that the geometry about each Mo is tetrahedral with a linear Mo(1)-N(4)-C(4) (175.6(5)°) and a shorter Mo(1)-N(4) distance of 1.740(5) Å than that in the corresponding neutral complex,[10] indicating strong π donation from N(4) to Mo(1). All Mo(1), N(4), C(4), C(4A), N(4A), and Mo(1A) are coplanar, and the dihedral angle N(4)-C(4)-C(4A)-N(4A) is nearly 180°. The triodide anion shows a symmetric linear structure. The I(1)-I(2) and I(2)-I(3) bond distances are 2.938(1) and 2.896(1) Å, which are in accord with the accepted value of 2.92 Å reported for the free triodide ion.[45] The angle I(1)-I(2)-I(3) is 177.22(3)°. Unfortunately, the dicationic complex [V V] can only be observed in solution but could not be isolated.

3 Discussion

Reversible β-hydrogen elimination for complexes of organoamide ligands is a rarely documented phenomenon.[46–52] Although **1** has been structurally characterized, its electronic structure was not fully understood. Owing to its paramagnetism, **1** has been subject to an EPR spectroscopic study, which provides us a good method of examining the nature of the SOMO of **1**. From experimental and simulated EPR spectroscopic data, it is believed that the unpaired electron is delocalized on molybdenum, the hydride ligand, and the three nitrogen atoms. In other words, the SOMO of **1** is a linear combination of all five atomic orbitals. Initially it was postulated that the cyclometallated

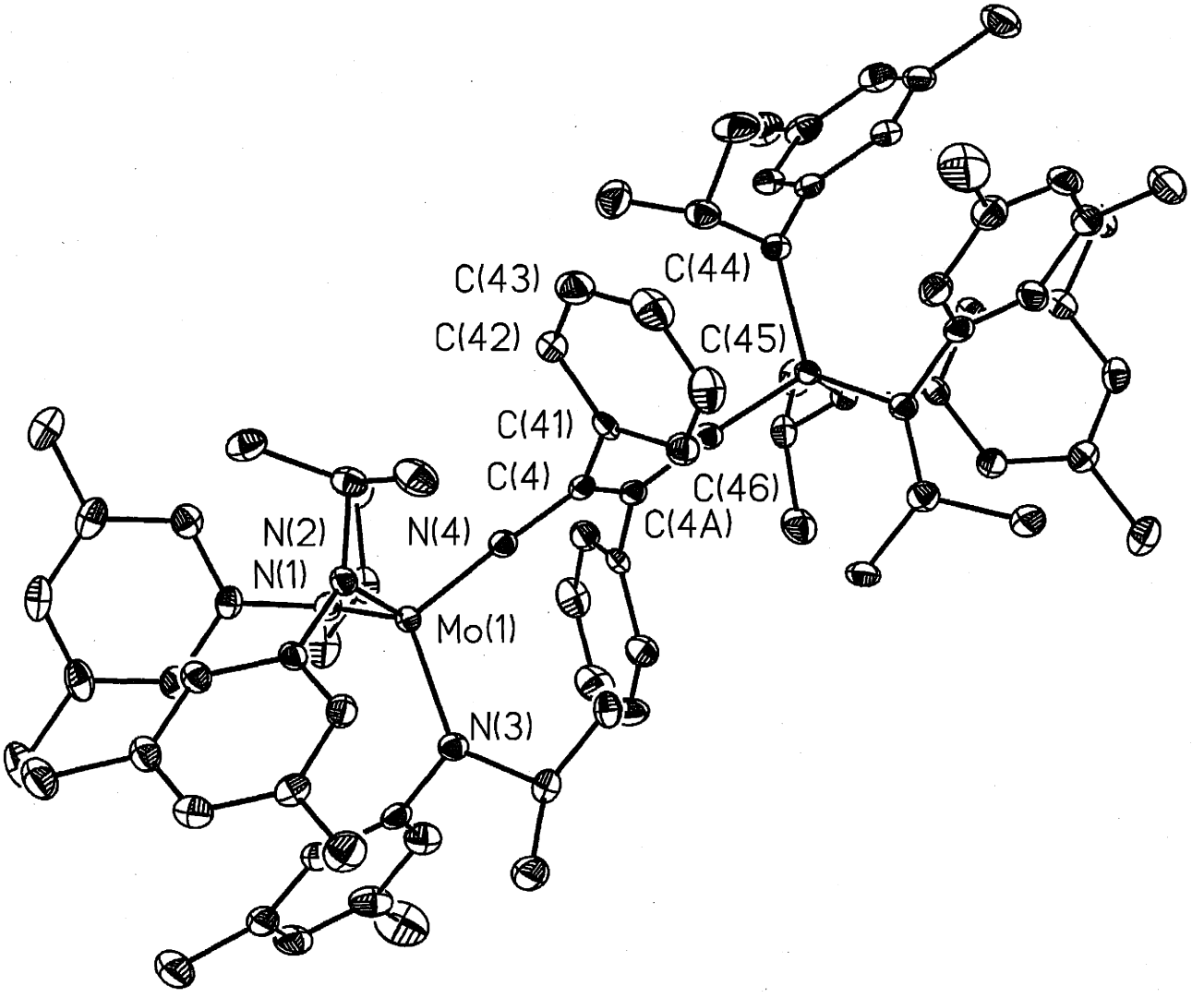

Figure 13: Thermal ellipsoid plot (35% probability) of [**2-NCPh**]$_2$[I_3]. Selected distances (Å) and angles (°): Mo(1)-N(1), 1.921(5); Mo(1)-N(2), 1.918(5); Mo(1)-N(3), 1.929(5); Mo(1)-N(4), 1.740(5); N(4)-C(4), 1.393(8); C(4)-C(4)*, 1.368(12); I(1)-I(2), 2.938(1); I(2)-I(3), 2.896(1); N(1)-Mo(1)-N(2), 110.7(2); N(2)-Mo(1)-N(3), 110.2(2); N(3)-Mo(1)-N(1), 111.3(2); N(4)-Mo(1)-N(1), 107.5(2); N(4)-Mo(1)-N(2), 107.4(2); N(3)-Mo-N(4), 109.6(2); C(4)-N(4)-Mo(1), 175.6(5); N(4)-C(4)-C(4)*, 120.6(7); I(3)-I(2)-I(1), 177.22(3).

nature of **1** would inhibit the type of reaction chemistry observed for related three-coordinate derivatives such as **3**. This proved not to be the case due to the reversibility of the β-hydrogen elimination. From a structural perspective, a striking feature is the parallel alignment of the imine ligand to the Mo-H vector. This orientation has been found in several octahedral *cis*-alkene hydride complexes of d^6-transition-metals including Re(I),[53] Os(II)[52,54,55] and Ir(III).[56] This preference has been explained on theoretical grounds to be the result of an interaction between the high-energy σ-(M-H) orbital and the π^* orbital of the olefin and iminium.[52,54,55] Therefore, the π^* orbital of the imine system can be expected to have a larger coefficient on the carbon than nitrogen and the orientation maximizing the overlap of this orbital with the (Mo-H) σ orbital places the imine carbon directly over the hydride. The representative molecular orbitals of these interactions are shown in Figure 14.

Although NCR coupling reaction mediated by transition-metals has been known for some time, most studies were performed with acetonitrile, which is a substrate and solvent, owing to the low solubility of the starting transition-metal complexes. Consequently, the mechanism of NCMe coupling reactions[23–27] has not been well studied. The most commonly accepted mechanism for NCMe coupling reactions was postulated to occur through a radical process in which the complexes $ML_n(\eta^1\text{-}NCCH_3)$ was believed to be the key intermediate. In this work, we obtained evidence to support this hypothesis. The reactions of **1** with the flourinated NCPh (4-fluorobenzonitrile and perfluorobenzonitrile) quickly form the coupling dimers. The presence of the electron-withdrawing fluorine atoms on NCPh reduce the energy for forming intermediates **1-η^1-NCR**. The asymmetric coupling of 9-anthracenecarbonitrile by **1** also supports the radical mechanism. In contrast to the two-electron reductive coupling of NCR occuring towards Ti(II),[27] Nb(III)[24,26] and Ta(III),[23,25]

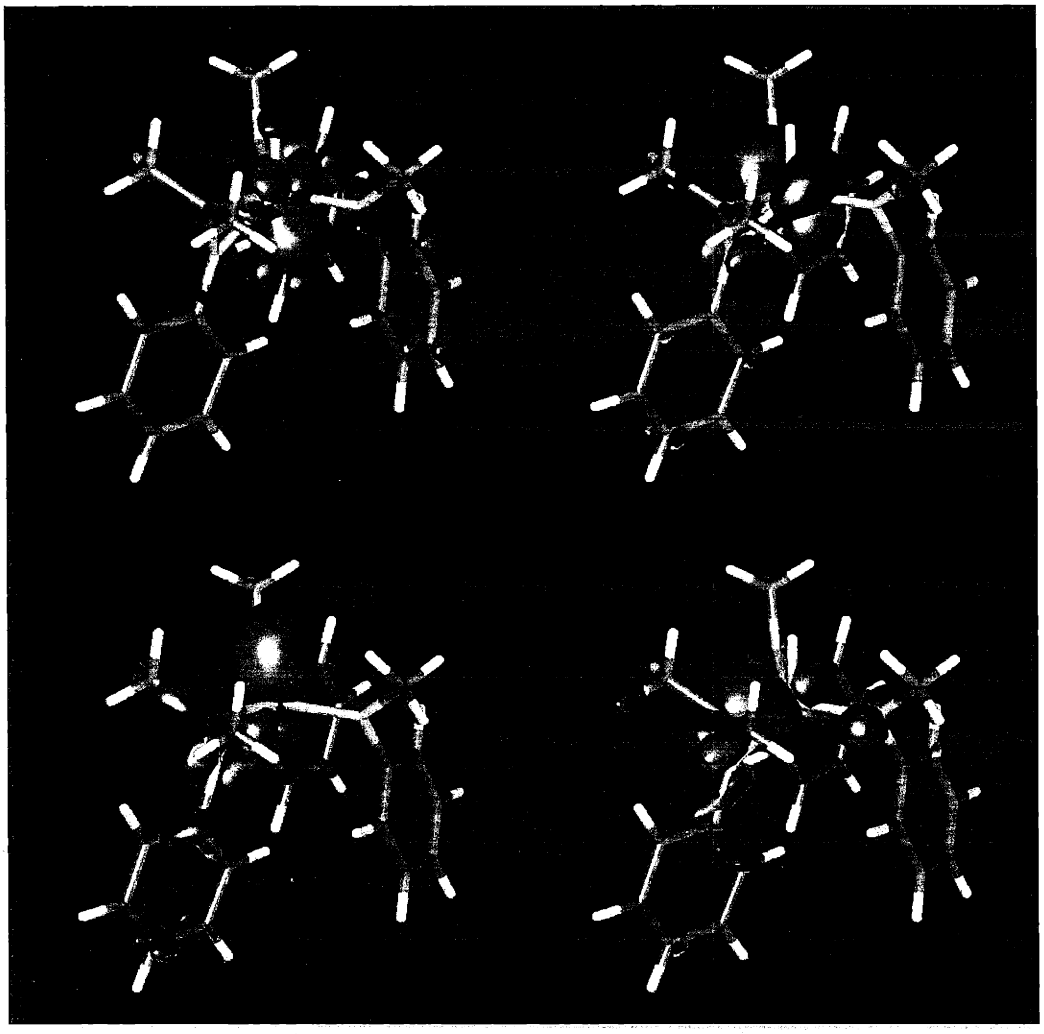

Figure 14: Pictured are molecular orbitals 116, 115, 112, and 106, clockwise from upper left. These correspond to the LUMO, SOMO, Mo-imine backbonding, and hydridic orbitals, respectively, of the model system $Mo(H)(Me_2CNPh)(NMePh)_2$ derived from X-ray and neutron diffraction studies of complex **1**. The calculation employed C_1 symmetry for the model system in agreement with the solid state structure determinations. EPR hyperfine couplings from the calculation are as follows: $A_{iso}(Mo) = 52$ MHz, $A_{iso}(H) = 49$ MHz, $A_{iso}(N_{imine}) = 3.9$ MHz, $A_{iso}(N_{amide}) = 7.2$ and 6.5 MHz. All of the foregoing are in good agreement with values determined experimentally with the exception of $A_{iso}(H)$; the origin of the latter discrepancy is not clear.

the mixing of **1** and an NCR in a 1:1 ratio results in one-electron nitrile coupling. Although these coupling dimers can be oxidized by one and two electrons on the electrochemical time scale, and the monocationic complexes can be isolated and structurally characterized, the dicationic complexes have not been obtained. It is believed that dicationic compounds [Mo(V), Mo(V)]$^{2+}$ are relatively unstable. The high spin nature of the monocationic salt [Mo(IV), Mo(V)]$^{1+}$ is due to its small HOMO-LUMO gap. It implies that upon oxidation, the stability of these dimers decrease. Although the postulate η^1-nitrile complex **2-η^1-NCPh** has not been observed, it is believed that **2-η^1-NCPh** is a very reactive species, because the energy of d_{z^2} orbital in **2-η^1-NCPh** is raised above that of d_{xz} and d_{yz} orbitals as a consequence of the binding of the nitrile donor to one of the apical sites. Consequently, **2-η^1-NCPh** could be a low-spin species and its high reactivity in part as a consequence of its low-spin configuration. Therefore, it can bind one more equiv NCPh to give **2-(η^1-NCPh)$_2$** readily. This might account for the observations that $[N_3N_F]Re$[57] ($[N_3N_F]^{3-}$ = $[(C_6F_5NCH_2CH_2)_3N]^{3-}$), $[N_3N]Mo$ ($[N_3N]$ = $[(Me_3SiNCH_2CH_2)_3N]$),[58] $Re(S\text{-}2,4,6\text{-}C_6H_2{}^iPr_3)_3(PPh_3)$,[59] and $[P_3P]Ru$ (P_3P = $(Ph_2PCH_2CH_2)_3P$)[60] have been proven to bind dinitrogen readily. The mechanism of NCR coupling reactions exemplified by NCPh and **1** is proposed in Scheme 2.

The single-crystal X-ray crystallographic studies reveal that the conformation in **2-(η^1-NCMes)$_2$** is essentially a "two-up, one-down" arrangement of the three equatorial amido ligand substituents. The preference for this orientation of three amido ligands parallel to the two axial nitrile ligands is interpreted to maximize the in-plane N to Mo π bonding.[2] This observation is also in agreement with the known structure of $[M(SAr)_3(CO)_2]^-$ (M = Mo, W), $[Mo(SAr)_3(CO)(\eta^1\text{-NCR})]^-$,[61,62] and $Re(SR)_3(\eta^1\text{-NCMe})_2$.[63] Investigation of **3** by molecular mechanics has also suggested this

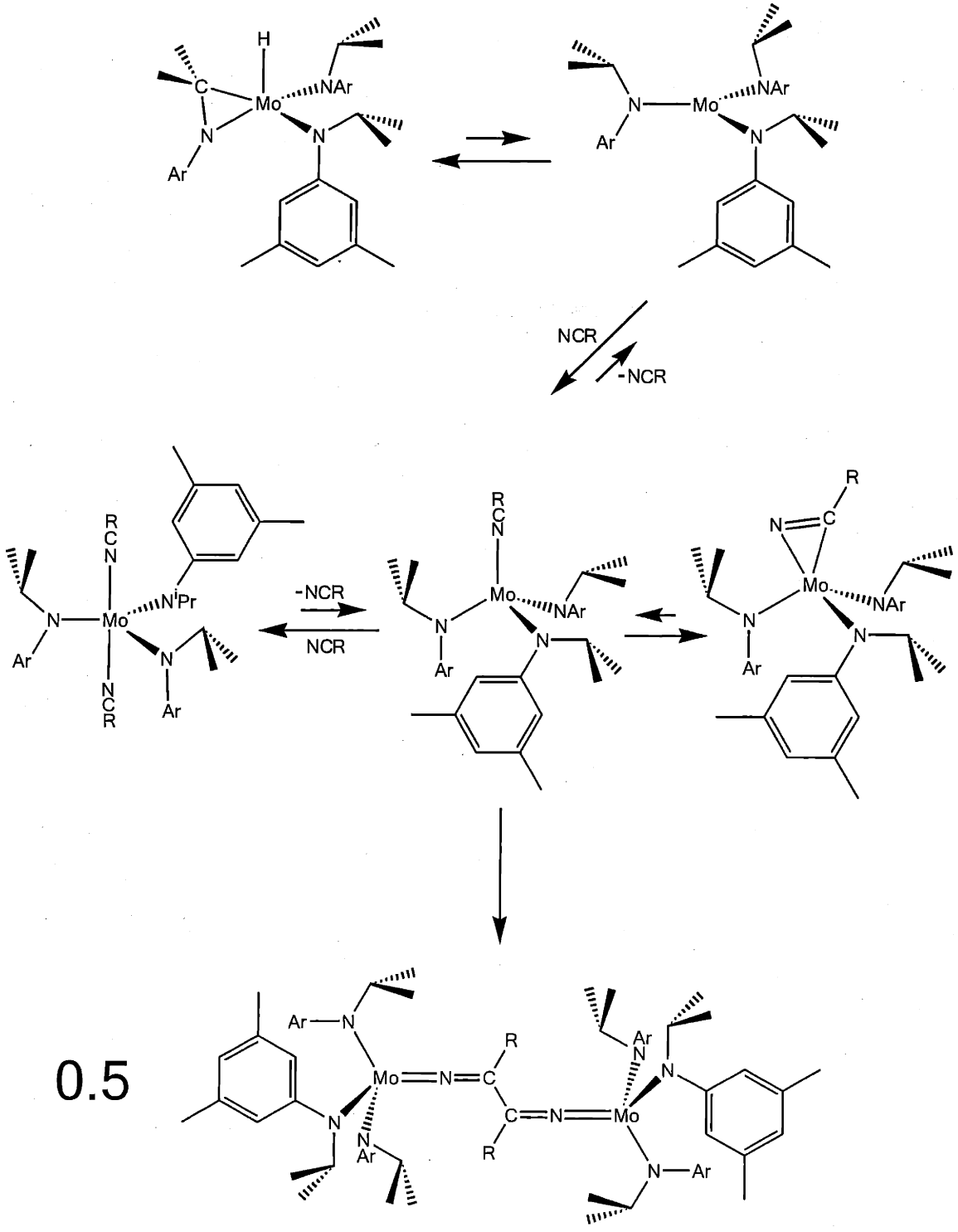

Scheme 2: Proposed mechanism for the coupling of NCR by **1**.

structure.[64] The asymmetric disposition of the three amido ligands observed here also provides a mechanism for reduction of steric crowding. The distance of Mo-N(5) 2.081(4) Å is a bit shorter than Mo-N(4) 2.097(4) Å due to the greater steric crowding about the latter.

Attempts to isolate **2-η^2-NCPh** complexes have been unsuccessful. Organonitriles NCR have $\pi_{||}$ and $\pi_{\perp}$ (orthogonal to MCN plane) orbitals which are lower in energy than alkynes, and this feature would decrease the stability of an η^2-nitrile complex relative to its carbon analogs, particularly for the case of electron-deficient metals. On the other hand, electron-rich metal systems can be stabilized through the relatively low-energy $\pi_{||}^*$ orbitals of the nitrile, which can interact more favorably with metal d_π electrons. In contrast to NCR, cyanamides are more electron rich and better σ donors. As a consequence, **2-η^2-NCNMe$_2$** can be isolated and characterized. Despite the electronic difference, it is believed that **2-η^2-NCR** (R = Ph or NMe_2) have similar spectroscopic properties which are reflected in NMR and EPR spectra. Unlike **2-η^2-alkyne**, which can be oxidized to give the cationic complexes [**2-η^2-alkyne**]$^+$.[65] Oxidation of **2-η^2-NCNMe$_2$** or **3-η^2-NCNMe$_2$** by adding half equiv of I_2 gives **2-I** or **3-I** and releases $NCNMe_2$.

The steric effect by substituting -^{i}Pr for -^{t}Bu in Mo(N[R]Ar)$_3$ (R = ^{i}Pr or ^{t}Bu) is also reflected in the reactions of **1** or **3** with organonitrile. The addition of different equiv of NCPh to **1-d_{18}** resulted in different products. However, the results of the reaction of **3** with NCPh were not affected by different concentrations of the latter. Only **3-η^2-NCPh** and [**3-NCPh**]$_2$ have been detected. The coupling of organonitriles NCR by **3** is much slower than by **1**. Besides, **3** does not show any reactivity towards bulky substrates such as benzophenone,[10] NCAnth, NCMes, and NC^{t}Bu. Unlike the anilide ligands -N[^{i}Pr]Ar in **1**, the ligands -N[^{t}Bu]Ar in **3** are more rigid, so all the complexes found based on this compound have pseudo-C_3 symmetry, until the discovery of **3-η^2-NCNMe$_2$**

(Figure 7). Although the mechanism for the nitrile cleavage reaction is still obscure, we believe the non-linear bridging nitrile dinuclear complex, namely **2**$_2$-μ, η^1, η^1-**NCPh** is the intermediate (Scheme 3), like the proposed transition state in the dinitrogen cleavage by **3**. This hypothesis is also supported by the observation that NCPh cannot be split by **3** because of the steric bulk of the ligands.

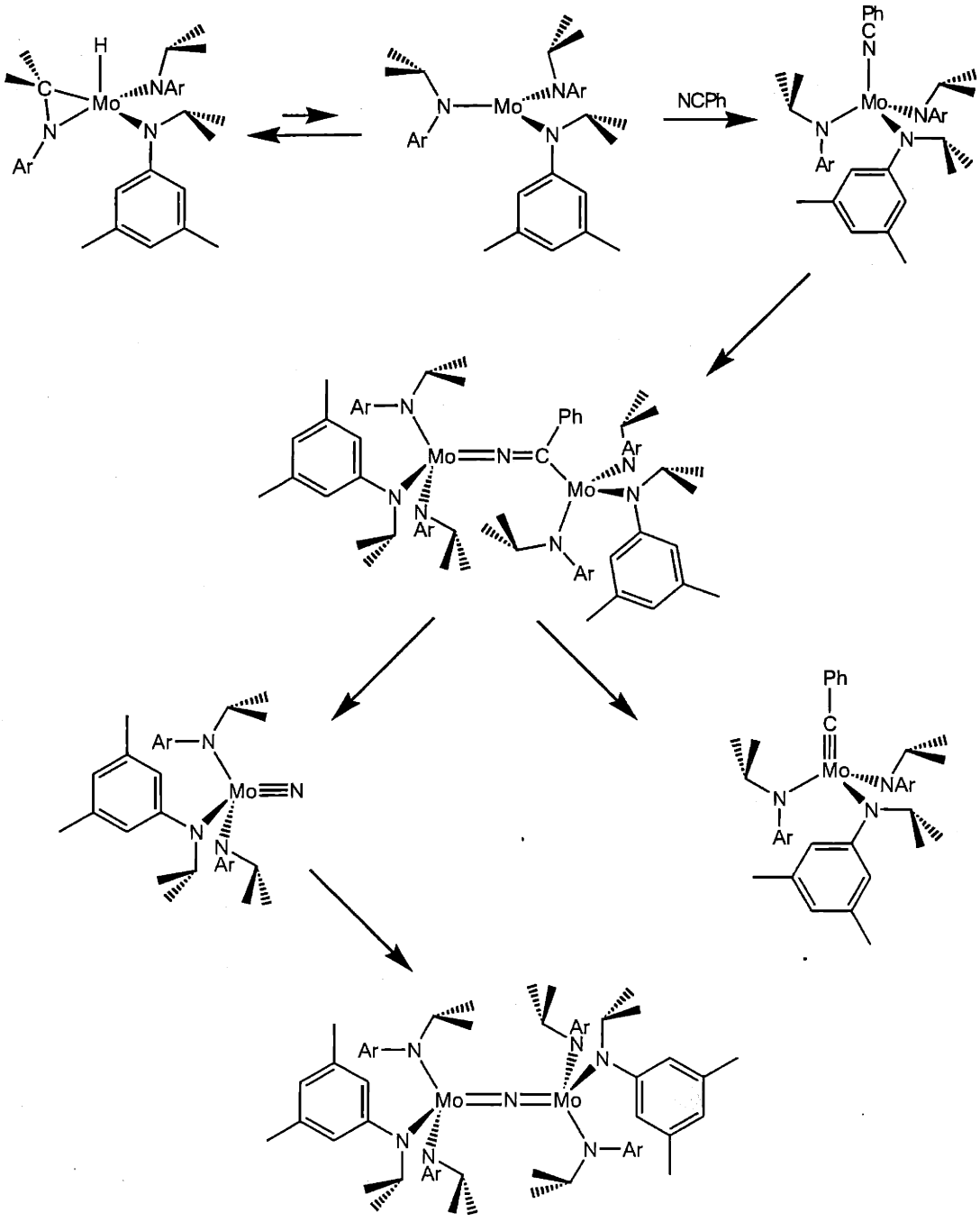

Scheme 3: Proposed mechanism for the cleavage of NCPh by **1**.

4 Experimental Section

4.1 General Considerations

Unless otherwise stated, all operations were performed in a Vacuum Atmospheres drybox under an atmosphere of purified dinitrogen or using Schlenk techniques under an argon atmosphere. Complexes **1**, **1-d_{18}**, and **3** were prepared according to the literature.[4,10] 9-anthracenecarbonitrile, benzonitrile, 4-dimethylaminobenzonitrile, 4-fluorobenzonitrile, 4-methoxybenzonitrile, pentafluorobenzonitrile, trimethylacetonitrile, 2,4,6-trimethylbenzonitrile were used as purchased from Lancaster Synthesis and dimethylcyanamide was obtained from Aldrich. Diethyl ether, benzene, *n*-pentane, *n*-hexane, and toluene were dried and deoxygenated by the method of Grubbs.[66] THF was distilled over Na/benzophenone and collected under nitrogen. C_6D_6 was degassed and dried over 4 Å molecular sieves. Celite, alumina, and 4 Å molecular sieves were dried in vacuo overnight at a temperature above 200 °C. The room temperature X-band EPR spectra of the complexes were recorded on a Bruker EMX spectrometer. Acquisition, simulation, and data post processing of the EPR spectra were performed by using an integrated WIN-EPR software package (Bruker). Cyclic voltammetry measurements were carried out using a Eco-Chemie Autolab potentiostat (pgstat20) and the GPES 4.3 software in conjuction with a three-electrode cell using 0.5 M $[NBu^n_4][PF_6]$ solutions in tetrahydrofuran. ^1H, ^2H, and ^{13}C NMR spectra were recorded on Varian VXR-500 or Varian XL-301 spectrometers. ^1H, ^2H, and ^{13}C chemical shifts are reported with respect to internal solvent (7.15 ppm and 128.38 (t) ppm (C_6D_6)). Elemental analysis for C, H, and N elemental analyses were conducted by H. Kolbe Mikroanalytisches Laboratorium, Mülheim an der Ruhr, Germany.

4.2 Syntheses of $DN(CDMe_2)Ar$ and $DN(CDMe_2)(3,5\text{-}C_6D_3Me_2)$ (Ar = 3,5-$C_6H_3Me_2$)

Since the preparations of these two anilines were carried out in essentially the same way, the preparation of $DNCDMe_2Ar$ is given in detail as an example. To a frozen solution of 9.377 g (0.223 mol) of lithium aluminum deuteride suspended in 250 mL of tetrahydrofuran were added dropwise a solution of 30 g (0.186 mol) of Me_2CNAr in 50 mL of tetrahydrofuran. Upon complete addition, the reaction mixture was stirred at room temperature and became light gray-green in color after overnight. The reaction vessel was cooled down in an ice water bath and slowly added D_2O and several portions of a dilute sodium potassium tartrate solution in D_2O, followed by two portions of D_2O. All organic material were extracted by adding 300 mL of petroleum ether. The organic layer was seperated from aqueous solution by separatory funnel. The solution was dried over anhydrous magnesium sulfate. A pale yellow oil was obtained upon removing all volatiles in vacuo. $DN(CDMe_2)Ar$ was obtained by distilling in vacuo and the yield was 77% (23.552 g, 0.143 mol) For $DN(CDMe_2)Ar$, ^1H NMR (C_6D_6, 19.8 °C): δ 6.40 (1 H, *para*), 6.15 (2 H, *ortho*), 2.21 (6 H, Ar-CH_3), 0.92 (6 H, -$CD(CH_3)_2$) ppm. ^1H NMR of $DN(CDMe_2)(3,5\text{-}C_6D_3Me_2)$ (C_6D_6, 19.8 °C): δ 2.21 (6 H, Ar-CH_3), 0.93 (6 H, -$CD(CH_3)_2$) ppm.

4.3 Syntheses of $Li(N(CDMe_2)Ar)\cdot Et_2O$, $LiNCDMe_2(3,5\text{-}C_6D_3Me_2)\cdot Et_2O$ (Ar = 3,5-$C_6H_3Me_2$)

Since the preparations of these two lithium anilides were carried out in essentially the same way, the preparation of $(Et_2O)LiNCDMe_2Ar$ is given in details. To a frozen solution of 23.0 g (0.139

mol) $DN(CDMe_2)Ar$ in 100 mL of *n*-pentane were added cold *n*-BuLi (105 mL, 1.6 M in hexanes, 0.168 mol). The resulting yellow solution was stirred for 60 min at room temperature and white precipitate formed. Upon reducing the volume of the slurry to one-third in vacuo, 18 mL of diethyl ether was added. After stirring the resulting mixture for 1 h, the mixture was stood in a cold trap in a liquid nitrogen bath for 30 min. A fine white powder (29.886 g, 0.122 mol, 87.7%) was collected by filteration, rinsed with cold *n*-pentane and dried in vacuo. For $Li(N(CDMe_2)Ar)\cdot Et_2O$, ^1H NMR (C_6D_6, 19.9 °C): δ 6.49 (s, 2H), 6.13 (s, 1H), 2.97 (q, 4H), 2.33 (s, 6H), 1.43 (s, 6H), 0.77 (t, 6H) ppm. ^{13}C NMR (C_6D_6, 19.9 °C): δ 160.38 (aryl *ipso*), 139.31 (aryl *meta*), 113.16 (aryl *para*), 111.00 (aryl *ortho*), 65.16 (OCH_2C_3), 47.34 ($CD(CH_3)_2$), 23.93 ($CD(CH_3)_2$), 22.10 (Ar-CH_3), 14.31 (OCH_2CH_3) ppm. For $LiNCDMe_2(3,5\text{-}C_6D_3Me_2)\cdot Et_2O$, ^1H NMR (C_6D_6, 19.9 °C): δ 2.97 (q, 4H), 2.33 (s, 6H), 1.43 (s, 6H), 0.77 (t, 6H) ppm. ^2H NMR (C_6H_6, 19.6 °C): δ 6.49 (s, 2D), 6.13 (s, 1D), 3.37 (s, 1D) ppm.

4.4 Syntheses of molybdenum metallaaziridine deuteride complexes **1-d_3** and $Mo(D)(\eta^2\text{-}Me_2CN(3,5\text{-}C_6D_3Me_2))(N[CDMe_2](3,5\text{-}C_6D_3Me_2))_2$ **(1-d_{12})**

Since the preparations of these two complexes were carried out in essentially the same way, the preparation of **2a** is given in details. To 22.0 g of $Li(N(CDMe_2)Ar)\cdot Et_2O$ (0.090 mol) in 350 mL of diethyl ether were added orange solid $MoCl_3(THF)_3$ (18.84 g, 0.045 mol). The resulting suspension was evacuated for 3 min and stirred at room temperature for 5.5 h. The resulting orange-brown suspension was filtered through a plug of Celite to remove LiCl and excess $MoCl_3(THF)_3$. A black solid was obtained upon removing all volatiles of the filtrate. The resulting solid was redissolved in 200 mL of diethyl ether and the resulting solution was concentrated to 180 mL in vacuo in a 300

mL of Schlenk flask. Big blocks of black crystals formed upon storing the solution under vacuum at −35 °C overnight. The desired product was isolated by filtration, and the yield was 60.0% (2 crops, totaling 10.67 g, 0.018 mol). ^{2}H NMR of **1-d_3** (C_6H_6, 19.6 °C): δ 5.84 ($\Delta\nu_{1/2}$= 41.8 Hz), −12.30 ($\Delta\nu_{1/2}$= 412.6 Hz) ppm. μ_{eff} = 2.04 μ_{B} (Evans' method, C_6D_6, 19.9 °C). For **1-d_{12}**, ^{2}H NMR (C_6H_6, 19.6 °C): δ 9.48 ($\Delta\nu_{1/2}$= 43.2 Hz), 3.45 ($\Delta\nu_{1/2}$= 95.7 Hz), −2.91 ($\Delta\nu_{1/2}$= 401.5 Hz) ppm. μ_{eff} = 2.11 μ_{B} (Evans' method, C_6D_6, 19.9 °C).

4.5 Synthesis of 2-(η^1-NCR)$_2$ (R = Mes and ^{t}Bu)

To 0.756 mmol of **1-d_{18}** in 10 mL of *n*-hexane were added 0.220 g (1.512 mmol) NCR (R = Mes and ^{t}Bu) in 5 mL of *n*-hexane. The resulting mixture became dark blue (R = 2,4,6-$C_6H_2(CH_3)_3$) quickly. The solution was concentrated to approximately 3 mL in vacuo. A crop of spectroscopically pure solid **2-(η^1-NCMes)$_2$** was formed in the solution, and collected as a dark blue powder by filtering. The yield was 52.1% (0.394 mmol). When R = ^{t}Bu, the solution was purple, a dark purple solid residue was obtained upon removing all volatiles, and was rinsed with cold pentane. The yield was 83%. For **2-(η^1-NCMes)$_2$**, ^{2}H NMR (diethyl ether, 19.5 °C): δ 3.21 ($\Delta\nu_{1/2}$= 22.1 Hz) ppm. μ_{eff} = 1.58 μ_{B} (SQuID). Anal. Calcd. for $C_{53}H_{70}N_5Mo$: C, 72.91; H, 7.93; N, 7.86. Found: C, 73.05; H, 7.96; N, 8.04. For **2-(η^1-NC^{t}Bu)$_2$**, ^{2}H NMR (diethyl ether, 19.5 °C): δ 4.08 Hz ($\Delta\nu_{1/2}$= 10.3 Hz) ppm. Anal. Calcd. for $C_{43}H_{66}N_5Mo$: C, 68.96; H, 8.88; N, 9.35. Found: C, 68.81; H, 8.69; N, 9.26.

4.6 Synthesis of [2-NCAnth]$_2$

To 0.680 mmol of **1** in 6 mL of diethyl ether were added 0.646 mmol 9-anthracenecarbonitrile supended in 10 mL of diethyl ether. The resulting mixture became purple quickly, and a purple precipitate formed in one min. After stirring for 1 hour, the purple solid [**2-NCAnth**]$_2$ was collected by filtration, rinsed with diethyl ether, and dried in vacuo. The isolated yield was 91 % (0.462 g, 0.294 mmol). ^{1}H NMR (C_6D_6, 19.9 °C): δ 8.21 (s, 1H), 8.16 (t, 2H), 7.76 (t, 2H), 7.22 (m, 4H), 7.06 (m, 4H), 7.00 (d, 2H), 6.56 (s, 6H), 6.37 (s, 6H), 6.32 (s, 6H), 4.62 (q, 3H), 4.21 (q, 3H), 2.10 (s, 18H), 2.08 (s, 18H), 1.14 (d, 18H), 1.06 (d, 18H) ppm. Anal. Calcd. $C_{96}H_{114}N_8Mo_2$: C, 73.35; H, 7.31; N, 7.13. Found: C, 73.24; H, 7.46; N, 7.02.

4.7 Synthesis of 2- and 3-η^2-NCNMe$_2$

To 0.407 g (0.633 mmol) of **1-d_{18}** in 8 mL of *n*-hexane were added 0.049 g (0.699 mmol) of $NCNMe_2$ in 2 mL of *n*-hexane. The resulting soultion turned green quickly and was stood at -35 °C upon concentrating to approximately 3 mL in vacuo. Crystalline product **3-η^2-NCNMe$_2$** was collected by filtration and rinsed with cold *n*-pentane. The isolated yield was 62.6% (0.282 g, 0.396 mmol). For **2-η^2-NCNMe$_2$**, ^{2}H NMR (diethyl ether, 19.9 °C): δ 8.68 ($\Delta\nu_{1/2}$= 63.1 Hz) ppm. μ_{eff} = 1.92 μ_B (Evans' method, C_6D_6, 19.9 °C). For **3-η^2-NCNMe$_2$**, ^{2}H NMR (diethyl ether, 19.9 °C): δ 7.06 ($\Delta\nu_{1/2}$= 76.6 Hz) ppm. μ_{eff} = 1.83 μ_B (Evans' method, C_6D_6, 19.9 °C). Anal. Calcd. for $C_{39}H_{60}N_5Mo$:: C, 67.41; H, 8.70; N, 10.08. Found: C, 67.46; H, 8.62; N, 10.06.

4.8 Synthesis of [2-NCPh]$_2$[I$_3$]

To 0.313 g (0.537 mmol) of **1-d$_{18}$** in 10 mL of diethyl ether were added 0.061 g (0.591 mmol) of NCPh. The resulting solution quickly turned to dark blue-green. An oily material was obtained upon removing all volatiles in vacuo. The oily residual was redissolved in 5 mL of diethyl ether to yield a green solution. To this green solution were added 0.103 g (0.812 mmol) of I_2 in 5 mL of diethyl ether. Maroon solid **[2-NCPh]$_2$[I$_3$]** precipitated rapidly and was isolated by filtration, and rinsed with hexane until the filtrate became colorless. This maroon solid was dried in vacuo and the yield was 86.2% (0.406 g). ^{2}H NMR (THF, 19.5 °C): δ 0.81 ($\Delta\nu_{1/2}$= 16.0 Hz) ppm. μ_{eff} = 3.74 μ_B (Evans' method, C_5D_5N, 19.9 °C). Anal. Calcd. for $C_{80}H_{106}N_8I_3Mo_2$: C, 54.83; H, 6.10; N, 4.80. Found: C, 54.91; H, 6.16; N, 4.73.

5 X-ray Crystallography

5.1 Crystal Structure of 2-(η^1-NCMes)$_2$

Crystals grown from a *n*-hexane solution at room temperature were coated with paratone *N* oil (Exxon) on a microscope slide. A large blue rod of approximate dimensions 0.42 × 0.21 × 0.19 mm was selected and mounted with wax on a glass fiber. A total of 19802 reflections ($-25 \leq h \leq 26$, $-11 \leq k \leq 12$,$-13 \leq l \leq 21$) were collected at 183(2) K in the θ range of 1.72 to 23.33 °, of which 7227 were unique (R_{int} = 0.0545). The radiation used was Mo-Kα (λ = 0.71073 Å, μ = 2.362 mm^{-1}). The structure was solved by direct methods (SHELXTL V5.0, G. M. Sheldrick and Siemens Industrial Automation, Inc., 1995) in conjunction with standard difference Fourier

techniques. All non-hydrogen atoms were refined anisotropically and hydrogen atoms were placed in calculated (d_{CH} = 0.96 Å) positions. The residual peak and hole electron density was 0.510 and −0.666 e·Å^{-3}. The least-squares refinement converged normally with residuals of R_1 = 0.0663, wR_2 = 0.1294, and GOF = 1.322 based on $I > 2\sigma I$. No significant extinction coefficient was necessary (0.0015(2)). Crystal and refinement data: Formula = $C_{53}H_{70}MoN_5$, space group $P2_1/c$, a = 23.7364(2) Å, b = 11.0300(2) Å, c = 19.2358(4) Å, α = 90 °, β = 93.686(1) °, γ = 90 °, Z = 4, V = 5025.8(1) Å^3, D_{calcd} = 1.154 g·cm^{-3}, $F(000)$ = 1860, R (all data based on F) = 0.0787, wR (all data based on F^2) = 0.1355.

5.2 Crystal Structure of [2-NCAnth]$_2$

Crystals grown from a diethyl ether solution at room temperature were coated with paratone N oil (Exxon) on a microscope slide. A large red plate of approximate dimensions 0.68 × 0.29 × 0.24 mm was selected and mounted with wax on a glass fiber. A total of 34731 reflections ($-20 \leq h \leq 20$, $-22 \leq k \leq 24$,$-24 \leq l \leq 19$) were collected at 183(2) K in the θ range of 1.30 to 23.27 °, of which 23728 were unique (R_{int} = 0.0431). The radiation used was Mo-Kα (λ = 0.71073 Å, μ = 2.362 mm^{-1}). The structure was solved by direct methods (SHELXTL V5.0, G. M. Sheldrick and Siemens Industrial Automation, Inc., 1995) in conjunction with standard difference Fourier techniques, and refined by full-matrix-block least-squares on F^2 using the BLOC card. Two crystallographically independent molecules were confined in the asymmetric unit. All non-hydrogen atoms were refined anisotropically and hydrogen atoms were placed in calculated (d_{CH} = 0.96 Å) positions. The residual peak and hole electron density was 1.157 and −0.491 e·Å^{-3}. The least-squares refinement converged normally with residuals of R_1 = 0.0736, wR_2 = 0.1661, and GOF = 1.328 based on $I >$

$2\sigma I$. No significant extinction coefficient was necessary (0.0015(2)). Crystal and refinement data: Formula = $C_{192}H_{228}Mo_4N_{16}$, space group $P\bar{1}$, a = 18.6762(2) Å, b = 21.6349(1) Å, c = 21.8544(3) Å, α = 85.142(1) °, β = 85.377(1) °, γ = 76.658(1) °, Z = 2, V = 8544(1) Å^3, D_{calcd} = 1.222 g·cm^{-3}, $F(000)$ = 3320, R (all data based on F) = 0.0816, wR (all data based on F^2) = 0.1738.

5.3 Crystal Structure of 3-η^2-NCNMe$_2$

Crystals grown from a diethyl ether solution at −35 °C were coated with paratone N oil (Exxon) on a microscope slide. A green block of approximate dimensions 0.28 × 0.23 × 0.09 mm was selected and mounted with wax on a glass fiber. A total of 12824 reflections ($-14 \leq h \leq 7$, $-21 \leq k \leq 19$, $-16 \leq l \leq 17$) were collected at 183(2) K in the θ range of 2.22 to 21.25 °, of which 4297 were unique (R_{int} = 0.3225). The radiation used was Mo-Kα (λ = 0.71073 Å, μ = 2.362 mm^{-1}). The structure was solved by direct methods (SHELXTL V5.0, G. M. Sheldrick and Siemens Industrial Automation, Inc., 1995) in conjunction with standard difference Fourier techniques. The large R_{int} of 32% and peak/hole map was associated with rapid decay of the crystal during data collection and weak reflections at high angles for 2θ. All non-hydrogen atoms were refined anisotropically and hydrogen atoms were placed in calculated (d_{CH} = 0.96 Å) positions. The residual peak and hole electron density was 1.324 and −2.594 e·Å^{-3}. The least-squares refinement converged normally with residuals of R_1 = 0.0750, wR_2 = 0.1481, and GOF = 1.129 based on $I > 2\sigma I$. No significant extinction coefficient was necessary (0.0006(2)). Crystal and refinement data: Formula = $C_{39}H_{60}MoN_5$, space group $P2_1/n$, a = 12.9183(13) Å, b = 19.099(2) Å, c = 15.748(2) Å, α = 90 °, β = 95.313(2) °, γ = 90 °, Z = 4, V = 3868.7(7) Å^3, D_{calcd} = 1.193 g·cm^{-3}, $F(000)$ = 1484, R (all data based on F) = 0.0889, wR (all data based on F^2) = 0.1567.

5.4 Crystal Structure of [2-NCPh]$_2$[I$_3$]

Crystals grown from a CH_2Cl_2/*n*-hexane solution at −35 °C were coated with paratone *N* oil (Exxon) on a microscope slide. A large red block of approximate dimensions 0.50 × 0.32 × 0.30 mm was selected and mounted with wax on a glass fiber. A total of 19795 reflections ($-22 \leq h \leq 20$, $-21 \leq k \leq 21$,$-22 \leq l \leq 27$) were collected at 183(2) K in the θ range of 1.45 to 23.26 °, of which 7010 were unique ($R_{\text{int}} = 0.0560$). The radiation used was Mo-Kα ($\lambda = 0.71073$ Å, $\mu = 2.362$ mm^{-1}). The structure was solved by direct methods (SHELXTL V5.0, G. M. Sheldrick and Siemens Industrial Automation, Inc., 1995) in conjunction with standard difference Fourier techniques. Two CH_2Cl_2 and one linear I_3 molecules were located in the asymmetric unit and were refined anisotropic. All non-hydrogen atoms were refined anisotropically and hydrogen atoms were placed in calculated ($d_{\text{CH}} = 0.96$ Å) positions. Symmetry transformations used to generate equivalent atoms: ♯1 −x, y, z+1/2; ♯2 −x, y, z+3/2. The residual peak and hole electron density was 2.082 and −1.050 e·Å^{-3}. The least-squares refinement converged normally with residuals of $R_1 = 0.0516$, $wR_2 = 0.1265$, and GOF = 1.322 based on $I > 2\sigma I$. No significant extinction coefficient was necessary (0.0001(2)). Crystal and refinement data: Formula = $C_{83}H_{110}Cl_2I_6Mo_2N_8$, space group $C2/c$, a = 20.0607(5) Å, b = 19.6646(5) Å, c = 24.8443(7) Å, $\alpha = 90$ °, $\beta = 95.380(1)$ °, $\gamma = 90$ °, $Z = 4$, $V = 9757.5(4)$ Å^3, $D_{calcd} = 1.624$ g·cm^{-3}, $F(000) = 4672$, R (all data based on F) = 0.0663, wR (all data based on F^2) = 0.1410.

References

1. Cummins, C. C. *Prog. Inorg. Chem.* **1998,** *47,* 685.

2. Cummins, C. C. *Chem. Commun.* **1998,** 1777.

3. Laplaza, C. E.; Cummins, C. C. *Science* **1995,** *268,* 861.

4. Laplaza, C. E.; Johnson, M. J. A.; Peters, J. C.; Odom, A. L.; Kim, E.; Cummins, C. C.; George, G. N.; Pickering, I. J. *J. Am. Chem. Soc.* **1996,** *118,* 8623.

5. Johnson, A. R.; Davis, W. M.; Cummins, C. C.; Serron, S.; Nolan, S. P.; Musaev, D. G.; Morokuma, K. *J. Am. Chem. Soc.* **1998,** *120,* 2071.

6. Cherry, J.-P. F.; Johnson, A. R.; Baraldo, L. M.; Tsai, Y.-C.; Cummins, C. C.; Kryatov, S. U.; Rybak-Akimova, E. V.; Capps, K. B.; Hoff, C. D.; Haar, C. M.; Nolan, S. P. *J. Am. Chem. Soc.* **2001,** *123,* accepted.

7. Laplaza, C. E.; Davis, W. M.; Cummins, C. C. *Angew. Chem. Int. Ed. Engl.* **1995,** *34,* 2042.

8. Peters, J. C.; Odom, A. L.; Cummins, C. C. *Chem. Commun.* **1997,** 1995.

9. Peters, J. C.; Cherry, J.-P.; Thomas, J. C.; Baraldo, L.; Mindiola, D. J.; Davis, W. M.; Cummins, C. C. *J. Am. Chem. Soc.* **1999,** *121,* 10053-10067.

10. Tsai, Y.-C.; Johnson, M. J. A.; Mindiola, D. J.; Cummins, C. C.; Klooster, W. T.; Koetzle, T. F. *J. Am. Chem. Soc.* **1999,** *121,* 10426.

11. Michelin, R. A.; Mozzon, M.; Bertani, R. *Coord. Chem. Rev.* **1996,** *147,* 299.

12. Walton, R. A. *Q. Rev., Chem. Soc* **1965,** *19,* 126.

13. Storhoff, B. N.; Lewis, H. C. *Coord. Chem. Rev.* **1977,** *23,* 1.

14. Kukushkin, Y. N. *Koord. Khim.* **1981,** *7,* 323.

15. Dunbar, K. R. *Comments Inorg. Chem.* **1992,** *13,* 313.

16. Kaim, W.; Moscherosch, M. *Coord. Chem. Rev.* **1994,** *129,* 157.

17. Murahashi, S.-I.; Naota, T. *Bull. Chem. Soc. Jpn.* **1996,** *69,* 1805.

18. Thomas, J. L. *J. Am. Chem. Soc.* **1975,** *97,* 5943.

19. McGilligan, B. S.; Wright, T. C.; Wilkinson, G.; Motevalli, M.; Hursthouse, M. B. *J. Chem. Soc., Dalton Trans.* **1988,** 1737.

20. Pombeiro, A. J.; Hughes, D. L.; Richards, R. L. *J. Chem. Soc., Chem. Commun.* **1988,** 1052.

21. Esjornson, D.; Bakir, M.; Fanwick, P. E.; Jones, K. S.; Walton, R. A. *Inorg. Chem.* **1990,** *29,* 2055.

22. Frausto da Silva, J. J. R.; Guedes da Silva, M. F. C.; Henderson, R. A.; Pombeiro, A. J.; Richards, R. L. *J. Organomet. Chem.* **1993,** *461,* 141.

23. Blight, D. G.; Deutscher, R. L.; Kepert, D. L. *J. Chem. Soc., Dalton Trans.* **1972,** 87.

24. Finn, P. A.; Schaefer, K, M.; Kilty, P. A.; McCarley, R. E. *J. Am. Chem. Soc* **1975,** *97,* 220.

25. Cotton, F. A.; Hall, W. *Inorg. Chem.* **1978,** *17,*.

26. Roskamp, E. J.; Pedersen, S. F. *J. Am. Chem. Soc.* **1987,** *109,* 3152.

27. Duchateau, R.; Williams, A. J.; Gambarotta, S.; Y., C. M. *Inorg. Chem.* **1991,** *30,* 4863.

28. Schrock, R. R.; Listemann, M. L.; Sturgeoff, L. G. *J. Am. Chem. Soc.* **1982,** *104,* 4291.

29. Chisholm, M. H.; Hoffman, D. M.; Huffman, J. C. *Inorg. Chem.* **1983,** *22,* 2903.

30. Chisholm, M. H.; Folting-Streib, K.; Tiedtke, D. B.; Lemoigno, F.; Eisentein, O. *Angew. Chem. Int. Ed. Engl.* **1995,** *34,* 110.

31. Seino, H.; Tanabe, Y.; Ishii, Y.; Hidai, M. *Inorg. Chim. Acta* **1998,** *280,* 163.

32. Chisholm, M. H.; Folting-Streib, K.; Lynn, M. L.; Tiedtke, D. B.; Lemoigno, F.; Eisentein, O. *Chem.-Eur. J.* **1999,** *5,* 2318.

33. Tanabe, Y.; Seino, H.; Ishii, Y.; Hidai, M. *J. Am. Chem. Soc* **2000,** *122,* 1690.

34. Evans, D. F. *J. Chem. Soc.* **1959,** 2003.

35. Mulay, L. N.; Boudreaux, E. A. *Theory and Applications of Molecular Paramagnetism and Theory and Applications of Molecular Diamagnetism;* Wiley Interscience: New York, 1976.

36. Danford, M. D.; Livingston, R. L. *J. Am. Chem. Soc.* **1955,** *77,* 2944.

37. Kessler, M.; Ring, H.; Trambarulo, R.; Gordy, W. *Phys. Rev.* **1950,** *79,* 54.

38. Silverstein, R. M.; Bassler, G. C.; Morrill, T. C. *SPECTROMETRIC IDENTIFICATION OF ORGANIC COMPOUNDS;* John Wiley & Sons, Inc.: , 5th ed.; 1991.

39. Covert, K. J.; Wolczanski, P. T.; Hill, S. A.; Krusic, P. J. *Inorg. Chem.* **1992,** *31,* 66.

40. Agapie, T.; Mindiola, D, J.; Cummins, C. C. *Submitted for publication* .

41. Morrison, W. H. J.; Krogsrud, S.; Hendrickson, D. N. *Inorg. Chem.* **1973,** *12,* 1998.

42. Bunel, E. E.; Campos, P.; Ruz, J.; Valle, L.; Chadwick, I.; Ana, M. S.; Gonzalez, G.; Manriquez, J. M. *Organometallics* **1988,** *7,* 474.

43. Atzkern, H.; Huber, B.; Köhler, F. H.; Müller, G.; Müller, R. *Organometallics* **1991,** *10,* 238.

44. Chukwu, R.; Hunter, A. D.; Santarsiero, B. D.; Bott, S. G. Atwood, J. L.; Chassaignac, J. *Organometallics* **1992,** *11,* 589.

45. Runsink, J.; Swen-Walstra, S.; Migchelsen, T. *Acta. Crystallogr., Sect. B.* **1972,** *28,* 1331.

46. Mares, F.; Diamond, S. E. *J. Organomet. Chem.* **1977,** *142,* C55.

47. Mayer, J. M.; Curtis, C. J.; Bercaw, J. E. *J. Am. Chem. Soc.* **1983,** *105,* 2651.

48. Bryndza, H. E.; Tam, W. *Chem. Rev.* **1988,** *88,* 1163.

49. Fryzuk, M. D.; Montgomery, C. D. *Coord. Chem. Rev.* **1989,** *95,* 1.

50. Driver, M. S.; Hartwig, J. F. *J. Am. Chem. Soc. 118,* 4206.

51. Hartwig, J. F. *J. Am. Chem. Soc. 118,* 7010.

52. Orth, S. D.; Barrera, J.; Rowe, S. M.; Helberg, L. E.; Harman, W. D. *Inorg. Chim. Acta* **1998,** *270,* 337.

53. Komiya, S.; Baba, A. *Organometallics* **1991,** *10,* 3105.

54. Johnson, T. J.; Albinati, A.; Koetzle, T. F.; Ricci, J.; Eisenstein, O.; Huffman, J. C.; Caulton, K. G. *Inorg. Chem.* **1994,** *33,* 4966.

55. Johnson, T. J.; Huffman, J. C.; Caulton, K. G.; Jackson, S. A.; Eisenstein, O. *Organometallics* **1989,** *8,* 2073.

56. Fernandez, M. J.; Rodriguez, L. A. O.; Lahoz, F. J. *J. Chem. Soc., Dalton Trans.* **1989,** 2073.

57. Neuner, B.; Schrock, R. R. *Organometallics* **1996,** *15,* 5-6.

58. O'Donoghue, M. B.; Davis, W. M.; Schrock, R. R. *Inorg. Chem.* **1998,** *37,* 5149.

59. Dilworth, J. R.; Hu, J.; Miller, J. R.; Hughes, D. L.; Zubieta, J. A. nad Chen, Q. *J. Chem. Soc. Dalton Trans.* **1995,** 3153.

60. Osman, R.; Pattison, D. L.; Perutz, R. N.; Bianchini, C.; Casares, J. A.; Peruzzini, M. *J. Am. Chem. Soc.* **1997,** *119,* 8459.

61. Dilworth, J. R.; Hutchinson, J.; Zubieta, J. *J. Chem. Soc., Chem. Commun.* **1983,** 1034.

62. Blower, P. J.; Dilworth, J. R.; Hutchinson, J.; Nicholson, T.; Zubieta, J. A. *J. Chem. Soc., Dalton Trans.* **1985,** 2639.

63. Blower, P. J.; Dilworth, J. R. *J. Chem. Soc., Dalton Trans.* **1985,** 2305.

64. Hahn, J.; Landis, C. R.; Nasluzov, V. A.; Neyman, K. M.; Rösch, N. *Inorg. Chem.* **1997,** *36,* 3947.

65. Tsai, Y.-C.; Diaconescu, P. L.; Cummins, C. C. *Organometallics* **2000,** *19,* 5260.

66. Pangborn, A. B.; Giardello, M. A.; Grubbs, R. H.; Rosen, R. K.; Timmers, F. J. *Organometallics* **1996,** *15,* 1518.

67. Wright, T. C.; Wilkinson, G.; Montevalli, M.; Hursthouse, M. B. *J. Chem. Soc., Dalton Trans.* **1986,** 2017.

68. Anderson, S. J.; Wells, F. J.; Wilkinson, G.; Hussain, B.; Hursthouse, M. B. *Polyhedron* **1987,** *6,* 1599-1601.

69. Barrera, J.; Sabat, M.; Harman, W. D. *Organometallics* **1993,** *12,* 4381.

70. Barrera, J.; Sabat, M.; Harman, W. D. *J. Am. Chem. Soc* **1991,** *113,* 8178.

71. Chetcuti, P. A.; Knobler, C. B.; Hawthorne, M. F. *Organometallics* **1986,** *5,* 1913.

72. Chetcuti, P. A.; Knobler, C. B.; Hawthorne, M. F. *Organometallics* **1988,** *7,* 650.

Chapter 2. Interaction of Styrene and Alkynes with a Masked Three-Coordinate Molybdenum(III) Complex: Preparation of Well-Defined Alkyne Metathesis Catalysts and Related Chemistry

October 29, 2001

1 Introduction

It has been reported that the three-coordinate molybdenum(III) complex Mo(N[R]Ar)$_3$ (R = C(CD$_3$)$_2$CH$_3$, **3** or ^{t}Bu, Ar = 3,5-C$_6$H$_3$Me$_2$) is a good platform for the synthesis of molybdenum-element (pnictogens: N[1–4] and P,[5] chalcogens: O, S, Se, and Te[6]) multiple bonds. Accordingly, alkylidyne complexes **3-CR** were reasonable targets since four-coordinate molybdenum(VI) alkylidyne complexes have been known for some time.[7] Indeed, the carbidomolybdenum(VI) anion, in which the terminal carbide ligand is derived from carbon monoxide through a stepwise reduction process,[8] and the corresponding methylidyne, generated by protonating the parent anion[8,9] or by "CH" transfer,[10] have been prepared in our group. In alternative fashion recalling the chop-chop reaction of Schrock,[11,12] a benzylidyne molybdenum(VI) complex PhCMo(N[^{i}Pr]Ar)$_3$ (**2-CPh**), formed *via* a reductive cleavage of benzonitrile by the molybdenum metallaaziridine-hydride complex Mo(H)(η^2-Me$_2$CNAr)(N[^{i}Pr]Ar)$_2$ (Ar = 3,5-C$_6$H$_3$Me$_2$, **1**), has been reported also.[13]

Only two types of reactions enabling the synthesis of tungsten and molybdenum alkylidyne complexes directly from alkynes have been reported to date.[11,14–25] Schrock *et al.* discovered that an alkyne can be split by a ditungsten complex W$_2$(O^{t}Bu)$_6$ to form trialkoxytungsten(VI) alkylidyne.[11] The less reactive analogous dimolybdenum species was limited to the cleavage of terminal alkynes.[14] Green[15–18] and Templeton[19–25] synthesized Fischer-type Mo(IV) and W(IV) alkylidyne complexes bearing a Cp (η^5-C$_5$H$_5$), Ind (η^5-indenyl), or Tp' (hydridotris(3,5-dimethylpyrazolyl)borate) ligand using terminal alkynes as the carbyne source. A common intermediate to form a carbyne is the L$_n$M-η^2-vinyl complex, observed by both groups.

Due to its amido ^{i}Pr substituent, complex **1** has been found to be more reactive than its

^{t}Bu-substituted counterpart (**3**) and an excellent platform for the activation of small molecules and organic functionalities.[13,26,27] We communicated earlier[26] that the Schrock-type Mo(VI) carbyne complexes can be prepared readily from **1** and Me_3SiCCH through complexation, oxidation, hydride addition, isomerization, and alcoholysis. The trialkoxytungsten(VI) alkylidyne complex ^{t}BuCW(O^{t}Bu)$_3$ has been employed in organic synthesis as an alkyne metathesis catalyst.[28–33] Trialkoxymolybdenum(VI) alkylidyne complexes, including the prototype ^{t}BuCMo(O^{t}Bu)$_3$, are known, but they have been subjected to little scrutiny as catalysts due to drawbacks inherent in the existing synthesis.[7]

Included in the present work is information on the complexation of styrene and alkynes by **1**, coupling of **2**-η^2-terminal alkyne complexes, and a series of transformations converting a Me_3SiCCH complex to a Schrock-type carbyne complex. Owing to the high yield of each step of the latter process, this method provides a facile synthesis of molybdenum(VI) alkylidyne complexes. It is shown that protolytic replacement of the N[^{i}Pr]Ar ligands with alkoxides or aryloxides gives trialkoxymolybdenum(VI) alkylidyne complexes, active catalysts for alkyne metathesis that are tolerant of a range of functionalities and function at 25 °C.

2 Results and Discussion

2.1 Synthesis, molecular structure, and EPR study of 2-η^2-H_2CCHPh

Addition of one equiv of styrene to Mo(H)(η^2-$(CD_3)_2CNAr$)(N[^{i}Pr-d_6]Ar)$_2$ (**1**-$\boldsymbol{d}_{18}$) in Et_2O resulted in formation of a yellow solution. Two signals in a 1:1 ratio were observed in ^{2}H NMR

spectra, as the CD_3 groups on each ligand are diastereotopic. The molecular structure of (η^2-H_2CCHPh)Mo(N[^{i}Pr]Ar)$_3$ (**2-η^2-H_2CCHPh**) is depicted in Figure 1. Remarkably, all three ^{i}Pr groups are located on one hemisphere, while the three 3,5-$C_6H_3Me_2$ substituents form a pocket encapsulating the bound styrene. The geometry at the metal center defies simple description. Carbon atoms C(41) and C(42) show partial positional disorder. They have been modeled as occupying two sites C(41A), C(41B) and C(42A), C(42B), respectively (C(41A) is 55% and C(42A) is 45% occupancy). The average Mo-N bond distance is 1.974(3) Å, this being normal for a π-donating amido ligand, and the Mo-C(41A), Mo-C(41B), Mo-C(42A), and Mo-C(42B) distances are 2.149(8), 2.195(9), 2.198(11), and 2.164(8) Å, respectively. A noteworthy feature is the presence of three agostic interactions involving the ^{i}Pr methine groups. The three Mo-N(1)-C(17), Mo-N(2)-C(27), and Mo-N(3)-C(37) angles are 112.2(3), 111.4(3), and 118.4(2)°, these being the three smallest such angles among structurally characterized complexes containing the fragment **2**.[13] The M···C distances also are characteristic of the agostic interactions. The Mo···C(17), Mo···C(27), and Mo···C(37) distances of 2.897(5), 2.860(4), and 2.975(5) Åare much shorter than those found for the single agostic interactions in Mo(CO)(dppe)$_2$ (3.50(2) Å),[34] Mo(CO)(d^{i}Bupe)$_2$ (3.007(4) Å),[35] W(CO)$_3$(PCy$_3$)$_2$ (2.945(6) Å),[36] and [Mn(CO)(dppe)$_2$]$^+$ (3.456(4) and 3.589(4) Å).[37] It did prove possible to locate and refine the positions of the three methine hydrogens, values for which therefore are reliable within the accuracy of the method. The true C-H distances (C(17)-H(17A): 0.86(6) Å, C(27)-H(27A): 0.95(5) Å, and (C(37)-H(37A): 0.88(5) Å) should be somewhat longer, since X-ray structure analysis systematically underestimates C-H distances.[13] The three interatomic distances Mo···H(17A), Mo···H(27A), and Mo···H(37A) are 2.61(6), 2.67(4), and 2.68(5) Å, respectively, significantly shorter than those found for the single agostic interactions in Mo(CO)(dppe)$_2$ (2.98(11) Å)[34] and [Mn(CO)(dppe)$_2$]$^+$ (2.89(6) and 2.98(6) Å),[37] and close to that in Mo(N(2,6-

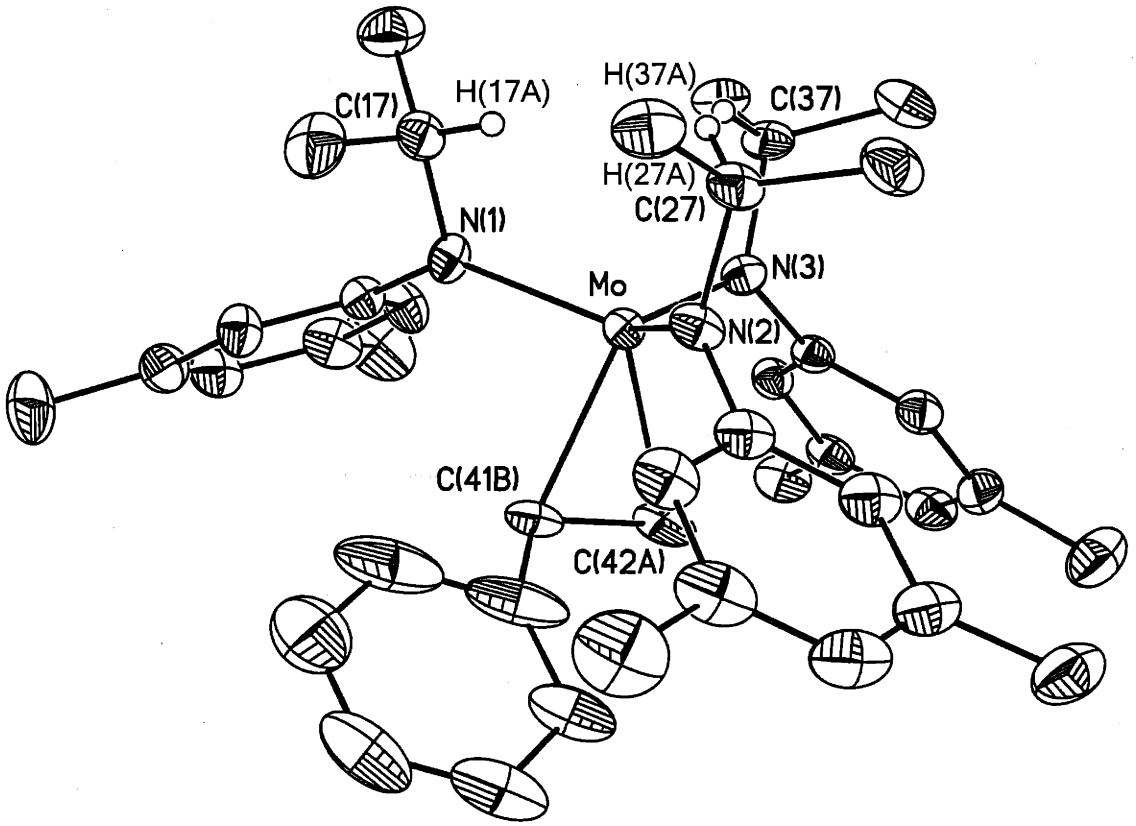

Figure 1: Thermal ellipsoid plot (35% probability) of **2-η^2-H_2CCPhH**. C(41A), C(42B), and all hydrogens except H(17A), H(27A), and H(37A) were omitted for clarity. Selected distances (Å) and angles (°): Mo-N(1), 1.990(3); Mo-N(2), 1.967(3); Mo-N(3), 1.964(3); Mo-C(41B), 2.149(8); Mo-C(42A), 2.198(11); C(41B)-C(42A), 1.204(17); N(1)-Mo(1)-N(2), 119.71(14); N(2)-Mo(1)-N(3), 113.93(14); N(3)-Mo(1)-N(1), 111.31(14); C(17)-N(1)-Mo, 112.2(3); C(27)-N(2)-Mo, 111.4(3); C(37)-N(3)-Mo, 112.2(3); 118.4(2); N(1)-Mo-C(41B), 88.2(3); N(2)-Mo-C(41B), 127.0(2); N(3)-Mo-C(41B), 91.7(3); N(1)-Mo-C(42A),119.1(4); N(2)-Mo-C(42A), 100.0(5); N(3)-Mo-C(42A), 88.3(4); C(42A)-C(41B)-Mo, 76.1(6); C(41B)-C(42A)-Mo, 71.7(7); C(41B)-Mo-C(42A), 32.1(4).

C_6H_3-^{i}Pr$_2$)$_2$Me$_2$ (2.585(8), 2.76(1), 2.598(5), and 2.755(5) Å).[38] The C-H (methine) stretching frequency is 2714 cm^{-1}, which is lower than that of a regular methine C−H stretch (2890 cm^{-1}).[39] These observations support the proposal of agostic interactions in complex **2-η^2-H_2CCHPh**.

In order to gain further information concerning the three β-agostic interactions, a geometry optimization calculation was performed on compound **2-η^2-H_2CCHPh** within the DFT framework.[40,41] To facilitate the calculations, the N(^{i}Pr)Ar ligands were modeled as NMe_2 groups. Indeed, further confirmation for the triple agostic interaction was obtained, as the three Mo···C distances were calculated to be in agreement with the crystallographically determined ones (2.860(4), 2.897(5), 2.975(5) Å and 2.85, 2.90, 3.08 Å for X-ray and DFT obtained values, respectively). This implies that despite the ligand simplification, the unsaturation of the metal center favors an arrangement of the ligands incorporating unusually short Mo···C distances typical of an agostic interaction.

In 1983 Brookhart and Green[42] coined the term "agostic" to describe interactions of this type. Since then, polyagostic interactions have been observed in several systems,[37,38,43–49] but those involving amido C-H bonds are still rare. To the best of our knowledge, the complex Cp^*_2TiN(Me)Ph[50] is the only such complex that displays a single, weak β-agostic Ti···CH interaction. The three-coordinate lanthanide complex Er(N[^{t}Bu](Si(CH$_3$)$_2$H))$_3$ shows three strong β-agostic Er···SiH interactions, where the three Er···H distances are 2.32(3), 2.41(3), and 2.37(3) Å.[51]

Magnetic susceptibility measurements (Evans' method)[52] indicate that **2-η^2-H_2CCHPh** possesses a single unpaired electron (μ_{eff} = 1.89 μ_B). The X-band EPR spectra of **2-η^2-H_2CCHPh**

were measured at room temperature in Et_2O solution (Figure 2). An isotropic signal at g_{iso} = 1.9741 with a line width of 8 Gauss and a coupling constant of 34.0 G ($A_{iso}{}^{95/97}$Mo) were obtained from the simulation. A noteworthy feature in the spectrum is the hyperfine splitting pattern. The main signal at g_{iso} = 1.9741 as well as the six satellites in the spectrum of **2-η^2-H_2CCHPh** are split into three signals *via* coupling to vinylic styrene hydrogens with a coupling constant of 9.0 G ($A_{iso}{}^{1}$H). There are in principle two possible assignments for the super-super hyperfine interactions. They may due to the three methine hydrogens in the ^{i}Pr substituents or due to the three vinylic styrene hydrogens. Since $A_{iso}{}^{2}$H is $\sim$ 1/7 $A_{iso}{}^{1}$H, deuteration of the methine position in the ^{i}Pr was undertaken as well as study of the effect of styrene-d_8. Figure 3 shows the EPR spectra of the isotopomers Mo(η^2-H_2CCHPh)(N(C[CD_3)$_2$D]Ar)$_3$ (**2-d_{21}-η^2-H_2CCHPh**) and **2-η^2-$D_2CCDC_6D_5$**. Clearly indicated is that the super-super hyperfine coupling stems from the interactions between the unpaired electron and the three vinylic styrene hydrogens. A coupling constant of 9.0 G ($A_{iso}{}^{1}$H) was obtained from the simulation. Simulations of the spectrum of **2-η^2-$D_2CCDC_6D_5$** were carried out under the assumption of a coupling constant of 1.3 G ($A_{iso}{}^{2}$H), which is much smaller than the line width (8 Gauss). The spectrum of **2-η^2-$D_2CCDC_6D_5$** was simulated successfully without changing any other parameters.

2.2 Syntheses and Redox Properties of 2-η^2-R^1CCR^2 (R^1 = Ph, R^2 = Ph, Me; R^1 = R^2 = Et; R^1 = H, R^2 = ^{t}Bu, $SiMe_3$)

Syntheses of simple monomeric d^3 alkyne complexes of molybdenum with no chelating or cyclopentadienyl ligands in the coordination sphere have not been reported previously. The green complexes **2-η^2-R^1CCR^2** were prepared upon addition of one equiv of R^1CCR^2 to **1** in Et_2O at room tem-

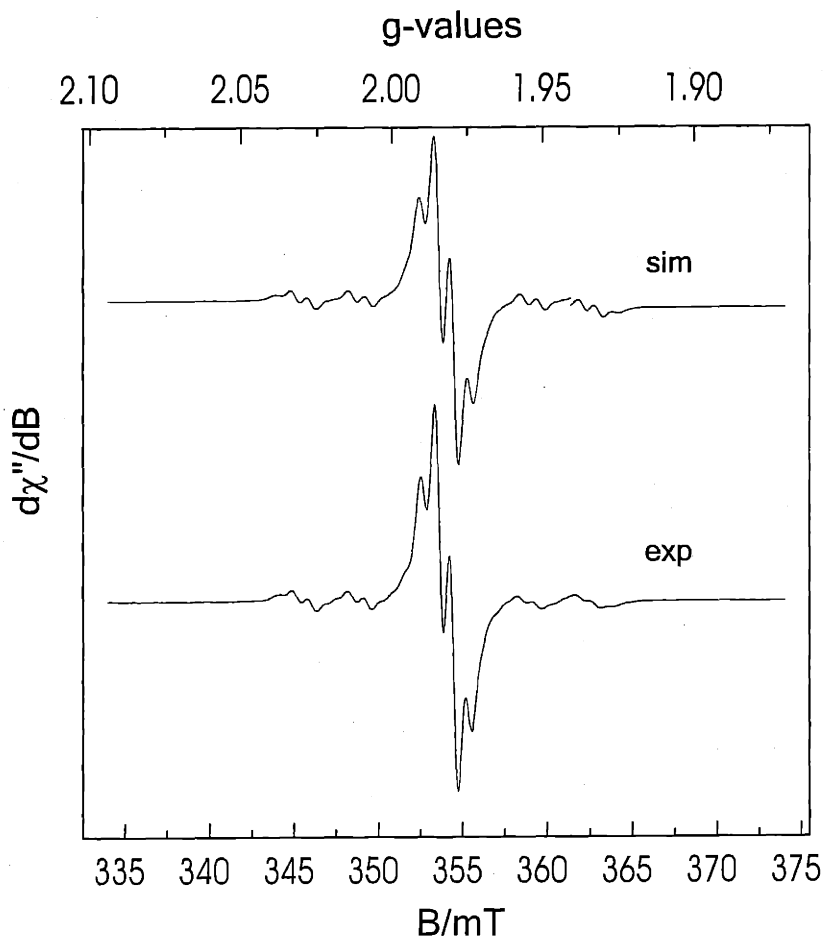

Figure 2: X-band EPR spectrum of **2-η^2-H_2CCPhH** recorded in n-pentane at 298 K. Experimental conditions: microwave frequency ν: 9.780 GHz, Power: 10.0 mW, Modulation amplitude: 1.0 G.

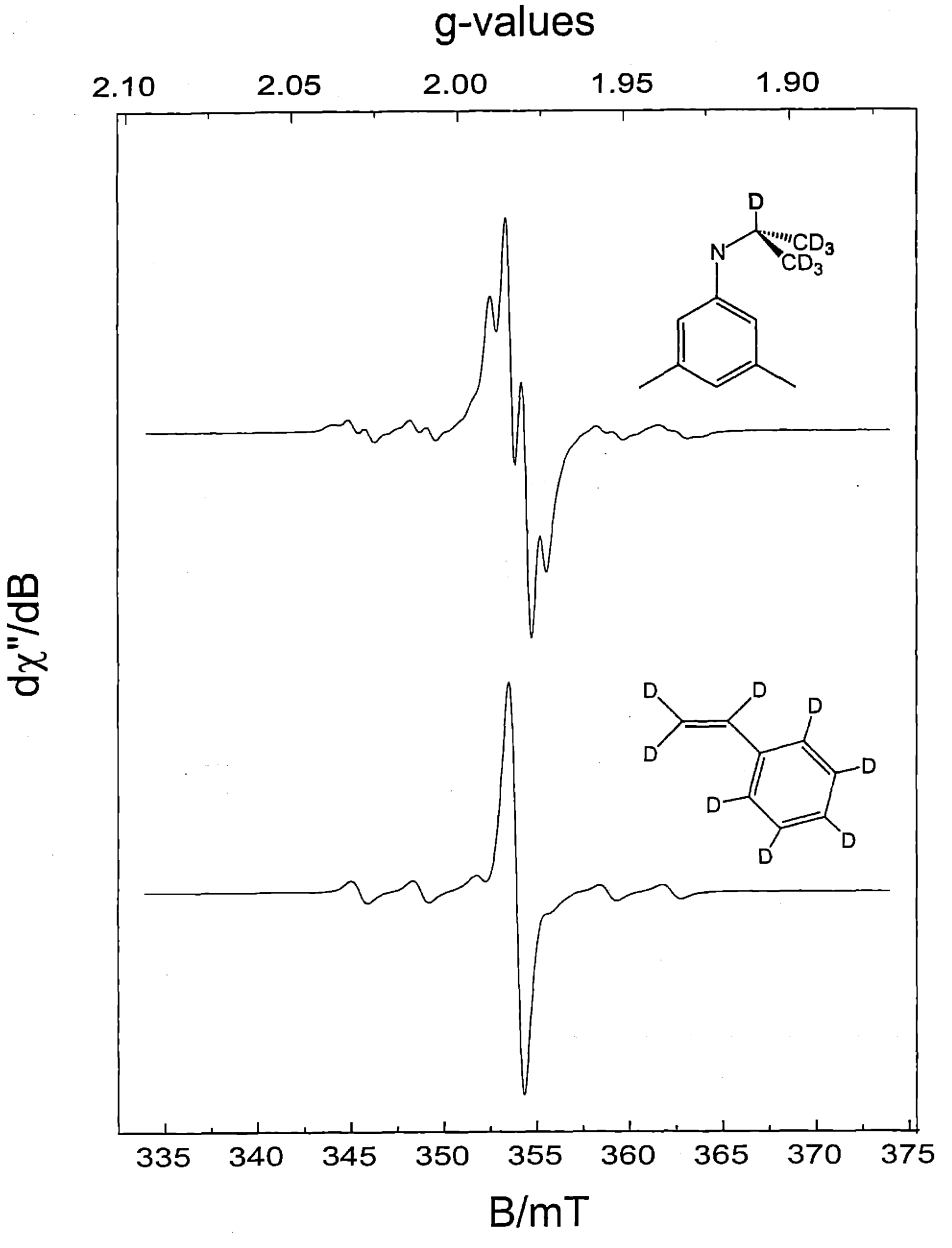

Figure 3: X-band EPR spectra of **2-d_{21}-η^2-H_2CCPhH** (top) and **2-η^2-D_2CCDPh-d_5** (bottom) recorded in *n*-pentane at 298 K. Experimental conditions: microwave frequency ν: 9.780 GHz, Power: 10.0 mW, Modulation amplitude: 1.0 G.

perature. The rate of formation of complexes **2-η^2-R^1CCR^2** was found to depend on the bulk of the alkyne. When $R^1 = R^2 = Ph$, the reaction was carried out under argon overnight (about 10% of **2_2-μ-N** formed when the reaction was conducted under dinitrogen[13]). However, the reactions of **1** with other alkynes were carried out under a dinitrogen atmosphere and were complete in several minutes. In concert with these observations, the more hindered Mo derivative **3** does not exhibit any reactivity towards diphenylacetylene. The new **2-η^2**-alkyne complexes are paramagnetic and have one unpaired electron (Evans' method),[52] so that deuterated anilide ligands N(^{i}Pr-d_6)Ar were used for monitoring the reactions by ^{2}H NMR spectroscopy, a single anilide ligand environment being observed. Although no structural data are available, it is believed that the alkynes coordinate to molybdenum in an η^2 manner, as found above for the styrene adduct **2-η^2-H_2CCHPh**.

A series of monocationic complexes **[2-η^2-R^1CCR^2]$^+$** can be prepared upon addition of one-half equiv of I_2 to neutral **2-η^2-R^1CCR^2**. For $R^1 = {}^t$Bu, $SiMe_3$, Ph and R^2 = H, the corresponding monocationic complexes can be prepared also by adding one equiv of the alkyne to **2-I**. Because of the low solubility of these iodide salts in hydrocarbon solvents, all were isolated in high yield (more than 88%). Acetylenic proton chemical shifts for **[2-η^2-RCCH]**[I] (R = ^{t}Bu, $SiMe_3$, and Ph) display low-field signals (9.68-10.89 ppm) indicative of four-electron donation from the alkynes.[20] This is consistent with the proton chemical shifts of the cyclopropenium ion (δ = 11.2 ppm) where two electrons are delocalized over three carbon π orbitals.[53] This analogy supports delocalization of the alkyne $\pi_\perp$ electron pair to a vacant dπ orbital in the Mo-C-C triangle which is isolobal with $C_3H_3^+$.[54] ^{13}C NMR chemical shifts for these **[2-η^2-R^1CCR^2]**[I] complexes are in the range of 203-174 ppm for the bound acetylenic carbons, typical of four-electron donor alkyne ligands.[20] An empirical correlation between alkyne $\pi_\perp$ donation and ^{13}C chemical shift for the bound alkyne

carbon atoms has been articulated previously.[55]

2.3 Synthesis of [2-RCCH]$_2$ (R = Ph or ^{n}Pr)

Addition of one equiv of phenylacetylene to **1-d$_{18}$** in *n*-pentane resulted in a color change from orange-brown to green, orange, and finally burgundy over a period of 2 days, while it took approximately 4 days for completion when 1-pentyne was employed. The green intermediates are formulated as **2-d$_{18}$-η^2-RCCH**, as supported by EPR (Figure 4) and ^{2}H NMR (Figure 5) spectroscopy, with *g* values and chemical shifts in good agreement with those for complexes **2-d$_{18}$-η^2-R^{1}CCR^2** (Table 1). The time resolved ^{2}H NMR spectra are shown in Figure 5. Over a period of 48 h, the ^{2}H NMR signal for **2-η^2-PhCCH** at 9.64 ppm decreased and finally disappeared, and a new resonance appeared at 6.66 ppm attributable to **[2-RCCH]$_2$**.

It was thought possible that phenylacetylene or 1-pentyne had rearranged to give a Mo(V) vinylidene complex.[56] However, this was not the case. The structure determined by an X-ray diffraction study, shown in Figure 6, indicates that **[2-PhCCH]$_2$** is the product of dimerization, generated from a two-electron (per Mo) reductive coupling of phenylacetylene. The geometry at molybdenum is pseudo-tetrahedral and the ligand orientation lends approximate C_{2h} symmetry to the molecule. The Mo-C(1) and C(2)-C(2A) distances are 1.955(4) and 1.372(8) Å, respectively, consistent with the presence of Mo=C and C=C double bonds. The C(2)-C(2A) bond distance is slightly longer than observed for the related complexes [CpFe(dppm)]$_2$(μ-CHCHCHCH)[57] (1.323(4) Å) and comparable to that observed for [Cp'(CO)$_2$Mn]$_2$(μ-C(OEt)CHCH(OEt)C)[58] (Cp' = η^5-C$_5$H$_4$Me) (1.366(20) Å). The average Mo-N distance is 1.982(3) Å, which is typical. Carpenter

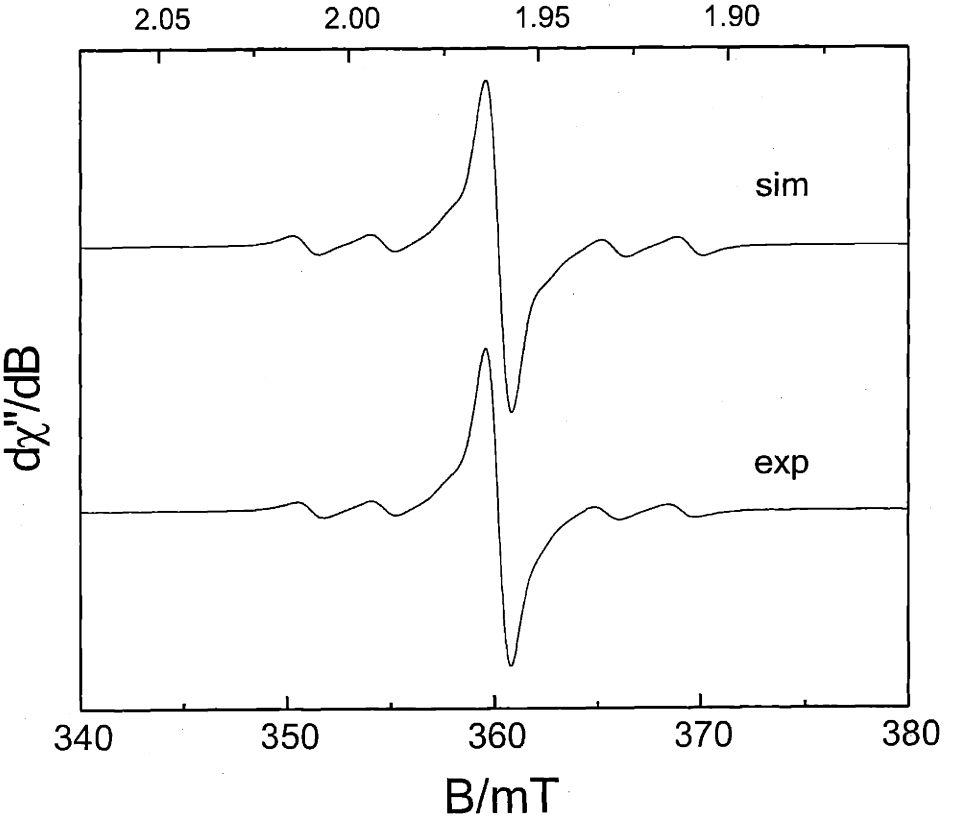

Figure 4: X-band EPR spectrum of **2-η^2-HCCPh** recorded in Et_2O at 298 K. Experimental conditions: microwave frequency ν: 9.858 GHz, Power: 20.1 mW, Modulation amplitude: 0.1 G

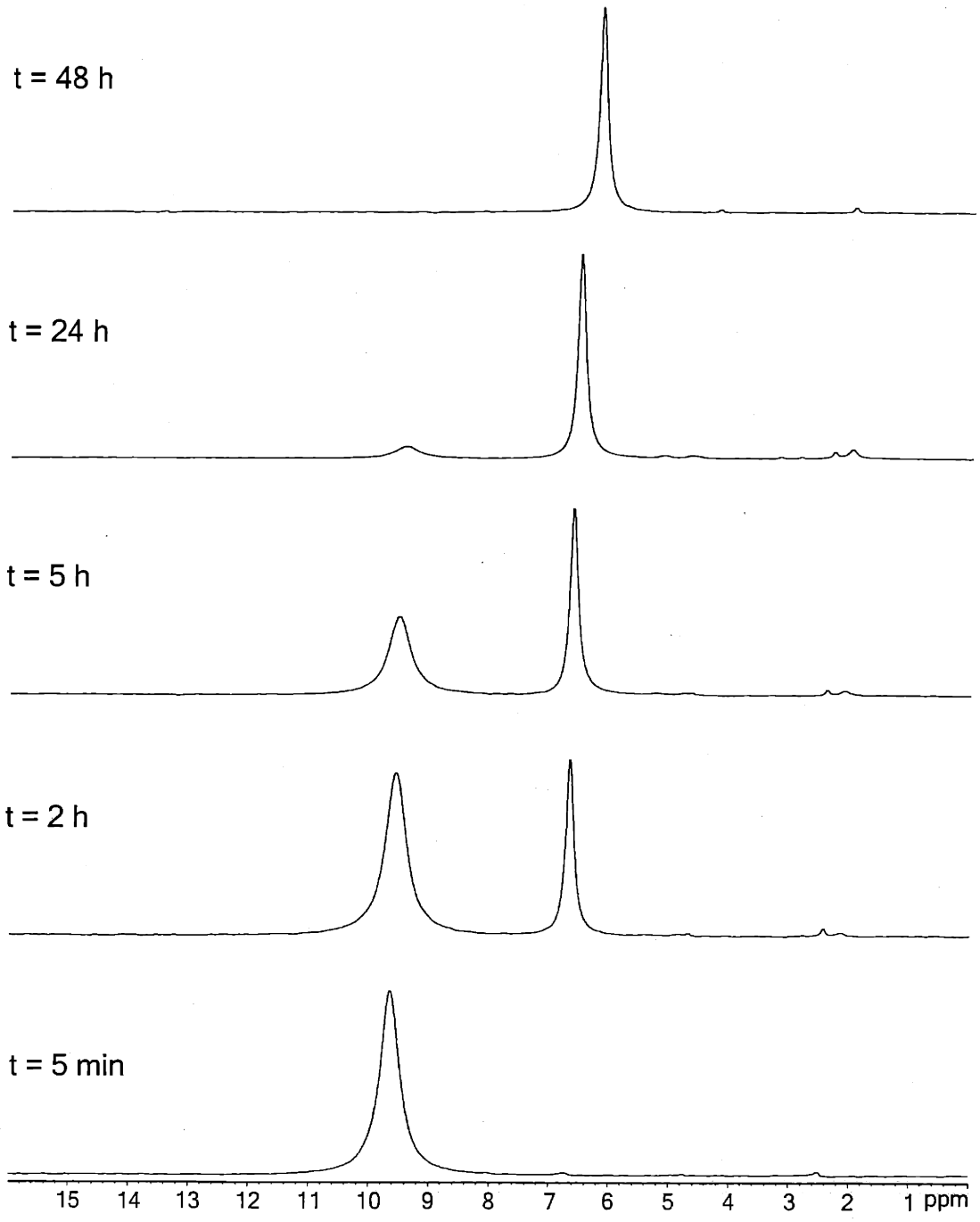

Figure 5: The dimerization of **2-η^2-HCCPh** (bottom) to form **[2-PhCCH]$_2$** (top) demonstrated by ^{2}H NMR spectra in Et_2O at 19.9 °C.

2-η^2-R^1CCR^2	g values	A_{iso} (G)	Chemical shifts (δ, ppm)
R^1 = Ph, R^2 = Ph	1.9488	34.5	8.46
R^1 = Ph, R^2 = Me	1.9543	35.4	9.64
R^1 = Et, R^2 = Et	1.9519	35.6	9.56
R^1 = H, R^2 = ^{t}Bu	1.9527	36.4	9.40
R^1 = H, R^2 = $SiMe_3$	1.9506	35.8	10.19
R^1 = H, R^2 = Ph	1.9548	37.2	9.64
R^1 = H, R^2 = ^{n}Pr	1.9532	37.0	9.41

Table 1: EPR and ^{2}H NMR spectroscopic data of **2-η^2-R^1CCR^2** recorded at room temperature.

et al.[59] described a related reaction in which phenylacetylene was 1e-coupled by [$NiBr(PEt_3)_2$] to give the [Ni(II) Ni(II)] complex (μ-PhCCHCHCPh)[$NiBr(PEt_3)_2]_2$. Alternatively, complex [**2-PhCCH**]$_2$ can be prepared by treating of **2-I** with one equiv of PhCCH in the presence of 1 equiv of Na/Hg.

Formation of the μ-bis(carbene)dimolybdenum complexes [**2-RCCH**]$_2$ (R = Ph or ^{n}Pr) might conceivably proceed *via* carbene or radical intermediates (Scheme 1).[60] The solution ^{2}H NMR data suggest that the dimerization of **2-η^2-RCCH** is irreversible. Moreover, there is no evidence for the presence of the *cis* isomer either in recrystallized samples or in the mother liquor. These dimers provide the first two cases where the four-electron reductive coupling of RCCH is effected by a mononuclear system. On the other hand, complexes **2-η^2-RCCH** (R = ^{t}Bu or $SiMe_3$) do not dimerize, an observation attributable to steric effects.

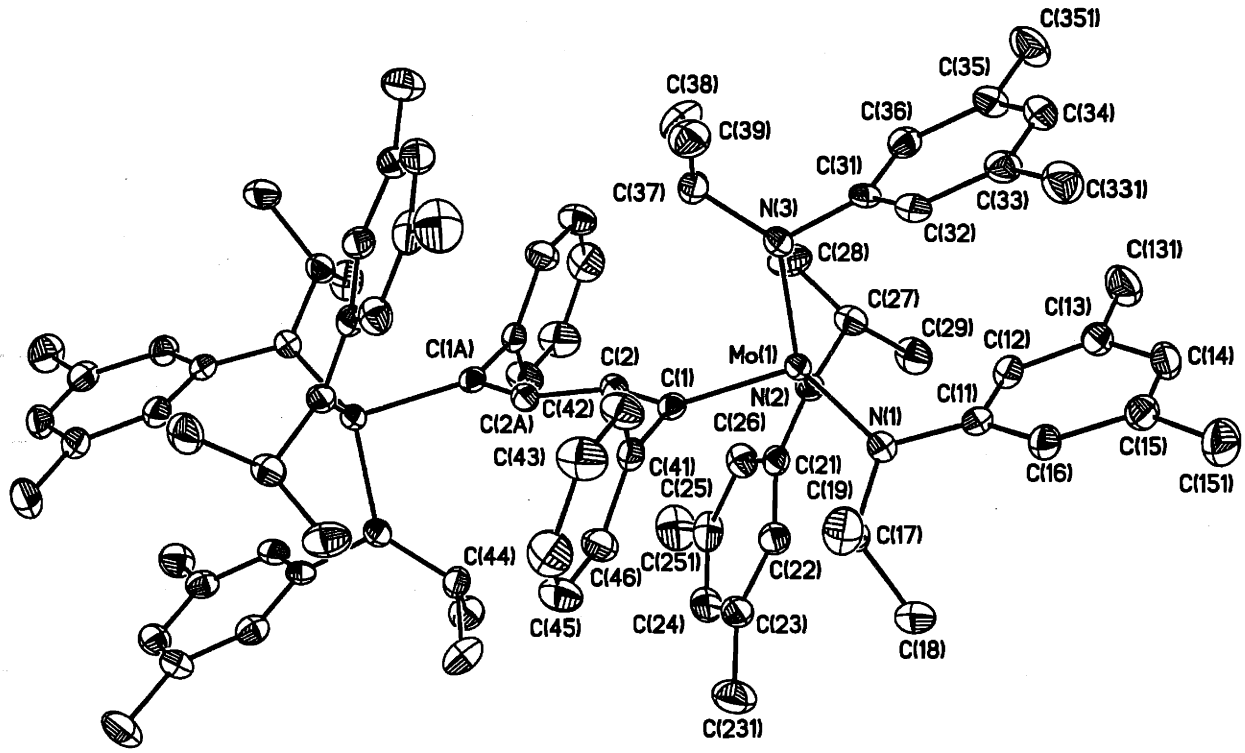

Figure 6: Thermal ellipsoid plot (35% probability) of [**2-PhCCH**]$_2$. Selected distances (Å) and angles (°): Mo(1)-N(1), 1.993(3); Mo(1)-N(2), 1.996(3); Mo(1)-N(3), 1.958(3); Mo(1)-C(1), 1.955(4); C(1)-C(2), 1.428(6); C(2)-C(2A), 1.372(8); N(1)-Mo(1)-N(2), 112.35(14); N(2)-Mo(1)-N(3), 117.13(14); N(3)-Mo(1)-N(1), 118.71(14); C(1)-Mo(1)-N(1), 111.6(2); C(1)-Mo(1)-N(2), 96.3(2); C(1)-Mo-N(3), 96.8(2); C(1)-C(2)-Mo, 120.3(3); C(1)-C(2)-C(2A), 127.0(5).

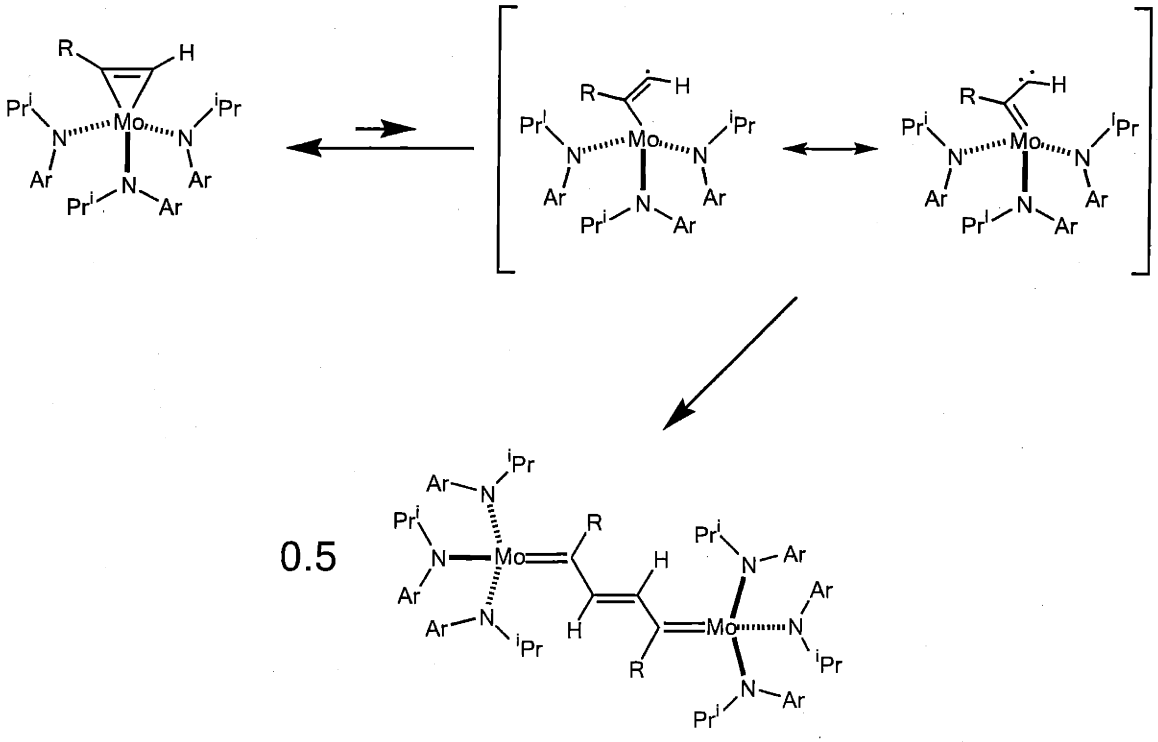

Scheme 1: Proposed mechanism for the dimerization of **2**-η^2-**RCCH**.

Both dimeric complexes [**2-PhCCH**]$_2$ and [**2-^{n}PrCCH**]$_2$ possess two unpaired electrons, μ_{eff} being 2.92 and 2.89 μ_B (Evans' method),[52] respectively. As a result, they both are [Mo(V) Mo(V)] complexes. The cyclic voltammogram of [**2-PhCCH**]$_2$ is shown in Figure 8. At low sweep rates ($v \leq 0.2$ V s^{-1}), complex [**2-PhCCH**]$_2$ exhibits two electrochemically reversible one-electron oxidation waves in THF at $E_{1/2} = -0.970$ and -0.614 V (vs. Fc/Fc$^+$). However, at higher sweep rates the first oxidation wave becomes quasi-reversible. Chemically, the violet diamagnetic dicationic salt [**2-PhCCH**]$_2^{2+}$ can be prepared by adding 5 equiv of I_2 or 2 equiv of ferrocenium or silver triflate to [**2-PhCCH**]$_2$ to yield [**2-PhCCH**]$_2$[I_{10}] or [**2-PhCCH**]$_2$(OTf)$_2$, respectively. The corresponding dark green monocationic complex [**2-PhCCH**]$_2^+$ can be prepared upon addition of one equiv of FcOTf or AgOTf to [**2-PhCCH**]$_2$, and characterized by ^{2}H NMR and EPR spectroscopy. Compound [**2-PhCCH**]$_2$(OTf) disproportionates slowly in solution to produce [**2-PhCCH**]$_2$ and [**2-PhCCH**]$_2$(OTf)$_2$. As a result, the purification of [**2-PhCCH**]$_2$(OTf) has so far been unsuccessful. Addition of a non-polar solvent (e.g. *n*-pentane) drives the reaction of equation 1 to the left, where [V V], [V VI], and [VI VI] denote [**2-PhCCH**]$_2$, [**2-PhCCH**]$_2^+$, and [**2-PhCCH**]$_2^{2+}$. Therefore, the relatively insoluble [**2-PhCCH**]$_2$(OTf)$_2$ is separated readily from [**2-PhCCH**]$_2$.

$$[V\ V] + [VI\ VI] \rightleftharpoons 2\,[V\ VI] \qquad (1)$$

The room-temperature X-band EPR spectra of both complexes [**2-PhCCH**]$_2$ and [**2-PhCCH**]$_2$(OTf) display an isotropic signal at $g_{iso} = 1.9724$ with a line-width of 8.5 G, which allows for detection of a well-resolved hyperfine structure attributed. A coupling constant of 29.8 G (A_{iso} Mo) was obtained from the simulation. Studies of previously reported mixed-valence [Fe(II) Fe(III)] and [Mn(0) Mn(I)] complexes [CpFe(dppm)]$_2$(μ-CHCHCHCH)$^+$[61] and [Cp'(CO)$_2$Mn]$_2$(μ-

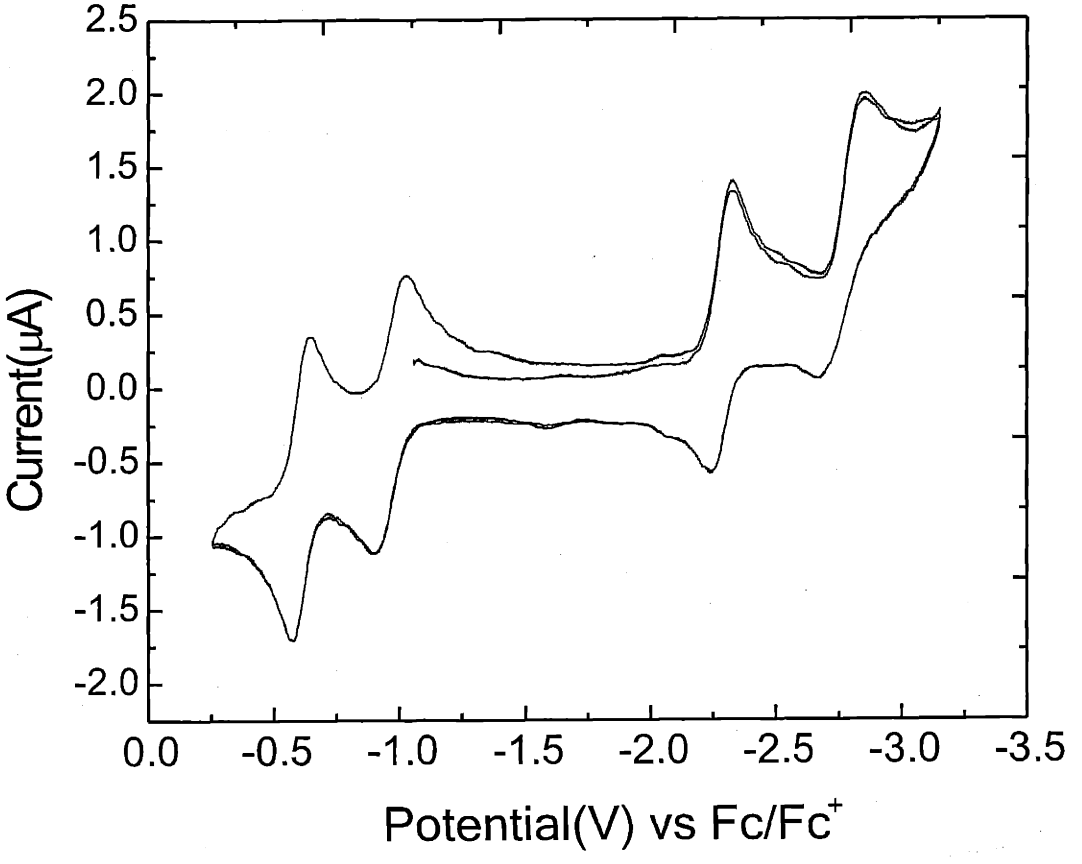

Figure 7: Cyclic voltammogram of $[\mathbf{2\text{-}PhCCH}]_2$.

C(OEt)CHCH(OEt)C)$^{-}$[58] suggested the unpaired electron to be delocalized over the two metal centers and coupled to the protons of the unsaturated bridges. Nevertheless, the experimental and simulated spectra of complexes [**2-PhCCH**]$_2$ and [**2-PhCCH**]$_2$(OTf) indicate that the two Mo centers do not communicate. Thus, the unpaired electron in the mixed-valence [Mo(V) Mo(VI)] complex is localized on the EPR time scale. On the other hand, since the ^{2}H NMR spectrum of [**2-PhCCH**]$_2$(OTf) shows a singlet, the unpaired electron in [**2-PhCCH**]$_2$(OTf) is delocalized on the NMR time scale. These observations are consistent with a type II [Mo(V) Mo(VI)] mixed-valence complex.[62]

Both compounds [**2-PhCCH**]$_2$ and [**2-^{n}PrCCH**]$_2$ show a startling lack of reactivity at 25 °C toward styrene, and even benzaldehyde, which usually reacts readily in a Wittig-like fashion with transition metal alkylidene complexes.[63–67] These observations are attributed to a combination of steric and electronic factors. An anilide nitrogen is a good σ and π donor, so [**2-PhCCH**]$_2$ and [**2-^{n}PrCCH**]$_2$ are construed to be 17-electron species without low-lying LUMO to which an incoming substrate can bind.

2.4 Syntheses of 2-η^2-vinyl complexes

Addition of one equiv of super hydride (LiHBEt$_3$) to [**2-η^2-R^{1}CCR^2**][I] (R^1 = H, R^2 = Ph, ^{t}Bu, or SiMe$_3$; R^1 = Ph, R^2 = Me, Ph; R^1 = R^2 = Et) in THF results in the formation of **2-η^2-vinyl** complexes, **2-η^2-R^{1}HCCR^2**.[26] For those cationic complexes bearing terminal alkyne ligands, hydride addition occurs regioselectively at the terminal carbon. In the case of R^1 = Ph and R^2 = Me, the hydride adds to the phenyl substituted alkyne carbon. Green has rationalized this

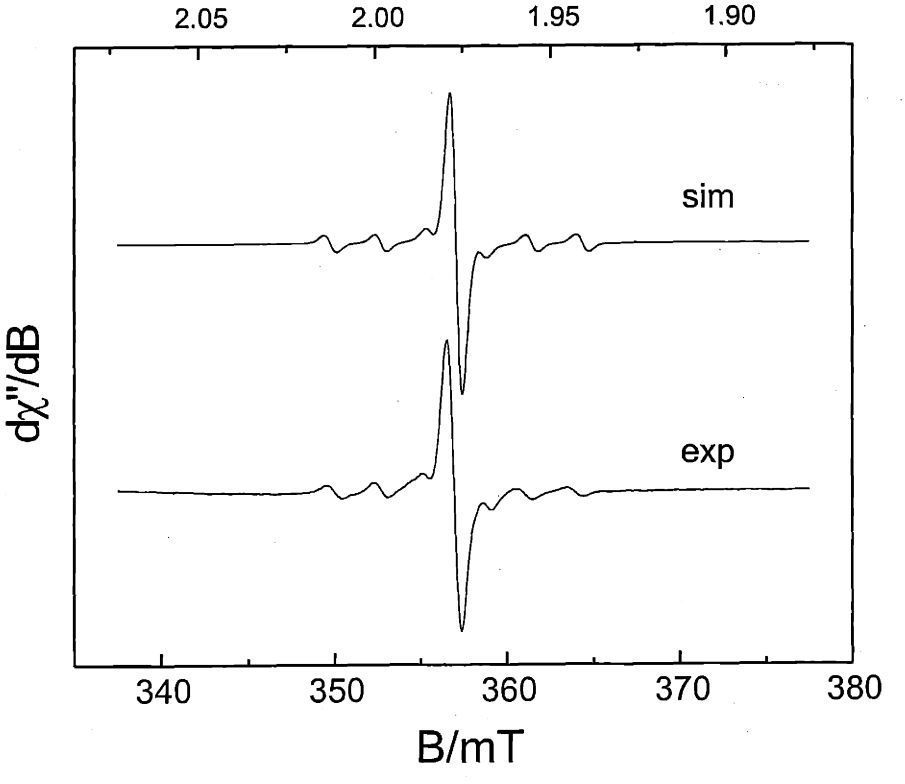

Figure 8: X-band EPR spectrum of [**2-PhCCH**]$_2$ (bottom) recorded in Et_2O at 298 K. Experimental conditions: microwave frequency ν: 9.849 GHz, Power: 20.02 mW, Modulation amplitude: 1.0 G.

regioselectivity for terminal alkynes in terms of a frontier-orbital controlled attack on the alkyne portion of the LUMO in conjunction with steric accessibility of the terminal site.[15]

^{13}C NMR spectroscopy is so far the preferred technique for identifying η^2-vinyl ligands in solution. The effective double-bond character of the Mo=C linkage is reflected in the low-field chemical shifts for α-carbons in the range of 290-266 ppm in this work.[25] The molecular structure of **2-η^2-H_2CCPh** is depicted in Figure 9. The most prominent geometrical feature in evidence for the η^2-H_2CCPh ligand is that the η^2-H_2CCPh ligand is bound asymmetrically to the metal through both carbon atoms; either a ring description or an η^2 descriptor highlights this point, and the asymmetric nature of the interaction is underscored by relevant metrical parameters. First, the Mo-C(2) bond distance is 1.920(3) Å, characteristic for a molybdenum-carbon double bond. Second, the Mo-C(1) bond distance is 2.169(4) Å, in the Mo-C single bond range. Third, the C(1)-C(2) bond distance is 1.423(5) Å, intermediate between typical C-C single and double bonds. According to the definition of an η^2-vinyl ligand by Templeton,[25] therefore, the two hydrogens on C(1) are approximately orthogonal to the MoC(1)C(2) plane and the distinction between *cis* and *trans* sites associated with the organic vinyl fragment is lost. Group 6 (Mo and W) d^4 η^2-vinyl complexes have been studied for some time by Green[15–18] and Templeton.[19–25] Nucleophilic addition to unsaturated d^4 alkyne complexes is the most common route to form η^2-vinyl complexes. In contrast, addition of nucleophiles to 2e donor alkyne ligands in coordinatively unsaturated complexes has been found to result in σ- or η^1-vinyl complexes.[68–70] No well-defined intermediate has been observed for such hydride addition reactions, but Green's work in this area is noteworthy.[16] Products of alkyl and aryl nucleophiles attack on alkyne complexes are relevant to this puzzle. Both direct attack at an alkyne carbon and initial attack at the metal are viable reaction pathways for

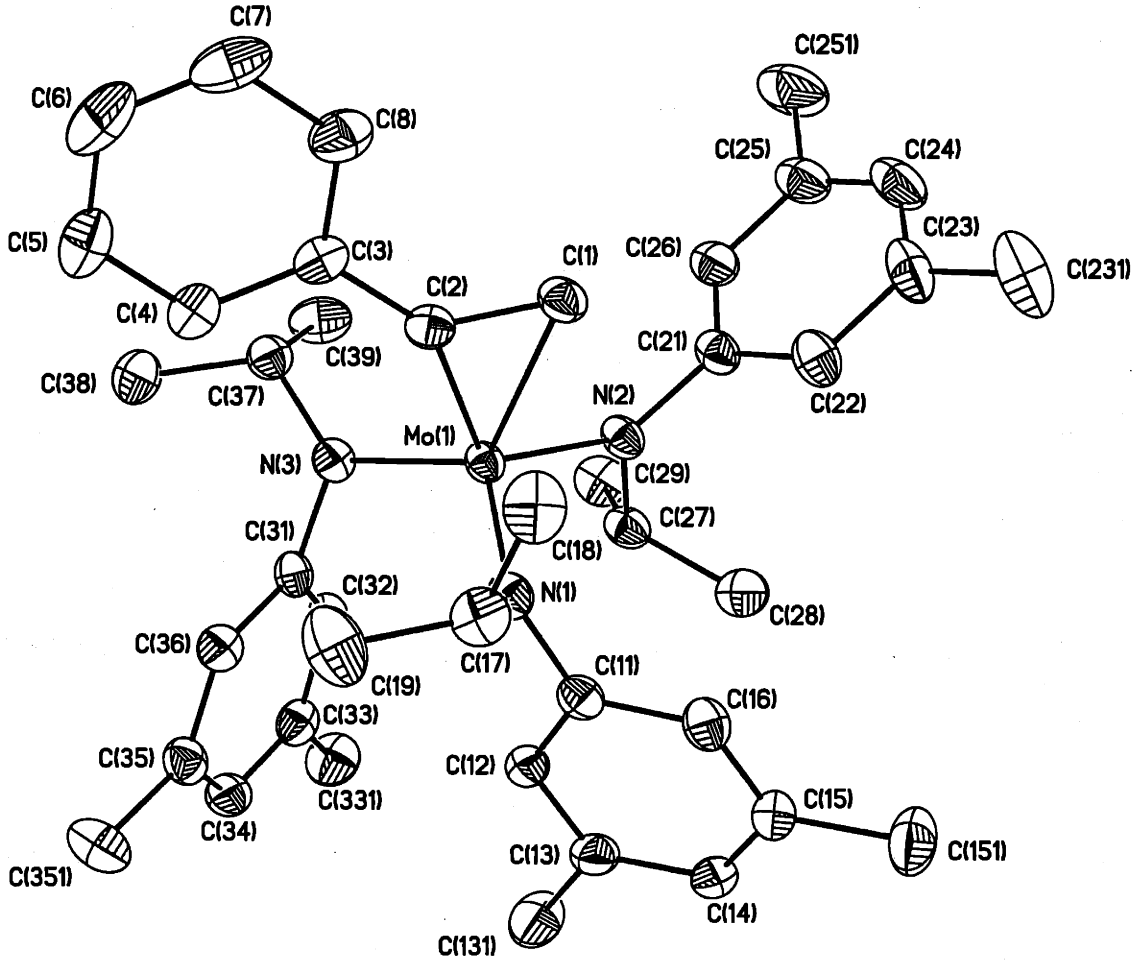

Figure 9: Thermal ellipsoid plot (35% probability) of **2-η^2-H_2CCPh**. Selected distances (Å) and angles (°): Mo(1)-C(1), 2.169(4); Mo(1)-C(2), 1.920(3); Mo(1)-N(1), 1.966(3); Mo(1)-N(2), 1.982(3); Mo(1)-N(3), 1.984(3); C(1)-C(2), 1.423(5); N(1)-Mo(1)-C(1), 100.77(14); N(2)-Mo(1)-C(1), 83.7(13); N(3)-Mo(1)-C(1), 123.88(14); C(2)-Mo(1)-N(1), 99.59(13); C(2)-Mo(1)-N(2), 119.56(13); C(2)-Mo(1)-N(3), 92.45(13); C(1)-C(2)-Mo(1), 79.4(2); C(2)-C(1)-Mo(1), 60.4(2); C(2)-Mo(1)-C(1), 40.2(2); N(1)-Mo(1)-N(2), 114.56(12); N(2)-Mo(1)-N(3), 109.75(12); N(3)-Mo(1)-N(1), 119.16(12).

alkyl nucleophiles.[16] Although hydride migrations from metal to ligand are expected to be more facile than alkyl migrations, direct attack of hydride at an alkyne carbon seems viable, especially for sterically-hindered metal centers.

An alternative synthesis of complex **2-η^2-$H_2CCSiMe_3$** is to add 0.6 equiv of H_2SnPh_2 to **2-η^2-$HCCSiMe_3$**. The diphenyltin formed as a byproduct[71] is polymeric and separated easily by filtration, so **2-η^2-$H_2CCSiMe_3$** was obtained readily upon recrystallization in 68% yield. This one-step reaction procedure has a distinct advantage over the oxidation/hydride-addition sequence employed previously.

2.5 Syntheses of Alkylidyne Complexes

Heating a toluene solution of **2-η^2-$H_2CCSiMe_3$** to 80 °C for 12 h induced isomerization to its alkylidyne counterpart, $Me_3SiCH_2CMo(N[^iPr]Ar)_3$ (**2-CCH_2SiMe_3**), the isomerization being thought to involve 1,2-trimethylsilyl migration.[17] Characteristic of the alkylidyne functional group is the α-carbon resonance at δ 302.0 ppm in the molecule's ^{13}C NMR spectrum. Heating other **2-η^2-vinyl** complexes does not lead to the analogous alkylidyne products; rather they are thermally stable.

Isomerization of d^4 Mo- and W-η^2-vinyl complexes to carbyne complexes is an important class of η^2-vinyl ligand transformations.[25] Thermolysis of the trimethylsilylvinyl complex (η^2-$H_2CCSiMe_3$)Mo(Ind)L_2 was found to result in 1,2-$SiMe_3$ migration to form a carbyne product, $Me_3SiCH_2CMo(Ind)L_2$.[17] Addition of hydride to $[(\eta^2\text{-}^iPrCCH)MoCpL_2]^+$ in the presence of excess $P(OMe)_3$ at room temperature allowed direct access to the carbyne product, $^iPrCH_2CMoCpL_2$.[16] Reaction of $[(\eta^2\text{-HCCH})WTp'(CO)_2]^+$ with $LiHBEt_3$ at $-78°C$ in THF forms a spectroscopi-

cally observable η^2-vinyl intermediate before forming the ethylidyne complex, MeCWTp'$(CO)_2$.[24] Trimethylsilyl migration for $(\eta^2$-$H_2CCSiMe_3)$WTp'$(CO)_2$ to form $Me_3SiCH_2CWTp'(CO)_2$ also has been documented.[24]

Schrock's trialkoxytungsten(VI) alkylidyne complexes, typified by $^tBuCW(O^tBu)_3$, have been employed recently for organic transformations.[31–33] Molybdenum analogs are expected to be more tolerant to a heteroatom functionality in the alkyne substrate than are the tungsten-based systems.[72] They also may be expected to exhibit different rate profiles. Although mechanistic aspects are not yet clear, the three-coordinate molybdenum(III) complex **3**, or its monohalo derivatives, have been found to be excellent alkyne metathesis catalyst precursors for the synthesis of large organic rings.[72] In contrast, complex **2-CCH$_2$SiMe$_3$** is unreactive towards acetylenes even under coaxing conditions (toluene solution, 80 °C, 24 h). Like the molybdenum methylidyne complex **3-CH**,[8,9] **2-CCH$_2$SiMe$_3$** contains three π-donating amido nitrogens. Therefore, **2-CCH$_2$SiMe$_3$** is an 18-electron species without low-energy LUMO to which an incoming alkyne can bind.

Treatment of complex **2-CCH$_2$SiMe$_3$** with 3 equiv of 1-adamantanol, 2-methyl-2-propanol, 1-adamantanethiol, S-2′-methoxy-[1,1′]binaphthalenyl-2-ol (HOAr*), or 2 equiv of 2,6-diphenylphenol generates $Me_3SiCH_2CMo(ER)_3$ (E = O or S) and Me_3SiCH_2CMo(O-2,6-diphenylphenyl)$_2$(N[^{i}Pr]Ar) in high yields (82-88%). With the exception of $Me_3SiCH_2CMo(O^tBu)_3$, which could not be separated from the HN^{i}PrAr by-product, all alkylidyne complexes were recrystallized from THF/*n*-pentane, as a result of minimal solubility in pentane. The α-carbon ^{13}C NMR chemical shifts were observed in the range 276 to 312 ppm. X-ray diffraction studies of Me_3SiCH_2CMo(O-1-Ad)$_3$[26] and Me_3SiCH_2CMo(O-2,6-diphenylphenyl)$_2$(N[^{i}Pr]Ar) (Figure 10) indicate that both compounds are monomeric and exhibit MoC bond lengths of 1.754(6) and 1.722(4) Å, respectively, consistent with

the observed ^{13}C NMR chemical shifts. A prominent structural feature for the latter is that the amido nitrogen remains planar and the Mo-N distance is 1.930(3) Å in keeping with its π-donating character. The two phenoxide ligand mean planes are almost mutually perpendicular. It may be presumed that $Me_3SiCH_2CMo(O\text{-}2,6\text{-}diphenylphenyl)_3$ would exhibit threefold symmetry, although the complex has eluded preparation. Evidently, 2,6-diphenylphenol is too bulky for the remaining anilide ligand.

With the exception of $Me_3SiCH_2CMo(S\text{-}1\text{-}Ad)_3$, these new alkylidyne derivatives show high reactivity towards acetylenes. For example, treatment of complex $Me_3SiCH_2CMo(O\text{-}1\text{-}Ad)_3$ in etheral solution with 10 equiv of 3-hexyne led to the formation of the propylidyne derivative, $EtCMo(O\text{-}1\text{-}Ad)_3$ in 92% yield at room temperature.[26] A further illustration of the alkyne metathesis capability of trialkoxymolybdenum(VI) alkylidyne complexes is the preparation of symmetrical non-volatile alkynes RCCR (Table 2) in high yields from corresponding precursor alkynes MeCCR, with 2-butyne as a volatile side product. The catalytic alkyne metathesis reactions were conducted in toluene at room temperature under dynamic vacuum using 2 mol% of $Me_3SiCH_2CMo(OAr^*)_3$, which was found to be the most efficient catalyst scrutinized. Purification of the alkyne product RCCR was accomplished *via* chromatography. The ethylidyne complex $MeCMo(O\text{-}1\text{-}Ad)_3$, formed in the course of these catalytic reactions, was observed spectroscopically.[26]

An alkoxide or phenoxide oxygen is a poorer σ- and π- donor than an amido nitrogen, rendering the metal more electron-deficient, facilitating the formation of base adducts. Figure 11 shows the molecular structure of the propylidyne THF adduct $EtCMo(O\text{-}1\text{-}Ad)_3(THF)$, which was prepared by adding THF to the propylidyne complex $EtCMo(O\text{-}1\text{-}Ad)_3$ in ethereal solution. The Mo-C(1) distance is 1.745(4) Å while the Mo-O(4) distance is 2.529(3) Å. In solution, according to ^1H NMR

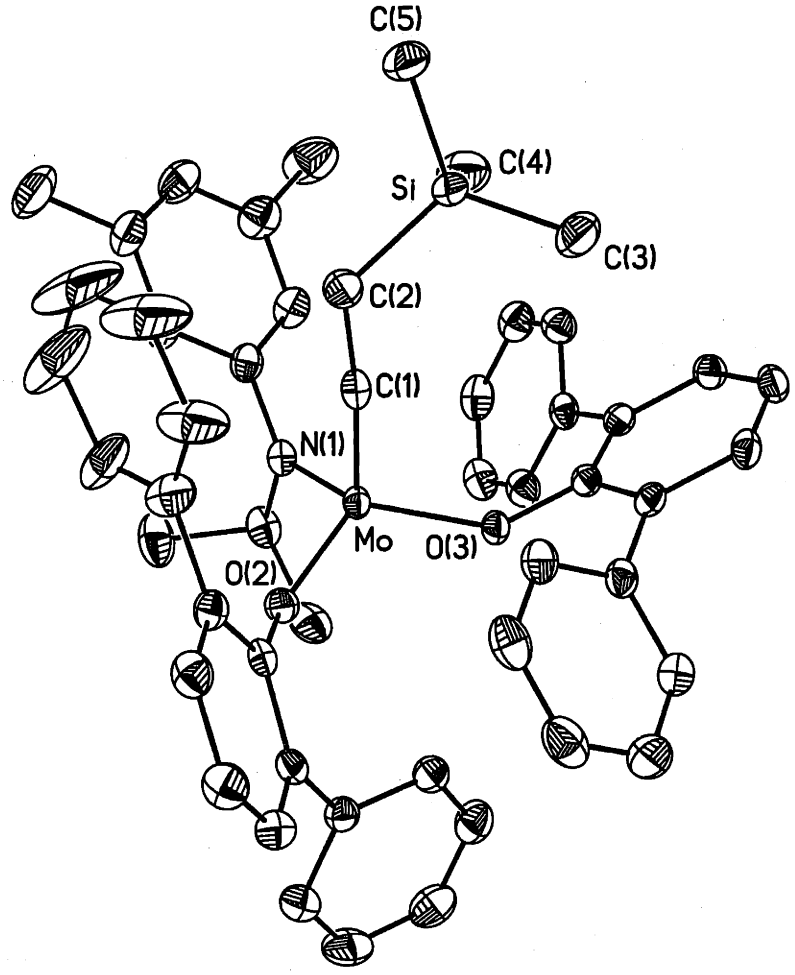

Figure 10: Thermal ellipsoid plot (35% probability) of $Me_3SiCH_2CMo(O\text{-}2,6\text{-}diphenylphenyl)_2(N[^iPr]Ar)$. Selected distances (Å) and angles (°): Mo-C(1), 1.722(4); Mo-N(1), 1.930(3); Mo-O(2), 1.944(3); Mo-O(3), 1.947(2); C(1)-Mo-N(1), 96.8(2); C(1)-Mo-O(2), 108.4(2); C(1)-Mo-O(3), 106.1(2); N(1)-Mo-O(2), 111.61(12); N(1)-Mo-O(3), 112.97(12); O(2)-Mo-O(3), 118.39(11).

data, the THF ligand dissociates. This observation is consistent with only a weak interaction between the Mo center and the THF ligand. The formation and structure of $EtCMo(O\text{-}1\text{-}Ad)_3(THF)$ supports the idea that trialkoxymolybdenum(VI) alkylidyne complexes are electron-deficient and accounts also for the low yields of alkyne metathesis products when the alkynes incorporates a donor atom. Complex $Me_3SiCH_2CMo(S\text{-}1\text{-}Ad)_3$ displays no reactivity towards ordinary acetylenes,[73] consistent with the strong π-donating nature of the thiolate ligands. The mixed-ligand derivative $Me_3SiCH_2CMo(O\text{-}2,6\text{-}diphenylphenyl)_2(N[^iPr]Ar)$ does exhibit alkyne metathesis activity. Further underscoring the alkyne metathesis capability of $Me_3SiCH_2CMo(O\text{-}2,6\text{-}diphenylphenyl)_2(N[^iPr]Ar)$ is the preparation of RCCR ($R = CH_2CH_2OTs$) in 74% yield from the precursor MeCCR. This reaction was conducted in toluene solvent under dynamic vacuum at ambient temperature using 10 mol % of $Me_3SiCH_2CMo(O\text{-}2,6\text{-}diphenylphenyl)_2(N[^iPr]Ar)$.

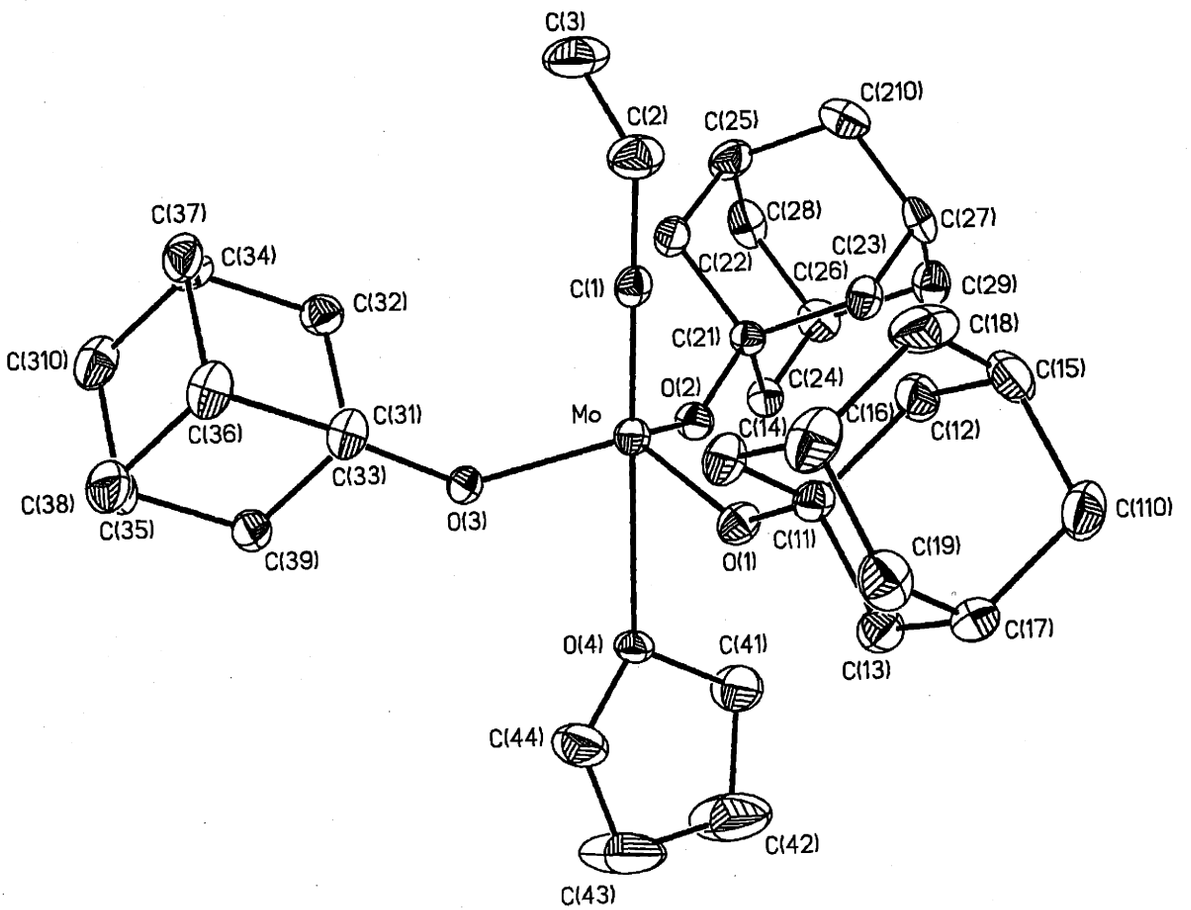

Figure 11: Thermal ellipsoid plot (35% probability) of the THF adduct alkylidyne compound EtCMo(O-1-Ad)$_3$(THF). Selected distances (Å) and angles (°): Mo-C(1), 1.745(4); Mo-O(1), 1.897(3); Mo-O(2), 1.899(3); Mo-O(3), 1.898(3); Mo-O(4), 2.529(3); C(1)-Mo-O(1), 102.6(2); C(1)-Mo-O(2), 104.7(2); C(1)-Mo-O(3), 103.9(2); O(1)-Mo-O(2), 114.45(11); O(3)-Mo-O(2), 115.59(12); O(1)-Mo-O(3), 113.56(12).

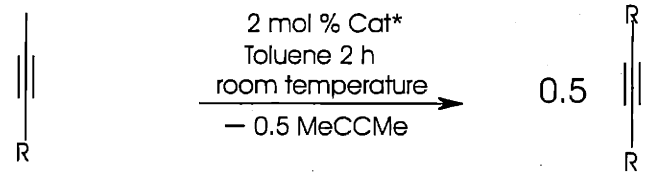

Cat* ≡

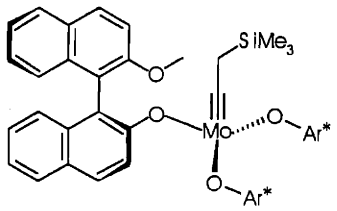

R	Isolated yield %
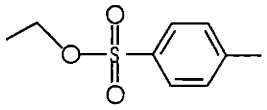	95
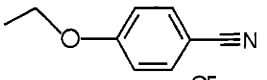	90
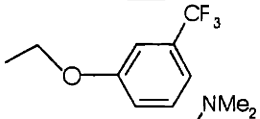	86
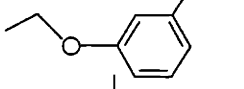	85
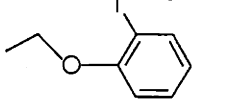	83
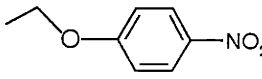	76
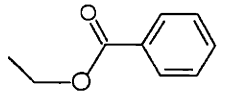	67
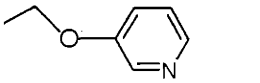	17
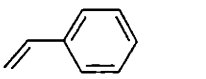	86

Table 2: The varied yields of alkyne *via* alkyne metathesis reactions catalyzed by $Me_3SiCH_2CMo(OAr^*)_3$

3 Summary and Conclusions

In conclusion, it has been demonstrated that the reactive and unsaturated metal fragment **2** binds readily to both terminal and internal alkynes, as well as to styrene. The odd-electron neutral green adducts thus obtained are of interest for their structural and other physicochemical properties, which have been probed in some detail. Of particular note is the observation that the sterically stressed styrene adduct provides an example of a triple-agostic interaction with three amido β hydrogens. Another key advance has been the utilization of a trimethylsilylacetylene adduct as the starting point for a high-yield synthesis of alkoxymolybdenum alkyne metathesis catalysts. Since the catalyst synthesis involves simple protolytic replacement of amido ligands, a variety of new catalysts now are seen to be readily accessible. Furthermore, the same protolytic replacement reaction allowed the synthesis of an alkylidyne species supported by thiolate ligands, this process being illustrative of a general method for incorporation of the molybdenum(VI) alkylidyne functionality.

4 Experimental Section

4.1 General considerations

Unless stated otherwise, all operations were performed in a Vacuum Atmospheres dry box under an atmosphere of purified dinitrogen or using Schlenk techniques under an argon atmosphere. Complexes **1** and **1-d_{18}**[13] S-2′-methoxy-[1,1′]binaphthalenyl-2-ol,[74] and Ph_2SnH_2[71] were prepared according to the published literature. Diphenylacetylene, 3,3-dimethyl-1-butyne, 3-hexyne, 1-pentyne, phenylacetylene, 1-phenyl-1-propyne, styrene, 2-methyl-2-propanol, 1-adamantanol, lithium triethylborohydride (1M in THF) were purchased from Aldrich, trimethylsilylacetylene was purchased from Alfa Aesar, and 2,6-diphenylphenol was purchased from Lancaster Synthesis. Diethyl ether, *n*-pentane, and *n*-hexane were dried and deoxygenated by the method of Grubbs.[75] THF was distilled over Na/benzophenone and collected under dinitrogen. C_6D_6 and $CDCl_3$ were degassed and dried over 4 Å molecular sieves. Celite, alumina, and 4 Å molecular sieves were dried in vacuo overnight at a temperature above 200 °C. The room temperature X-band EPR spectra were recorded on a Bruker EMX spectrometer. Acquisition, simulation, and data post processing of the liquid solution spectra were performed by using an integrated WIN-EPR software package (Bruker). Cyclic voltammetry measurements were carried out using a Eco-Chemie Autolab potentiostat (pgstat20) and the GPES 4.3 software in conjuction with a three-electrode cell using 0.5 M $[NBu^n_4][PF_6]$ solutions in tetrahydrofuran. ^1H, ^2H, and ^{13}C NMR spectra were recorded on a Varian XL-501 spectrometer. Chemical shifts are reported with respect to internal solvent (7.15 ppm (^1H and ^2H) and 128.39 (t) (^{13}C) ppm (C_6D_6)). Elemental analyses for C, H, and N were performed by H. Kolbe Mikroanalytisches Laboratorium, Mülheim an der Ruhr, Germany.

4.2 Synthesis of 2-η^2-H_2CCHPh

To 0.402 g (0.669 mmol) of **1-d_{18}** in 10 mL of *n*-pentane were added 0.087 g (0.835 mmol) of styrene. The resulting mixture became yellowish green. After stirring for 1 hour, all volatile material were removed in vacuo, and a dark brown solid residue was washed with cold *n*-pentane. The dark brown solid was dried in vacuo. Total yield = 0.338 g (71.6%). ^{2}H NMR (Et_2O, 19.3 °C) δ: 8.50 ($\Delta\nu_{1/2}$= 48 Hz), 7.41 ($\Delta\nu_{1/2}$= 34 Hz) ppm. μ_{eff} = 1.89 μ_B. Anal. Calcd. for $C_{41}H_{56}N_3Mo$: C, 71.70; H, 8.22; N, 6.12. Found: C, 71.59; H, 8.16; N, 6.11.

4.3 Oxidation of 2-η^2-H_2CCHPh

To 0.212 g (0.309 mmol) of **2-η^2-PhC(H)CH_2** in 5 mL of diethyl ether were added 0.039 g (0.155 mmol) of I_2 in 5 mL of diethyl ether. The mixture became green right away. The ^{1}H NMR spectrum indicated the presence of **2-I** and styrene.

4.4 Syntheses of 2-d_{18}-η^2-R^1CCR^2 (R^1 = Ph, R^2 = Ph, Me; R^1 = R^2 = Et; R^1 = H; R^2 = ^{t}Bu, $SiMe_3$)

Since the preparation of all these complexes was carried out in essentially the same way, the preparation of **2-d_{18}-η^2-PhCCPh** is given in detail. To 1.011 g (1.683 mmol) of **1-d_{18}** in 20 mL of diethyl ether under argon were added 0.300 g (1.683 mmol) of diphenylacetylene in 5 mL of diethyl ether. The resulting mixture was stirred at room temperature, and its color became green from orange-brown overnight. Diethyl ether was removed in vacuo, and the oily residual was dissolved in

5 mL of hexamethyldisiloxane, and the green solution was stored in a freezer at −35 °C. One crop of crystals (0.829 g, 1.064 mmol, 63.2%) was collected by suction filtration after 2 days. **2-d_{18}-η^2-PhCCPh**: ^{2}H NMR (Et_2O, 19.8 °C) δ: 8.46 ($\Delta\nu_{1/2}$= 57 Hz) ppm. μ_{eff} = 1.84 μ_B (Evans' method, C_6D_6, 19.8 °C). Anal. Calcd. for $C_{47}H_{58}N_3Mo$: C, 74.19; H, 7.68; N, 5.52. Found: C, 74.33; H, 7.76; N, 5.67. **2-d_{18}-η^2-PhCCMe**: ^{2}H NMR (Et_2O, 20.3 °C) δ: 9.64 ($\Delta\nu_{1/2}$= 29.0 Hz) ppm. **2-d_{18}-η^2-EtCCEt**: ^{2}H NMR (Et_2O, 20.3 °C) δ: 9.56 ($\Delta\nu_{1/2}$= 24.0 Hz) ppm. **2-d_{18}-η^2-^{t}BuCCH**: ^{2}H NMR (Et_2O, 20.3 °C) δ: 9.40 ($\Delta\nu_{1/2}$= 24.0 Hz) ppm. **2-d_{18}-η^2-Me_3SiCCH**: ^{2}H NMR (Et_2O, 20.3 °C) δ: 10.19 ($\Delta\nu_{1/2}$= 34.4 Hz) ppm.

4.5 Synthesis of [2-η^2-R^1CCR^2][I] (R^1 = Ph, R^2 = Ph, Me; R^1 = R^2 = Et; R^1 = H; R^2 = ^{t}Bu, $SiMe_3$)

Since the preparation of all these complexes was carried out in essentially the same way, the preparation of [2-η^2-PhCCPh][I] is given in detail. To 0.313 g (0.411 mmol) of 2-η^2-PhCCPh in 10 mL of *n*-pentane were added 0.052 g (0.206 mmol) of I_2 in 3 mL of diehtyl ether. A yellow solid started to precipitate out of the green solution. After stirring for 2 hours, 0.327 g (0.368 mmol, 89.5%) of yellow solid were collected by suction filtration and dried in vacuo. [2-η^2-PhCCPh][I]: ^{1}H NMR ($CDCl_3$, 19.8 °C): δ: 7.34 (br, 4H), 7.14 (br, 4H), 6.78 (br, 2H), 6.23 (s, 9H, *ortho* and *para*-3,5-$C_6H_3Me_2$), 4.44 (q, 3H, methine), 2.11 (s, 18H, 3,5-$C_6H_3\mathit{Me}_2$), 0.88 (d, 18H, -CHMe_2) ppm. ^{13}C NMR ($CDCl_3$, 19.8 °C): δ: 185.52, 141.60, 137.82, 132.17, 129.86, 129.48, 128.05, 127.52, 125.32, 58.83, 21.73, 20.47 ppm. Anal. Calcd. for $C_{47}H_{58}N_3IMo$: C, 63.58; H, 6.58; N, 4.73. Found: C, 63.69; H, 6.72; N, 4.89.

[**2-η^2-PhCCMe**][I]: 89%, ^{1}H NMR ($CDCl_3$, 20.1 °C): δ: 7.66 (d, 2H), 7.62 (t, 2H), 7.56 (t, 1H), 6.96 (s, 3H, *para*-3,5-$C_6H_3Me_2$), 6.38 (s, 6H, *ortho*-3,5-$C_6H_3Me_2$), 4.36 (q, 3H, methine), 2.53 (s, 3H, -CH_3), 2.27 (s, 18H, 3,5-C_6H_3*Me*$_2$), 0.96 (d, 18H, -CH*Me*$_2$) ppm. ^{13}C NMR ($CDCl_3$, 19.8 °C): δ: 202.88, 194.63, 143.85, 139.15, 131.79, 131.62. 130.65, 130.56, 129.51, 126.20, 59.07, 22.47, 21.51 ppm.

[**2-η^2-EtCCEt**][I]: 92%, ^{1}H NMR (C_6D_6, 20.1 °C): δ: 6.81 (s, 6H, *ortho*-3,5-$C_6H_3Me_2$), 6.75 (s, 3H, *para*-3,5-$C_6H_3Me_2$), 5.16 (q, 3H, methine), 3.03 (q, 4H, -C*H*$_2$CH$_3$), 2.30 (s, 18H, 3,5-C_6H_3*Me*$_2$), 1.18 (d, 18H, -CH*Me*$_2$), 1.08 (t, 3H, -CH_2C*H*$_3$) ppm. ^{13}C NMR (C_6D_6, 20.1 °C): δ: 192.17, 147.02, 139.17, 129.98, 126.63, 57.70, 27.34, 23.20, 21.93, 14.83 ppm.

[**2-η^2-^{t}BuCCH**][I]: 91% ^{1}H NMR ($CDCl_3$, 20.1 °C): δ: 9.55 (s, 1H, ^{t}BuCC*H*), 6.80 (s, 3H, *para*-3,5-$C_6H_3Me_2$), 6.19 (s, 6H, *ortho*-3,5-$C_6H_3Me_2$), 4.04 (q, 3H, methine), 2.12 (s, 18H, 3,5-C_6H_3*Me*$_2$). 1.34 (s, 9H, ^{t}Bu), 0.83 (d, 18H, -CH*Me*$_2$) ppm. ^{13}C NMR ($CDCl_3$, 19.8 °C): δ: 190.26, 177.37, 138.73, 130.21, 125.39, 59.43, 38.73, 31.15, 22.31, 21.03 ppm.

[**2-η^2-Me$_3$SiCCH**][I]: 95%, ^{1}H NMR ($CDCl_3$, 20.1 °C): 9.68 (s, 1H, Me_3SiCC*H*), 6.86 (s, 3H, *para*-3,5-$C_6H_3Me_2$), 6.22 (s, 6H, *ortho*-3,5-$C_6H_3Me_2$), 4.06 (q, 3H, methine), 2.18 (s, 18H, 3,5-C_6H_3*Me*$_2$), 0.86 (d, 18H, -CH*Me*$_2$), 0.41 (s, 9H, *Me*$_3$SiCCH) ppm. ^{13}C NMR ($CDCl_3$, δ): 188.60, 174.16, 142.56, 138.78, 130.39, 125.80, 59.09, 21.77, 21.13, 0.41. Anal. Calcd for $C_{38}H_{58}N_3IMoSi$: C, 56.50; H, 7.24; N, 5.20. Found: C, 56.38; H, 7.21; N, 5.12 ppm.

4.6 Syntheses of [2-d_{18}-RCCH]$_2$, R = Ph, ^{n}Pr

To 0.998 g (1.661 mmol) of **1-d_{18}** in 15 mL of *n*-pentane were added 0.339 g (3.322 mmol) of phenylacetylene. The resulting mixture became green and then burgundy in 30 min, and a red precipitate started to precipitate out of solution. After stirring overnight, 0.792 g (0.563 mmol, 67.8%) of brick-red solid were collected by suction filtration, and washed with *n*-pentane. [**2-d_{18}-PhCCH**]$_2$: ^{2}H NMR (Et_2O, 19.8 °C): δ: 6.66 ($\Delta\nu_{1/2}$= 32 Hz) ppm. μ_{eff} = 2.96 μ_B (Evans' method, C_6D_6, 19.8 °C). Anal. Calcd. for $C_{82}H_{108}N_6Mo_2$: C, 71.91; H, 7.95; N, 6.14. Found: C, 72.08; H, 8.07; N, 6.25. [**2-d_{18}-^{n}PrCCH**]$_2$: ^{2}H NMR (Et_2O, 19.8 °C): δ 6.76 ($\Delta\nu_{1/2}$= 16 Hz) ppm. μ_{eff} = 2.87 μ_B (Evans' method, C_6D_6, 19.8 °C).

4.7 Syntheses of [2-PhCCH]$_2$[O_3SCF_3]$_2$

To 0.346 g (0.253 mmol) of [**2-PhCCH**]$_2$ in 10 mL of diethyl ether were added 0.169 g (0.504 mol) [$(C_5H_5)_2Fe$][O_3SCF_3] in 10 mL of THF. The resulting mixture became violet and was stirred for 2 hours. All volatile material were removed in vacuo. The solid residue was collected on a frit and washed with *n*-pentane until the filtrate is colorless. The yield was 92.1% (0.389 g, 0.233 mmol). ^{1}H NMR (C_5D_5N, 20.1 °C) δ: 7.82 (t, 2H, Ph), 7.62-7.58 (m, 6H, Ph), 7.07 (s, 6H, *para*-3,5-$C_6H_3Me_2$), 6.62 (s, 2H, PhCC*H*), 6.33 (s, 6H, *ortho*-3,5-$C_6H_3Me_2$), 4.33 (q, 6H, methine), 2.33 (s, 36H, 3,5-C_6H_3*Me*$_2$), 1.01 (d, 36H, CH*Me*$_2$) ppm. Anal. Calcd. for $C_{84}H_{108}N_6F_6Mo_2O_6S_2$: C, 60.49 ; H, 6.53 ; N, 5.04. Found: C, 60.61; H, 6,67; N, 5.17.

4.8 Synthesis of [2-η^2-PhCCH][I]

To 0.467 g (0.658 mmol) of **2-I** in 15 mL of *n*-pentane were added 0.134 g (1.312 mmol) phenylacetylene. A yellow solid started to precipitate out of the green solution in 5 min. After stirring overnight, 0.482 g (0.594 mmol, 90.3%) of yellow solid were collected by suction filtration, washed with *n*-pentane until the filtrate colorless, and dried in vacuo. ^{1}H NMR ($CDCl_3$, 19.8 °C) δ: 10.28 (s, 1H, *H*CCPh), 7.90 (d, 2H, HCC*Ph*), 7.64 (d, 3H, HCC*Ph*), 6.97 (s, 3H, *para*-Ar), 6.34 (s, 6H, *ortho*-Ar), 4.23 (q, 3H, methine), 2.25 (s, 18H, Ar-*Me*), 0.95 (d, 18H, CH*Me*$_2$) ppm. ^{13}C NMR ($CDCl_3$, δ): 178.76, 174.61, 142.28, 139.17, 133.34, 132.87, 130.96, 129.71, 126.60, 59.94, 21.86, 21.52 ppm. Anal. Calcd. for $C_{41}H_{54}N_3IMo$: C, 60.67; H, 7.18; N, 5.18. Found: C, 60.81; H, 7.30; N, 5,31.

4.9 Reduction of [2-d_{18}-η^2-PhCCH][I]

To 0.223 g (0.269 mmol) [**2-d_{18}-η^2-PhCCH**][I] in 10 mL of tetrahydrofuran were added 1 equiv of 0.5% Na/Hg. The resulting mixture gradually became green to orange and burgundy in 2 hour. ^{2}H NMR spectrum of the burgundy solution showed the formation of [**2-PhCCH**]$_2$.

4.10 Synthesis of 2-η^2-R^1(H)CCR^2 (R^1 = Ph, R^2 = Ph, Me; R^1 = R^2 = Et; R^1 = H; R^2 = ^{t}Bu, SiMe$_3$)

Since the preparation of all these complexes was carried out in essentially the same way, the preparation of **2-η^2-H$_2$CCSiMe$_3$** is given in detail.

Method 1: To 5.120 g (6.338 mmol) of [**2-η^2-HCCSiMe$_3$**][I] in 125 mL of tetrahydrofuran were added LiHBEt$_3$ (1.0 M in THF, 7.0 mL, 7.0 mmol). A color change from orange to dark yellow was quickly observed. All volatile material were removed in vacuo after 1 h, and the yellow solid was extracted into 200 mL of *n*-pentane. The resulting solution was filtered through a plug of Celite, and the removal of solvent generated 4.063 g (5.958 mmol, 94% yield) of yellow solid **2-η^2-H$_2$CCSiMe$_3$**.

Method 2: To 4.214 g of **1** (7.076 mmol) in 50 mL of diethyl ether were added 1.2 equiv of HCCSiMe$_3$. The resulting mixture gradually turned green in a few minutes. After stirring for 1 h, all volatile material were removed in vacuo, and the oily residual was dissolved in 20 mL of *n*-pentane. To this green solution were added 0.6 equiv of H_2SnPh_2. The green solution gradually became yellow in 15 min. After stirring for 3 h, the solution was filtered through a plug of Celite and a light brown oily residue was obtained upon removal of all volatile material in vacuo. The complex **2-η^2-H$_2$CCSiMe$_3$** was isolated in 68% after recrystallization from *n*-pentane at -35 °C. ^{1}H NMR (C_6D_6, 20.1 °C) δ: 6.64 (s, 3H, *para*-3,5-$C_6H_3Me_2$), 6.63 (s, 6H, *ortho*-3,5-$C_6H_3Me_2$), 4.22 (q, 3H, methine), 3.33 (s, 2H, H_2CCSiMe$_3$), 2.22 (s, 18H, 3,5-$C_6H_3Me_2$), 1.23 (d, 18H, CHMe_2), 0.07 (s, 9H, H$_2$CCSiMe_3) ppm. ^{13}C NMR (C_6D_6, δ): 287.10 (H$_2$CCSiMe$_3$), 152.64, 137.70, 126.23, 126.10, 58.49, 55.73, 23.76, 21.90, 0.11 ppm. Anal. Calcd. for $C_{38}H_{59}N_3MoSi$: C, 66.93; H, 8.72; N, 6.16. Found: C, 67.06; H, 8.65; N, 6.08.

2-η^2-H$_2$CCPh: 92% (method 1), ^{1}H NMR (C_6D_6, 20.1 °C) δ: 7.81 (d, H$_2$CCPh, 2H), 7.30 (t, H$_2$CCPh, 2H), 6.91 (t, H$_2$CCPh, 1H), 6.73 (s, 6H, *ortho*-3,5-$C_6H_3Me_2$), 6.66 (s, 3H, *para*-3,5-$C_6H_3Me_2$), 4.28 (q, 3H, methine), 2.83 (s, 2H, H_2CCPh), 2.18 (s, 18H, 3,5-$C_6H_3Me_2$), 1.02 (d, 18H, CHMe_2) ppm. ^{13}C NMR (C_6D_6, 20.1 °C): δ: 266.45 (H$_2$CCPh), 151.18, 140.66, 138.01, 128.68,

128.58, 127.36, 126.94, 58.86, 25.74, 24.11, 21.86. Anal. Calcd. for $MoC_{41}H_{55}N_3$: C, 71.80; H, 8.08; N, 6.13. Found: C, 71.92; H, 8.02; N, 6.19 ppm.

2-η^2-H_2CC^tBu: 82% (method 1), ^{1}H NMR (C_6D_6, 20.1 °C) δ: 6.61 (s, 3H, *para*-3,5-$C_6H_3Me_2$), 6.58 (s, 6H, *ortho*-3,5-$C_6H_3Me_2$), 4.06 (q, 3H, methine), 3.21 (s, 2H, H_2CC^tBu), 2.18 (s, 18H, 3,5-$C_6H_3Me_2$), 1.41 (s, 9H, ^{t}Bu), 1.23 (d, 18H, $CHMe_2$) ppm. ^{13}C NMR (C_6D_6, 20.1 °C) δ: 289.27 (H_2CC^tBu), 153.38, 137.61, 126.06, 125.74, 56.31, 47.26, 39.26, 29.54, 23.77, 21.92 ppm.

2-η^2-Ph(H)CCMe: 89% (method 1), ^{1}H NMR (C_6D_6, 20.1 °C) δ: 7.82 (d, 2H, *ortho*-Ph), 7.33 (t, 2H, *meta*-Ph), 6.93 (t, 1H, *para*-Ph), 6.76 (s, 6H, *ortho*-3,5-$C_6H_3Me_2$), 6.68 (s, 3H, *para*-3,5-$C_6H_3Me_2$), 4.25 (q, 3H, methine), 2.21 (s, 18H, 3,5-$C_6H_3Me_2$), 1.75 (s, 1H, Ph(H)CCMe), 1.28 (s, 3H, Ph(H)CCMe), 1.02 (d, 18H, $CHMe_2$) ppm. ^{13}C NMR (C_6D_6, 20.1 °C) δ: 271.90 (Ph(H)CCMe), 150.36, 140.08, 137.71, 129.53, 128.30, 127.44, 127.06, 59.23 (br), 46.32, 25.62, 24.11, 21.85 ppm.

2-η^2-Ph(H)CCPh: 92% (method 1), ^{1}H NMR (C_6D_6, 20.1 °C) δ: 7.92 (d, 2H, Ph), 7.30-6.61 (18H, *ortho, para*-3,5-$C_6H_3Me_2$, Ph), 4.50 (br, 3H, methine), 2.19 (s, 1H, Ph(H)CCPh) 2.15 (s, 18H, 3,5-$C_6H_3Me_2$), 0.96 (br, 18H, $CHMe_2$) ppm. ^{13}C NMR (C_6D_6, 20.1 °C) δ: 263.33 (Ph(H)CCPh), 149.96, 139.02, 137.82, 130.52, 129.44, 129.27, 129.20, 128.94, 127.73, 127.48, 127.29, 50.11, 23 ppm.

2-η^2-Et(H)CCEt: 87% (method 1), ^{1}H NMR (C_6D_6, 20.1 °C) δ: 6.72 (s, 6H, *ortho*-3,5-$C_6H_3Me_2$), 6.67 (s, 3H, *para*-3,5-$C_6H_3Me_2$), 4.27 (q, 3H, methine), 3.46 (q, 2H, -CH_2CH_3), 2.75 (t, 1H, Et(H)CCEt), 2.23 (s, 18H, 3,5-$C_6H_3Me_2$), 1.71 (m, 2H, -CH_2CH_3), 1.21 (d, 18H, $CHMe_2$), 0.87 (m, 6H, -CH_2CH_3) ppm. ^{13}C NMR (C_6D_6, 20.1 °C) δ: 289.19 (Et(H)CCEt), 152.04, 137.47, 127.51, 126.30, 58.03, 53.44, 37.38, 29.92, 24.28, 21.92, 18.14, 14.01 ppm.

4.11 Synthesis of $Me_3SiCH_2CMo(O\text{-}1\text{-}Ad)_3{\cdot}HN^iPrAr$

A solution of 4.000 g (5.866 mmol) of **2-η^2-$H_2CCSiMe_3$** in 50 mL of toluene contained in a 300 mL Schlenk flask fitted with a Westoff stopcock was heated at 80 °C for 12 h. The reaction mixture became brown from bright yellow indicating the formation of **2-CCH_2SiMe_3**. ^{1}H NMR (C_6D_6, 20.1 °C): δ: 6.66 (s, 6H, *ortho*-3,5-$C_6H_3Me_2$), 6.55 (s, 3H *para*-3,5-$C_6H_3Me_2$), 4.38 (q, 3H, methine), 2.49 (s, 2H, CCH_2SiMe_3), 2.13 (s, 18H, 3,5-$C_6H_3Me_2$), 1.36 (d, 18H, $CHMe_2$), -0.01 (s, 9H, CCH_2SiMe_3) ppm. ^{13}C NMR (C_6D_6, 20.1 °C): δ: 302.00 (CCH_2SiMe_3). 153.62 (aryl ipso) , 137.95 (aryl meta), 125.38 (aryl para), 124.92 (aryl ortho), 61.49 ($CHMe_2$), 44.69 (CCH_2SiMe_3), 26.07 (Ar-CH_3), 21.76 ($CHMe_2$), -0.48 (CCH_2SiMe_3) ppm. After being cooled to room temperature, to the solution was added a solution containing 2.679 g (17.598 mmol) of 1-adamantanol in 30 mL of tetrahydrofuran. The solution was stirred for 20 h, and the volume of the solution was reduced to 10 mL in vacuo. Upon cooling (liq N_2, 1h), an off-white solid was obtained. The desired product (4.192 g , 5.162 mmol, 88.0% yield) was isolated by filtration and washed with cold pentane. ^{1}H NMR (C_6D_6, 20.1 °C) δ: 6.39 (s, 1H, *para*-3,5-$C_6H_3Me_2$), 6.15 (s, 2H, *ortho*-3,5-$C_6H_3Me_2$), 3.39 (q, 1H, methine), 3.28 (s, 2H, CCH_2SiMe_3), 2.20 (s, 6H, 3,5-$C_6H_3Me_2$), 2.14 (br, 9H, O-1-*Ad*), 2.05 (br, 18H, O-1-1*Ad*), 1.59 (q, 18H, O-1-*Ad*), 0.94 (d, 6H, $CHMe_2$), 0.27 (s, 9H, CCH_2SiMe_3) ppm. ^{13}C NMR (C_6D_6, 20.1 °C) δ: 289.04 (CCH_2SiMe_3), 148.38 (aryl ipso), 138.88 (aryl meta), 119.70 (aryl para), 112.14 (aryl ortho), 77.60 ($CHMe_2$), 47.74 (O-1-Ad), 47.15 (CCH_2SiMe_3), 37.05 (O-1-Ad), 32.06 (O-1-Ad), 23.39 (Ar-CH_3), 22.11 ($CHMe_2$), 0.22 (CCH_2SiMe_3) ppm. Anal. Calcd. for $C_{46}H_{73}NMoO_3Si$: C, 68.03; H, 9.06; N, 1.72. Found: C, 67.87; H, 9.11; N, 1.68.

4.12 Synthesis of $Me_3SiCH_2CMo(S\text{-}1\text{-}Ad)_3$

The bright yellow compound $Me_3SiCH_2CMo(S\text{-}1\text{-}Ad)_3$ was prepared and purified in a similar way as that of $Me_3SiCH_2CMo(O\text{-}1\text{-}Ad)_3{\cdot}HN^iPrAr$. The isolated yield was 77.6%. ^1H NMR (C_6D_6, 20.3 °C) δ: 3.75 (s, 2H, CCH_2SiMe_3), 2.42 (9H, S-1-*Ad*), 1.95 (br, 18H, S-1-*Ad*), 1.58 (q, 18H, S-1-*Ad*), 0.94 (d, 6H, $CHMe_2$), 0.27 (s, 9H, CCH_2SiMe_3) ppm. ^{13}C NMR (C_6D_6, 20.3°C) δ: 289.04 (CCH_2SiMe_3), 77.60 ($CHMe_2$), 47.74 (S-1-Ad), 47.15 (CCH_2SiMe_3), 37.05 (S-1-Ad), 32.06 (S-1-Ad), 23.39 (Ar-CH_3), 22.11 ($CHMe_2$), 0.22 (CCH_2SiMe_3) ppm. Anal. Calcd. for $C_{35}H_{56}MoS_3Si$: C, 60.30; H, 8.10; S, 13.80. Found: C, 60.18; H, 8.03; S, 13.72.

4.13 Synthesis of optically pure alkylidyne complex $Me_3SiCH_2CMo(OAr^*)_3$ (Ar* = (S-2′-methoxy-[1,1′]binaphthalenyl-2)

The brick-red compound $Me_3SiCH_2CMo(OAr^*)_3$ was prepared and purified in a similar way as that of compound $(Me_3SiCH_2C)Mo(O\text{-}1\text{-}Ad)_3{\cdot}HN^iPrAr$. The isolated yield was 82%. ^1H NMR (C_6D_6, 20.3 °C) δ: 7.87 (q), 7.81(d), 7.57 (d), 7.51 (d), 7.39 (d), 7.35 (d), 7.17 (d), 7.06 (q), 6.90 (t), 6.84 (d), 3.39 (s, OMe), 3.02 (s, CCH_2SiMe_3), −0.19 (s, $SiMe_3$) ppm. ^{13}C NMR ($CDCl_3$, 20.3 °C) δ: 310.35 (CCH_2SiMe_3), 134.28, 129.42, 129.18, 128.99, 128.52, 128.38, 127.82, 126.16, 125.46, 122.75, 22.53, 21.35, -0.81 ppm. Anal. Calcd. for $C_{68}H_{59}MoO_6Si$: C, 74.71; H, 5.16. Found: C, 74.62; H, 5.24.

4.14 Synthesis of $Me_3SiCH_2CMo(O\text{-}2,6\text{-}diphenylphenyl)_2(N[^iPr]Ar)$

The off-white compound $Me_3SiCH_2CMo(O\text{-}2,6\text{-}diphenylphenyl)_2(N[^iPr]Ar$ was prepared and purified in a similar way as that of compound $Me_3SiCH_2CMo(O\text{-}1\text{-}Ad)_3{\cdot}HN^iPrAr$. The isolated yield was 79.9%. ^1H NMR (C_6D_6, 19.9 °C) δ: 7.54 (d, 8H, Ph), 7.20 (m, 12H, Ph), 7.08 (t, 4H, Ph), 6.92 (t, 2H, Ph), 6.52 (s, 1H, *para*-Ar), 6.17 (s, 2H, *ortho*-Ar), 3.46 (s, 1H, methine), 2.17 (s, 6H, Ar-Me_2), 1.61 (s, CH_2SiMe_3), 0.77 (d, 6H, $CH(CH_3)_2$), −0.60 (s, 9H, CH_2SiMe_3). ^{13}C NMR (C_6D_6, 20.1 °C) δ: 312.20 (CCH_2SiMe_3), 162.86, 161.86, 141.22, 137.43, 133.29, 131.24, 130.54, 130.09, 128.80, 127.05, 122.52, 121.28, 59.48, 45.02, 21.58, −1.37. Anal. Calcd. for $C_{52}H_{53}MoNO_3Si$: C, 73.65; H, 6.30; N, 1.65. Found: C, 73.74; H, 6.39; N, 1.61.

4.15 Synthesis of $EtCMo(O\text{-}1\text{-}Ad)_3(THF)$

To a solution containing 0.991 g $Me_3SiCH_2CMo(O\text{-}1\text{-}Ad)_3{\cdot}HN^iPrAr$ (1.220 mmol) in 10 mL of diethyl ether were added 10 equiv of 3-hexyne. After stirring overnight, a white solid precipitated out and all volatile material were removed in vacuo, leaving a white solid being $EtCMo(O\text{-}1\text{-}Ad)_3$ as the product. The solid (0.663 g, 1.122 mmol, 92% yield) was collected by filtration and washed with cold *n*-pentane. Compound $EtCMo(O\text{-}1\text{-}Ad)_3(THF)$ was prepared by dissolving $EtCMo(O\text{-}1\text{-}Ad)_3$ in minimum amount of tetrahydrofuran. Crystals of $EtCMo(O\text{-}1\text{-}Ad)_3(THF)$ were obtained by adding *n*-hexane to tetrahydrofuran solution and the resulting solution was stood at −35 °C. ^1H NMR ($CDCl_3$, 20.1 °C) δ: 3.57 (br, 4H, THF), 3.17 (q, 2H, CCH_2CH_3, 2.19 (br, 9H, O-1-Ad), 1.83 (br, 18H, O-1-Ad), 1.72 (br, 4H, THF), 1.63 (q, 18H, O-1-Ad), 1.21 (t, 3H, CCH_2CH_3) ppm. ^{13}C NMR ($CDCl_3$, 20.0 °C) δ: 288.77 (CCH_2CH_3), 67.57 (THF), 46.92 (O-1-Ad), 36.59 (O-1-Ad),

36.29 (O-1-Ad), 31.55 (O-1-Ad), 30.10 (CCH_2CH_3), 25.37 (THF), 15.06 (CCH_2CH_3). Anal. Calcd. for $C_{37}H_{58}MoO_4$: C, 67.05; H, 8.82. Found: C, 66.94; H, 8.50.

4.16 Catalytic alkyne metathesis reactions

To a solution of $Me_3SiCH_2CMo(OAr^*)_3$ (0.030 g, 0.003 mmol) in 40 mL of toluene were added $TsOCH_2CH_2CCCH_3$ (0.331 g, 1.389 mmol). The resulting solution turned dark reddish-brown quickly and was stirred at room temperature under dynamic vacuum until all volatile material were evaporated (about 2 h). The solid residue was purified by flash column chromatography with hexane/ethyl acetate ar the eluent. Removal of all volatile material provided the desired symmetric alkyne product as a white solid (0.279 g, 95%). ^{1}H NMR (C_6D_6, 20.3 °C)δ: 7.71 (d, 4H, aryl ortho), 6.77 (d, 4H, aryl meta), 3.73 (t, 4H, $TsOCH_2$-), 2.00 (t, 4H, $TsOCH_2CH_2CC$-), 1.89 (s, 6H, -OTs) ppm. ^{13}C NMR (C_6D_6, 20.2 °C) δ: 145.12 (TsO-), 134.09 (TsO-), 130.36 (TsO-), 128.58 (TsO-), 77.59 (-CC-), 68.36 ($TsOCH_2$-), 21.60 (TsO-), 20.00 ($TsOCH_2CH_2CC$-) ppm. Anal. Calcd. for $C_{20}H_{22}S_2O_6$: C, 56.85; H, 5.25. Found: C, 56.83; H, 5.24.

(4-$NCC_6H_4OCH_2CH_2C)_2$: ^{1}H NMR ($CDCl_3$, 20.3 °C) δ: 7.59 (d, 4H, *meta*-4-$NCC_6H_4OCH_2CH_2$), 6.96 (d, 4H, *ortho*-4-$NCC_6H_4OCH_2CH_2$), 4.10 (t, 4H, 4-$NCC_6H_4OCH_2CH_2$), 2.70 (t, 4H, 4-$NCC_6H_4OCH_2CH_2$) ppm.

(3-$CF_3C_6H_4OCH_2CH_2C)_2$: ^{1}H NMR ($CDCl_3$, 20.1 °C) δ: 7.40 (t, 2H, *meta*-3-$CF_3C_6H_4OCH_2CH_2$), 7.21 (d, 2H, *para*-3-$CF_3C_6H_4OCH_2CH_2$), 7.16 (s, 2H, *ortho*-3-$CF_3C_6H_4OCH_2CH_2$), 7.10 (d, 2H, *ortho*-3-$CF_3C_6H_4OCH_2CH_2$), 4.11 (t, 4H, 3-$CF_3C_6H_4OCH_2CH_2$), 2.70 (t, 4H, 3-$CF_3C_6H_4OCH_2CH_2$) ppm.

(3-$Me_2NC_6H_4OCH_2CH_2C)_2$: ^{1}H NMR ($CDCl_3$, 20.3 °C) δ: 7.15 (t, 2H, *meta*-3-$Me_2NC_6H_4OCH_2CH_2$), 6.38 (d, 2H, *para*-3-$Me_2NC_6H_4OCH_2CH_2$), 6.31 (s, 2H, *ortho*-3-$Me_2NC_6H_4OCH_2CH_2$), 6.29 (d, 2H, *ortho*-3-$Me_2NC_6H_4OCH_2CH_2$), 4.07 (t, 4H, 3-$Me_2NC_6H_4OCH_2CH_2$), 2.67 (t, 4H, 3-$Me_2NC_6H_4$-OCH_2CH_2) ppm.

(2-$IC_6H_4OCH_2CH_2C)_2$: ^{1}H NMR (C_6D_6, 20.3 °C) δ: 7.64 (d, 2H, *meta*-2-IC_6H_4O-CH_2CH_2), 6.84 (t, 2H, *para*-2-$IC_6H_4OCH_2CH_2$), 6.36 (t, *meta*-2-$IC_6H_4OCH_2CH_2$), 6.31 (d, 2H, *ortho*-2-$IC_6H_4OCH_2CH_2$), 3.63 (t, 4H, 2-$IC_6H_4OCH_2CH_2$), 2.42 (t, 4H, 2-$IC_6H_4OCH_2CH_2$) ppm.

(4-$O_2NC_6H_4OCH_2CH_2C)_2$: ^{1}H NMR ($CDCl_3$, 20.3 °C) δ: 8.21 (d, 4H, *meta*-4-$O_2NC_6H_4OCH_2CH_2$), 6.97 (d, 4H, *ortho*-4-$O_2NC_6H_4OCH_2CH_2$), 4.15 (t, 4H, 4-$O_2NC_6H_4OCH_2CH_2$), 2.73 (t, 4H, 4-$O_2NC_6H_4OCH_2CH_2$) ppm.

($C_6H_5C(O)OCH_2CH_2C)_2$: ^{1}H NMR ($CDCl_3$, 19.9 °C) δ: 8.05 (d, 4H, *ortho*-$C_6H_5C(O)OCH_2CH_2$), 7.57 (t, 2H, *para*-$C_6H_5C(O)OCH_2CH_2$), 7.44 (t, 4H, *meta*-$C_6H_5C(O)OCH_2CH_2$), 4.40 (t, 4H, $C_6H_5C(O)OCH_2CH_2$), 2.65 (t, 4H, $C_6H_5C(O)OCH_2CH_2$) ppm.

(3-$C_6H_4NOCH_2CH_2C)_2$: ^{1}H NMR ($CDCl_3$, 20.1 °C) δ: 8.33 (d, 2H, *para*-3-$C_6H_4NOCH_2CH_2$), 8.23 (t, 2H, *meta*-3-$C_6H_4NOCH_2CH_2$), 7.22 (s, 2H, *ortho*-3-$C_6H_4NOCH_2CH_2$), 7.21 (d, 2H, *ortho*-3-$C_6H_4NOCH_2CH_2$), 4.09 (t, 4H, 3-$C_6H_4NOCH_2CH_2$), 2.65 (t, 4H, 3-$C_6H_4NOCH_2CH_2$) ppm.

($C_6H_5CHCHC)_2$: ^{1}H NMR (C_6D_6, 20.1°C) δ: 7.10 (d, 4H, *ortho*-C_6H_5CHCH), 7.03-6.98 (m, 8H, *meta, para*-C_6H_5CHCH and C_6H_5CHCH), 6.34 (d, 2H, C_6H_5CHCH) ppm.

4.17 Crystal Structure of 2-η^2-H_2CCHPh

Crystals were grown from a saturated diethyl ether solution at -35 °C. Inside the glove-box, the crystals were quickly moved from a scintillation vial to a microscope slide containing Paratone N (an Exxon product) oil. Under the microscope a dark brown block of approximate dimensions $0.28 \times 0.26 \times 0.16$ mm^3 was selected and mounted on a glass fiber using wax. A total of 7285 reflections were collected ($-10 \leq h \leq 9$, $-13 \leq k \leq 13$, $-20 \leq l \leq 18$) in the θ range of 2.42 to 23.35 °, of which 5349 were unique ($R_{int} = 0.0722$). The structure was solved using the Patterson method (SHELXTL V5.1, G. M. Sheldrick and Siemens Industrial Automation, Inc., 1997) in conjunction with standard difference Fourier techniques. All non-hydrogen atoms were refined anisotropically. Some of the hydrogen atoms were found in the electronic density map. The rest of the hydrogen atoms were placed in calculated ($d_{CH} = 0.96$ Å) positions. The carbon atoms C41 and C42 appear slightly disordered and they have been modeled as occupying two sites C41A, C41B and C42A, C42B, respectively (C41A is 55 % and C42A is 45 % occupancy). The residual peak and hole electron density were 1.430 and -2.144 e·Å^{-3}, respectively. A semi-empirical absorption correction was applied based on pseudo-psi-scans with maximum and minimum transmission equal to 0.9424 and 0.9021, respectively. The least squares refinement converged normally with residuals of R_1=0.0564, wR_2=0.1436 based on $I > 2\sigma I$ and GOF = 1.127 (based on F^2). No extinction coefficient was applied to the refinement. Crystal and refinement data: formula = $C_{41}H_{53}N_3Mo$, space group $P\bar{1}$, $a = 9.062(1)$ Å, $b = 12.268(2)$ Å, $c = 18.414(3)$ Å, $\alpha = 90.927(3)$ °, $\beta = 94.659(3)$ °, $\gamma = 111.361(2)$ °, $Z = 2$, $V = 1897.(5)$ Å^3, $D_{calcd} = 1.197$ g·cm^{-3}, $F(000) = 724$, R (all data based on F) = 0.0580, wR (all data based on F^2) = 0.1452.

4.18 Crystal Structure of [2-PhCCH]$_2$

Crystals grown from a Et_2O solution at room temperature were coated with Paratone N oil (Exxon) on a microscope slide. A red block of approximate dimensions 0.35 × 0.24 × 0.18 mm was selected and mounted with wax on a glass fiber. A total of 14726 reflections ($-18 \leq h \leq 15$, $-14 \leq k \leq 12$, $-20 \leq l \leq 18$) were collected at 183(2) K in the θ range of 1.37 to 23.27 °, of which 5260 were unique ($R_{int} = 0.0586$). The radiation used was Mo-Kα ($\lambda = 0.71073$ Å, $\mu = 2.362$ mm^{-1}). The structure was solved by Direct methods (SHELXTL V5.0, G. M. Sheldrick and Siemens Industrial Automation, Inc., 1995) in conjunction with standard difference Fourier techniques. All non-hydrogen atoms were refined anisotropically and hydrogen atoms were placed in calculated ($d_{CH} = 0.96$ Å) positions. The residual peak and hole electron density was 0.477 and −0.363 e·Å^{-3}. The least square refinement converged normally with residuals of $R_1 = 0.0435$, $wR_2 = 0.0896$, and GOF = 1.086 based on $I > 2\sigma I$. No significant extinction coefficient was necessary (0.0006(2)). Crystal and refinement data: Formula = $C_{82}H_{108}Mo_2N_6$, space group $P2_1/n$, $a = 16.9568(3)$ Å, $b = 12.89190(10)$ Å, $c = 18.4714(4)$ Å, $\alpha = 90$ °, $\beta = 114.6850(10)$ °, $\gamma = 90$ °, $Z = 2$, $V = 3668.95(11)$ Å^3, $D_{calcd} = 1.240$ g·cm^{-3}, $F(000) = 1452$, R (all data on F) = 0.0727, wR (all data based on F^2) = 0.1086.

4.19 Crystal Structure of 2-η^2-H_2CCPh

Crystals grown from a Et_2O solution at −35 °C were coated with Paratone N oil (Exxon) on a microscope slide. A red block of approximate dimensions 0.22 × 0.19 × 0.15 mm was selected and mounted with wax on a glass fiber. A total of 7590 reflections ($-10 \leq h \leq 11$, $-13 \leq k \leq 13$, $-16 \leq$

$l \leq 18$) were collected at 183(2) K in the θ range of 2.57 to 23.27 °, of which 5294 were unique (R_{int} = 0.0390). The radiation used was Mo-Kα (λ = 0.71073 Å, μ = 2.362 mm^{-1}). The structure was solved by Direct methods (SHELXTL V5.0, G. M. Sheldrick and Siemens Industrial Automation, Inc., 1995) in conjunction with standard difference Fourier techniques. All non-hydrogen atoms were refined anisotropically and hydrogen atoms were placed in calculated (d_{CH} = 0.96 Å) positions. The residual peak and hole electron density was 0.477 and −0.363 e·Å^{-3}. The least square refinement converged normally with residuals of R_1 = 0.0435, wR_2 = 0.0896, and GOF = 1.086 based on $I > 2\sigma I$. No significant extinction coefficient was necessary (0.0006(2)). Crystal and refinement data: Formula = $C_{41}H_{55}MoN_3$, space group $P\bar{1}$, a = 9.9106(8) Å, b = 12.045(1) Å, c = 16.805(1) Å, α = 83.946(2) °, β = 84.247(2) °, γ = 71.376(1) °, Z = 2, V = 1885.7(3) Å^3, D_{calcd} = 1.208 g·cm^{-3}, $F(000)$ = 728, R (all data on F) = 0.0487, wR (all data based on F^2) = 0.1047.

4.20 Crystal structure of $Me_3SiCH_2CMo(O\text{-}2,6\text{-}diphenylphenyl)_2(N[^iPr]Ar)$

Crystals were grown from a saturated diethyl ether solution at −35 °C. The crystals were quickly moved from a scintillation vial to a microscope slide containing Paratone N (an Exxon product) oil. Under the microscope a colorless block of approximate dimensions 0.30 × 0.27 × 0.24 mm^3 was selected and mounted on a glass fiber using wax. A total of 9909 reflections were collected (−9 ≤ h ≤ 11, −14 ≤ k ≤ 15, −19 ≤ l ≤ 19) in the θ range of 2.47 to 23.28 °, of which 7044 were unique (R_{int} = 0.0478). The structure was solved using the Patterson method (SHELXTL V5.1, G. M. Sheldrick and Siemens Industrial Automation, Inc., 1997) in conjunction with standard difference Fourier techniques. All non-hydrogen atoms were refined anisotropically and the hydrogen atoms were placed in calculated (d_{CH} = 0.96 Å) positions. The residual peak and hole electron

density were 0.983 and -0.827 e·Å^{-3}, respectively. A semi-empirical absorption correction was applied based on pseudo-psi-scans with maximum and minimum transmission equal to 0.3898 and 0.1925, respectively. The least squares refinement converged normally with residuals of R_1=0.0522, wR_2=0.1338 based on $I > 2\sigma I$ and GOF = 1.123 (based on F^2). No extinction coefficient was applied to the refinement. Crystal and refinement data: formula = $C_{57}H_{64}NO_2SiMo$, space group $P\bar{1}$, a = 10.628(3) Å, b = 13.529(4) Å, c = 17.882(5) Å, α = 88.791(4) °, β = 88.969(4) °, γ = 77.243(4) °, Z = 2, V = 2506.8(11) Å^3, D_{calcd} = 1.218 g·cm^{-3}, $F(000)$ = 970, R (all data based on F) = 0.0554, wR (all data based on F^2) = 0.1361.

4.21 Crystal structure of EtCMo(O-1-Ad)$_3$(THF)

Crystals were grown from a saturated tetrahydrofuran solution layered with hexane at -35 °C. The crystals were quickly moved from a scintillation vial to a microscope slide containing Paratone N (an Exxon product) oil. Under the microscope an orange plate of approximate dimensions 0.28 × 0.15 × 0.13 mm^3 was selected and mounted on a glass fiber using wax. A total of 13486 reflections were collected ($-35 \leq h \leq 25$, $-14 \leq k \leq 13$, $-20 \leq l \leq 24$) in the θ range of 2.46 to 23.28 °, of which 4858 were unique (R_{int} = 0.0470) The structure was solved using the Patterson method (SHELXTL V5.1, G. M. Sheldrick and Siemens Industrial Automation, Inc., 1997) in conjunction with standard difference Fourier techniques. All non-hydrogen atoms were refined anisotropically and the hydrogen atoms were placed in calculated (d_{CH} = 0.96 Å) positions. The residual peak and hole electron density were 0.398 and -0.472e·Å^{-3}, respectively. A semi-empirical absorption correction was applied based on pseudo-psi-scans with maximum and minimum transmission equal to 0.8911 and 0.6844, respectively. The least squares refinement converged normally with residuals

of $R_1 = 0.0505$, $wR_2 = 0.0879$ based on $I > 2\sigma I$ and GOF = 1.144 (based on F^2). No extinction coefficient was applied to the refinement. Crystal and refinement data: formula = $C_{74}H_{116}O_8Mo_2$, space group *C2/c*, $a = 31.730(5)$ Å, $b = 12.922(2)$ Å, $c = 22.449(3)$ Å, $\alpha = 90$ °, $\beta = 132.477(2)$ °, $\gamma = 90$ °, $Z = 4$, $V = 6788.8(18)$ Å^3, $D_{calcd} = 1.297$ g·cm^{-3}, $F(000) = 2832$, R (all data based on F) = 0.0731, wR (all data based on F^2) = 0.0943.

References

1. Laplaza, C. E.; Cummins, C. C. *Science* **1995,** *268,* 861.

2. Laplaza, C. E.; Johnson, A. R.; Cummins, C. C. *J. Am. Chem. Soc.* **1996,** *118,* 709.

3. Laplaza, C. E.; Johnson, M. J. A.; Peters, J. C.; Odom, A. L.; Kim, E.; Cummins, C. C.; George, G. N.; Pickering, I. J. *J. Am. Chem. Soc.* **1996,** *118,* 8623.

4. Cummins, C. C. *Chem. Commun.* **1998,** 1777.

5. Laplaza, C. E.; Davis, W. M.; Cummins, C. C. *Angew. Chem. Int. Ed. Engl.* **1995,** *34,* 2042.

6. Johnson, A. R.; Davis, W. M.; Cummins, C. C.; Serron, S.; Nolan, S. P.; Musaev, D. G.; Morokuma, K. *J. Am. Chem. Soc.* **1998,** *120,* 2071.

7. McCullough, L. G.; Schrock, R. R.; Dewan, J. C.; Nurdzek, J. C. *J. Am. Chem. Soc.* **1985,** *107,* 5987.

8. Peters, J. C.; Odom, A. L.; Cummins, C. C. *Chem. Commun.* **1997,** 1995.

9. Greco, J. B.; Peters, J. C.; Baker, T. A.; Davis, W. M.; Cummins, C. C.; Wu, G. *J. Am. Chem. Soc.* **2001,** *123,* 5003.

10. Agapie, T. A.; Cummins, C. C. *unpublished results* .

11. Schrock, R. R.; Listemann, M. L.; Sturgeoff, L. G. *J. Am. Chem. Soc.* **1982,** *104,* 4291.

12. Chisholm, M. H.; Hoffman, D. M.; Huffman, J. C. *Inorg. Chem.* **1983,** *22,* 2903.

13. Tsai, Y.-C.; Johnson, M. J. A.; Mindiola, D. J.; Cummins, C. C.; Klooster, W. T.; Koetzle, T. F. *J. Am. Chem. Soc.* **1999,** *121,* 10426.

14. Strutz, H.; Schrock, R. R. *Organometallics* **1984,** *3,* 1600.

15. Allen, S. R.; Beevor, R. G.; Green, M.; Norman, N. C.; Orpen, A. G.; Williams, I. D. *J. Chem. Soc. Dalton Trans.* **1985,** 435.

16. Green, M. *J. Organomet. Chem.* **1986,** *300,* 93.

17. Allen, S. R.; Beevor, R. G.; Green, M.; Orpen, A. G.; Paddick, K. E.; Williams, I. D. *J. Chem. Soc. Dalton Trans.* **1987,** 591.

18. Carfagna, C.; Carr, N.; Deeth, R. J.; Dossett, S. J.; Green, M.; Mahon, M. F.; Vaughn, C. *J. Chem. Soc. Dalton Trans.* **1996,** 415.

19. Brower, D. C.; Birdwhistell, K. R.; Templeton, J. L. *Organometallics* **1986,** *5,* 94.

20. Templeton, J. L. *Adv. Organomet. Chem.* **1989,** *29,* 1.

21. Feng, S. G.; Templeton, J. L. *Organometallics* **1992,** *11,* 2168.

22. Morrow, J. R.; Tonker, T. L.; Templeton, J. L. *J. Am. Chem. Soc.* **1985,** *107,* 6956.

23. Frohnapfel, D. S.; Enriquez, A. E.; Templeton, J. L. *Organometallics* **2000,** *19,* 221.

24. Frohnapfel, D. S.; White, P. S.; Templeton, J. L. *Organometallics* **2000,** *19,* 1497.

25. Frohnapfel, D. S.; Templeton, J. L. *Coord. Chem. Rev.* **2000,** *206,* 199.

26. Tsai, Y.-C.; Diaconescu, P. L.; Cummins, C. C. *Organometallics* **2000,** *19,* 5260.

27. Tsai, Y.-C.; Meyer, K.; Mindiola, D. J.; Cummins, C. C. *submitted* .

28. Freudenberger, J. H.; Schrock, R. R.; Churchill, M. R.; Rheingold, A. L.; Ziller, J. W. *Organometallics* **1984,** *3,* 1563.

29. Listemann, M. L.; Schrock, R. R. *Organometallics* **1985,** *4,* 74.

30. Schrock, R. R. *Polyhedron* **1995,** *14,* 3177.

31. Fürstner, A.; Seidel, G. *Angew. Chem. Int. Ed. Engl.* **1998,** *37,* 1734.

32. Fürstner, A.; Guth, O.; Rumbo, A.; Seidel, G. *J. Am. Chem. Soc.* **1999,** *121,* 11108.

33. Fürstner, A.; Rumbo, A. *J. Org. Chem* **2000,** *65,* 2608.

34. Sato, M.; Tatsumi, T.; Kodama, T.; Hidai, M.; Uchida, T.; Uchida, Y. *J. Am. Chem. Soc.* **1978,** *100,* 447.

35. Luo, X.-L.; Kubas, G. J.; Burns, C. J.; Butcher, R. J.; Bryan, J. C. *Inorg. Chem.* **1995,** *34,* 6538.

36. Wasserman, H. J.; Kubas, G. J.; Ryan, R. R. *J. Am. Chem. Soc.* **1986,** *108,* 2294.

37. King, W. A.; Scott, B. L.; Eckert, J.; Kubas, G. J. *Inorg. Chem.* **1999,** *38,* 1069.

38. Cole, J. M.; Gibson, V. C.; Howard, J. A. K.; McIntyre, G. J.; Walker, G. L. P. *Chem. Commun.* **1998,** 1829.

39. Pavia, D. L.; Lampman, G. M.; Kriz, G. S. *Introduction to Spectroscopy;* Saunders College Publishing: , second ed.; 1996.

40. Baerends, E. J.; Ellis, D. E.; Ros, P. *Chem Phys.* **1973,** *2,* 41.

41. Versluis, L.; Ziegler, T. *J. Chem. Phys.* **1988,** *88,* 322.

42. Brookhart, M.; Green, M. L. H. *J. Organomet. Chem.* **1983,** *250,* 395.

43. Otsuka, S.; Yoshida, T.; Matsumoto, M.; Nakatsu, K. *J. Am. Chem. soc.* **1976,** *98,* 588.

44. Huang, D.; Streib, W. E.; Eisenstein, O.; Caulton, K. G. *Angew. Chem., Int. Ed. Engl.* **1997,** *36,* 2004.

45. Evans, W. J.; Anwander, R.; Ziller, J. W.; Khan, S. I. *Inorg. Chem.* **1995,** *34,* 5927.

46. Cooper, A. C.; Clot, E.; Huffman, J. C.; Streib, W. E.; Maseras, F.; Eisenstein, O.; Caulton, K. G. *J. Am. Chem. Soc.* **1999,** *121,* 97.

47. Ujaque, G.; Cooper, A. C.; Maseras, F.; Eisenstein, O.; Caulton, K. G. *J. Am. Chem. Soc.* **1998,** *120,* 361.

48. King, W. A.; Luo, X.-L.; Scott, B. L.; Kubas, G. J.; Zilm, K. W. *J. Am. Chem. Soc.* **1996,** *118,* 6782.

49. Braga, D.; Grepioni, F.; Biradha, K.; Desiraju, G. R. *J. Chem. Soc., Dalton Trans.* **1996,** 3925.

50. Lukens, Jr., W. W.; Smith III, M. R.; Andersen, R. A. *J. Am. Chem. Soc.* **1996,** *118,* 1719.

51. Rees, Jr., W. S.; Just, O.; Schumann, H.; Weimann, R. *Angew. Chem., Int. Ed. Engl.* **1996,** *35,* 419.

52. Evans, D. F. *J. Chem. Soc.* **1959,** 2003.

53. McDonald, J. W.; Corbin, J. L.; Newton, W. E. *J. Am. Chem. Soc.* **1975,** *97,* 1970.

54. Hoffmann, R. *Angew. Chem. Int. Ed. Engl.* **1982,** *21,* 711.

55. Templeton, J. L.; Ward, B. C. *J. Am. Chem. Soc.* **1980,** *102,* 3288.

56. Bruneau, C.; Dixneuf, P. H. *Acc. Chem. Res.* **1999,** *32,* 311. And references therein.

57. Etzenhouser, B. A.; Chen, Q.; Sponsler, M. B. *Organometallics* **1994,** *13,* 4176.

58. Rabier, A.; Lugan, N.; Mathieu, R.; Geoffroy, G. L. *Organometallics* **1994,** *13,* 4676.

59. Lawrie, C. J.; Gable, K. P.; Carpenter, B. K. *Organometallics* **1989,** *8,* 2274.

60. Duchateau, R.; Williams, A. J.; Gambarotta, S.; Y., C. M. *Inorg. Chem.* **1991,** *30,* 4863.

61. Etzenhouser, B. A.; Cavanaugh, M. D.; Spurgeon, H. N.; Sponsler, M. B. *J. Am. Chem. Soc.* **1994,** *116,* 2221.

62. Robin, M. B.; Day, P. *Adv. Inorg. Chem. Radiochem.* **1967,** *10,* 247.

63. Kauffmann, T.; Ennen, B.; Sander, J.; Wieschollek, R. *Angew. Chem., Int. Ed. Engl.* **1983,** *22,* 244.

64. Clift, S. M.; Schwartz, J. *J. Am. Chem. Soc.* **1984,** *106,* 8300.

65. Aguero, A.; Kress, J.; Osborn, J. A. *J. Chem. Soc., Chem. Commun.* **1986,** 531.

66. Freudenberger, J. H.; Schrock, R. R. *Organometallics* **1986,** *5,* 398.

67. Feldman, J.; Schrock, R. R. *Prog. Inorg. Chem.* **1991,** *39,* 1.

68. Reger, D. L.; McElligot, P. J. *J. Am. Chem. Soc.* **1980,** *102,* 5923.

69. Reger, D. L.; Klaeren, S. A.; Babin, J. E.; Adams, R. D. *Organometallics* **1988,** *7,* 181.

70. Reger, D. L. *Acc. Chem. Res.* **1988,** *21,* 229.

71. Kuivila, H. G. *Synthesis* **1970,** 499.

72. Fürstner, A.; Mathes, C.; Lehmann, C. W. *J. Am. Chem. Soc.* **1999,** *121,* 9453.

73. Murdzek, J. S.; Blum, L.; Schrock, R. R. *Organometallics* **1988,** *7,* 436.

74. Takahashi, M.; Ogasawara, K. *Tetrahedron: Asymmetry* **1997,** *8,* 3125.

75. Pangborn, A. B.; Giardello, M. A.; Grubbs, R. H.; Rosen, R. K.; Timmers, F. J. *Organometallics* **1996,** *15,* 1518.

Chapter 3. Dinitrogen Cleavage by Three-Coordinate Molybdenum(III) Complexes Accelerated by Lewis Bases

October 29, 2001

1 Introduction

The detailed information of spontaneous[1–4] thermal cleavage of dinitrogen by three-coordinate molybdenum complexes was given a while ago.[5] It has been shown that the molybdenum(III) complexes Mo(H)(η^2-$(CD_3)_2CNAr$)(N[^{i}Pr-d_6]Ar)$_2$ (**1**), a mask of Mo(N[^{i}Pr-d_6]Ar)$_3$ (**2**) (Ar = 3,5-$C_6H_3Me_2$),[6–9] and Mo(N[^{t}Bu-d_6]Ar)$_3$ (**3**) effect the six-electron reductive cleavage of dinitrogen (1 atm, −35 to 30 °C)[5,6,10,11] to provide the bridging and terminal nitrido complexes **2**$_2$-μ-**N** and **3-N**, respectively. A previous mechanistic study[5] showed that the key intermediate in the splitting of dinitrogen by **3** was a bridging-dinitrogen dimolybdenum complex **3**$_2$-μ-N_2 ([**3-N**]$_2$) which was formed during a slow (76 h) incubation period at −35 °C (1 atm N_2).[5] Complex [**3-N**]$_2$ ultimately converts to two equiv of the terminal nitrido compound **3-N**. The rate-determining step to form the bridging-dinitrogen dimolybdenum complex [**3-N**]$_2$ is believed the binding of dinitrogen to **3**. Presumably, the equilibrium constant for dinitrogen capture by **3** is small at ambient temperature. Thus, this relatively slow rate of the formation of the proposed end-on bound dinitrogen intermediate **3-N**$_2$ to that of subsequent reaction with another equiv of **3** to generate [**3-N**]$_2$ renders the observation of the putative **3-N**$_2$ difficult. This intermediate **3-N**$_2$ has not been observed experimentally thus far while many mononuclear end-on bound dinitrogen compounds have been well characterized.[12]

We also showed that the splitting of dinitrogen (1 atm, 25 °C) by **3** could be accelerated in the presence of a sodium amalgam.[13] The electrochemical and synthetic experiments revealed that the anionic dinitrogen complex [**3-N**$_2$]$^-$ is the key intermediate in the acceleration of dinitrogen splitting by **3** under such conditions. In the presence of an electron acceptor, [**3-N**$_2$]$^-$ reacted with

3 to give the neutral N_2-bridged complex [**3-N**]$_2$, which in turn split into two equiv of the terminal nitrido complex **3-N**. Sodium amalgam in this system functioned as a redox catalyst accelerating the conversion of **3** to [**3-N**]$_2$.

Inspired by the finding that the O_2 uptake ability of the square-planar complex Co(salen) (salen: bis(2-hydroxybenzaldehyde)ethylenediimine) was dramatically enhanced (> 1500 times) upon addition of one equiv of pyridine, which coordinated to Co(salen) to give the square-pyramidal complex Co(salen)(pyridine),[14] we decided to explore possible strategies for accelerating dinitrogen binding to **1** or **3** in the presence of various types of organic bases. The geometric adjustment from square-planar to square-pyramidal is necessary for the Co(II) complex to achieve the appropriate electronic configuration for O_2 uptake since the energy of the d_{z^2} orbital needs to be raised above that of the d_{xy} orbital to give a $(d_{xz})^2(d_{yz})^2(d_{xy})^2(d_{z^2})^1$ configuration.[15,16] Similarly and relevant to N_2 uptake, several groups have recently discovered end-on bound dinitrogen trigonal-bipyramidal transition-metal complexes bearing a donor ligand trans to dinitrogen, e.g. $[N_3N_F]Re(N_2)$ ($[N_3N_F]^{3-}$ = $[(C_6F_5NCH_2CH_2)_3N]^{3-}$),[17] $[N_3N]Mo(N_2)$ ($[N_3N]^{3-} = [(Me_3SiNCH_2CH_2)_3N]^{3-}$),[18] Re(S-2,4,6-$C_6H_2{}^iPr_3$)$_3$($PPh_3$)($N_2$),[19] and $[P_3P]Ru(N_2)$ (P_3P = $(Ph_2PCH_2CH_2)_3P$).[20] Interestingly, the reaction of complex **1** with one equiv of 2,4,6-$NCC_6H_2Me_3$ gave a 1:1 mixture of complex **2-(η^1-2,4,6-$NCC_6H_2Me_3$)$_2$** and **1** instead of a mono-adduct complex **2-(η^1-2,4,6-$NCC_6H_2Me_3$)**.[8] This observation implies that the complex **2-η^1-2,4,6-$NCC_6H_2Me_3$** is a better nucleophile than **2**. Similarly, N_2 uptake ability of **1** or **3** could be enhanced in the presence of a Lewis base due to the nucleophilic Lewis base adduct, and subsequently, the rate of N_2 cleavage could be increased.

Herein reported is the acceleration of dinitrogen splitting by **1** or **3**, which is a consequence of accelerated dinitrogen uptake by **1** or **3** in the presence of a Lewis base. The proposed mechanism

of the dinitrogen cleavage was ascertained by comparing the reactivities of **1** and **3**.

2 Results

2.1 Dinitrogen cleavage by complex 1 in the presence of Lewis bases (2,6-dimethylpyrazine, pyridine, 4-dimethylaminopyridine, 1-methylimidazole, potassium hydride, and 2,4,6-collidine)

Under a dinitrogen atmosphere, addition of one equiv of 2,6-dimethylpyrazine to a solution of **1** in Et_2O resulted in a quick color change from orange-brown to intense purple. ^2H NMR of the purple solution showed a new signal at 7.20 ppm ($\Delta\nu_{1/2}$= 26 Hz). After stirring for 5 h, this peak disappeared and the signal of $\mathbf{2_2}$-μ-**N** was observed. Similarly, when Et_2O solution of **1** were stirred in the presence of one equiv of pyridine or 4-dimethylaminopyridine, the initial orange-brown color of **1** acquired the intense purple color of $\mathbf{2_2}$-μ-N within 3 h or 2 h. Monitoring these reactions by ^2H NMR spectroscopy showed that a steady consumption of orange-brown **1** coincided with the formation of the bridging-nitrido dimolybdenum complex $\mathbf{2_2}$-μ-**N**. The broad signals at 7.64 ppm ($\Delta\nu_{1/2}$= 309 Hz in the presence of pyridine), and 8.24 ppm ($\Delta\nu_{1/2}$= 303 Hz in the presence of 4-dimethylaminopyridine), indicative of paramagnetic species, were also observed. When two equiv of pyridine or 4-dimethylaminopyridine were employed, the signal of **1** completely disappeared indicated by ^2H NMR spectroscopy while the new broad signal remained. Based on these observations, it is very likely that an organic base coordinates to **2** reversibly. This assumption is also supported by the dissolution of **1** in 2,4,6-collidine. Upon disolving **1** in 2,4,6-collidine, ^2H

NMR spectrum only showed the signals of **1**, and the rate of the formation $\mathbf{2}_2$-μ-**N** was not affected at all. Based on the above observation, the degree of the interaction between **1** and an organic base is a function of the steric bulk of bases. Under vacuum, **1** was found to react with one equiv of 1-methylimidazole generating a new species at 5.36 ppm with $\Delta\nu_{1/2}$= 525 Hz indicated by ^{2}H NMR spectroscopy. Under a dinitrogen atmosphere and in the presence of one equiv of 1-methylimidazole, the Et_2O solution of **1** acquired an intense purple color in 5 min in which 87% of $\mathbf{2}_2$-μ-**N** was isolated. Interestingly, the nitride complex **2-N** was also isolated in about 8% yield from the above reaction. Previously, the only way to prepare **2-N** was *via* the nitrogen atom transfer from $Cr(N)(O^tBu)_3$,[6] but never directly from dinitrogen. Complex **1** also split dinitrogen rapidly in the presence of potassium hydride in THF solvent. As the reaction mixture was stirred over a period of several hours, the intense purple color gradually diminished, initially turning green and finally acquiring an orange-brown color. A ^{1}H NMR spectrum of said mixture indicated that the nitrido complex **2-N** and the anionic dinitrogen salt $[(THF)_xK][\mathbf{2}\text{-}\mathbf{N}_2]$ had formed. The green solution was characterized as the anionic salt $[(THF)_xK][\mathbf{2}_2\text{-}\mu\text{-}\mathbf{N}]$.[21]

2.2 Dinitrogen cleavage by complex 3 in the presence of Lewis bases (2,6-dimethylpyrazine, pyridine, 4-dimethylaminopyridine, 1-methylimidazole, potassium hydride, and 2,4,6-collidine)

In contrast to the reactions of **1** with N-containing organic bases, ^{2}H NMR spectroscopy did not reveal new signals from the reaction of **3** with 1-methylimidazole, pyridine, and pyridine derivatives in the absence of dinitrogen. However, addition of one equiv of 2,6-dimethylpyrazine to a solution of **3** in Et_2O resulted in a color change from bright orange to intense violet, giving a new broad

peak at 11.40 ppm ($\Delta\nu_{1/2}$= 626 Hz) in ^{2}H NMR. The intensity of this new peak increased as more 2,6-dimethylpyrazine was added to the solution of **3** (Figure 1).

Under a dinitrogen atmosphere, **3** also rapidly split dinitrogen to form **3-N** in the presence of Lewis bases. Et_2O or THF solutions of **3**, when stirred in the presence of such bases under a dinitrogen atmosphere, acquired the intense pink color of intermediate [**3-N**]$_2$ within 2 h. The preliminary rates of dinitrogen cleavage determined by ^{2}H NMR spectroscopy are shown in Figures 2, 3, and 4, which represent the reactions of **3** and dinitrogen in the presence of one equiv of 4-dimethylaminopyridine (in Et_2O), 1-methylimidazole (in Et_2O), and ten equiv of potassium hydride (in THF), respectively. Although ten equiv of potassium hydride was employed, the exact amount of potassium hydride in solution is not certain becasue of its poor solubility in THF. In addition, potassium hydride did not accelerate the splitting of dinitrogen by **3** in an Et_2O solution even up to twenty equiv, because of its solubility in Et_2O. ^{2}H NMR spectroscopy also revealed that a steady consumption of orange **3** coincided with the formation of the dinuclear complexes [**3-N**]$_2$ and **3-N**. As the reaction mixtures were stirred over a period of several hours (24, 8, and 6 h in the presence of 4-dimethylaminopyridine, potassium hydride, and 1-methylimidazole, respectively), the intense pink color of [**3-N**]$_2$ gradually diminished, and the final solution acquired a red-brown color of **3-N**. ^{2}H NMR spectroscopy of the solution revealed complete consumption of both the starting material **3** and the intermediate [**3-N**]$_2$. Analysis of the final reaction products by ^{1}H NMR spectroscopy indicated that the nitride complex **3-N** was formed in high yields (85, 91, and 94% in the presence of 4-dimethylaminopyridine, 1-methylimidazole, and potassium hydride, respectively).

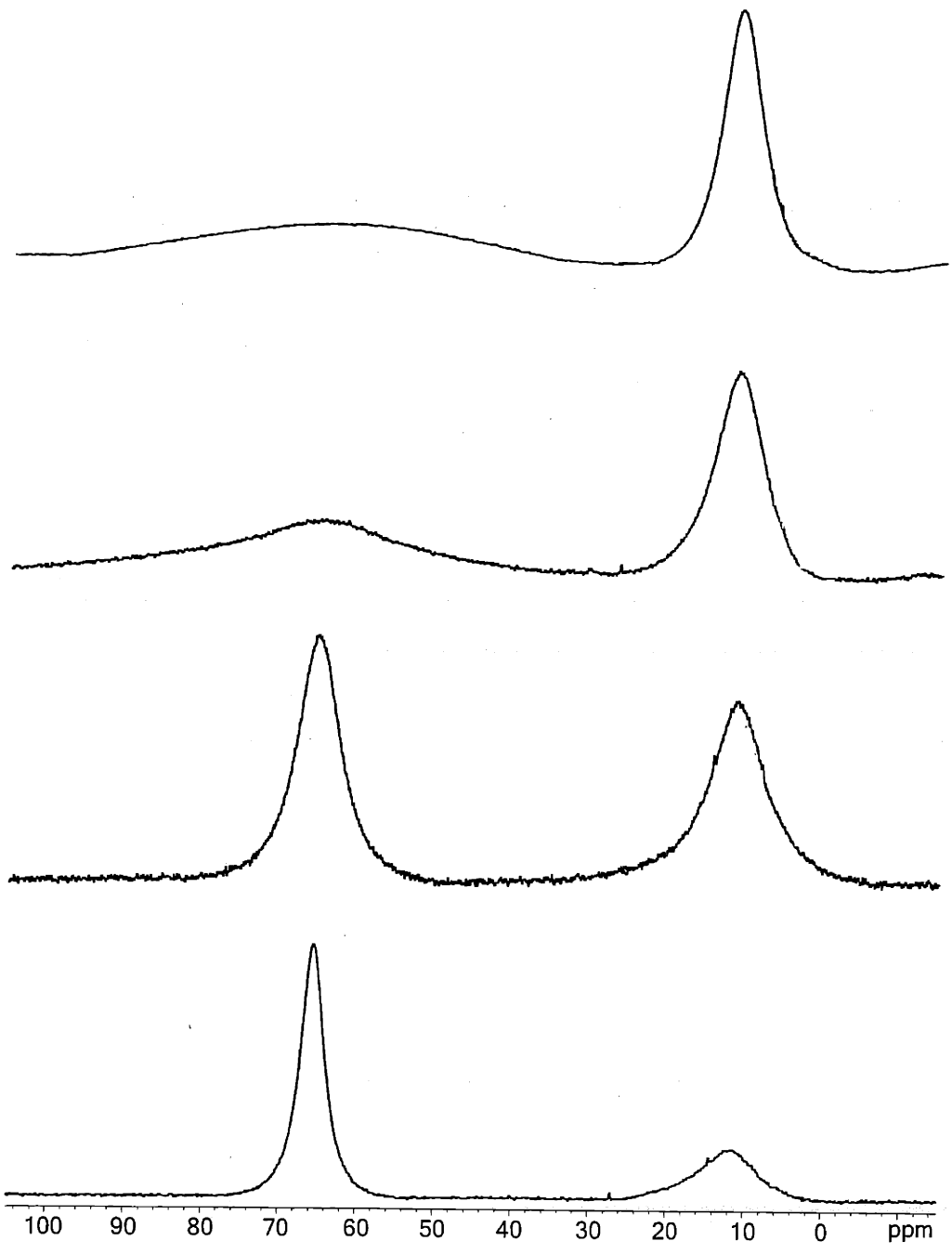

Figure 1: ^{2}H NMR spectra of the reactions of **3** with one, two, five, and ten equiv of 2,6-dimethylpyrazine (from bottom to top). The left peak is **3** and the right is postulated to be the intermediate **3-2,6-$C_4H_2N_2Me_2$**.

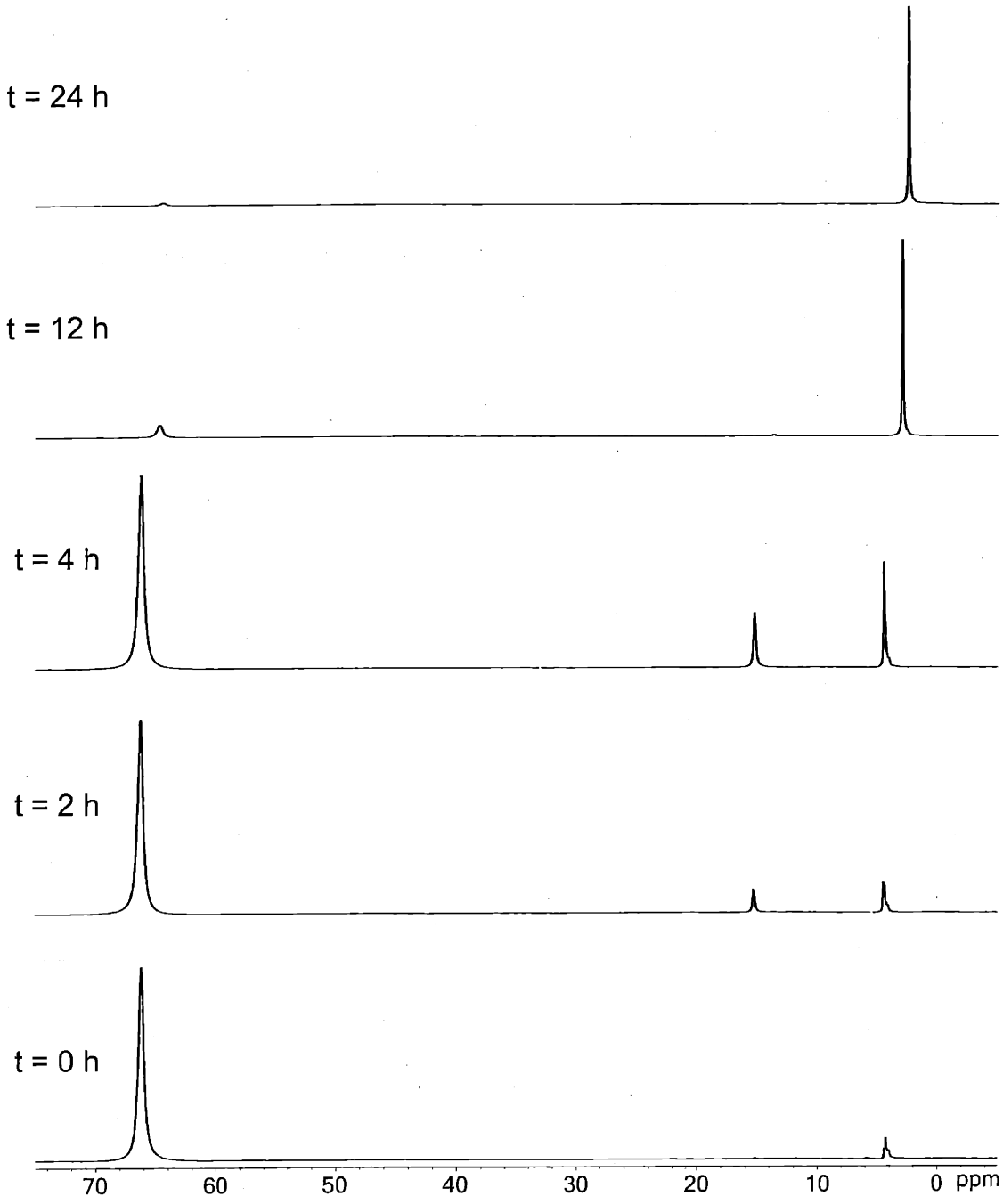

Figure 2: ^{2}H NMR spectra of the reactions of **3** with dinitrogen in the presence of one equiv of 4-dimethylaminopyridine in Et_2O. The signals from left to right are for **3**, [**3-N**]$_2$, and **3-N**, respectively.

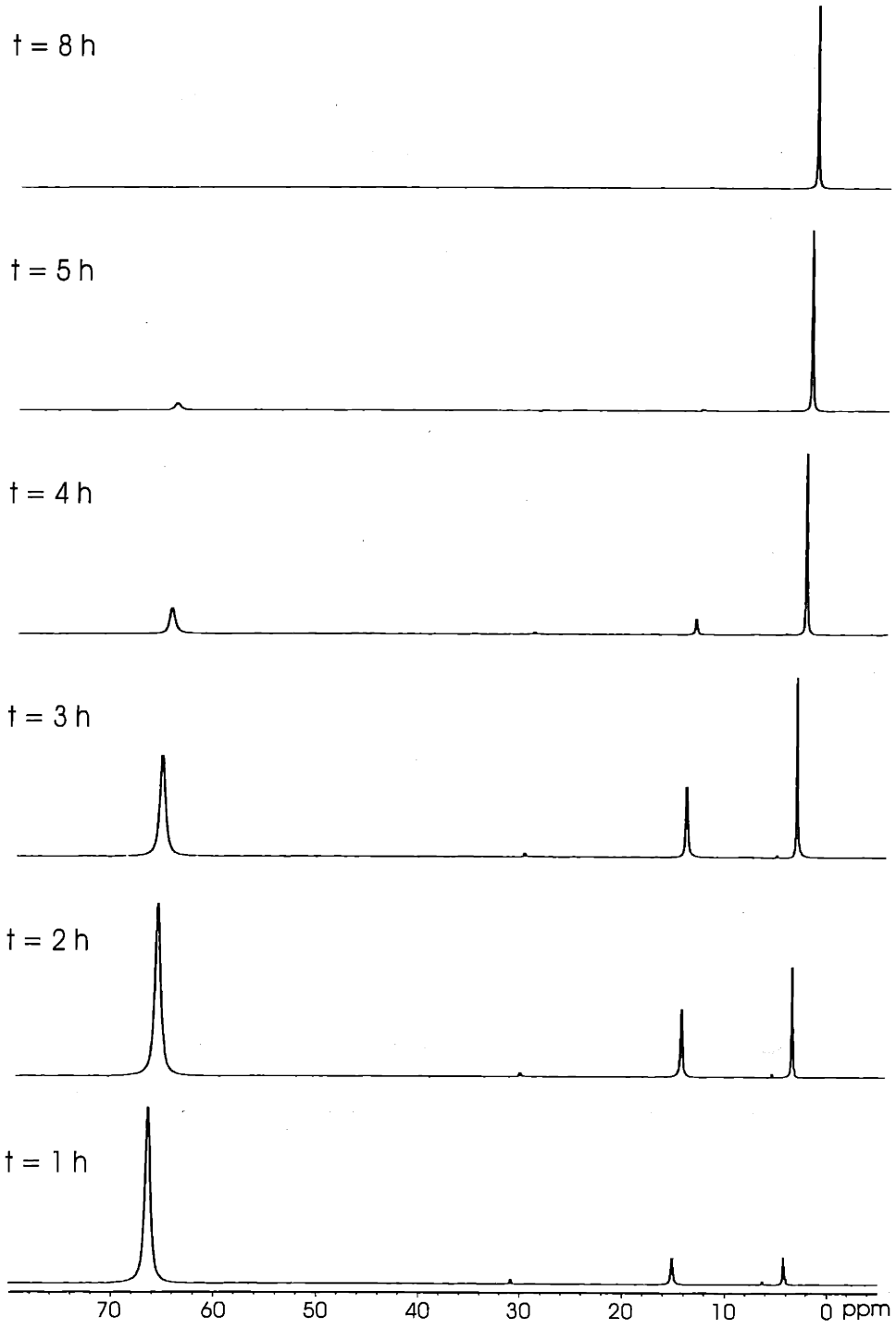

Figure 3: ^{2}H NMR spectra of the reactions of **3** with dinitrogen in the presence of one equiv of 1-methylimidazole in Et_2O. The signals from left to right are for **3**, [**3-N**]$_2$, and **3-N**, respectively.

3 Discussion

The foregoing results establish that the rate of dinitrogen cleavage by **1** or **3** is dramatically accelerated at ambient temperatures in the presence of organic bases and potassium hydride. Evidence from ^{2}H NMR spectroscopy suggested that the intermediates **2-L** (L = 2,6-dimethylpyrazine, pyridine, 4-dimethylaminopyridine, 1-methylimidazole) and **3-L** (L = 2,6-dimethylpyrazine) were formed. Some of the intermediates **3-L** (L = pyridine, 4-dimethylaminopyridine, 1-methylimidazole) were not, however, observed experimentally. As determined in the reaction of **3** with different amounts of 2,6-dimethylpyrazine (Figure 1), the binding constant of a Lewis base to **3** is very small. There are two reasons that could accout for this observation. First, the steric bulk of the three ^{t}Bu substituents prevents bulky substrates from accessing to the Mo center.[8] Second, the high-spin nature of **3**, presumably as a consequence of the relatively small energy difference between the d_{z^2} orbital and degenerate d_{xz} and d_{yz} orbitals,[5] makes complex **3** unfavorable in the interactions with pure σ- or π-donor ligands.[11] Due to the smaller ^{i}Pr groups, most of the ntermediates **2-L** could be detected. This base adduct **2-L** is in equilibrium with **1** and L in sloution.

We speculate that the intermediates **2-L** and **3-L** formed upon addition of L to **1** and **3** are relatively reactive species. It is expected that the d_{z^2} orbitals in **2-L** and **3-L** are pushed well above the energy of the d_{xz} and d_{yz} orbitals as a consequence of the binding of L donors to one of the apical sites. Therefore, **2-L** and **3-L** could be low-spin species and their high energy and reactivity in part a consequence of their low-spin configurations (cf. the high spin **2** and **3**). The base adducts **2-L** and **3-L** have been proposed to be more efficient for back-bonding to dinitrogen than **2** and **3**, respectively..[22] In addition to the literature precedent provided by Schrock,[17,18,23] Bianchini,[20] and

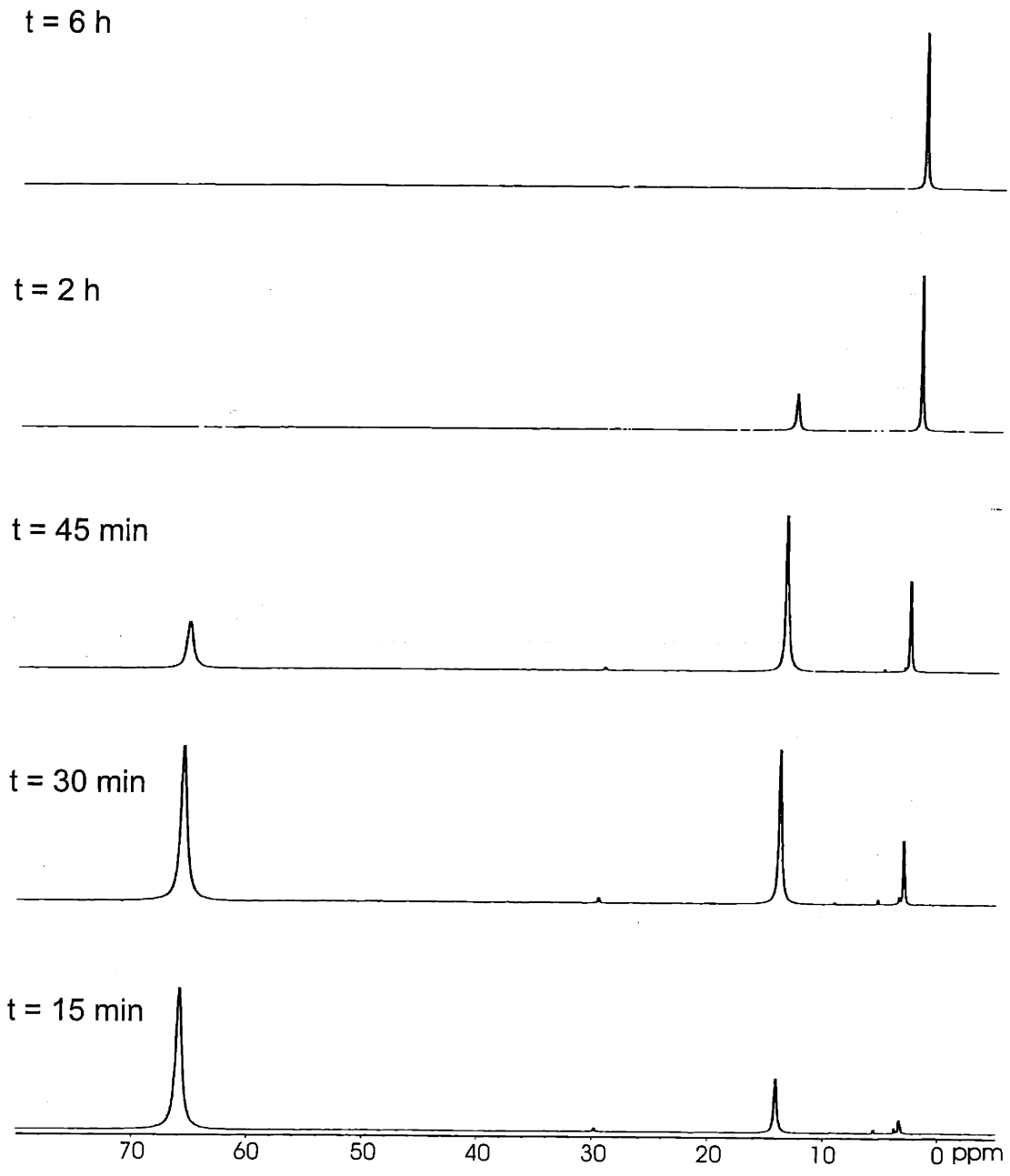

Figure 4: ^{2}H NMR spectra of the reactions of **3** with dinitrogen in the presence of ten equiv of potassium hydride in THF. The signals from left to right are for **3**, [**3-N**]$_2$, and **3-N**, respectively.

Dilworth,[19] this hypothesis is supported by the fact that **2-(η^1-2,4,6-NCC$_6$H$_2$Me$_3$)$_2$** is stable but **2-η^1-2,4,6-NCC$_6$H$_2$Me$_3$** has not been observed. The observation that the rate of dinitrogen cleavage by **1** did not increase in neat 2,4,6-collidine, which does not interact with **1** generating **2-L** indirectly supports our assumption as well.

The rate of dinitrogen cleavage is dependent on the nature of L. In general, a smaller and good σ- or even π-donor base is more efficient in accelerating the scission of dinitrogen. This generalization is reflected in Figures 2, 3, and 4; the reactions of **3** with dinitrogen in the presence of a variety of bases. Figure 2 shows the rate of the reaction of **3** with dinitrogen in the presence of 4-dimethylaminopyridine and it suggests that the rate of forming the pink intermediate [**3-N**]$_2$ is much smaller than those in Figure 3 (in the presence of 1-methylimidazole) and Figure 4 (in the presence of potassium hydride). In these three reactions, the initial rates of the formation of [**3-N**]$_2$ are faster than the rates of decomposition ($t_{1/2} \approx 30$ min) to form two equiv of **3-N**.[5] In Figure 4, the formation of complex [**3-N**]$_2$ is much faster than the formation of **3-N**. Hence, **3-H**$^-$ is so far the best species for enhancing the capture of dinitrogen by **1** or **3**. One might argue that an electron (the smallest but strongest base) should be better than the other bases for assisting **1** or **3** in binding dinitrogen. However, this is not the case. A previous study[13] indicated that **3** could not be reduced to form its corresponding anion. Although dinitrogen cleavage is dramatically accelerated at ambient temperature by the presence of Na/Hg, the formation of **3-N$_2$** is still slow.[13]

The dinitrogen cleavage reaction mediated by **1** or **3** is slow at ambient temperature because the ability to capture dinitrogen by **1** or **3** is weak.[5] Although the rate of splitting dinitrogen could be increased by the presence of Na/Hg, the rate-determining-step is still the binding of dinitrogen to **3**.[13] The presence of a Lewis base enhanced the ability of **1** or **3** to bind dinitrogen. The proposed

mechanism corresponding to this work is depicted in Figure 5. Due to the reversible binding of the apical base, the proposed intermediates **(2-L)**$_2$-μ-**N**$_2$ or **(3-L)**$_2$-μ-**N**$_2$ would lose L quickly to give the dimolybdenum dinitrogen complexes [**2-N**]$_2$ or [**3-N**]$_2$. It had been predicted, on theoretical grounds, that a dinitrogen splitting reaction for the complex [Mo(^{t}BuMe$_2$SiNCH$_2$CH$_2$)$_3$N]$_2$(μ-N$_2$)[24] would be an endothermic process.[22] It is worth noting that the purple intermediate dimolybdenum dinitrogen complex [**3-N**]$_2$ was detected by ^{2}H NMR spectroscopy (Figures 2-4), but the corresponding complex [**2-N**]$_2$ still was not observed. This is attributed to the small ^{i}Pr groups. Over the course of dinitrogen cleavage, a postulated zigzag-shaped (C_{2h}) transition state (TS) with an elongated NN bond and shortened Mo-N$_2$ bonds is involved.[5] Accordingly, the linear intermediate [**2-N**]$_2$ can transform into a C_{2h} TS, and subsequently rapidly decompose to **2-N**. The ease of forming **2**$_2$-μ-**N** (not **3**$_2$-μ-**N**) instead of **2-N** from the dinitrogen cleavage reaction also supports this hypothesis.

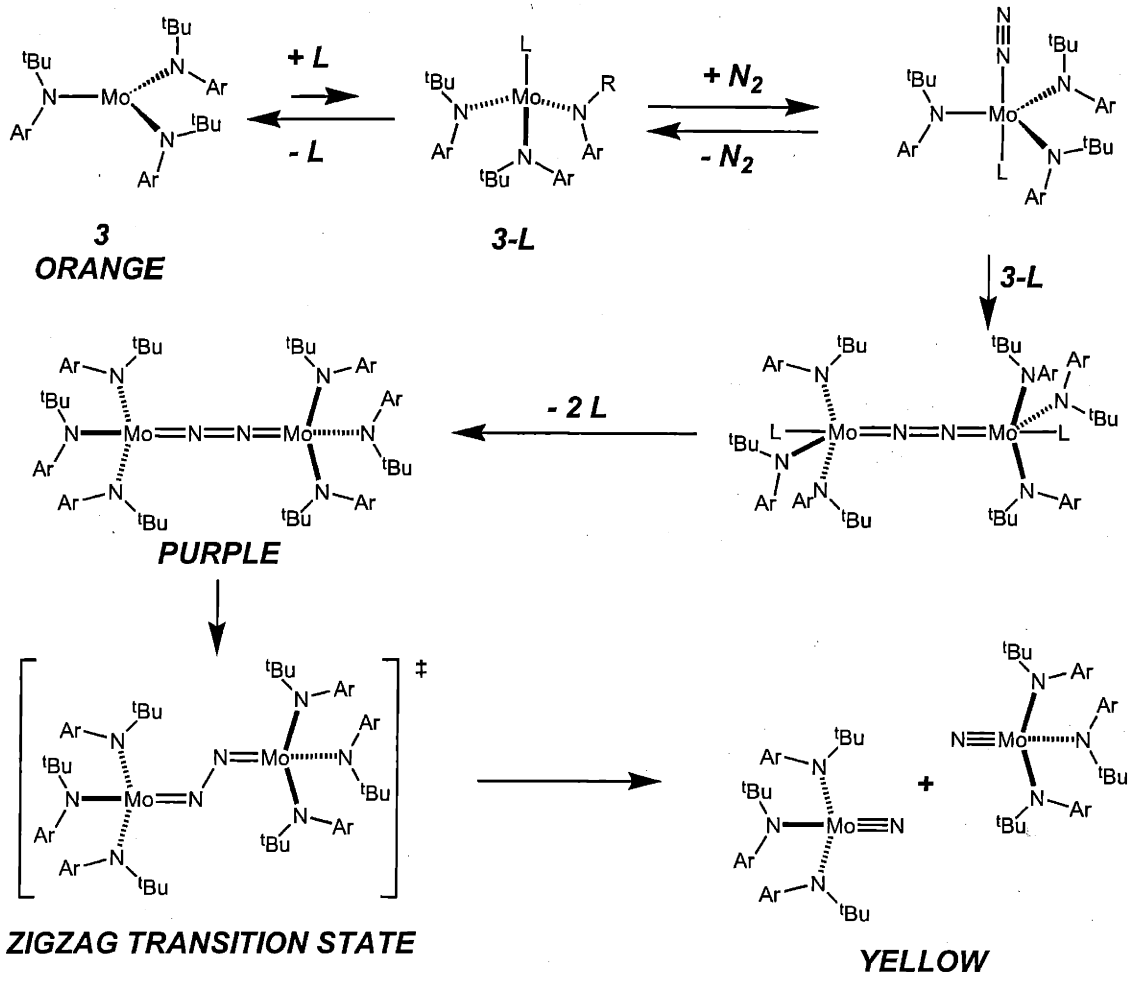

Figure 5: Proposed mechanism of the dinitrogen cleavage by **3** in the presence of a Lewis base.

4 Coucluding Remarks

Findings presented here corroborate the proposal that dinitrogen cleavage by three-coordinate molybdenum amide complexes is accelerated by the presence of bases. The proposed active complexes **2-L** or **3-L** (L = 2,6-dimethylpyrazine, pyridine, 4-dimethylaminopyridine, 1-methylimidazole, hydride anion) were found to bind dinitrogen readily at ambient temperature. The ability of **1** or **3** to bind dinitrogen in the presence of L is a function of the size and basicity of L. With a small but

strong base, the rate of forming the purple intermediate dimolybdenum dinitrogen complex [**3-N**]$_2$ can be larger than that of its conversion to the nitrido product, **3-N**. Especially attractive is the fact that the proposed dinitrogen cleavage mechanism in this work is easily achieved by comparing the different observations from sterically different complexes **1** and **3**.

5 Experimental Section

5.1 General considerations

Unless otherwise stated, all operations were performed in a Vacuum Atmospheres drybox under an atmosphere of purified nitrogen or using Schlenk techniques under an argon atmosphere. Complexes **1**, and **3** were prepared according to the precedent literature.[5,6] 2,6-dimethylpyrazine, pyridine, 4-dimethylaminopyridine, 1-methylimidazole, and 2,4,6-collidine were purchased from Alfa Azar and potassium hydride was purchased from Aldrich Chemical Co. Diethyl ether, benzene, *n*-pentane, and toluene were dried and deoxygenated by the method of Grubbs.[25] THF was distilled over Na/benzophenone and collected under nitrogen. C_6D_6 was degassed and dried over 4 Å molecular sieves. Celite, alumina, and 4 Å molecular sieves were dried in vacuo overnight at a temperature above 200 °C. An NMR data was collected on Varian VXR-500 or Varian XL-301 spectrometers. ^1H, ^2H, and ^{13}C chemical shifts are reported with respect to internal solvent (7.15 ppm and 128.38 (t) ppm (C_6D_6)).

5.2 Reactions of complex 1 with two equiv of Lewis bases (1-methylimidazole, 4-dimethylaminopyridine, pyridine, 2,6-dimethylpyrazine under vacuum and neat 2,4,6-trimethylpyridine)

To a solution of **1-*d*$_{18}$** (0.232 g, 0.386 mmol) in 2 mL of Et_2O were added 1-methylimidazole (0.063 g, 0.772 mmol). The resulting mixture was immediately loaded in an NMR tube and was degassed by 3 cycles of freezing-thawing-and-pumping. ^2H NMR spectroscopy exhibited no signals for **1**

but a new resonance signal at 5.36 ppm ($\Delta\nu_{1/2}$= 525 Hz) (8.24 ppm with $\Delta\nu_{1/2}$= 303 Hz for 4-dimethylaminopyridine; 7.64 ppm with $\Delta\nu_{1/2}$= 309 Hz for pyridine; and 7.20 ppm with $\Delta\nu_{1/2}$= 26 Hz for 2,6-dimethylpyrazine). When **1** (0.189 mg, 0.314 mmol) was dissolved in neat 2,4,6-collodine, ^{2}H NMR only displayed the signals for **1**.

5.3 Syntheses of 2_2-N from 1 and dinitrogen with the presence of one equiv of 1-methylimidazole, 4-dimethylaminopyridine, pyridine, 2,6-dimethylpyrazine

To a solution of **1** (0.673 g, 1.155 mmol) in 8 mL of *n*-pentane at room temperature were added 0.095 g of 1-methylimidazole. The resulting mixture became purple accompanied by the precipitation **2_2-N**. After stirring for 10 min, the solution was stripped to about 3 mL, and black **2_2-N** was collected on a frit by filtration and dried in vacuo. The yield was 87 %. The filtrate was concentrated to about 1 mL and stored in a freezer at -35 °C. Yellow crystals of **2-N** were collected on a frit by filtration and dried in vacuo. The yield was 8%. When the base was 4-dimethylaminopyridine, the isolated yield of **2_2**-N was 92% in 2 h; when the base was pyridine, the yield of **2_2-N** was 91% in 3 h; when the base was 2,6-dimethylpyrazine, the yield of **2_2-N** was 85% overnight. No **2-N** was observed in the latter 3 reactions.

5.4 Syntheses of 3-N from 3 and dinitrogen in the presence of one equiv of 1-methylimidazole, 4-dimethylaminopyridine, pyridine, 2,6-dimethylpyrazine, and ten equiv of potassium hydride

To a solution of **3** (0.661 g, 1.058 mmol) in 8 mL of Et_2O at room temperature were added 0.0869 g of 1-methylimidazole. The resulting mixture was stirred for 30 min during which it became dark pink. After 24 h, the solution turned amber. ^1H NMR analysis of the crude material obtained upon removing the volatiles revealed that **3**-N had formed cleanly. The nitrido complex **3-N** was isolated in 91% yield upon recrystallization (*n*-pentane, −35 °C). For the other bases, the yield of **3-N** was 85% (4-dimethylaminopyridine), 83% (pyridine), and 74% (2,6-dimethylpyrazine) all in 24 h, and 94% (potassium hydride).

References

1. Clentsmith, G. K. B.; Bates, V. M. E.; Hitchcock, P. B.; Cloke, F. G. N. *J. Am. Chem. Soc.* **1999,** *121,* 10444.

2. Mindiola, D. J.; Meyer, K.; Cherry, J.-P. F.; Baker, T. A.; Cummins, C. C. *Organometallics* **2000,** *19,* 1622.

3. Caselli, A.; Solari, R.; Scopelliti, R.; Floriani, C.; Re, N.; Rizzoli, C.; Chiesi-Villa, A. *J. Am. Chem. Soc.* **2000,** *122,* 3652.

4. Solari, E.; Silva, C. D.; Iacono, B.; Hesschenbrouck, J.; Rizzoli, C.; Scopelliti, R.; Floriani, C. *Angew. Chem. Int. Ed.* **2001,** *40,* 3907.

5. Laplaza, C. E.; Johnson, M. J. A.; Peters, J. C.; Odom, A. L.; Kim, E.; Cummins, C. C.; George, G. N.; Pickering, I. J. *J. Am. Chem. Soc.* **1996,** *118,* 8623-8638.

6. Tsai, Y.-C.; Johnson, M. J. A.; Mindiola, D. J.; Cummins, C. C.; Klooster, W. T.; Koetzle, T. F. *J. Am. Chem. Soc.* **1999,** *121,* 10426.

7. Tsai, Y.-C.; Diaconescu, P. L.; ; Cummins, C. C. *Organometallics* **2000,** *19,* 5260.

8. Tsai, Y.-C.; Meyer, K.; Mindiola, D. J.; Cummins, C. C. *Manuscript in preparation* .

9. Tsai, Y.-C.; Durá-Vilá, V.; Diaconescu, P. L.; Cummins, C. C. *Manuscript in preparation* .

10. Laplaza, C. E.; Cummins, C. C. *Science* **1995,** *268,* 861.

11. Cummins, C. C. *Chem. Commun.* **1998,** 1777-1786.

12. Fryzuk, M. D.; Johnson, S. A. *Coord. Chem. Rev.* **2000,** *200-202,* 379 and references therein.

13. Peters, J. C.; Cherry, J.-P.; Thomas, J. C.; Baraldo, L.; Mindiola, D. J.; Davis, W. M.; Cummins, C. C. *J. Am. Chem. Soc.* **1999,** *121,* 10053-10067.

14. Cesarotti, M.; Gullotti, A.; Pasini, A.; Ugo, R. *J. Chem. Soc. Dalton Trans.* **1977,** 757.

15. Carter, M. J.; Rillema, P. P.; Basolo, F. *J. Am. Chem. Soc.* **1974,** *96,* 392.

16. Meier, I. K.; Pearlstein, R. M.; Ramprasad, D.; Pez, G. P. *Inorg. Chem.* **1997,** *36,* 1707.

17. Neuner, B.; Schrock, R. R. *Organometallics* **1996,** *15,* 5-6.

18. O'Donoghue, M. B.; Davis, W. M.; Schrock, R. R. *Inorg. Chem.* **1998,** *37,* 5149.

19. Dilworth, J. R.; Hu, J.; Miller, J. R.; Hughes, D. L.; Zubieta, J. A. nad Chen, Q. *J. Chem. Soc. Dalton Trans.* **1995,** 3153.

20. Osman, R.; Pattison, D. L.; Perutz, R. N.; Bianchini, C.; Casares, J. A.; Peruzzini, M. *J. Am. Chem. Soc.* **1997,** *119,* 8459.

21. Cherry, J.-P. F.; Stephens, F. H.; Johnson, M. J. A.; Diaconescu, P. L.; Cummins, C. C. *Submitted to Inorg. Chem.* .

22. Cui, Q.; Musaev, D. G.; Svensson, M.; Sieber, S.; Morokuma, K. *J. Am. Chem. Soc.* **1995,** *117,* 12366-12367.

23. Kol, M.; Schrock, R. R.; Kempe, R.; Davis, W. M. *J. Am. Chem. Soc.* **1994,** *116,* 4382.

24. Shih, K.-Y.; Schrock, R. R.; Kempe, R. *J. Am. Chem. Soc.* **1994,** *116,* 8804.

25. Pangborn, A. B.; Giardello, M. A.; Grubbs, R. H.; Rosen, R. K.; Timmers, F. J. *Organometallics* **1996,** *15,* 1518.

Chapter 4. Activation of E-H Bonds (E = Sn or P) by Three-Coordinate Molybdenum(III) Complexes

October 29, 2001

1 Introduction

The activation of the Si-H bond in hydrosilanes by a low oxidation state transition-metal complex is well understood.[1] Many "classical" (two-center, two-electron) and "nonclassical" (three-center, two-electron) hydrido silyl metal complexes have been charactrized since Graham first reported the mononuclear σ-complex $Cp(CO)_2Mn(\eta^2\text{-}HSiPh_3)$.[2] The nonclassical interaction involves partial addition of the Si-H bond to the metal center. Other descriptive terms that have been used to describe the nonclassical interaction include σ-complexation or an agostic interaction. A σ-complex can be an intermediate, a transition state in an oxidative addition reaction, or an isolated complex. Schubert has proposed that the oxidative addition pathway is initiated when the H atom in the Si-H unit approaches the metal. The Si-H component then pivots to place the Si atom near the metal center, increasing the transition-metal-Si interaction and weakening the Si-H bond.[3]

The three-coordinate Mo(III) complex $Mo(N[^tBu]Ar)_3$ ($^tBu = C(CD_3)_2CH_3$, $Ar = 3,5\text{-}C_6H_3Me_2$) (**3**) can split dinitrogen[4,5] and nitrous oxide[6,7] and has been used for the synthesis of triply bonded functional groups such as a terminal phosphide[8] and a terminal carbide.[9] This unique reactivity can be comprehended in terms of the electronic structure of the compound. Complex **3** has a sterically protected, three-fold symmetric "pocket" which is composed of three ^tBu groups. As a result, the Mo center has only three orbitals available to bond to additional ligands: two π orbitals (d_{xz} and d_{yz}) and a σ orbital (d_{z^2}). The fact that the two frontier π orbitals are degenerate in the C_3-symmetric complex **3** creates a favorable environment for a metal-ligand triple bond formation. Owing to its dinimished steric bulk, the molybdenum metallaaziridine hydride complex $Mo(H)(\eta^2\text{-}Me_2C{=}NAr)(N[^iPr]Ar)_2$ (**1**), which behaves as a mask of $Mo(N[^iPr]Ar)_3$ (**2**), is more reactive than

$Mo(N[^tBu]Ar)_3$. For example, benzophenone,[10] alkynes,[10,11] and organonitriles[12] coordinate to **2** in an η^2 fashion, but exhibit no reaction with **3**.[10]

The orbital interactions that occur between the Si-H unit and the metal center coincide with the extent of oxidation addition for such nonclassical complexes. A σ-interaction can exist between a metal d-orbital and the Si-H σ-bonding orbital. A π-component may arise when an occupied metal d_π-orbital interacts with the Si-H σ^*-antibonding orbital. If sufficient π back-bonding occurs, weakening of the Si-H bond ensues and can results in full cleavage of the Si-H bond. The substituents at either silicon or the metal center can have significant impacts on the oxidative addition pathway. Although silanes bearing either electronegative or electron-donating groups have been reported to react with transition-metal centers, it is generally observed that electron-rich, late transition-metal centers or electron-withdrawing groups at silicon tend to result in full oxidative addition of the silane. In general, sterically unencumbering and electronegative groups bound to silicon favor an oxidative addition reaction. Increased electron density at the metal center or electrophilic properties at silicon increases the π back-bonding and leads to full oxidative addition.

Hydrostannanes have been extensively used as intermediates in the synthesis of organotin compounds and as selective reducing agents in organic synthesis. Their special characteristics can be attributed in large part to the fact that the tin-hydrogen bond is both weaker and less polar than e.g. boron-hydrogen and aluminum-hydrogen bonds. The greater basicity of the Sn-H bond relative to the H-H, H-C, or Si-H bond makes the Sn-H unit a better σ-donor.[13] In addition, the greater accessibility of the σ^*-orbital allows the Sn-H unit to be a better π-acceptor. The nature of the σ-donor or π-acceptor ability of the Sn-H σ^* unit may potentially be tuned by the substituents on tin. The possibility of a three-center bond involving a SnR_3 ligand has been considered since Schu-

bert *et al.* reported the first example of a transition-metal-hydrogen-tin three-center, two-electron bond in the Mn complex $(MeCp)(CO)_2Mn(H)SnPh_3$.[14] Accordingly, several transition-metal hydrido stannyl complexes[15–18] stabilized by Cp or arene and CO ligands have been prepared. The photochemical decarbonylation of metal tricarbonyl complexes followed by addition of $HSnR_3$ has led to a variety of Cp and arene-hydride-SnR_3 complexes of Mn[14] and Cr.[15,18]

It is noteworthy that the P-H bond strength [$D(H\text{-}PH_2 = 83.9$ kcal/mol][19] is close to those for Si-H and Sn-H [cf. $D(H\text{-}SiR_3) = 92.0\text{-}79.0$ and $D(H-Sn^nBu_3) = 74.0$ kcal/mol].[20,21] Therefore, the implication is that the activation of P-H bonds by transition-metal complexes may be a possibility. For instance, Wolczanski *et al.* reported the synthesis of $(silox)_3Ta{=}EPh$ [silox = $OSi(^tBu)_3$ and E = N, P, or As][22] *via* 1,2-H_2-elimination. This work has inspired us to explore the chemistry of alkyl- or arylphosphine with the coordinately unsaturated Mo(III) complexes studied in our group.

Reported herein are the syntheses and characterizations of complexes **2-η^2-HSnR$_3$** (R = ^{n}Bu or Ph), [**2-SnPh$_2$**]$_2$, **3-SnPh$_3$**, **3-H**, **2-PHR** (R = Ph, cyclohexyl, 2,4,6-mesityl), and **3-PHPh** *via* the activation of the respective E-H bond (E = Sn or P) by **1** or **3**.

2 Results and Discussion

2.1 Synthesis 2-η^2-HSnR$_3$ (R = ^{n}Bu or Ph)

Addition of one equiv of $HSnR_3$ (R = ^{n}Bu or Ph) to $Mo(H)(\eta^2\text{-}(CD_3)_2CNAr)(N[^iPr\text{-}d_6]Ar)_2$ (**1-d_{18}**) in THF, Et_2O, or n-C_5H_{12} solution resulted in a color change from orange-brown to brownish-yellow (R = ^{n}Bu) or greenish-yellow (R = Ph). ^{2}H NMR spectra displayed one broad signal for each

reaction at 9.41 ($\Delta\nu_{1/2}$= 46 Hz, R= ^{n}Bu) ppm and 9.11 ($\Delta\nu_{1/2}$= 50 Hz, R = Ph) ppm, respectively, indicative of paramagnetism. However, the room temperature X-band EPR spectra of the former reaction only showed the signal of **1-d_{18}**,[12] suggesting that HSn^{n}Bu$_3$ reversibly coordinated to **2** and the adduct decomposed in a dilute (< 1 mM) solution. Consequently, crystals of this new compound were grown in the presence of excess HSn^{n}Bu$_3$ in a n-C_5H_{12} solution that was stored at −35 °C. The X-ray crystallographic study revealed that this new compound was the hydrido stannyl complex Mo(η^2-HSn^{n}Bu$_3$)(N[^{i}Pr]Ar)$_3$ (**2-η^2-HSn^{n}Bu$_3$**). The ORTEP diagram of **2-η^2-HSn^{n}Bu$_3$** is shown in Figure 1.

The hydrostannane ligand HSn^{n}Bu$_3$ coordinates to **2** *via* the Sn−H bond to form a σ-complex. The geometry at Mo is better described as a distorted tetrahedron with the Sn-H moiety occupying one coordinate site. In particular, we were able to locate and refine the position of the hydride ligand, which was reliable only within the accuracy of the method (the true Sn-H and Mo-H distances should be somewhat longer, since X-ray structure analyses systematically underestimate M-H distances). The location of the hydride on HSn^{n}Bu$_3$ was determined by X-ray crystallography, and the position is consistent with the geometry. The angles Sn-Mo-N(1) (86.36(7)°) and Sn-Mo-N(3) (91.31(8)°) are close to 90° while the angle Sn-Mo-N(2) (128.08(8))° is much larger. Accordingly, the hydride is coplanar with Sn, Mo, and N(2). The bond distances for Mo-Sn, Sn-H, and Mo-H are 2.7787(3), 2.16(4), and 1.61(4) Å, respectively. It was noted that the Mo-Sn bond distance is considerably shorter than the expected distance of 3.00 Å based on the sum of covalent radii (1.61 + 1.39 Å) for these two atoms.[23–26] The difference in the shortening of the Mo-Sn bond is a result of a considerable increase in the s-orbital electron density of the Mo-Sn bond, due to the tin nucleus.[27] The Sn-H distance found in **2-η^2-HSn^{n}Bu$_3$** (2.16(4) Å) is only about 0.45

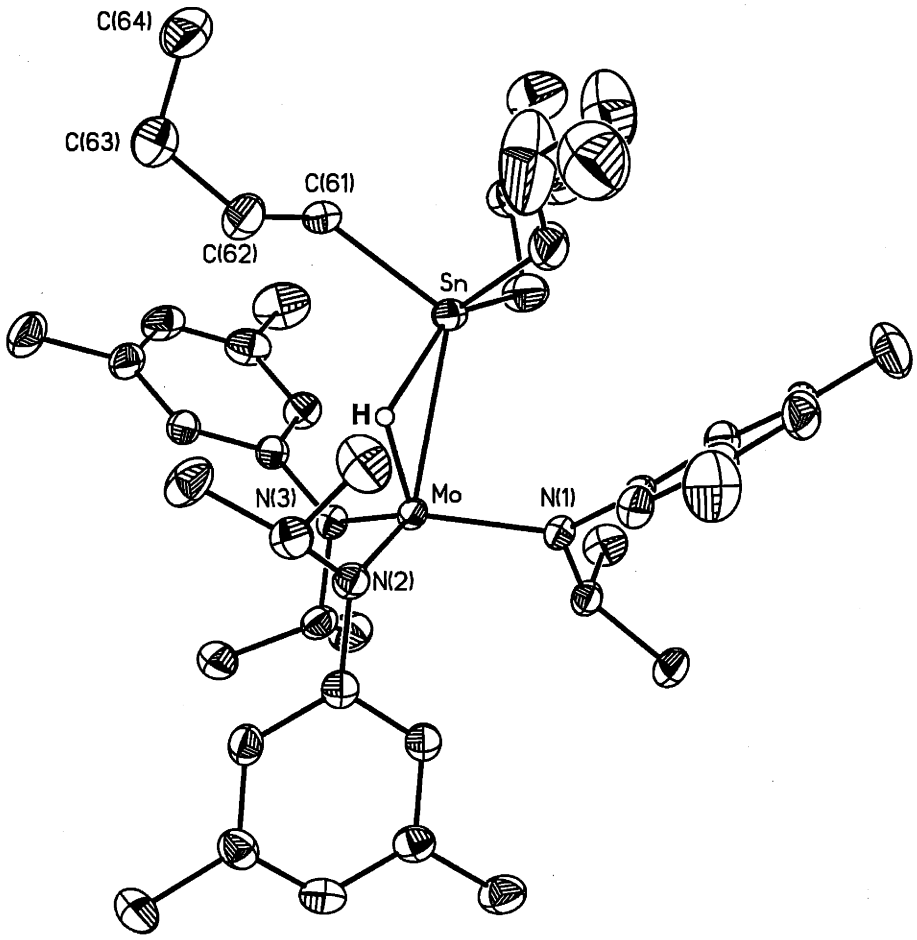

Figure 1: Thermal ellipsoid plot (35% probability) of **2-η^2-HSn^{n}Bu$_3$**. Selected distances (Å) and angles (°): Sn-H, 2.170(4); Sn-Mo, 2.7787(3); Mo-H, 1.61(4); Mo-N(1), 1.991(2); Mo-N(2), 1.999(3); Mo-N(3), 1.940(3); H-Mo-Sn, 50.7(14); N(1)-Mo-Sn, 86.36(7); N(2)-Mo-Sn, 128.08(8); N(3)-Mo-Sn, 91.31(8); N(1)-Mo-N(2), 114.8(1); N(2)-Mo-N(3), 115.0(1); N(3)-Mo-N(1), 117.4(1).

Å (21%) longer than those in methyl-substituted stannanes[28,29] and $[(Me_3Si)_2CH_2]_2SnH(OH)$[30] and is therefore indicative of a bonding interaction between Sn and H. The H-Mo-Sn angle in **2-η^2-HSn^{n}Bu$_3$** is 50.70(14)°, which is too small to suggest that the Sn and H atoms occupy two coordination sites around the Mo center. Rather, the stannane HSn^nBu_3 ligand should be considered as one ligand such that the Sn−H bond occupies one coordinate site, with the hydride forming a delocalized, three-center two-electron bond involving Sn and Mo. Table 1 summarizes some metric parameters of the known hydrido stannyl complexes $M(\eta^2\text{-}HSnR_3)L_n$.

Complexes	Mo-Sn (Å)	Sn-H (Å)	H-Mo-Sn (°)
Me-$Cp(CO)_2Mn(\eta^2\text{-}HSnPh_3)$[14]	2.636(1)	2.16(4)	55(2)
1,3,5-$C_6H_3Me_3(CO)_2Cr(\eta^2\text{-}HSnPh_3)$[15]	2.7016(6)	2.02(4)[a]	48.0(1)[b]
$Cp(NO)(PPh_3)Cr(\eta^2\text{-}HSnPh_3)$[16]	2.6690(7)	1.84*	42*
$Rh(NCBPh_3)(H)(SnPh_3)(PPh_3)_2$[17]	2.559(1)	2.31(5)	64(2)
1,4-$C_6H_4(OMe)_2(CO)_2Cr(\eta^2\text{-}HSnPh_3)$[18]	2.688(3)	2.23*	56*
2-η^2-HSn^{n}Bu$_3$	2.7787(3)	2.16(4)	50.70(14)

Table 1: Structural data of complexes with a moiety of $M(\eta^2\text{-}HSnR_3)L_n$. a: 1.95 Å[31], b: 45°[31], *: calculated.

In contrast to the low stability of **2-η^2-HSn^{n}Bu$_3$** in solution, the hydrido stannyl compound **2-η^2-HSnPh$_3$** was found to have a stronger interaction between Mo and the Sn-H bond. Figures 2 and 3 show the X-band EPR spectra of **2-η^2-HSnPh$_3$** and its deuterated isotopomer **2-η^2-DSnPh$_3$**. The most prominent difference in the spectra is the splitting pattern evinced by **2-η^2-HSnPh$_3$** and its deutero analog **2-η^2-DSnPh$_3$**. The main signal as well as the six satellites in **2-η^2-HSnPh$_3$**

are split into two intense signals through coupling of the electron with a nucleus of spin $I = 1/2$. The spectrum of the deuterated isotopomer **2-η^2-DSnPh$_3$** does not exhibit this additional super-hyperfine structure, so this feature must arise from coupling to the hydride ($A_{iso}{}^2$H is $\approx 1/7\ A_{iso}{}^1$H). Moreover, the stannane ligand in compound **2-η^2-HSn^{n}Bu$_3$** can be replaced by HSnPh$_3$. Addition of one equiv of HSnPh$_3$ to **2-η^2-HSn^{n}Bu$_3$** produced the green-yellow complex **2-η^2-HSnPh$_3$**. However, HSn^{n}Bu$_3$ cannot substitute the HSnPh$_3$ ligand in complex **2-η^2-HSnPh$_3$**. The binding of HSnR$_3$ to a low-valent transition-metal complex to form a three-center bonded adduct is believed to occur by two complementary processes: (1) σ activation, involving a transfer of electron density from the Sn-H σ bond to a vacant orbital of σ symmetry on the metal and (2) σ^* activation, in which electron density is transfered from a filled orbital of π symmetry on the metal to the σ^* Sn-H antibonding orbital. σ activation is favored in the case where electron-withdrawing substituents are present on transition-metal and electron-donating substituents (cf. ^{n}Bu) are on Sn. Conversely, σ^* activation is supported by electron-donating substituents (cf. anilide ligands) on transition-metal and electron-withdrawing substituents (Ph) on Sn.[17,31–34] Therfore, **2-η^2-HSn^{n}Bu$_3$** should have stronger Sn-H interactions than that observed in the hydrido stannyl compound **2-η^2-HSnPh$_3$**,.[18] i.e., compound **2-η^2-HSnPh$_3$** exhibits a greater extent of oxidative addition than complex **2-η^2-HSn^{n}Bu$_3$**.

A bis-stannyl metal complex is a common by-product in synthesizing hydrido atnnyl complexes. For example, the syntheses of Me-Cp(CO)$_2$Mn(η^2-HSnPh$_3$) and 1,4-C$_6$H$_4$(OMe)$_2$(CO)$_2$Cr-(η^2-HSnPh$_3$) were contaminated with Me-Cp(CO)$_2$Mn(SnPh$_3$)$_2$ and 1,4-C$_6$H$_4$(OMe)$_2$(CO)$_2$Cr(SnPh$_3$)$_2$, espectively.[35,36] However, complexes **2-η^2-HSnR$_3$** (R = ^{n}Bu or Ph) can be prepared in high yield in the presence of excess of HSnR$_3$ in organic solvents. None of bis-stannyl complexes

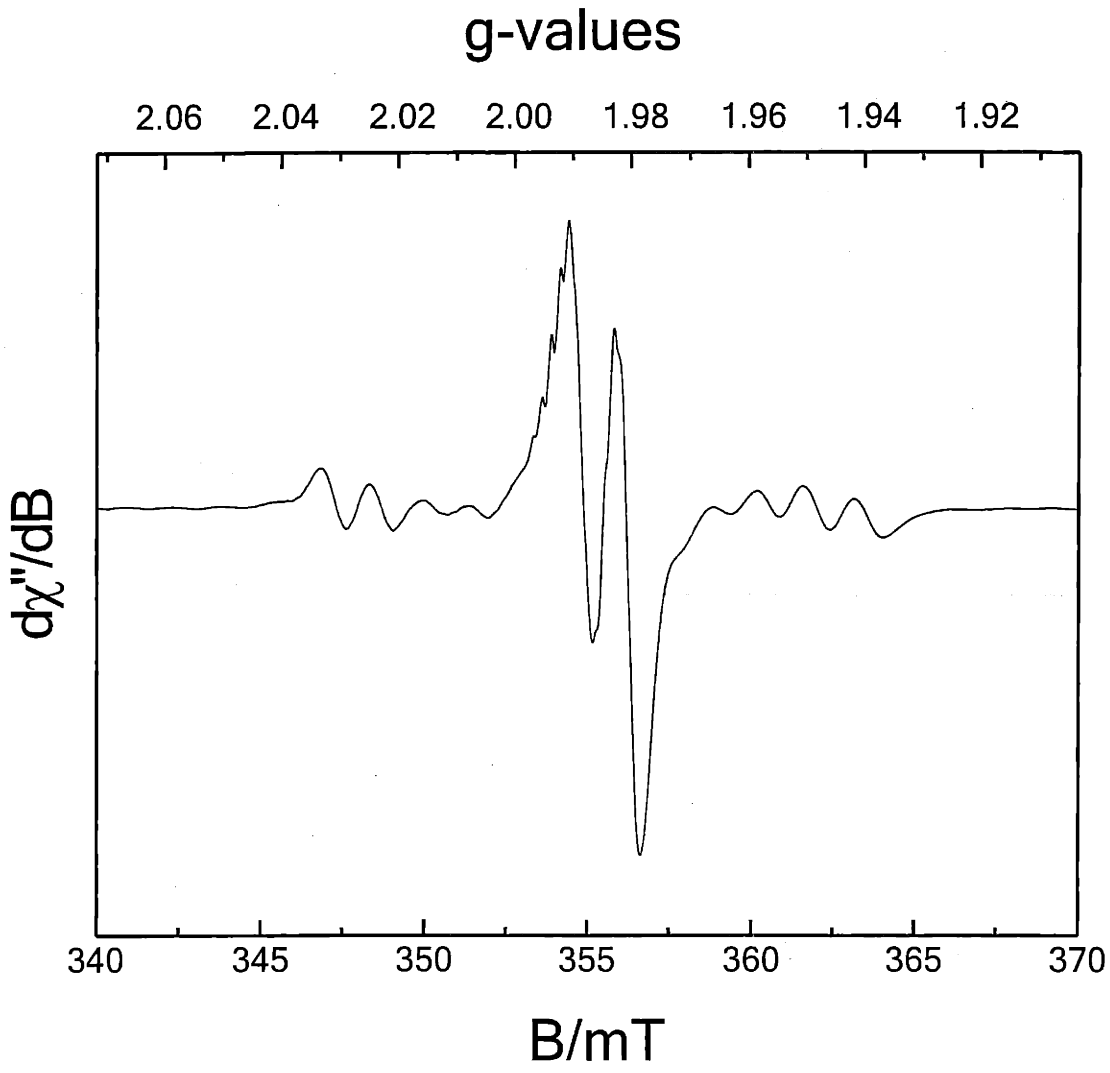

Figure 2: X-band EPR spectrum of **2-η^2-HSnPh$_3$** recorded in n-C_5H_{12} at 300 K Experimental conditions: microwave frequency ν: 9.858 GHz, power: 20.1 mW, modulation amplitude: 0.1 G.

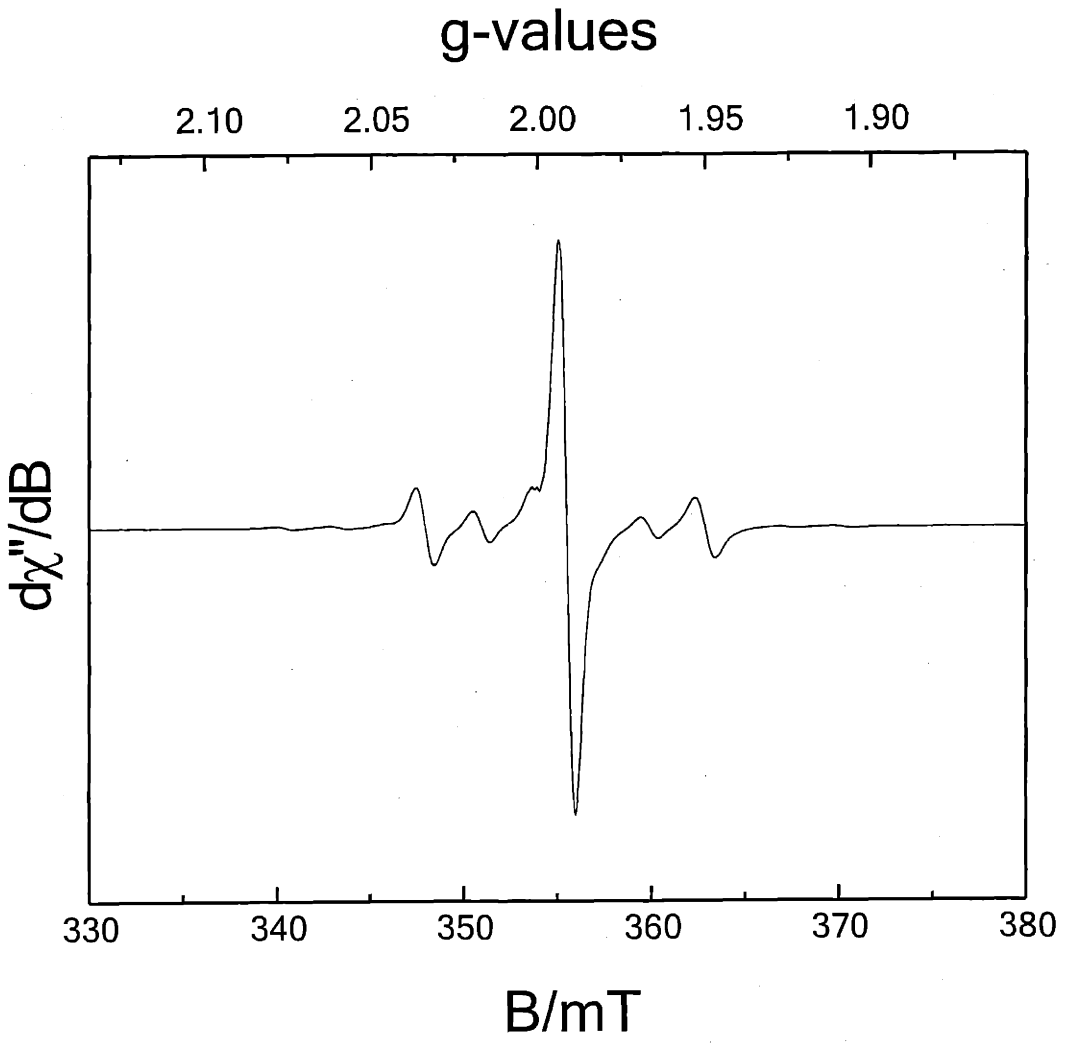

Figure 3: X-band EPR spectrum of **2-η^2-DSnPh$_3$** recorded in n-C_5H_{12} at 300 K Experimental conditions: microwave frequency ν: 9.858 GHz, power: 20.1 mW, modulation amplitude: 0.1 G.

$Mo(SnR_3)_2(N[^iPr]Ar)_3$ **2-$(SnR_3)_2$** has been detected experimentally. This can be explained by the steric bulk of the anilide ligands that prevent a second $HSnR_3$ from accessing the Mo center.

In general, the hydrido stannyl compounds **2-η^2-$HSnR_3$** are not stable in solution. The stannane ligands can be replaced easily by organic nitriles. Both complexes reacted rapidly with one equiv of NCPh to yield **2-NC(H)Ph**. ^2H NMR spectra revealed that the stannane ligands were completely replaced by NCPh to initially form **2-η^2-NCPh** and **2-$(\eta^1$-NCPh$)_2$**.[12] Subsequent hydride transfer from free $HSnR_3$ to **2-η^2-NCPh** or **2-$(\eta^1$-NCPh$)_2$** produced **2-NC(H)Ph**. Moreover, both **2-η^2-HSn^nBu_3** and **2-η^2-$HSnPh_3$** slowly reacted with dinitrogen to form **2_2-N**.

2.2 Reactions of 3 with $HSnR_3$ (R = ^{n}Bu or Ph)

In contrast to the reactions between **1** and $HSnR_3$, hydrido stannyl complexes **3-η^2-$HSnR_3$** were not produced in the reactions of **3** with $HSnR_3$ (R = ^{n}Bu or Ph). ^2H NMR spectra revealed two signals in both reactions. When R = Ph, peaks at 29.5 and 12 ppm (ca. 1.3:1 ratio) were detected while signals at 29.5 and 23.5 ppm (ca. 1.3 : 1 ratio as well) were observed in the case of R = ^{n}Bu. We assigned the signal at 29.5 ppm to $Mo(H)(N[^tBu]Ar)_3$ (**3-H**)[37] and those at 12 and 23.5 ppm to $Mo(SnPh_3)((N[^tBu]Ar)_3)$ (**3-$SnPh_3$**) and $Mo(Sn^nBu_3)((N[^tBu]Ar)_3)$ (**3-Sn^nBu_3**), respectively. However, none of these complexes could be isolated due to their good solubility in commonly-used solvents. ^1H NMR spctra exhibited the signals for R_3SnSnR_3. The forest green compound **3-$SnPh_3$** can be synthesized independently in 48 % isolated yield *via* a salt metathesis reaction from **3**-I and $KSnPh_3$.[38] An ORTEP diagram of **3-$SnPh_3$** is depicted in Figure 4. Salient bond distances and angles are given in the figure caption.

The solid state structure exhibits pseudo mirror symmetry, which contains N(2). The two pseudo mirror-related aryl rings engage in a parallel π-stacked arrangement, with *tert*-butyl groups oriented distal with respect to the center of the molecule. The third aryl group is essentially bisected by the pseudo mirror plane. The Mo-Sn bond distance of 2.8131(5) Å is also shorter than the expected value (ca. 3.0 Å, *vide supra*). Complex **3-SnPh$_3$** exhibits paramagnetism in solution with $\mu_{\text{eff}} = 2.99\ \mu_{\text{B}}$. It is speculated that the high-spin nature of the d^2 species **3-SnPh$_3$** is due to the fact that it possesses C_3 symmetry in solution. Therefore, the d_{xz} and d_{yz} orbitals (taking the Mo-Sn vector as the C_3 and z axes) are degenerate in C_3 symmetry. Proposed mechanism for the formation of **3-H**, **3-SnR$_3$**, and R_3SnSnR_3 is depicted in Figure 5. A major difference between **2** and **3** is the steric bulk: i.e. an increase from ^{i}Pr to ^{t}Bu. Hence, $HSnR_3$ molecules are too bulky to coordinate to **3** in an η^2 manner, and it is believed that the $HSnR_3$ molecules coordinate to the metal center through a linear Sn-H-Mo three center two-electron bond instead, similar to the known η^1-borane complexes.[39,40] Consequently, **3-H** and a radical intermediate [$\cdot SnR_3$] were produced and, subsequently, the latter either reacted with **3** to form **3-SnR$_3$** or dimerized to yield R_3Sn-SnR_3. Since the ratio (1.3:1) of **3-H/3-SnR$_3$** is close to 1, formation of **3-SnR$_3$** is apparently faster than the dimerization of [$\cdot SnR_3$].

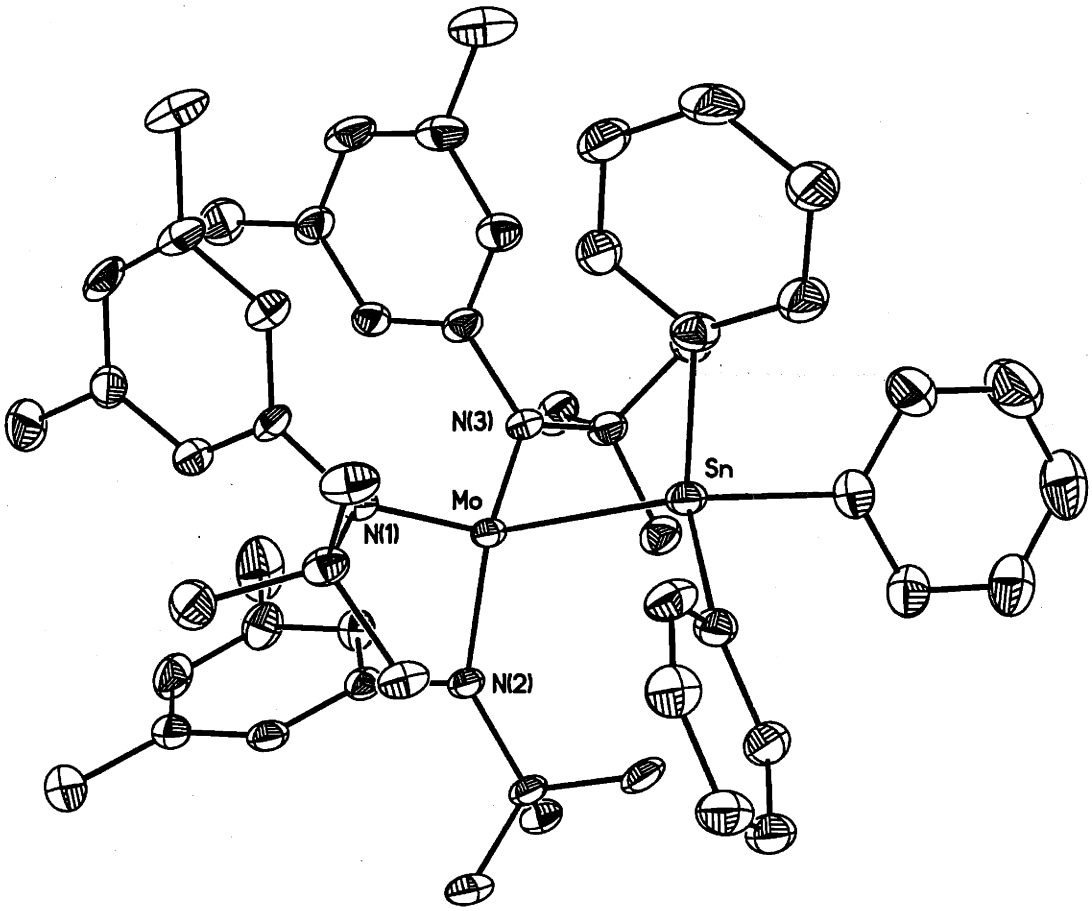

Figure 4: Thermal ellipsoid plot (35% probability) of **3-SnPh$_3$**. Selected distances (Å) and angles (°): Mo-Sn, 2.8131(5); Mo-N(1), 1.941(3); Mo-N(2), 1.982(3); Mo-N(3), 1.934(3); N(1)-Mo-Sn, 103.6(1); N(2)-Mo-Sn, 117.1(1); N(3)-Mo-Sn, 96.8(1); N(1)-Mo-N(2), 106.9(1); N(2)-Mo-N(3), 114.0(1); N(3)-Mo-N(1), 118.2(1).

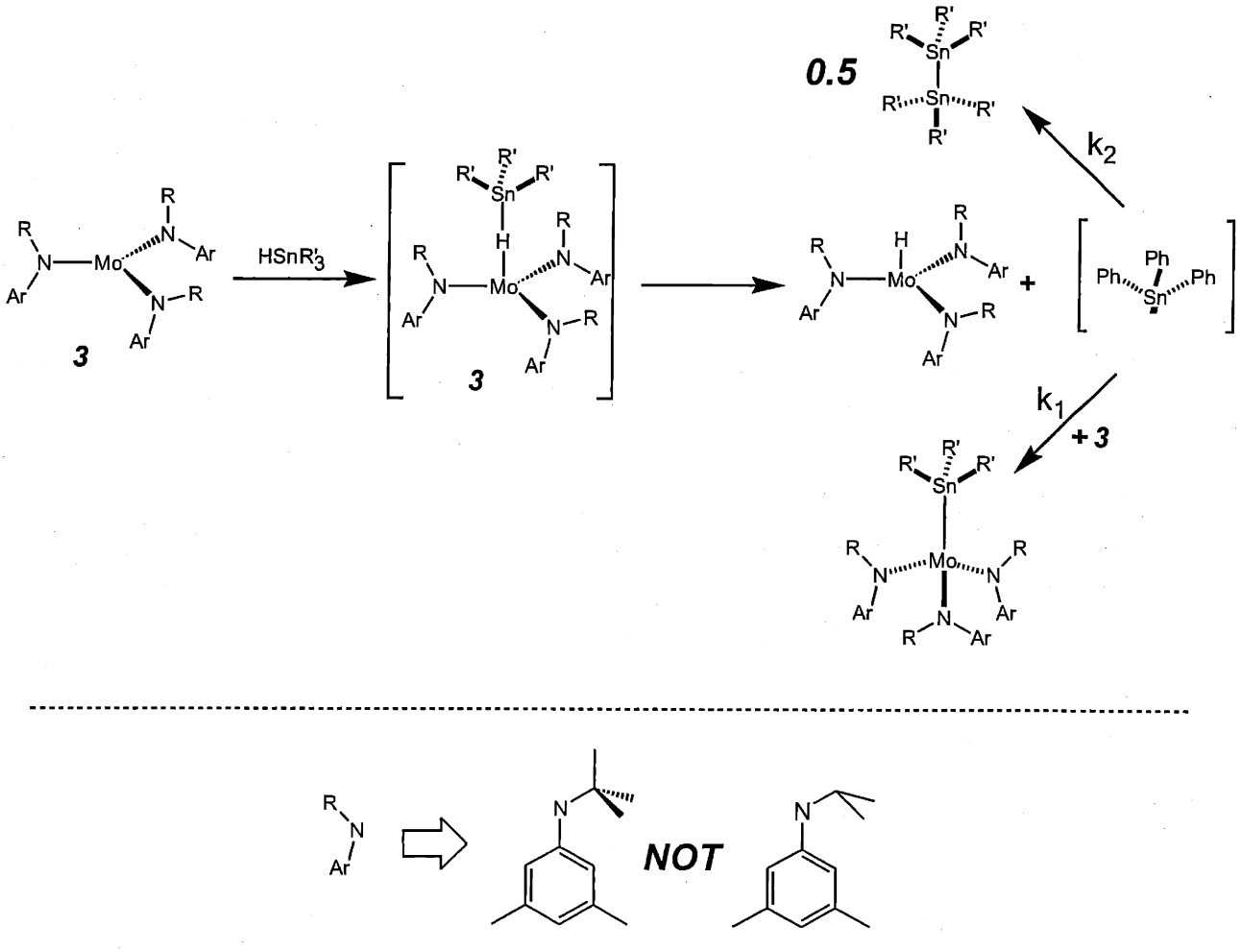

Figure 5: Proposed mechanism for the reactions of **3** with hydrostannane.

2.3 Synthesis and structure of [2-$SnPh_2$]$_2$

Schiesser *et al.*[41] have pointed out that the rates of hydrogen transfer from hydrostannanes are related to the bulk of the substituents on Sn atom: i.e. small hydrostannanes have higher hydride transfer rates. In addition, Tilley *et al.* prepared polystannanes by the dehydropolymerization of secondary hydrostannanes H_2SnR_2 *via* σ-bond metathesis catalyzed by zirconocene complexes.[42–44] Therefore, we suspected that dihydrostannanes H_2SnR_2 would be good hydrogen sources for making Mo(H)(N[^{i}Pr]Ar)$_3$) (**2-H**) or **3-H**. However, addition of one equiv of H_2SnR_2 (R = ^{n}Bu or Ph) to **1** in Et_2O solution resulted in a vigorous hydrogen gas evolution and a rapid color change from orange-brown to green, following the formation of a green precipitate. The green diamagnetic solid is insoluble in hydrocarbon solvents but soluble in aromatic or polar solvents. An X-ray diffraction study revealed the green compound to be a dimeric complex [**2-SnPh$_2$**]$_2$. An ORTEP diagram of [**2-SnPh$_2$**]$_2$ is shown in Figure 6. Salient bond distances and angles are given in the figure caption.

The centrosymmtric molecule consists of a zigzag chain of four pseudotetrahedral metal atoms and is reminiscent of the tetrastannane $Ph_3Sn(^tBu_2Sn)_2SnPh_3$, which also has a tetrametallic chain.[45] The Sn-Sn bond distances in the latter are 2.83 (outer) and 2.87 Å (inner). The distances of Mo-Sn and Sn-Sn in compound [**2-SnPh$_2$**]$_2$ are 2.8054(4) and 2.8372(5) Å, respectively. Both Sn atoms are in a distorted tetrahedral environment, with bond angles Mo-Sn-C(41) = 106.57(8), Mo-Sn-C(51) = 110.81(9), Mo-Sn-Sn(A) = 127.61(1), C(41)-Sn-Sn(A) = 103.56(9), and C(51)-Sn-Sn(A) = 102.65(8)°. This is common for tin-transition-metal compounds because such bonds have strong *s* character, with the remaining bonds having stronger *p* character.[46] Complex [**2-SnPh$_2$**]$_2$

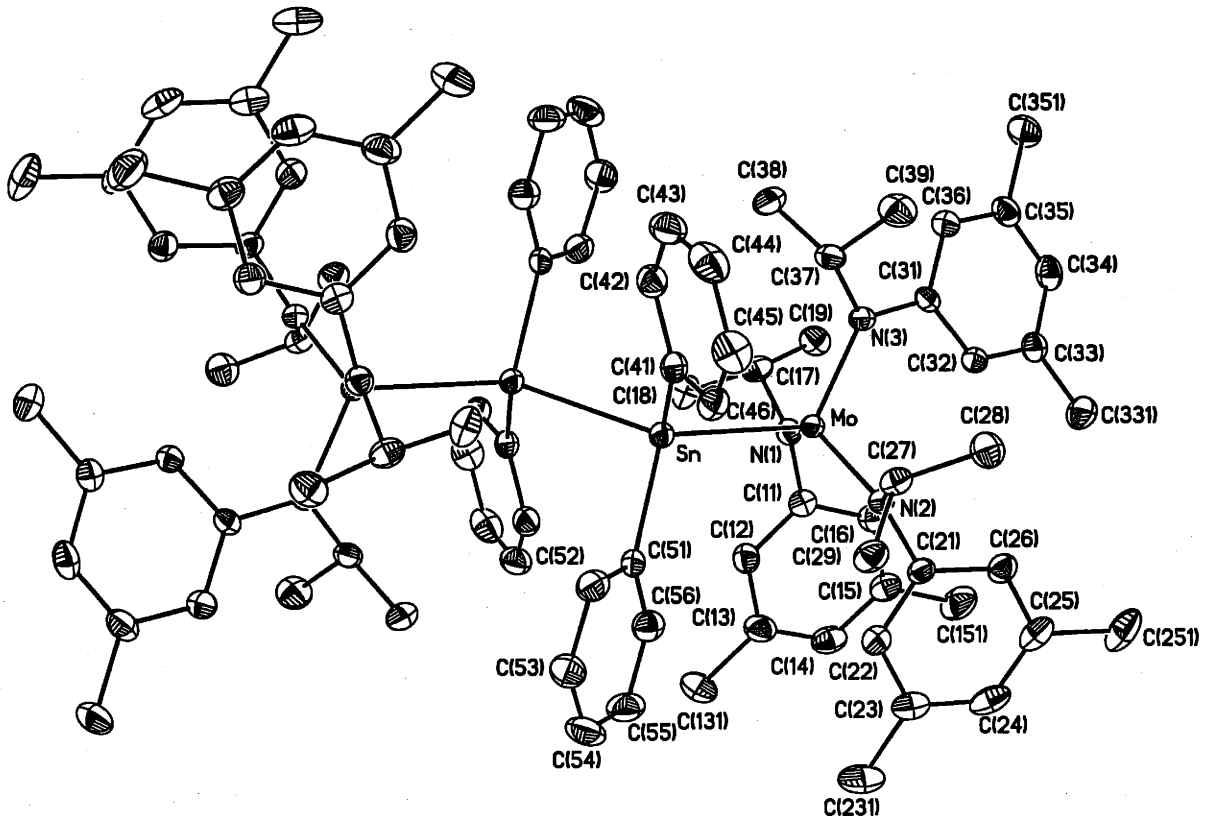

Figure 6: Thermal ellipsoid plot (35% probability) of $[\mathbf{2\text{-}SnPh_2}]_2$. Selected distances (Å) and angles (°): Sn-Mo, 2.8054; Sn-Sn(A), 2.8372(5); Mo-N(1), 1.889(3); Mo-N(2), 1.908(3); Mo-N(3), 1.980(3); C(41)-Sn-C(51), 103.1(1); C(41)-Sn-Mo, 106.57(8); C(51)-Sn-Mo, 110.81(9); Mo-Sn-Sn(A), 127.61(1); N(1)-Mo-N(2), 124.5(1); N(2)-Mo-N(3), 106.7(1); N(3)-Mo-N(1), 104.4(1); Sn-Mo-N(1), 106.80(8); Sn-Mo-N(2), 103.96(8); Sn-Mo-N(3), 110.13(8).

is stable in solid state, but thermally unstable in solution. The X-band EPR spectra of both [**2-SnPh$_2$**]$_2$ and [**2-Sn^{n}Bu$_2$**]$_2$ displayed the signals for complex **1** and the unidentified organotin by-products are likely *cyclo*-hexameric $(R_2Sn)_6$ or polymeric $(R_2Sn)_2$.[44]

Proposed mechanism for the formation of [**2-SnPh$_2$**]$_2$ from the reaction of **1** with H_2SnPh_2 and the decomposition of [**2-SnPh$_2$**]$_2$ are both illustrated in Figure 7. Dihydrostannane H−SnHR$_2$ coordinates to **2** *via* Sn−H bond to from **2-η^2-HSnHR$_2$**. Subsequently, the H−Sn bond oxidatively adds to **2** to produce **2-(H)(SnHR$_2$)**, which loses H_2 *via* an 1,2-H_2-elimination process[22] to give the intermediate stannylidene complexes [**2-SnR$_2$**]. The stannylidene intermediate [**2-SnR$_2$**] then dimerizes to give [**2-SnR$_2$**]$_2$. Unlike the stable pnictide complexes (silox)$_3$Ta(EPh) (E = N, P or As),[22] that have strong Ta(d_π)-E(p_π) interaction, the intermediate [**2-SnR$_2$**] dimerizes to produce [**2-SnR$_2$**]$_2$, a result of weak Mo(d_π)-Sn(p_π) interactions. The decomposition of [**2-SnR$_2$**]$_2$ suggests the possible application of making polystannane catalytically *via* dehydropolymerization of secondary hydrostannanes H_2SnR_2 by **1**.

2.4 Synthesis and structure of 3-H

Unlike the reactions of **1** and H_2SnR_2, in which H_2 was a by-product, no H_2 evolution was observed in the reactions of **3** with H_2SnR_2 (R = Ph or ^{n}Bu). Instead, a paramagnetic brick-red Mo(IV) complex **3-H** was isolated in 92% yield. H_2SnPh_2 was found to be more reactive than $H_2Sn^nBu_2$ for making **3-H**. This conclusion was supported by the observation that two equiv of $H_2Sn^nBu_2$ was employed to achieve a complete formation of **3-H** but only 0.6 equiv of H_2SnPh_2 was needed to prepare **3-H**. This result might be explained by the fact that H_2SnPh_2 is more unstable than

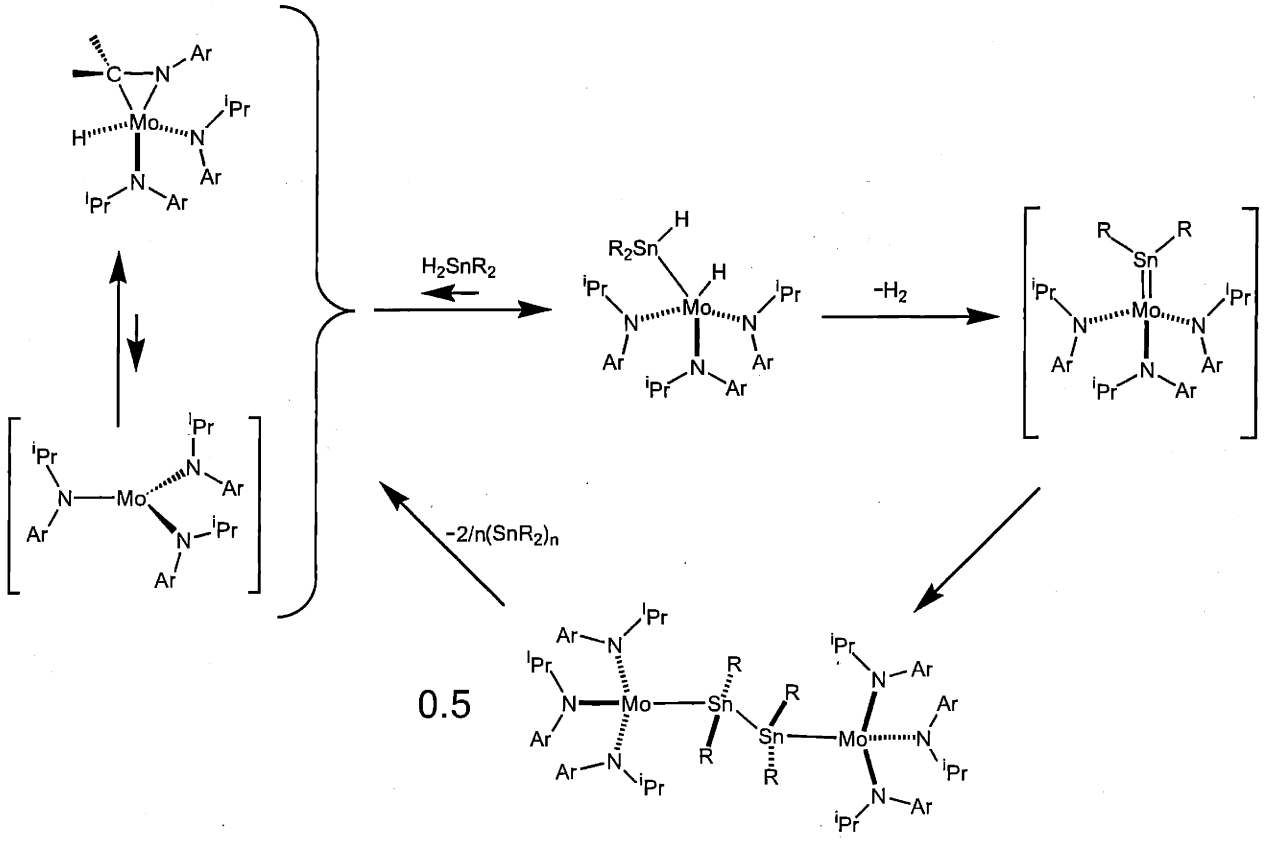

Figure 7: Proposed mechanism for the formation of $[\mathbf{2\text{-}SnR_2}]_2$.

$H_2Sn^nBu_2$ at room temperature.[47] The solid state structure of **3-H** is shown in Figure 8.

It clearly shows that the intramolecular packing conformation is such that the three 3,5-$C_6H_3Me_2$ substituents are on one side of the trigonal plane and the three ^{t}Bu groups occupy on the other. The geometry of the Mo-N_3 unit is trigonal planar with the sum of N-Mo-N angles = 356.23°. Similarly, the sum of the three N-Mo-N angles in complexes **3**[5] and Mo(Cl)(N[^{t}Bu]Ar)$_3$) (**3-Cl**)[48] are 357.7(3)° and 350.5(1)°, respectively. The planarity at Mo can be attributed to the lack of π interaction between molybdenum and the hydride ligand. The sum of the three N-Mo-N angles in complex **3-Cl** is slightly smaller than that for **3-H** because of the presence of a π interaction between molybdenum and the chloride ligand, as well as the relative bulk of the Cl atom. The Mo-H bond distance of 1.57 Å is shorter than that of the Mo-H bond (1.69(5) Å) in compound **1**, but is close to the distance of the W-H bond (between 1.57 and 1.59 Å) in the compound [$(Me_3SiCH_2CH_2N)_3$N]WH.[49] The Mo-H and Mo-D (which was prepared by using D_2SnR_2) stretching frequency were located at 1860 and 1334 cm^{-1} (calcd. 1315 cm^{-1}). Proposed mechanism for the formation of **3-H** is shown in Figure 9. Based on the reactions of **3** with $HSnR_3$, it is likely that the intermediate **3-η^1-HSnHR$_2$** forms first and subsequently decomposes to produce **3-H** and a radical intermediate [·$SnHR_2$]. The putative species [·$SnHR_2$] then reacts with **3** to give [**3-SnHR$_2$**]. Following this, the intermediate [**3-SnHR$_2$**] decomposes to generate **3-H** and [SnR_2], which polymerizes readily to give $[SnR_2]_n$.

The magnetic susceptibility of complex **3-H** was determined by using Evans' method[50,51] and it was found that μ_{eff} = 3.09 μ_B, close to the spin-only value for a d^2 complex (2.83 μ_B). This megnetic property can be explained in terms of the electronic structure of **3-H**. Since there is no π interaction between the hydride ligand and molybdenum in **3-H**, the half-occupied π orbitals

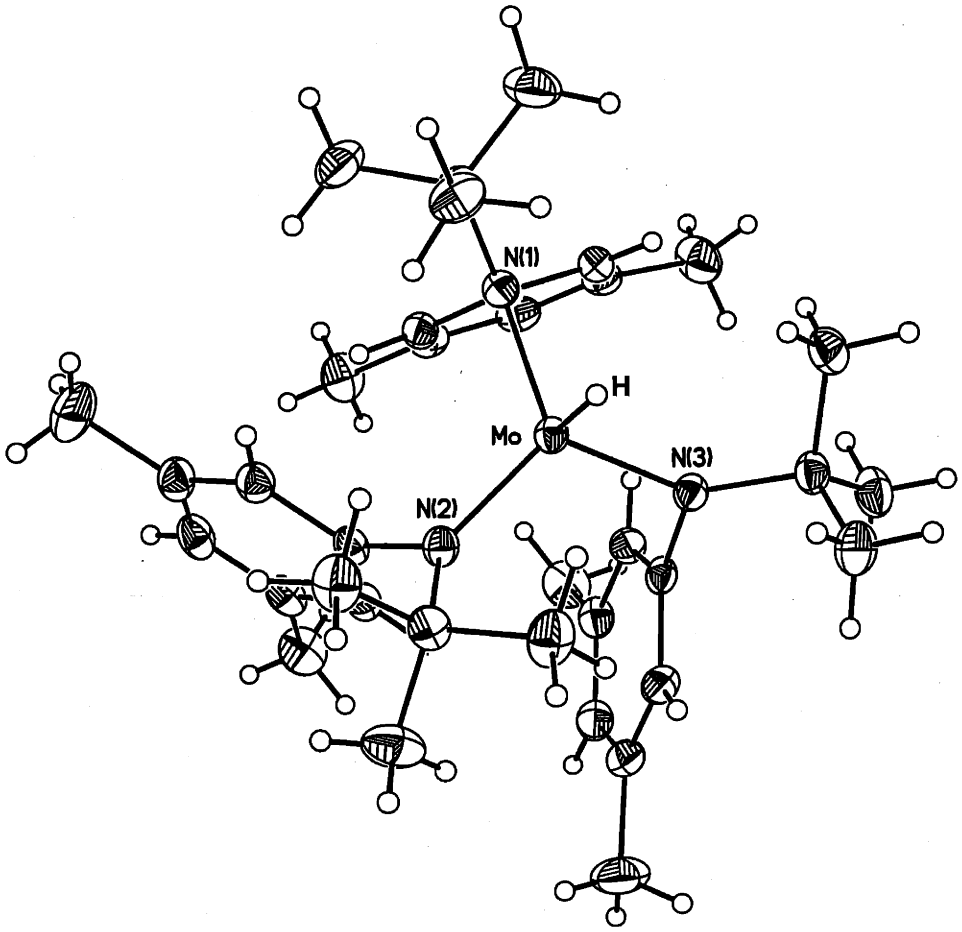

Figure 8: Thermal ellipsoid plot (35% probability) of **3-H**. Selected distances (Å) and angles (°): Mo-H, 1.58(3); Mo-N(1), 1.967(2); Mo-N(2), 1.960(2); Mo-N(3), 1.957(2); N(1)-Mo-N(2), 119.46(8); N(2)-Mo-N(3), 116.75(8); N(3)-Mo-N(1), 120.02(8); H-Mo-N(1), 98(1); H-Mo-N(2), 96(1); H-Mo-N(3), 95(1).

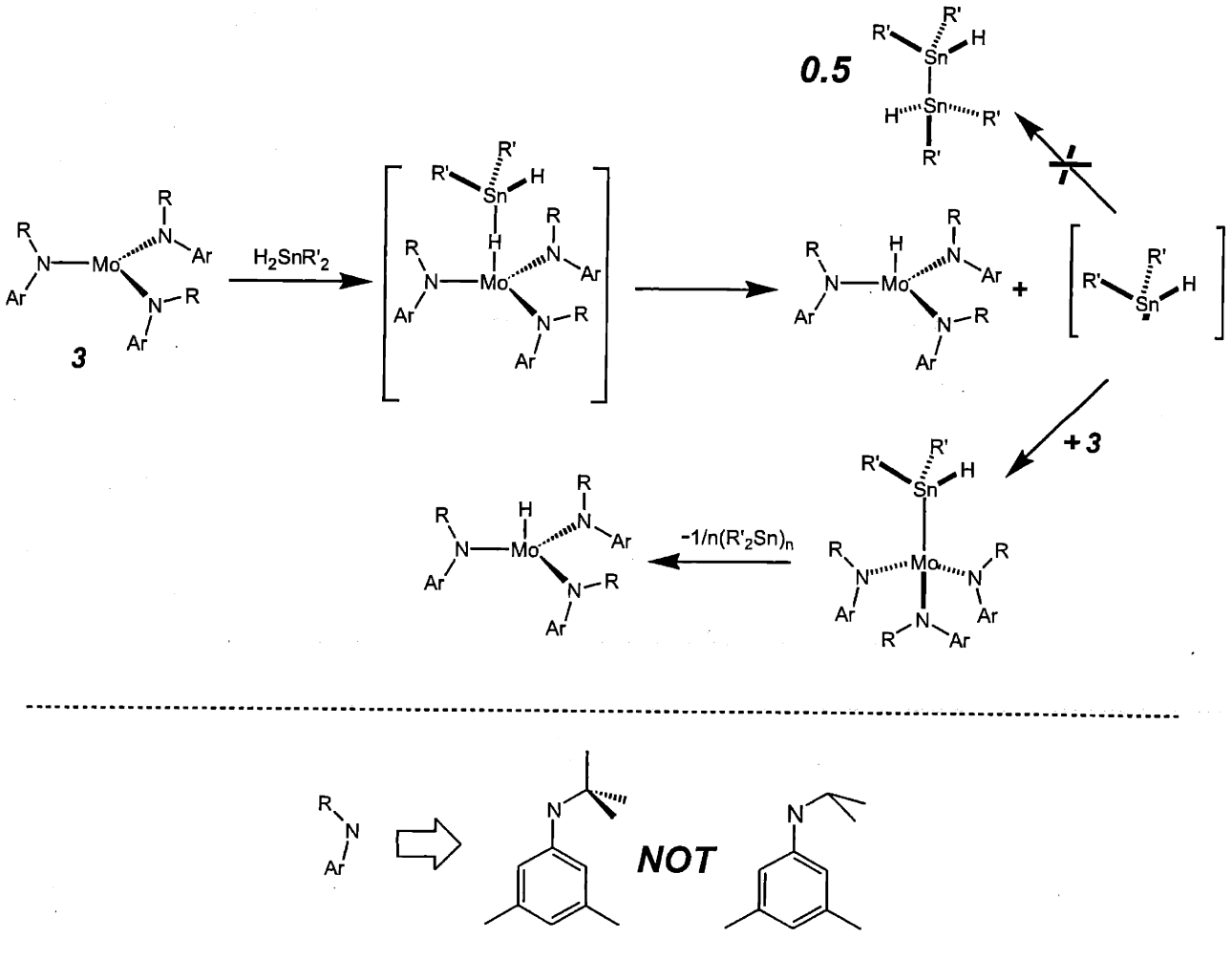

Figure 9: Proposed mechanism for the formation of **3-H**.

(d_{xz} and d_{yz}, taking the Mo-H vector as the C_3 axis and z axis) remain intact in complex **3-H**. Hence, the C_3 symmetric **3-H** is expected to remain paramagnetic with two unpaired electrons in the degenerate d_{xz} and d_{yz} orbitals.

The hydride ligand in compound **3-H** is exchangeable with H_2. The deuterated isotopomer **3-D** reacted with H_2 (4 atm) at room temperature to produce **3-H**, which was identified by IR. Although the metathesis reaction is still obscure, Schrock's.[49] W(VI) trihydride complex $[(Me_3SiNCH_2CH_2)_3N]WH_3$ that was prepared by treating $[(Me_3SiNCH_2CH_2)_3N]WH$ with H_2 may provide a solution to the result of the reaction of **3-D** with H_2. A Mo(VI) trihydride **3-H$_3$** is therefore postulated as an intermediate in this process, as shown in Figure 10. Complex **3-H** forms upon the release of HD from **3-DH$_2$**. The intermediate **3-DH$_2$** has not been identified, so it is assumed that the metathesis reaction is fast.

2.5 Reactions of 3 and 1-d_{18} with H_2PPh

Addition of one equiv of PH_2Ph to **3** in Et_2O solution resulted in a slow color change from bright orange to brownish-yellow. Complex **3** disappeared after overnight, and compounds **3-H** (δ 30 ppm) and Mo(PHPh)(N[^{t}Bu]Ar)$_3$ (**3-PHPh**) (δ 3.0 ppm) formed, as revealed by ^{2}H and ^{1}H NMR spectroscopy. The ratio of **3**-H to **3**-PHPh was 1:1. After another 12 h, the ratio decreased to approximately 1:1.5. However, addition of ten equiv of PH_2Ph to **3** gave **3-PHPh** exclusively in 1 h. Reaction of **3-H** with ten equiv of H_2PPh generated **3-PHPh** as well, but the reaction did not occur if one equiv of H_2PPh was added to **3-H**. ^{31}P NMR spectrum of **3-PHPh** displayed a broad peak at 161.8 ppm. On the other hand, the reaction of **1-d_{18}** and one equiv of H_2PPh

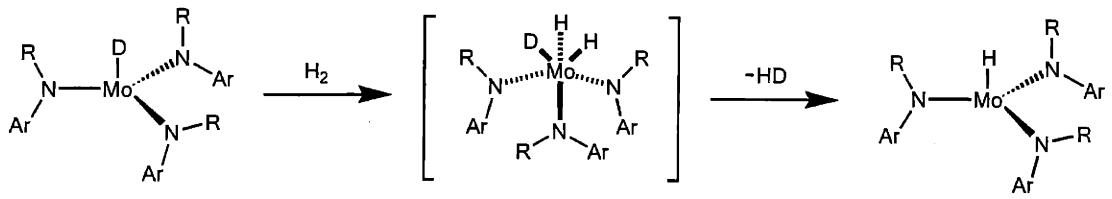

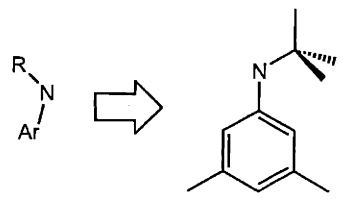

Figure 10: Proposed mechanism for the reaction of **3-H** with H_2.

resulted in the formation of a purple solution, which disappeared quickly and became brownish-yellow to give Mo(PHPh)(N[^{i}Pr-d_6]Ar)$_3$ (**2-d_{18}-PHPh**) as the only observable product (Figure 11). Importantly, hydrogen evolution occured over the course of the reaction. ^{31}P NMR spectra of **2-d_{18}-PHPh** exhibited a doublet at 118.4 ppm (J_{PH} = 293 Hz). However, when half an equiv of PH_2Ph was added to **1-d_{18}** at −35 °C, a signal at 18 ppm ($\Delta\nu_{1/2}$= 14 Hz) was observed in the ^{2}H NMR spectra (Figure 11) and the ratio of this peak to **2-d_{18}-PHPh** was about 1:1. When sterically bulky H_2P-2,4,6-$C_6H_2Me_3$ (H_2PMes) was employed, the reaction became slow (indicated by ^{2}H NMR spectroscopy) and no significant H_2 evolution was observed. The signal at 18 ppm was observed in this reaction as well, but it disappeared in 3 h to give Mo(PHMes)(N[^{i}Pr-d_6]Ar)$_3$ (**2-d_{18}-PHMes**) as the final product, as determined by ^{1}H NMR spectroscopy. The ^{31}P NMR spectra for **2-d_{18}-PHMes** also dispalyed a doublet at 89.9 ppm (J_{PH} = 287 Hz). Based on the above results, we speculate that the signal at 18 ppm corresponds to **2-d_{18}-H**.

Hydrostannane H-Sn^{n}Bu$_3$ has a higher energy Sn-H σ^* antibonding orbital than that for H-SnPh$_3$ and complex **2-η^2-HSn^{n}Bu$_3$** has a stronger Sn-H interaction than that in complex **2-η^2-HSnPh$_3$**, suggesting that alkylphosphines will have stronger P-H bonds than arylphosphine. Therefore, slower reaction of **1-d_{18}-H** with alkylphosphines than for **1-d_{18}-H** and arylphosphines is expected. Indeed, the rate of the fromation of **2-d_{18}-PHCy** was diminished as compared to that of the formation of **2-d_{18}-PHPh** and **2-d_{18}-PHMes**. Addition of one equiv of PH_2Cy (Cy = cyclohexyl) to **1-d_{18}** in Et_2O under 1 atm of dinitrogen resulted in a quick color change from orange-brown to intense purple; solid (**2-d_{18}**)$_2$-**N** formed rapidly. However, when the reaction was conducted under vacuum, ^{2}H NMR spectra displayed a signal at 5 ppm, which decreased over a period of 12 h, and the purple solution gradually turned orange-brown. ^{1}H and ^{2}H NMR spectra

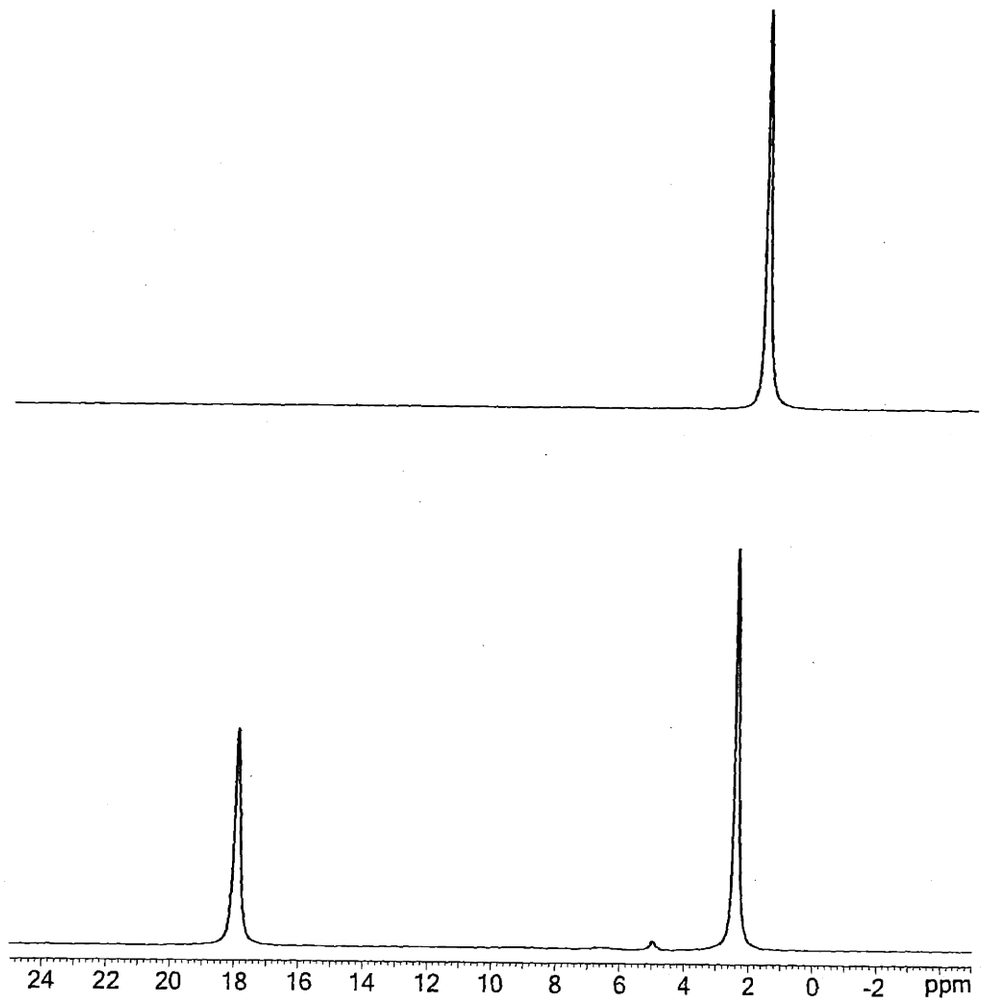

Figure 11: ^{2}H NMR specta of the reactions of **1-d_{18}** and 1 (top) and 0.5 (bottom) equiv of PH_2Ph, respectively. The signal at 18 ppm (bottom) is **2-d_{18}-H** and the signals aroud 2 ppm is **2-d_{18}-PHPh**.

revealed that compound Mo(PHCy)(N[^{i}Pr-d_6]Ar)$_3$ (**2-d_{18}-PHCy**) was the only observable product (Figure 12). It is presumed that the signal at 5 ppm was the adduct **2-d_{18}-PH$_2$Cy**, which has a much longer lifetime than the analogous intermediate **2-d_{18}-PH$_2$Ph**. Surprisingly, the proposed intermediate **2-d_{18}-H** at 18 ppm was not observed as shown in Figure 12. This observation suggests that the activation of the P-H bond is the rate-determining step. Unlike the stable **3-H**, the proposed intermediate **2-d_{18}-H** is very reactive; it disappeared in the reaction of **1-d_{18}** and half equiv of H_2PPh over a period of 4 h, and was not observed at all in the reaction of **1-d_{18}** with one equiv of PH_2Cy. Because the chemical shift of **2-d_{18}-PHPh** in the reaction of **1-d_{18}** with PH_2Ph moved from 2.7 ppm to 1.6 ppm,[50] we speculate that **2-d_{18}-H** is paramagnetic,[50] and the geometry at Mo is trigonal planar. The diamagnetism of **3-PHPh**, **2-d_{18}-PHPh**, **2-d_{18}-PHMes**, and **2-d_{18}-PHCy** can be ascribed to the donation of the phosphorus lone pair to one of the metal's d_π orbitals and the consequent pairing of the two d electrons in the remaining π orbital. The proton and deuterium NMR spectra suggest that these compounds are C_{3v} symmetric on the NMR time scale requiring that the phenylphosphido ligand rotates readily with respect to the three amido ligands. Schrock *et al.*[52] also prepared M(IV) phenylphosphido complexes [(Me$_3$SiNCH$_2$CH$_2$)$_3$N]M-PHPh (M = Mo, W), which also exhibit diamagnetic character.

Proposed mechanism for the formation of phenylphosphido complexes is shown in Figure 13. In contrast to the formation of imido, phosphinidene and arsinidene complexes (silox)$_3$Ta(EPh) (E = N, P, or As) from reactions of Ta(silox)$_3$ and EH_2Ph,[22] Mo(V) phosphinidene complexes Mo(PPh)(N[R]Ar)$_3$, (R = ^{i}Pr or ^{t}Bu) were not observed. Instead, PH_2Ph oxidatively adds to two Mo(N[R]Ar)$_3$ (R = ^{i}Pr-d_6 or ^{t}Bu-d_6) molecules yielding Mo(H)(N[R]Ar)$_3$ and Mo(PHPh)(N[R]Ar)$_3$. Subsequently, the complex Mo(H)(N[R]Ar)$_3$ reacts with H_2PPh to form Mo(PHPh)(N[R]Ar)$_3$ and

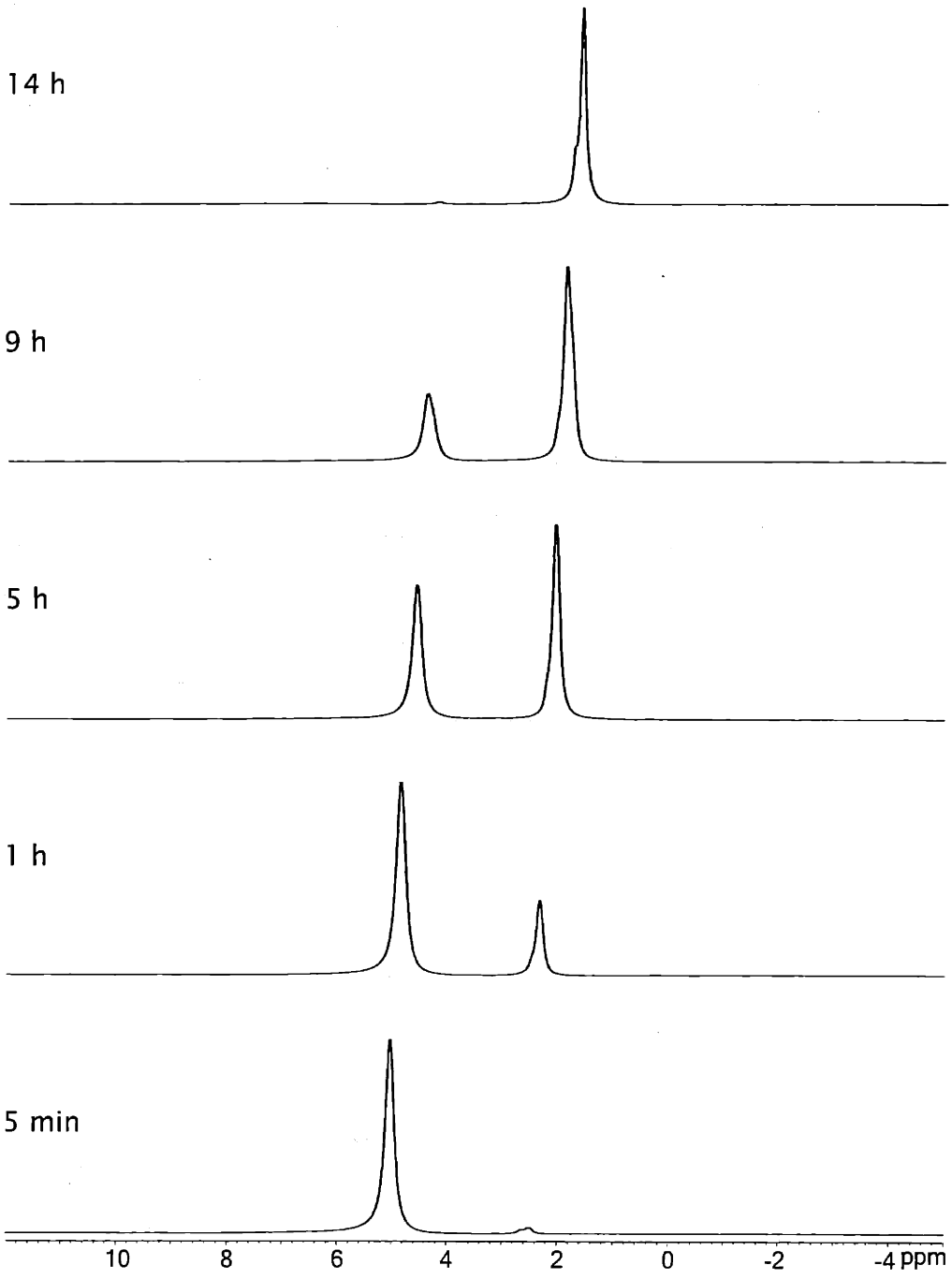

Figure 12: ^{2}H NMR specta of the reaction of **1-d_{18}** and 1 equiv of PH_2Cy in Et_2O at room temperature.

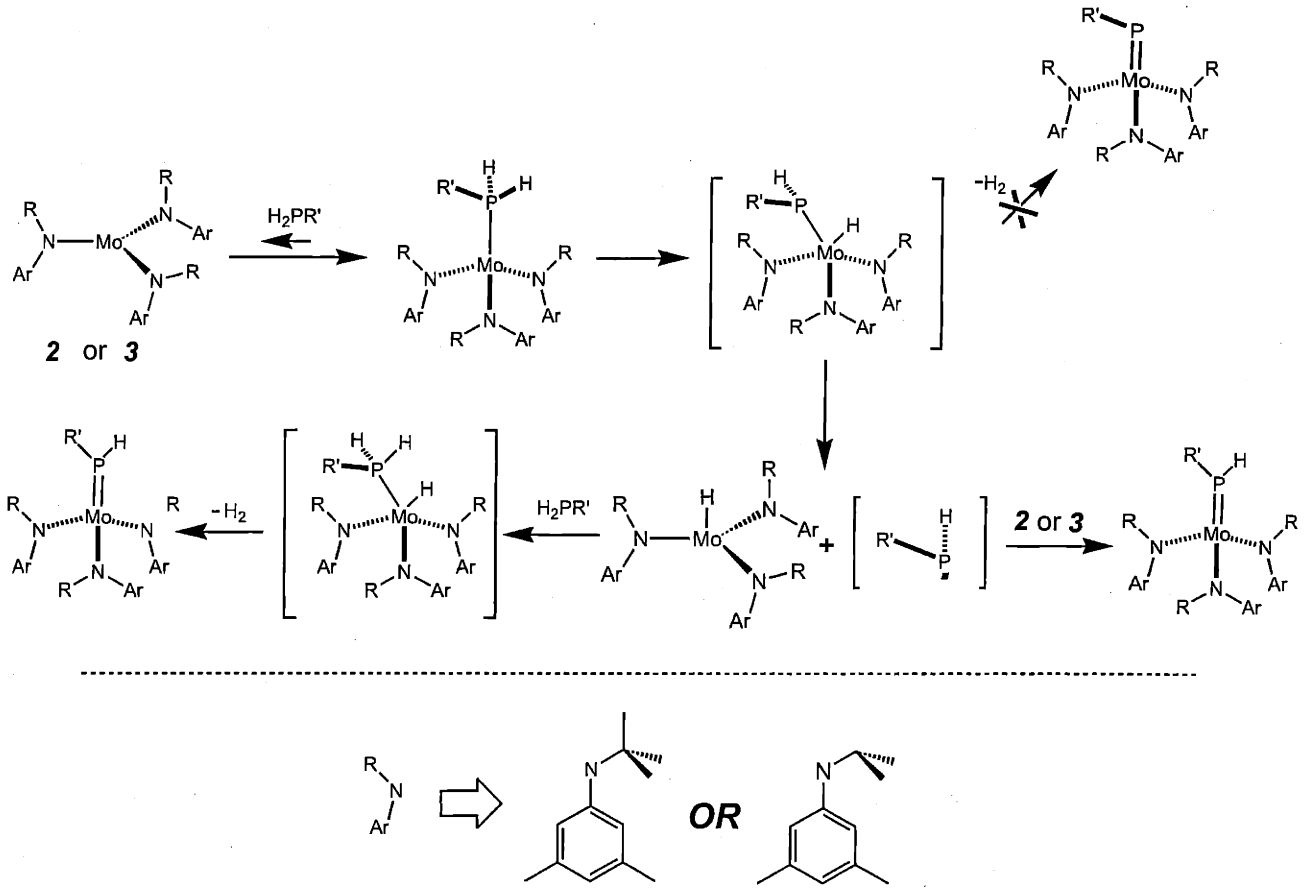

Figure 13: Proposed mechanism for the formation of **2-PHPh** or **3-PHPh**.

H_2 as the by-product. The fact that **1-d_{18}-H** is more reactive than **3-H** because of steric effects is consistent with the observation of rapid H_2 evolution in the reaction of **1-d_{18}** with 1 equiv of H_2PPh, as compared to the reaction of **3** and PH_2Ph which slowly produced H_2.

3 Concluding Remarks

We have shown that the reactivity of **1** and **3** towards Sn-H depends on electronic and steric effects. $HSnR_3$ coordinates to **2** in an η^2-manner. The X-ray structural data of **2-η^2-HSn^{n}Bu$_3$** reveals that HSn^nBu_3 coordinates to Mo *via* an Sn−H bond. Substituents at tin were also found to have a great effect on the stability of the hydrido stannyl compounds. Complex **2-η^2-HSn^{n}Bu$_3$** dissociates in dilute solution (¡ 1 mM) on the EPR time scale and the ligand HSn^nBu_3 can be replaced by one equiv of $HSnPh_3$ to form **2-η^2-HSnPh$_3$**. Alternatively, **2-η^2-HSnPh$_3$** can also be independently prepared from the direct reaction of **1** with $HSnPh_3$. Interestingly, **2-η^2-HSnPh$_3$** is more stable in solution than **2-η^2-HSn^{n}Bu$_3$**, and the EPR data shows the super hyperfine coupling of the unpaired electron on Mo to H. This observation suggests that the hydrido stannyl complex **2-η^2-HSnPh$_3$** has a greater degree of oxidative addition than **2-η^2-HSn^{n}Bu$_3$**, although they both react with dinitrogen and benzonitrile to give **2$_2$-N** and **2-NCHPh**, respectively. As such, we believe that the hydrido stannyl complex **2-η^2-HSn^{n}Bu$_3$** has higher degree of Sn-H interaction than **2-η^2-HSnPh$_3$**. Due to the steric bulk of the ^{t}Bu substituent in compound **3**, $HSnR_3$ cannot bind to **3** *via* a Sn-H bond. The three products **3-H**, **3-SnR$_3$**, and R_3SnSnR_3 were observed instead from the reactions of **3** and $HSnR_3$ *via* oxidative addition to two molecules of **3**.

The dihydrostannanes are more reactive than the tin monohydride compounds because of one additional Sn-H bond. It is found that H_2SnR_2 can lose H_2 to provide the putative stannylene fragment. In the reactions of **1** and H_2SnR_2, **[2-SnR$_2$]$_2$** was formed *via* the Sn-H oxidative addition to **1** and subsequent 1,2-H_2-elimination to give stannylidene complexes, which dimerized to form **[2-SnR$_2$]$_2$**. On the other hand, H_2SnR_2 can also lose a stannylene fragment to provide two H

atoms. In the reactions of **3** with H_2SnR_2, **3-H** was formed in high yield generating $(R_2Sn)_n$ as a by-product.

Activation of the P-H bond by **1** and **3** was also possible. Both **1** and **3** reacted with PH_2Ph to give compounds **2-PHPh** and **3-PHPh**, respectively. The mechanism for the formation of complexes **2-PHR** and **3-PHR** was examined in detail. One of the P-H bonds oxidatively added to two Mo centers to form Mo-H and Mo-PHR. Mo-H subsequently reacted with H_2PR to form another equiv of Mo-PHR. The ease of the activation of the P-H bond is also dependent on the substituents on P and the bulk of the molybdenum complexes. As we have determined, a P-H bond in cyclohexylphosphine is more difficult to be activated than those in arylphosphines because the former have higher energy σ^* symmetry orbitals.

4 Experimental Section

4.1 General considerations

Unless otherwise stated, all operations were performed in a Vacuum Atmospheres drybox under an atmosphere of purified nitrogen or using Schlenk techniques under an argon atmosphere. Complexes **1**, **1-d_{18}**, **3**, hydrostannanes, and dihydrostannanes were prepared according to the published procedure.[5,10,47] Phenylphosphine and cyclohexylphosphine were purchased from Strem Chemical Co. Mesitylphosphine was prepared according to the literature.[53] Diethyl ether, benzene, *n*-pentane, and toluene were dried and deoxygenated by the method of Grubbs.[54] THF was distilled over Na/benzophenone and collected under nitrogen. C_6D_6 was degassed and dried over 4 Å molecular sieves. Celite, alumina, and 4 Å molecular sieves were dried in vacuo overnight at a temperature above 200 °C. The room temperature X-band EPR spectra of the complexes were recorded on a Bruker EMX spectrometer. Acquisition, simulation, and data post processing of the liquid solution spectra were performed by using an integrated WIN-EPR software package (Bruker). Varian VXR-500 or Varian XL-301 spectrometers were used to collect all nuclear magnetic resonance spectra. ^{1}H, ^{2}H, and ^{13}C chemical shifts are reported with respect to internal solvent (7.15 ppm and 128.38 (t) ppm (C_6D_6)). C, H, and N elemental analyses were performed by H. Kolbe Mikroanalytisches Laboratorium, Mülheim an der Ruhr, Germany.

4.2 Synthesis of 2-d_{18}-η^2-$HSnR_3$ (R = ^{n}Bu and Ph)

To an orange-brown solution of **1-d_{18}** (0.512 g, 0.852 mmol) in 10 mL of *n*-pentane or Et_2O were added a solution of 0.273 g (0.937 mmol) of HSn^nBu_3 in 2 mL of Et_2O. The resulting mixture quickly turned into yellow and was stirred for 10 min. All volatiles were removed in vacuo. The solid residue was collected on a frit and washed with cold *n*-pentane and dried in vacuo. The yields of **2-d_{18}-η^2-$HSnPh_3$** and **2-d_{18}-η^2-HSn^nBu_3** were 72% and 69%, respectively. Crystals of **2-η^2-HSn^nBu_3** were grown from *n*-pentane in the presence of excess of HSn^nBu_3 at −35 °C. For **2-η^2-HSn^nBu_3**, ^{2}H NMR (Et_2O, 20.1 °C): δ = 9.41 ($\Delta\nu_{1/2}$= 46 Hz) ppm. μ_{eff} = 2.01 μ_B (Evans' method, C_6D_6, 19.9 °C). Anal. Calcd. for $C_{45}H_{47}N_3MoSn$: C, 61.86; H, 8.77; N, 4.81. Found: C, 61.76; H, 8.79; N, 4.79. For **2-η^2-$HSnPh_3$**, ^{2}H NMR (Et_2O, 19.9 °C): δ 9.11 ($\Delta\nu_{1/2}$= 50 Hz) ppm. μ_{eff} = 1.94 μ_B (Evans' method, C_6D_6, 20.3 °C). Anal. Calcd. for $C_{51}H_{64}N_3MoSn$: C, 65.60; H, 6.91; N, 4.50. Found: C, 65.78; H, 7.03; N, 4.40.

4.3 Reaction of 2-d_{18}-η^2-HSn^nBu_3 with $HSnPh_3$

To a yellow solution of **2-η^2-HSn^nBu_3** (0.232 g, 0.260 mmol) in 2 mL of Et_2O were added 1.1 equiv of $HSnPh_3$. The resulting solution turned into intense yellow quickly. The ^{2}H NMR spectroscopy exhibited the signal of **2-η^2-$HSnPh_3$** (*vide supra*).

4.4 Reactions of 3 and $HSnR_3$ (R = ^{n}Bu and Ph)

To an orange solution of **3** (0.463 g, 0.720 mmol) in 5 mL of Et_2O were added 1 equiv of $HSnR_3$. The resulting solution turned into dark reddish-brown slowly and was stirred for 24 h. The ^2H NMR spectroscopy exhibited two signals for each reaction. Both reactions produced **3-H** (29.5 ppm) and **3-SnR$_3$** (23.5 ppm, when R = ^{n}Bu; 12 ppm, when R = Ph). None of these products can be purified due to their good solubility in commonly used solvents.

4.5 Synthesis of 3-$SnPh_3$

To a suspension of 0.0249 g (0.620 mmol) of potassium hydride, washed with dry hexane, in 5 mL of THF in a 20 mL vial were added dropwise a solution of 0.218 g (0.620 mmol) of triphenylstannane in 5 mL of THF at room temperature. Hydrogen evolution was observed, and a green-yellow color developed rapidly. The solution was stirred for 1 h and was added to a dark green solution of 0.477 g (0.620 mmol) of **3-I** in 10 mL of Et_2O in a 100 mL round-bottom flask. The resulting mixture was stirred for 12 h and filtered through a plug of celite. Upon removal of solvents in vacuo, an oily residue was obtained. The residue was extracted with 10 mL of *n*-pentane and the forest green solution was stored at −35 °C to give 0.295 g of dark green crystals of **3-SnPh$_3$**. The yield was 48%. ^2H NMR (Et_2O, 20.1 °C): δ 10.93 ($\Delta\nu_{1/2}$= 14.2 Hz) ppm. μ_{eff} = 2.99 μ_B (Evans' method, C_6D_6, 20.1 °C). Anal. Calcd for $C_{54}H_{51}D_{18}N_3MoSn$: C 65.32, ; H, 8.83; N, 4.32. Found: C, 65.41; H, 8.74; N, 4.25.

4.6 Synthesis of [2-$SnPh_2$]$_2$

To an orange-brown solution of **1** (0.534g, 0.862 mmol) in 5 mL of Et_2O were added dropwise a solution of 0.237 g (0.862 mmol) of Ph_2SnH_2 in 5mL of Et_2O. A violent hydrogen gas evolution was observed. The resulting mixture turned into green color and then green precipitate formed rapidly. The suspension was stirred for 30 min and filtered. The green solid was collected on a frit by filtration, washed with *n*-pentane, and dried in vacuo. The yield was 79.4%. ^{1}H NMR (C_6D_6, 20.3 °C): δ 8.73 (s, 8 H, *meta*-Ph), 7.98 (d, 8 H, *ortho*-Ph), 7.55 (t, 4 H, *para*-Ph), 5.81 (s, 12 H, *ortho*-$C_6H_3Me_2$), 5.33 (s, 6 H, *para*-$C_6H_3Me_2$), 3.08 (br, 36 H, -C(H)Me_2), 1.74 (s, 36 H, $C_6H_3Me_2$). Anal. Calcd for $C_{90}H_{116}N_6Mo_2Sn_2$: C, 63.17; H, 6.83; N, 4.91. Found: C, 62.97; H, 6.90; N, 4.81.

4.7 Synthesis of 3-H

To an orange solution of 1.864 g (2.90 mmol) of **3** in 20 mL of Et_2O in a 50 mL round-bottom flask were added dropwise a solution of 1.364 g (5.80 mmol) of $H_2Sn^nBu_2$ or 0.480 g (1.74 mmol) of H_2SnPh_2 in 5 mL of Et_2O. The resulting solution turned into dark red rapidly and was stirred for 1 h. The dark red solution was filter through a plug of Celite. Upon removal of all volatiles, a brick-red solid was obtained and extracted into a minimum amount of *n*-pentane and was stored at −35 °C to give 1.718 g of brick-red powder (92% yield). ^{2}H NMR (Et_2O, 20.1 °C): δ 29.3 ($\Delta\nu_{1/2}$= 11 Hz) ppm. ^{1}H NMR (C_6D_6, 20.1 °C): δ 28.40 (s, 27 H, ^{t}Bu), −7.64 (s, 18 H, $C_6H_3Me_2$), −18.62 (br, 6 H, *ortho*-$C_6H_3Me_2$), −27.15 (s, 3 H, *para*-$C_6H_3Me_2$) ppm. IR: ν_{Mo-H}: 1860 cm^{-1}, ν_{Mo-D}: 1334 cm^{-1}. μ_{eff} = 3.09 μ_B (Evans' method, C_6D_6, 19.8 °C). Anal. Calcd for $C_{36}H_{55}N_3Mo$: C,

63.17; H, 6.83; N, 4.91. Found: C, 62.97; H, 6.90; N, 4.81.

4.8 Synthesis of 2-NC(H)Ph

Method 1: To a cold solution of 0.040 g (0.39 mmol) of benzonitrile in 10 mL of Et_2O, stored at -35 °C for 30 min, were added 0.242 g (0.390 mmol) of **1**. The resulting mixture became dark blue rapidly and was stirred for 10 min. One equiv of $HSnR_3$ or 0.6 equiv of H_2SnR_2 (R = ^{n}Bu and Ph) was added to the dark blue solution. The solution turned into maroon quickly and was stirred for 1 h. Upon removal of volatile materials provided a dark oily residue. ^{1}H NMR spectroscopy displayed 90% of **2-NC(H)Ph** and 10% of HN(^{i}Pr)Ar. ^{1}H NMR (C_6D_6, 20.2 °C): δ 7.57 (s, 1 H, -NC(*H*)Ph), 7.19 (t, 2 H, *meta*-Ph), 7.01 (t, 1 H, *para*-Ph), 6.86 (d, 2 H, *ortho*-Ph), 6.65 (s, 6 H, *ortho*-$C_6H_3Me_2$), 6.60 (s, 3 H, *para*-$C_6H_3Me_2$), 4.38 (q, 3 H, methine), 2.12 (s, 18 H, C_6H_3*Me*$_2$), 1.21 (d, 18 H, C(H)*Me*$_2$) ppm.

Method 2: To a cold solution of 0.430 mmol of **2-η^2-HSnR$_3$** (R = ^{n}Bu and Ph) in 6 mL of Et_2O, stored at -35 °C for 30 min, were added a solution of 0.044 g (0.430 mmol) of benzonitrile in 2 mL of Et_2O. The resulting mixture turned from yellow to maroon and was stirred for 1 h. Upon removal of all volatiles produced a dark oily residue. The ^{1}H NMR spectra exhibited a mixture of 95% of **2-NC(H)Ph** and 5% of HN(^{i}Pr)Ar.

4.9 Reaction of 3 with PH_2Ph

To an orange solution of 0.376 g (0.585 mmol) of **3** in 5 mL of Et_2O were added a solution of 0.065 g (0.590 mmol) of phenylphosphine in 2 mL of Et_2O. The resulting mixture slowly turned into reddish-brown and was stirred for 12 h. The ^2H NMR spectra displayed the signal of **3-H** (29.78 ppm) and **3-PHPh** (2.92 ppm) in approximately 1:1 ratio. When 10 equiv of phenylphosphine was employed, the signal of **3-H** disappeared in the ^2H NMR spectra and the signal of **3-PHPh** (1.85 ppm) remained. Upon removal of all volatiles in vacuo from the latter reaction resulted in a dark brown oily residue of **3-PHPh**. ^1H NMR (C_6D_6, 19.9 °C): δ 9.92 (d, $^1J_{HP}$ = 315 Hz) , 7.83 (t, 2 H, *meta*-Ph), 7.21 (t, 2 H, *ortho*-Ph), 7.01 (t, 1 H, *para*-Ph), 6.59 (s, 3 H, *para*-$C_6H_3Me_2$), 6.54 (s, 6 H, *ortho*-$C_6H_3Me_2$), 2.17 (s, 18 H, $C_6H_3\mathit{Me}_2$), 1.32 (s, 9 H, $CC\mathit{H}_3(CD_3)_2$) ppm. ^{31}P NMR (Et_2O, 19.9 °C): δ 161.80 ($\Delta\nu_{1/2}$= 2530 Hz) ppm.

4.10 Synthesis of 2-d_{18}-PHMes (Mes = 2,4,6-$C_6H_2Me_3$)

To an orange-brown solution of 0.362 g (0.567 mmol) of **1-d_{18}** in 5 mL of Et_2O were added a solution of 0.086 g (0.567 mmol) of 2,4,6-trimethylphenylphosphine in 2 mL of Et_2O. The reaction was monitored by ^2H NMR spectroscopy, which displayed signals of **1-d_{18}** and new peaks at 17.96 ($\Delta\nu_{1/2}$= 17.8 Hz) and 2.52 ppm in the early stage. The solution was stirred for 2 h and the ^2H NMR spectra exhibited only the signal at 1.77 ppm. Upon removal of solvent in vacuo provided a dark brown oily residue of **2-d_{18}-PHMes**. ^1H NMR (C_6D_6, 20.1 °C): δ 8.58 (d, 1 H, $^1J_{HP}$ = 288 Hz), 6.86 (s, 2 H, *meta*-Mes), 6.60 (s, 3 H, *para*-$C_6H_3Me_2$), 6.55 (s, 6 H, *ortho*-$C_6H_3Me_2$), 4.50 (q, 3 H, methine), 2.67 (s, 9 H, 2,4,6-$C_6H_2\mathit{Me}_3$), 2.15 (s, 18 H, $C_6H_3\mathit{Me}_2$), 1.19 (d, 18 H, C(H)Me_2)

ppm. ^{13}C NMR (C_6D_6, 20.1 °C): δ 150.26, 139.16, 138.89, 137.60, 135.78, 129.67 (d, C_{ipso}), 126.88, 125.71, 61.04, 24.82, 24.70, 23.95, 21.84 ppm. ^{31}P NMR (Et_2O, 20.1 °C): δ 89.94 (d, J_{PH} = 287 Hz) ppm. Anal. Calcd. for $C_{42}H_{60}N_3MoP$: C, 68.74; H, 8.24; N, 5.73. Found: C, 68.86; H, 8.20; N, 5.66.

4.11 Synthesis of 2-PHPh

To an orange-brown solution of 0.347 g (0.560 mmol) of **1** in 10 mL of Et_2O were added *via* pipet a solution of 0.062 g (0.560 mmol) of phenylphosphine in 5 mL of Et_2O. Evolution of hydrogen was observed, and a brownish-yellow solution developed rapidly. The solution was stirred for 1 h and all volatiles were removed in vacuo. An oily residue of **2-PHPh** was obtained. ^{1}H NMR (C_6D_6, 20.3 °C): δ 8.81 (d, 1 H, $^1J_{HP}$ = 285 Hz) 7.77 (t, 2 H, *meta*-Ph), 7.21 (t, 2 H, *ortho*-Ph), 7.01 (t, 1 H, *para*-Ph), 6.62 (s, 3 H, *para*-$C_6H_3Me_2$), 6.56 (s, 6 H, *ortho*-$C_6H_3Me_2$), 4.43 (q, 3 H, methine), 2.15 (s, 18 H, $C_6H_3\mathit{Me}_2$), 1.16 (d, 18 H, C(H)Me_2) ppm. ^{13}C NMR (C_6D_6, 20.3 °C): δ 150.97, 137.69, 131.09 (d, C_{ipso}), 128.77, 128.70, 126.91, 126.28, 126.09, 61.03 (C(H)Me_2), 24.01, 21.89 ppm. ^{31}P NMR (Et_2O, 20.3 °C): δ 118.39 (d, J_{PH} = 293 Hz) ppm. Anal. Calcd. for $C_{39}H_{36}D_{18}N_3MoP$: C, 65.98; H, 10.22; N, 5.92. Found: C, 65.89; H, 10.15; N, 5.84.

To a cold solution of 0.020 g (0.179 mmol) of phenylphosphine in 2 mL of Et_2O, stored at −35 °C for 30 min, were added 0.228 g (0.357 mmol) of **1-d_{18}**. The resulting mixture was stirred for 5 min during which it became dark reddish-brown. ^{2}H NMR (Et_2O, 20.2 °C): δ 18.24 ($\Delta\nu_{1/2}$= 14 Hz), 2.70 ppm. The solution was stirred overnight and the signal at 18.24 ppm disappeared but the peak at 2.70 ppm (**2-d_{18}-PPhH**) remained.

4.12 Synthesis of 2-PHCy (Cy = cyclohexyl)

To an orange-brown solution of 0.336 g (0.527 mmol) of **1-d_{18}** in 5 mL of Et_2O were added a solution of 0.062 g (0.527 mmol) of cyclohexylphosphine in 2 mL of Et_2O. The resulting mixture turned into intense purple rapidly and was evacuated for 1 min. The reaction was monitored by ^2H NMR spectroscopy, which displayed a peak at 5.02 ($\Delta\nu_{1/2}$= 14 Hz) in the early stage. After stirring overnight, the solution became orange-brown and the removal of solvent in vacuo produced a dark oily residue of **2-PHCy**. ^1H NMR (C_6D_6, 20.1 °C): δ 8.52 (d, 1 H, $^1J_{HP}$ = 260 Hz), 6.71 (s, 6 H, *ortho*-$C_6H_3Me_2$), 6.64 (s, 3 H, *para*-$C_6H_3Me_2$), 4.37 (q, 3 H, methine), 2.20 (s, 18 H, $C_6H_3\mathit{Me}_2$), 2.04 (br, 2 H, Cy), 1.77 (br, 4 H, Cy), 1.58 (br, 1 H, Cy), 1.30 (br, 4 H, Cy), 1.20 (d, 18 H, C(H)Me_2) ppm. ^{13}C NMR (C_6D_6, 20.1°C): δ 153.15, 137.57, 126.23, 125.75, 61.04, 48.57, 34.91, 28.59 (d), 26.92, 24.10, 21.92 ppm. ^{31}P NMR (Et_2O, 20.1 °C): δ 173.13 (d, J_{PH} = 265 Hz) ppm. Anal. Calcd. for $C_{39}H_{60}N_3MoP$: C, 67.13; H, 8.67; N, 6.02. Found: C, 67.28; H, 8.78; N, 5.88.

4.13 X-ray crystal structure of 2-η^2-HSn^nBu_3

Crystals of **2-η^2-HSn^nBu_3** were grown from a saturated pentane solution at -35 °C. Inside the glove-box, the crystals were quickly moved from a scintillation vial to a microscope slide containing Paratone *N* (an Exxon product) oil. Under the microscope a dark brown block of approximate dimensions 0.72 × 0.44 × 0.32 mm^3 was selected and mounted on a glass fiber using wax. A total of 17971 reflections were collected ($-12 \leq h \leq 8$, $-22 \leq k \leq 25$, $-19 \leq l \leq 19$) in the θ range of 2.39 to 23.28 °, of which 6605 were unique (R_{int} = 0.0444) The structure was solved using direct methods

(SHELXTL V5.1, G. M. Sheldrick and Siemens Industrial Automation, Inc., 1997) in conjunction with standard difference Fourier techniques. All non-hydrogen atoms were refined anisotropically. All hydrogen atoms were found in the electronic density map and refined isotropically, with the exception of H44C, H64D and the hydrogen atoms belonging to C51, C52, C54, C63, C351 which were placed in calculated (d_{CH} = 0.96 Å) positions. The residual peak and hole electron density were 0.968 and −0.911 e·Å^{-3}, respectively. A semi-empirical absorption correction was applied based on pseudo-psi-scans with maximum and minimum transmission equal to 0.7736 and 0.5811, respectively. The least squares refinement converged normally with residuals of R_1 = 0.0303, wR_2 = 0.0722 based on $I > 2\sigma I$ and GOF = 1.123 (all data based on F^2). No extinction coefficient was applied to the refinement. Crystal and refinement data: formula = $C_{45}H_{76}N_3MoSn$, space group *P2(1)/n*, a = 11.2324(7) Å, b = 23.026(1) Å, c = 17.844(1) Å, α = 90 °, β = 94.049(1) °, γ = 90 °, Z = 4, V = 4603.5(5) Å^3, D_{calcd} = 1.261 g·cm^{-3}, $F(000)$ = 1836, R (all data based on F) = 0.0337, wR (all data based on all F^2) = 0.0748.

4.14 X-ray crystal structure of 3-$SnPh_3$

Inside the glove-box, crystals of **01154** grown from a concentrated pentane solution at −35 °C were coated with Paratone *N* oil (an Exxon product) on a microscope slide. A dark emerald plate of approximate dimensions 0.26 × 0.22 × 0.05 mm^3 was selected and mounted with wax on a glass fiber. A total of 10083 reflections ($-13 \leq h \leq 14$, $-14 \leq k \leq 9$, $-18 \leq l \leq 17$) were collected at 183(2) K in the θ range of 2.05 to 23.29 °, of which 7001 were unique (R_{int} = 0.0414). The structure was solved by direct methods (SHELXTL V5.1, G. M. Sheldrick and Siemens Industrial Automation, Inc., 1997) in conjunction with standard difference Fourier techniques.

All non-hydrogen atoms were refined anisotropically and all hydrogen atoms were found in the electronic density map with the exception of H23C that was placed in calculated (d_{CH} = 0.96 Å) position. The residual peak and hole electron density were 0.859 and −0.738 e·Å^{-3}, respectively. A semi-empirical absorption correction was applied based on pseudo-psi-scans with maximum and minimum transmissions equal to 0.9615 and 0.8205, respectively. The least squares refinement converged normally with residuals of R_1 = 0.0389, wR_2 = 0.0995 based on $I > 2\sigma I$ and GOF = 1.092 (all data based on F^2). No extinction coefficient was applied to the refinement. Crystal and refinement data: Formula = $C_{54}H_{69}N_3SnMo$, space group $P\bar{1}$, a = 13.0062(8) Å, b = 13.3583(8) Å, c = 16.760(1) Å, α = 102.642(1) °, β = 90.291(1) °, γ = 118.284(1) °, Z = 2, V = 2481.9(3) Å^3, D_{calcd} = 1.304 g·cm^{-3}, $F(000)$ = 1012, R (all data based on F) = 0.0450, wR (all data based on F^2) = 0.1036.

4.15 X-ray crystal structure of [2-SnPh$_2$]$_2$

Inside the glove box, crystals of [**2-SnPh$_2$**]$_2$ grown from a concentrated diethyl ether solution at −35 °C were coated with Paratone N oil (an Exxon product) on a microscope slide. A green plate of approximate dimensions 0.43 × 0.23 × 0.11 mm^3 was selected and mounted with wax on a glass fiber. A total of 9438 reflections ($-11 \leq h \leq 13$, $-13 \leq k \leq 9$, $-19 \leq l \leq 19$) were collected at 183(2) K in the θ range of 2.40 to 23.27 °, of which 6523 were unique (R_{int} = 0.0263). The structure was solved by direct methods (SHELXTL V5.1, G. M. Sheldrick and Siemens Industrial Automation, Inc., 1997) in conjunction with standard difference Fourier techniques. All non-hydrogen atoms were refined anisotropically. All hydrogen atoms were located in the electronic density map and refined isotropically, with the exception of the hydrogen atoms belonging to

C231 and to the solvent carbon atoms which were placed in calculated (d_{CH} = 0.96 Å) positions. The residual peak and hole electron density were 1.166 and −0.377 e·Å^{-3}, respectively. A semi-empirical absorption correction was applied based on pseudo-psi-scans with maximum and minimum transmission equal to 0.9127 and 0.7123, respectively. The least squares refinement converged normally with residuals of R_1 = 0.0292, wR_2 = 0.0705 based on $I > 2\sigma I$ and GOF = 1.027 (all data based on F^2). No extinction coefficient was applied to the refinement. Crystal and refinement data: formula = $MoC_{49}H_{68}N_3Sn$, space group $P\bar{1}$, a = 12.4397(9) Å, b = 12.5551(9) Å, c = 17.426(1) Å, α = 103.906(1) °, β = 92.215(1) °, γ = 117.065(1) °, Z = 2, V = 2317.7(3) Å^3, D_{calcd} = 1.332 g·cm^{-3}, $F(000)$ = 966, R (all data based on F) = 0.0336, wR (all data based on F^2) = 0.0728.

4.16 X-ray crystal structure of 3-H

Inside the glove-box, crystals of **3-H** grown from a concentrated diethyl ether solution at -35 °C were quickly moved from a scintillation vial to a microscope slide containing Paratone N (an Exxon product) oil. Under the microscope a ruby red block of approximate dimensions 0.52 × 0.40 × 0.26 mm^3 was selected and mounted on a glass fiber using wax. A total of 13457 reflections were collected ($-12 \leq h \leq 12$, $-19 \leq k \leq 19$, $-20 \leq l \leq 10$) in the θ range of 2.59 to 23.30 °, of which 4991 were unique (R_{int} = 0.0354) The structure was solved by direct methods (SHELXTL V5.1, G. M. Sheldrick and Siemens Industrial Automation, Inc., 1997) in conjunction with standard difference Fourier techniques. All non-hydrogen atoms were refined anisotropically. All hydrogen atoms were placed in located in the electronic density map and refined isotropically. The residual peak and hole electron density were 0.230 and −0.389 e·Å^{-3}, respectively. A semi-empirical absorption correction

was applied based on pseudo-psi-scans with maximum and minimum transmission equal to 0.9023 and 0.8175, respectively. The least squares refinement converged normally with residuals of $R_1 = 0.0299$, $wR_2 = 0.0744$ based on $I > 2\sigma I$ and GOF = 1.150 (all data based on F^2). No extinction coefficient was applied to the refinement. Crystal and refinement data: formula = $C_{36}H_{55}N_3Mo$, space group *P2(1)/n*, $a = 11.208(1)$ Å, $b = 17.152(2)$ Å, $c = 18.296(2)$ Å, $\alpha = 90$ °, $\beta = 99.044(2)$ °, $\gamma = 90$ °, $Z = 4$, $V = 3473.4(6)$ Å^3, $D_{\text{calcd}} = 1.197$ g·cm^{-3}, $F(000) = 1366$, R (all data based on F) = 0.0314, wR (all data based on F^2) = 0.0752.

References

1. Corey, J. Y.; Braddock-Wilking, J. *Chem. Rev.* **1999,** *99,* 175.

2. Graham, W. A. G. *J. Organomet. Chem.* **1986,** *300,* 81.

3. Schubert, U. *Adv. Organomet. Chem.* **1990,** *30,* 151.

4. Laplaza, C. E.; Cummins, C. C. *Science* **1995,** *268,* 861.

5. Laplaza, C. E.; Johnson, M. J. A.; Peters, J. C.; Odom, A. L.; Kim, E.; Cummins, C. C.; George, G. N.; Pickering, I. J. *J. Am. Chem. Soc.* **1996,** *118,* 8623.

6. Laplaza, C. E.; Odom, A. L.; Davis, W. M.; Cummins, C. C.; Protasiewicz, J. D. *J. Am. Chem. Soc.* **1995,** *117,* 4999-5000.

7. Cherry, J.-P. F.; Johnson, A. R.; Baraldo, L. M.; Tsai, Y.-C.; Cummins, C. C.; Kryatov, S. U.; Rybak-Akimova, E. V.; Capps, K. B.; Hoff, C. D.; Haar, C. M.; Nolan, S. P. *J. Am. Chem. Soc.* **2001,** *123,* 7271.

8. Laplaza, C. E.; Davis, W. M.; Cummins, C. C. *Angew. Chem. Int. Ed. Engl.* **1995,** *34,* 2042.

9. Peters, J. C.; Odom, A. L.; Cummins, C. C. *Chem. Commun.* **1997,** 1995.

10. Tsai, Y.-C.; Johnson, M. J. A.; Mindiola, D. J.; Cummins, C. C.; Klooster, W. T.; Koetzle, T. F. *J. Am. Chem. Soc.* **1999,** *121,* 10426.

11. Tsai, Y.-C.; Durá-Vilá, V.; Diaconescu, P. L.; Cummins, C. C. *Manuscript in preparation* .

12. Tsai, Y.-C.; Meyer, K.; Mindiola, D. J.; Cummins, C. C. *submitted* .

13. Crabtree, R. H. *Angew. Chem., Int. Ed. Engl.* **1993,** *35,* 789.

14. Schubert, U.; Kunz, E.; Harkers, B.; Willnecker, J.; Meyer, J. *J. Am. Chem. Soc.* **1989,** *111,* 2572.

15. Piana, H.; Kirchgäßner, U.; Schubert, U. *Chem. Ber.* **1991,** *124,* 743.

16. Legzdins, P.; Shaw, M. J.; Batchelor, R. J.; Einstein, W. B. *Organometallics* **1995,** *14,* 4721.

17. Carlton, L.; Weber, R.; Levendis, D. C. *Inorg. Chem.* **1998,** *37,* 1264.

18. Khaleel, A.; Klabunde, K.; Johnson, A. *J. Organomet. Chem.* **1999,** *572,* 11.

19. Berkowitz, J.; Ellison, G. B.; Gutman, D. *J. Phys. Chem.* **1994,** *98,* 2744.

20. Kanabus-Kaminska, J. M.; Hawari, J. A.; Griller, D.; Chatgilialoglu, C. *J. Am. Chem. Soc.* **1987,** *109,* 5267.

21. Dickhaut, J.; Giese, B. *Org. Synth.* **1992,** *70,* 164.

22. Bonanno, J. B.; Wolczanski, P. T.; Lobkovsky, E. B. *J. Am. Chem. Soc.* **1994,** *116,* 11159.

23. Bennett, M. J.; Mason, R. *Proc. Chem. Soc.* **1963,** 273.

24. Doedens, R. J.; Dahl, L. F. *J. Am. Chem. Soc.* **1965,** *87,* 2576.

25. Wilson, F. C.; Shoemaker, D. P. *J. Chem. Phys.* **1957,** *27,* 809.

26. Olsen, D. H.; Rundle, R. E. *Inorg. Chem.* **1963,** *2,* 1310.

27. Protsky, A. N.; Bulychev, B. M.; Soloveichik, G. L.; Belsky, V. K. *Inorg. Chim. Acta* **1986,** *115,* 121.

28. Linde, D. R. *J. Chem. Phys.* **1951,** *19,* 1605.

29. Beagley, B.; Mcaloon, K.; Freeman, J. M. *Acta Crystallogr., Part B* **1974,** *30,* 444.

30. Schager, F.; Goddard, R.; Seevogel, K.; Pörschke, K.-R. *Organometallics* **1998,** 1546.

31. Saillard, J.-Y.; Hoffmann, R. *J. Am. Chem. Soc.* **1984,** *106,* 2006.

32. Fitzpatrick, N. J.; McGinn, M. A. *J. Chem. Soc., Dalton Trans.* **1985,** 1637.

33. Lichtenberger, D. L.; E., K. G. *J. Am. Chem. Soc* **1986,** *108,* 2560.

34. Rabaâ, H.; Saillard, J.-Y.; Schubert, U. *J. Organomet. Chem.* **1987,** *330,* 397.

35. Glavee, G. N.; Jagirdar, R. B.; Schneider, J. J.; Klabunde, K. J.; Radonovich, L. J.; Dodd, K. *Organometallics* **1992,** *11,* 1043.

36. Jagirdar, R. B.; Palmer, R.; Klabunde, K. J.; Radonovich, L. J. *Inorg. Chem.* **1995,** *34,* 278.

37. Peters, J. C.; Cummins, C. C. *unpublished results* .

38. Corriu, R.; Guerin, C.; Kolani, B. *Inorg. Synth.* **1989,** *25,* 110.

39. Shimoi, M.; Nagai, S.-I.; Ichikawa, M.; Kawano, Y.; Katoh, K.; Uruichi, M.; Ogino, H. *J. Am. Chem. Soc.* **1999,** *121,* 11704.

40. Kakizawa, T.; Kawano, Y.; Shimoi, M. *Organometallics* **2001,** *20,* 3211.

41. Dakternieks, D.; Henty, D. J.; Schiesser, C. H. *J. Phys. Org. Chem.* **1999,** *12,* 233.

42. Imori, T.; Tilley, T. D. *J. Chem. Soc., Chem. Commun.* **1993,** 1607.

43. Imori, T.; Lu, V.; Cai, H.; Tilley, T. D. *J. Am. Chem. Soc.* **1995,** *117,* 9931.

44. Lu, V.; Tilley, T. D. *Macromolecules* **2000,** *33,* 2403.

45. Adams, S.; Dräger, M. *Angew. Chem., Int. Ed. Engl.* **1987,** *26,* 1255.

46. Ho, B. Y. K.; Zuckerman, J. J. *J. Organomet. Chem.* **1973,** *49,* 1.

47. Kuivila, H. G. *Synthesis* **1970,** 499.

48. Fürstner, A.; Mathes, C.; Lehmann, C. W. *J. Am. Chem. Soc.* **1999,** *121,* 9453.

49. Dobbs, A. A.; Schrock, R. R.; Davis, W. M. *Inorg. Chim. Acta* **1997,** *263,* 171.

50. Evans, D. F. *J. Chem. Soc.* **1959,** 2003.

51. Bottomley, F.; Lin, I. J. B. *J. Chem. Soc., Dalton Trans.* **1981,** 271.

52. Mösch-Zanetti, N. C.; Schrock, R. R.; Davis, W. M.; Wanninger, K.; Siedel, S. W.; O'Donoghue, M. B. *J. Am. Chem. Soc.* **1997,** *119,* 11037.

53. Oshikawa, T.; Yamashita, M. *Chem. Ind. (London)* **1985,** 126.

54. Pangborn, A. B.; Giardello, M. A.; Grubbs, R. H.; Rosen, R. K.; Timmers, F. J. *Organometallics* **1996,** *15,* 1518.

Curriculum Vitae

Education M.S., Chemistry, National Taiwan Normal University (June 1994)
B.S., Chemistry, National Taiwan Normal University (June 1991)

Experience Professor Christopher C. Cummins, MIT
Research Assistant July. 1998 –Present
Discovery and characterization of three coordinate based organometallic system. One objective is to activate organic functional groups by an unusual hydride-imine molybdenum complex.

Department of Chemistry, MIT
Teaching Assistant Sept. 1997 – June 1998
Responsible for aiding undergraduate students in needing laboratory assistance, including the operation of dry box and Schlenk line and the syntheses and characterizations of organometallic compounds.

Department of Chemistry, National Taiwan Normal University
Teaching Assistant July 1994 – July 1997
Responsible for aiding undergraduate students in needing laboratory assistance, includingthesyntheses and characterizatons of inorganic compounds.

Publications

1. Yi-Chou Tsai, Karsten Meyer, Daniel J. Mindiola, and Christopher C. Cummins,"Complexation, Coupling, and Cleavage of Organonitriles by a Masked Three-Coordinate Molybdenum(III) Complex: Spectroscopic Characterization and Mechanistic Investigations," manuscript in preparation.

2. Yi-Chou Tsai, Víctor Durá Vilá, Paula L. Diaconescu, Masaki Shimizu, Stephen Buchwald, and Christopher C. Cummins, "Interaction of Styrene and Alkynes with a Masked Three-Coordinate Molybdenum(III) Complex: Preparation of Well-Defined Alkyne Metathesis Catalysts and Related Chemistry," manuscript in preparation.

3. Yi-Chou Tsai, Paula L. Diaconescu, and Christopher C. Cummins, "Activation of E-H Bonds (E = Sn or P) by Three-Coordinate Molybdenum(III) Complexes," manuscript in preparation.

4. Yi-Chou Tsai and Christopher C. Cummins, "Dinitrogen Cleavage by Three-Coordinate Molybdenum(III) Complexes Accelerated by Lewis Bases," manuscript in preparation.

5. Daniel J. Mindiola, Yi-Chou Tsai, Ryuichiro Hara, Qinghao Chen, Karsten Meyer, and Christopher C. Cummins, "Bimetallic μ-Cyanoimide Complexes Prepared by NCN Group Transfer," *Chem. Comm.* **2001,** 125.

6. Yi-Chou Tsai, Paula L. Diaconescu, and Christopher C. Cummins, "Facile Synthesis of Trialkoxymolybdenum(VI) Alkylidyne Complexes for Alkyne Metathesis," *Organometallics*, **2000,** *19*, 5260.

7. Yi-Chou Tsai, Marc J. A. Johnson, Daniel J. Mindiola, Christopher C. Cummins, Wim T. Klooster, and Thomas F. Koetzle, "A Cyclometallated Resting State for a Reactive Molybdenum Amide: Favorable Consequences of β-Hydrogen Elimination Including Reductive Cleavage, Coupling, and Complexation," *J. Am. Chem. Soc.*, **1999**, *121*, 10426.

8. J.-J Cherng, Y.-C. Tsai, C.-H. Ueng, G.-H. Lee, S.-M. Peng, and M. Shieh, "New Synthesis of $[SFe_3(CO)_9]^{2-}$ and Its Reactiviry toward Electrophiles," *Organometallics* , **1998**, *17*, 255.

9. K.-C. Huang, Y.-C. Tsai, G.-H. Lee, S.-M. Peng, and M. Shieh, "Syntheses and X-ray Structures of a Series of Chalcogen-Containing Manganese Carbonylates $[E_2Mn_3(CO)_9]^-$, $[E_8C_2Mn_2(CO)_6]^{2-}$, and $[E_2Mn_4(CO)_{12}]^{2-}$ (E= Se, S)," *Inorg. Chem.* **1997**, *36*, 4421.

10. M. Shieh, Y.-C. Tsai, J.-J Cherng, M.-H. Shieh, H.-S. Chen, and C. H. Ueng, "Reactivity of $[SeFe_3(CO)_9]^{2-}$ with Electrophiles: Formation of $[SeFe_2Ru_3(CO)_{14}]^{2-}$, $[SeFe_3(CO)_9(\mu\text{-HgI})]^-$, $Fe_2(CO)_6(\mu\text{- SeCHPhSe})$, and $Se_2Fe_2(CO)_6(\mu\text{-}CH_2)_2$," *Organometallics*, **1997**, *16*, 456.

11. M. Shieh, M.-H. Shieh, Y.-C. Tsai, and C.-H. Ueng, " Transformations of Selenium-Iron Carbonylates in Hieber's Synthesis: Isolation of an Intermediate Complex $[PhCH_2NMe_3]_2[Se_6Fe_6(CO)_{12}]$," *Inorg. Chem.* **1995**, *34*, 5088.

12. M. Shieh, P.-F. Chen, Y.-C. Tsai, M.-H. Shieh, S.-M. Peng, and G.-H. Lee, "Facile Syntheses and Transformations of a Series of Tellurium- Iron Carbonyl Clusters: Crystal Structures of $[PhCH_2NMe_3]_2[Te_6Fe_8(CO)_{24}]$, $Fe_2(CO)_6(\mu\text{-}TeCHCl_2)_2$, and $Fe_2(CO)_6(\mu\text{-}TeCHPhTe)$," *Inorg. Chem.* **1995**, *34*, 2251.

13. M. Shieh and Y.-C. Tsai, "Preparation of $[SeFe_3(CO)_9]^{2-}$ and Its Derivatives $[\{SeFe_3(CO)_9\}_2M]^{2-}$(M= Hg, Cd)," *Inorg. Chem.* **1994**, *33*, 2303.

Acknowledgments

This thesis would not have been possible without the support and guidance of many people throughout my life. First of all, I would like to thank my research advisor Kit Cummins for providing me with countless opportunities during the course of my studies at MIT, as well as the occasional prodding that an advisor can provide. I am grateful to Kit for his patience and for having such a love of inorganic chemistry and I am hoping to approach his level of chemical knowledge someday. I also want to thank Kit for the hundreds of times I have knocked on his office door with questions about innumerable things, he is always there and I have never been turned away. Kit also taught me many practical things which I am sure will benefit throughout my career, and has been a great person to work with.

Many thanks are due to the multitude of unique individuals whom I was fortune enough to cross paths with in the Cummins group. I would especially like to thank Dr. Daniel Mindiola for his guidance during my early years of graduate studies. Dan is an energetic, enthusiastic, knowledgeable, funny and very handy chemist. I also want to thank him for his enthusiastic help with X-ray crystallography. Dan is currently a post-doc at the University of Chicago and looking for a job in academia. I believe he will be a willing, capable, and thoughtful teacher. Dr. Jane Greco, my box-mate, taught me how to do chemistry in a dry box. John-Paul Cherry, a nonlinear thinker, came the same time as I did and is leaving the same time as I am. John-Paul is not only a good friend but also a good mentor. He always has different viewpoints on chemistry and life in general. He also taught me how to appreciate my life. The crystal structures make up a big part of my thesis, and I owe Paula Diaconescu a big thank you for mounting the crystals and solving the structures. Paula is not only a great crystallographer but a very talented synthetic inorganic chemist. She has a big success in uranium chemistry. I hope she continues to do well. Fran Stephens, the master of phosphorus chemistry, is like a sister. I am grateful to Fran for establishing the inventory of chemical reagents. With her efforts, doing chemistry in the Cummins Group became more efficient than before. The newest members of the group, Joshua Figueroa, Arjun Mendiratta, and Víctor Durá-Vilá. Josh (aka La La), my box-mate, a very talented and knowledgeable chemist. He prepared a niobium metallaaziridine hydride complex which many people had dreamed about.

Because of his success, I can not use 'the' for molybdenum metallaaziridine hydride any more. With his efforts, our dry box is now a very clean working place. Arjun is also very knowledgeable. He always has stimulating ideas for me at group meetings. Víctor is not only doing neat experiments but also does computational works. His excellent works truly help me understand the electronic structures of my compounds. Good luck to them.

Acknowledgment goes to many intelligent post-docs. Dr. Luis Baraldo (in Argentina) taught me electrochemistry. Dr. Karsten Meyer (at UCSD) taught me EPR spectroscopy. I am also grateful to Karsten for his patience and great enthusiasm, which has been truly inspiring me for the past few years. Dr. Dan Millward (in California), Dr. Masaharu Toriyama (in Japan), Dr. Paul Chirik (at Cornell), Dr. Ryuichiro Hara, Dr. Mish Barybin (at The University of Kansas), Dr. Justin Brask (my Canadian box-mate), and Dr. Booyong Lim shared their invaluable experience with me. I must also thank Dr. Masaki Shimizu (at Kyoto University in Japan), who came to MIT working with Professor Buchwald) collaborated with me on the alkyne metathesis project and taught me how to run column chromatography. Discussion about chemistry with them is always enjoyable. These discussions helped shaped the way I put the thesis together.

Traditionally, the bright UROPs make a lot of contributions to this group, and I am lucky to work with some of them. Nuch Sangtrirutnugul (Berkeley), Theo Agapie (Caltech), and Han Sen Soo. They all have excellent achievements and their works impact me and our group in a very positive way. I believe they all will have wonderful future.

I want to thank Gabriella Browne and Allison Kelesey as well. With their help, I could finish my forth-year seminar and thesis defense without any trouble. Both of them have been tremendous support for the group.

There are many other people to thank. Dr. Lan-Chang Liang (Schrock), an assistant professor in Taiwan now, Jennifer Jamieson (Schrock), Parisa Mehrkhodavandi (Schrock), Dr. Evan Freiberg (Davison), Dr. Alan Heyduk (Nocera) Brad Pistorio (Nocera), David Manke (Nocera), and David Krodel (Nocera) shared their experience with me. I really enjoy talking with them, and they always cheer me up.From the Department of Chemistry Instrumentation Facility, I would like to

acknowledge Jeff Simpson, Mark Wall, and David Bray for their assistance with various NMR and EPR experiments. I would also like to thank my thesis committee, Professor Lippard and Schrock, for an instructive defense and their valuable suggestions about the thesis.

I am deeply indebted to my wife Jui-Fen, who tolerated many late nights and bad moods during the course of my studies. For her patience, support, and love I am eternally grateful. She is going to give birth of our first baby in the mid December. I feel that we have grown together throughout this experience, and hopefully we will continue to do so for the remainder of my career and life.

I would like to regard this thesis as a remark for my staying at MIT. I would like to expand the spirit that I learned from here to my entire career. After all, I would like to thank my parents and brothers for their love and support throughout the course of my studies and life.